Holography, hydrodynamics and flows

Novak, Igor

UNIVERSITÉ DE GENÈVE
Section de Physique
Département de Physique Théorique

FACULTÉ DES SCIENCES
Professeur Julian Sonner

HOLOGRAPHY, HYDRODYNAMICS AND FLOWS

THÈSE

présentée à la Faculté des Sciences de l'Université de Genève
pour obtenir le grade de Docteur ès sciences, mention Physique

par

Igor NOVAK

de

Daruvar (Croatie)

Thèse N° 5522

GENÈVE
Atelier d'impression de l'Université de Genève
Decembre 2020

UNIVERSITÉ DE GENÈVE

FACULTÉ DES SCIENCES

DOCTORAT ÈS SCIENCES, MENTION PHYSIQUE

Thèse de Monsieur Igor NOVAK

intitulée :

«Holography, Hydrodynamics And Flows»

La Faculté des sciences, sur le préavis de Monsieur J. SONNER, professeur associé et directeur de thèse (Département de physique théorique), Monsieur K. KRUSE, professeur ordinaire (Département de biochimie) et Monsieur J. HARTONG, professeur (School of Mathematics, University of Edinburgh, Edinburgh, United Kingdom), autorise l'impression de la présente thèse, sans exprimer d'opinion sur les propositions qui y sont énoncées.

Genève, le 2 décembre 2020

Thèse - 5522 -

Le Doyen

N.B. - La thèse doit porter la déclaration précédente et remplir les conditions énumérées dans les "Informations relatives aux thèses de doctorat à l'Université de Genève".

MEMBERS OF THE JURY

Prof. Dr. Julian Sonner
Département de Physique Théorique
Université de Genève, Switzerland

Prof. Dr. Karsten Kruse
Département de Physique Théorique
Université de Genève, Switzerland

Dr. Jelle Hartong
School of Mathematics
University of Edinburgh, United Kingdom

PUBLICATIONS

This thesis is based on the following publications:

[1] Igor Novak, Julian Sonner, and Benjamin Withers. "Overcoming Obstacles in Nonequilibrium Holography." In: *Phys. Rev.* D98.8 (2018), p. 086023. DOI: 10.1103/PhysRevD.98.086023. arXiv: 1806.08655 [hep-th].

[2] Igor Novak, Julian Sonner, and Benjamin Withers. "Hydrodynamics without boosts." In: *JHEP* 07 (2020), p. 165. DOI: 10.1007/JHEP07(2020)165. arXiv: 1911.02578 [hep-th].

[3] Igor Novak, Julian Sonner, and Benjamin Withers. "To be published." In: ().

Nous ne pouvons connaître tous les faits et il faut choisir ceux qui sont dignes d'être connus. Si l'on en croyait Tolstoï, les savants feraient ce choix au hasard, au lieu de le faire, ce qui serait raisonnable, en vue des applications pratiques. Les savants, au contraire, croient que certains faits sont plus intéressants que d'autres, parce qu'ils complètent une harmonie inachevée, ou parce qu'ils font prévoir un grand nombre d'autres faits. S'ils ont tort, si cette hiérarchie des faits qu'ils postulent implicitement, n'est qu'une illusion vaine, il ne saurait y avoir de Science pour la Science, et par conséquent il ne saurait y avoir de Science. Quant à moi, je crois qu'ils ont raison, et, par exemple, j'ai montré plus haut quelle est la haute valeur des faits astronomiques, non parce qu'ils sont susceptibles d'applications pratiques, mais parce qu'ils sont les plus instructifs de tous.

Ce n'est que par la Science et par l'Art que valent les civilisations. On s'est étonné de cette formule: la Science pour la Science; et pourtant cela vaut bien la vie pour la vie, si la vie n'est que misère; et même le bonheur pour le bonheur, si l'on ne croit pas que tous les plaisirs sont de même qualité, si l'on ne veut pas admettre que le but de la civilisation soit de fournir de l'alcool aux gens qui aiment à boire.

Toute action doit avoir un but. Nous devons souffrir, nous devons travailler, nous devons payer notre place au spectacle, mais c'est pour voir; ou tout au moins pour que d'autres voient un jour.

Tout ce qui n'est pas pensée est le pur néant; puisque nous ne pouvons penser que la pensée et que tous les mots dont nous disposons pour parler des choses ne peuvent exprimer que des pensées; dire qu'il y a autre chose que la pensée, c'est donc une affirmation qui ne peut avoir de sens.

Et cependant – étrange contradiction pour ceux qui croient au temps – l'histoire géologique nous montre que la vie n'est qu'un court épisode entre deux éternités de mort, et que, dans cet épisode même, la pensée consciente n'a duré et ne durera qu'un moment. La pensée n'est qu'un éclair au milieu d'une longue nuit.

Mais c'est cet éclair qui est tout.

— HENRI POINCARÉ, *Valeur de la science*

Dedicated to my wife Petra.

ACKNOWLEDGEMENTS

It's almost hard to believe it's been four years since I've arrived to Geneva to start my PhD. It's been quite a journey. Let me thank, first and foremost, Julian Sonner who has given me this unique opportunity and from whom I've learned so much. I want to thank him for his patience and guidance, for his support, both professional and personal. I am grateful and honored to have been his student. It's hard to imagine a better mentor.

I want to thank Ben Withers, who has been almost as a second mentor to me, for all the fruitful and interesting discussions about physics. Always approachable and open to lending a hand, Ben has taught me many things, especially numerical GR and debugging my own rusty code. Julian and Ben have been wonderful collaborators, and remain sources of inspiration.

I'm grateful for the people who I've come to meet, work, share the office with, and befriend in the past four years - Manuel, Pranjal, Goran, Arunabha, Manus, Tomas, Szabolcs, Santi, Adrian. Thank you for being my colleagues and, more importantly, my friends. Going to the office may be drab for some people, but not for me, and that is mostly thanks to the wonderful people I got to work with.

I want to thank the members of the jury, Prof. Karsten Kruse and Dr. Jelle Hartong for taking the time to read my thesis and agreeing to oversee my defence.

Let me thank my family, especially my parents Gordana and Kazimir, whose unconditional support, love and sacrifice have made me the man that I am, as corny as it may sound. It is difficult to express in words how supportive they have been, in whatever pursuit, dream or ambition I had.

Last, but certainly not least (quite the opposite, in fact), I want to thank my wife, Petra. It's not easy being 900 km apart for almost four years, and yet, in spite of that, grow ever closer. Without you there would be no thesis to read. Thank you for being my partner and best friend, for your unrelenting support, for keeping me sane, and for your love.

REMERCIEMENTS

C'est presque difficile de croire que cela fait quatre ans que je suis arrivé à Genève pour commencer mon doctorat. Ç'a été tout un voyage. Permettez-moi d'abord et avant tout de remercier Julian Sonner qui m'a offert cette occasion unique et dont j'ai tant appris. Je souhaite le remercier pour sa patience et ses conseils, pour son soutien, tant professionnel que personnel. Je suis reconnaissant et honoré d'avoir été son élève. Il est difficile d'imaginer un meilleur mentor.

Je souhaite remercier Ben Withers, qui a été presque comme un deuxième mentor pour moi, pour toutes les discussions fructueuses et intéressantes sur la physique. Toujours accessible et prêt à aider, Ben m'a appris beaucoup de choses, en particulier le GR numérique et le débogage de mon code. Julian et Ben ont été de merveilleux collaborateurs et restent des sources d'inspiration.

Je suis reconnaissant aux personnes avec qui j'ai rencontré, travaillé, partagé le bureau et je suis devenu ami au cours des quatre dernières années - Manuel, Pranjal, Goran, Arunabha, Manus, Tomas, Szabolcs, Santi, Adrian. Merci d'être mes collègues et, plus important encore, mes amies. Aller au bureau peut être terne pour certaines personnes, mais pas pour moi, et c'est surtout grâce aux personnes formidables avec lesquelles j'ai travaillé.

Je souhaite remercier les membres du jury, Prof. Karsten Kruse et Dr. Jelle Hartong d'avoir pris le temps de lire ma thèse et d'avoir accepté de superviser ma soutenance.

J'aimerais remercier ma famille, en particulier mes parents Gordana et Kazimir, dont le soutien inconditionnel, l'amour et le sacrifice ont fait de moi l'homme que je suis. Il est difficile d'exprimer avec des mots à quel point ils m'ont soutenu, quelle que soit la poursuite, le rêve ou l'ambition que j'avais.

Enfin, mais non des moindres (bien au contraire, en fait), j'aimerais remercier ma femme, Petra. Ce n'est pas facile d'être distants de 900 km pendant près de quatre ans et, malgré cela, de se rapprocher de plus en plus. Sans toi, il n'y aurait pas de thèse à lire. Merci d'être ma partenaire et meilleure amie, pour ton soutien indéfectible, pour me garder sain d'esprit et pour ton amour.

CONTENTS

Résumé xxi
Summary and outline xxiii

I INTRODUCTION 1

1 HOLOGRAPHY 3
1.1 Elements of conformal symmetry . . . 3
1.2 Anti-de Sitter spaces . . . 7
1.3 AdS/CFT correspondence . . . 8
1.3.1 GKPW formula and the holographic dictionary . . . 10

2 HYDRODYNAMICS 13
2.1 Non-relativistic hydrodynamics . . . 13
2.1.1 Ideal fluids . . . 14
2.1.2 Incompressible, irrotational and steady flows . . . 17
2.1.3 Dissipative fluids . . . 18
2.2 Relativistic hydrodynamics . . . 21
2.2.1 Zeroth-order hydrodynamics . . . 22
2.2.2 First-order hydrodynamics . . . 23
2.2.3 Entropy current . . . 27
2.3 Non-relativistic hydrodynamics revisited: Newton-Cartan . . . 28
2.3.1 Elements of Newton-Cartan geometry . . . 28
2.3.2 Hydrodynamics . . . 30

II THE SHOWCASE 33

3 OVERCOMING OBSTACLES IN NONEQUILIBRIUM HOLOGRAPHY 35
3.1 Introduction . . . 35
3.2 Universal modes in gravity and hydrodynamics . . . 38
3.2.1 Definition of stationary collective modes . . . 38
3.2.2 A simple hydrodynamic example . . . 42
3.2.3 Charged hydrodynamics . . . 44
3.2.4 Neutral hydrodynamics . . . 49
3.2.5 Reissner-Nordström AdS . . . 50
3.2.6 Spatial Collective Modes in a large number of dimensions . . . 57
3.2.7 BTZ black hole . . . 59
3.3 Black Janus: a fully non-linear analytic example . . . 61
3.3.1 One-point functions . . . 62
3.3.2 Extracting the SCM . . . 63
3.4 Nonlinear solutions: steady states without Killing horizons . . . 66
3.4.1 Numerical method . . . 66
3.4.2 Results . . . 69
3.5 Summary and Discussion . . . 72

4 HYDRODYNAMICS WITHOUT BOOSTS 79
4.1 Introduction . . . 79
4.2 Non-boost-invariant hydrodynamics . . . 80

4.2.1 The ideal fluid . . . 81
4.2.2 Dissipative corrections . . . 82
4.2.3 Entropy current . . . 87
4.2.4 Hydrodynamic shear mode . . . 93
4.3 Special cases . . . 94
4.3.1 Lorentz boosts . . . 94
4.3.2 Galilean boosts . . . 98
4.3.3 Lifshitz scale invariance . . . 99
4.4 Discussion . . . 101
5 FLOWS WITHOUT BOOSTS 103
5.1 Introduction . . . 103
5.2 The Setup . . . 103
5.3 Flow in a 2D channel . . . 104
5.3.1 Flow characterization . . . 107
5.3.2 Planar Poiseuille flow . . . 108
5.3.3 3D Poiseuille flow in a pipe . . . 111
5.3.4 Planar Couette flow . . . 113
5.4 Taylor-Couette flow . . . 115
5.5 (In)stability of the Poiseuille flow . . . 118
5.6 Discussion . . . 121

III APPENDIX 123
A EQUATIONS OF STATE 125
A.1 Conformal equation of state . . . 125
A.2 Reissner-Nordström AdS_{d+1} equation of state . . . 125
B EXTRACTING THE HOLOGRAPHIC STRESS TENSOR 127
B.1 Near-boundary solution in FG coordinates . . . 127
B.2 Converting from FG to $\xi = 0$ coordinate system . . . 128

BIBLIOGRAPHY 129

LIST OF FIGURES

Figure 2.1 Chuck Close, *Self-Portrait* (2000-2001), oil on canvas. This large painting is divided into numerous elements, each, when viewed close-up (no pun intended), has it's own distinct features, colors, even patterns. However, when viewed from afar ("coarse-graining" in a sense) they constitute a different whole, an almost continuous, realistic portrait. . . 14

Figure 3.1 Schematic illustration of the nonequilibrium steady state corresponding to flow across an obstacle. Far to the left ($x \to -\infty$) and far to the right ($x \to +\infty$) the flow returns to a steady, homogeneous flow, different on each side. In the vicinity of the obstacle (hatched region) the flow is nonlinearly deformed. Connecting these two regions are a set of spatial collective modes which describe the exponential (and sometimes oscillatory) spatial relaxation back to equilibrium. 36

Figure 3.2 Schematic illustration of the nonequilibrium steady state of the type depicted in Figure 3.1 in a boosted frame where the upstream fluid is at rest (here we have allowed for a fluid flow incident angle θ). This corresponds to the time-dependent process of dragging a co-dimension one obstacle (hatched region) through a fluid at rest. As in Figure 3.1 the fluid returns to a steady homogeneous flow far from the obstacle, and the spatial collective modes describe this process, indicated here by the spatial profiles of a bow wave and a wake. 37

Figure 3.3 (color figure) poles of the Fourier transform of the 'decay to the right' correlation function, $\hat{G}^{[\searrow]}(k)$, and of the 'decay to the left' correlation function, $\hat{G}^{[\swarrow]}(k)$, in this order, and as defined in the text. The blue contour corresponds to the region to the right of the obstacle, and the green contour to the left. 41

Figure 3.4 (color figure) Spectrum of SCMs in the transverse channel for values of $\mu = 1.0$ (left panel) and $\mu = 1.5$ (right panel). The motion of the imaginary part of the complex momentum is shown as a function of background velocity. Parts of the spectrum where the mode is purely imaginary are shown in orange, while blue dots correspond to the parts where the mode has non-trivial imaginary and real parts. These behaviors transition into each other at the collision points indicated by turquoise diamonds. The red dashed line shows the SCM as predicted in our charged hydrodynamic effective theory. 53

Figure 3.5 The critical exponent in the transverse channel for $\mu = 1.0$, exhibited by the function $\alpha(v)$ defined in (3.88). It can be seen that the mean-field value of $\alpha = 1/2$ is approached at the critical velocity, v_c. 54
Figure 3.6 Behaviour of the critical velocity for flows of a holographic plasma at finite charge density as a function of μ/T, above which the transverse channel SCM wavevector develops a real part, and the spatial relaxation becomes oscillatory. For specific values of μ/T these transitions are shown by the turquoise diamonds in Figure 3.4. 55
Figure 3.7 (color figure) Spectrum of SCMs in the longitudinal channel for values of $\mu = 1.0$ (left panel) and $\mu = 1.5$ (right panel). As before purely imaginary-k poles are shown in orange, while poles with both imaginary and real parts are shown in blue. In the longitudinal channel there are two kinds of pole collisions, where these behaviors transition into one another, one indicated by turquoise diamonds, and the other by yellow diamonds. Green and yellow lines show the predictions on the basis of our hydrodynamic effective theory. 56
Figure 3.8 The critical exponent in the longitudinal channel for $\mu = 1.0$, as exhibited by the function $\alpha(v)$ defined in (3.88). As for the analogous transition in the transverse channel Figure 3.5, the value mean-field value $\alpha = 1/2$ is approached at the critical velocity, v_c. 56
Figure 3.9 Behaviour of the critical velocity for flows of a holographic plasma at finite charge density as a function of μ/T, above which the longitudinal channel SCM wavevector develops a real part and the spatial relaxation becomes oscillatory. For specific values of μ/T these transitions are shown by the turquoise diamonds in Figure 3.7. The dashed line indicates the hydrodynamic estimate for this collision point, $v_c^{\text{hydro.}}$ given in (3.91). 57
Figure 3.10 (color figure) First three modes of the spectrum of SCM of a neutral CFT_2 at temperature T, as deduced from the mode spectrum of the boosted BTZ solution. The positive branches correspond to k_+ modes, while the negative branches correspond to k_- modes. 60
Figure 3.11 Coordinates for the black Janus solution. The defect is located at the origin $p = 0$. We reach the asymptotic regions on either side by taking $p \to \infty$ with angular coordinate $\mu = \pm\mu_0$. In the asymptotic regions the scalar field approaches the limiting value $\phi(\pm\mu_0) = \pm 2 \log\left(\frac{1+\sqrt{m}}{\sqrt{1-m}}\right)$. . . . 62

Figure 3.12 (color figure) Analytic structure in the complex momentum plane for the black Janus solution. At finite temperature we have two sectors of SCM along the positive and negative imaginary axis (we summarize all poles, that is both those of $G^{[\searrow]}(k)$ and $G^{[\swarrow]}(k)$ in the same figure). In the $T \to 0$ limit these condense into a continuum in the form of two branch cuts along positive and negative imaginary axes. This continuum, for example, manifests itself as a power-law decay at large distances (3.122) or as a discontinuity in the spectral representation of the two point function. 65

Figure 3.13 A sketch of the domain used for the numerical construction of holographic non-equilibrium steady states. The spatial field theory direction is compactified using coordinate ρ as defined in (3.138). The '$\times$'s mark the points where boundary conditions are imposed to fix moduli of the solution. The gray filled region schematically indicates the presence of the obstacle, in the sense that far to the left or to the right the bulk is described by an equilibrium solution with spatial collective modes. 68

Figure 3.14 Convergence tests of the numerical method for non-Killing black branes describing NESS. We show the approach to the continuum limit of the ξ^a vector, whose maximum value on the numerical grid approaches zero as a power law with order (a) 4.4, (b) 4.2, (c) 4.2. 70

Figure 3.15 Flow profiles for solution (a): subsonic-to-subsonic non-equilibrium steady flow at incidence parameter $\theta = \pi/4$. In this case the fluid is rarefied, refracted and sped up by the obstacle. Note that $v_L^y = v_R^y$. The tails visible in these spatial profiles are the spatial collective modes. 71

Figure 3.16 Flow profiles for solution (b): subsonic-to-subsonic non-equilibrium steady flow at normal incidence. Here the fluid is rarefied and sped up by the obstacle. The tails visible in these spatial profiles are the spatial collective modes. 72

Figure 3.17 Flow profiles for solution (c): supersonic-to-supersonic non-equilibrium steady flow at normal incidence. Here the fluid is compressed and slowed through its encounter with the obstacle. The tails visible in these spatial profiles are the spatial collective modes. 73

Figure 3.18 Comparing the asymptotics of solution (a) to the spatial collective modes appropriate to each asymptotic equilibrium region. The points are given by derivatives of the spatial profiles of solution (a), according to the definition (3.142). The spatial collective modes are shown by the coloured solid lines. Note that a non-hydrodynamic mode is excited in the transverse channel on the downstream side. 74

Figure 3.19 Matching the downstream asymptotics of the subsonic flow solution (b) (left column) and the supersonic flow solution (c) (right column) to spatial collective modes. Upper panels show the leading pole structure in the complex-k plane as computed in [9] in the neutral case of relevance here, and in section 3.2.5 with finite charge density. Lower panels show the asymptotic behaviour of ε using log-linear axes. The black dots are the nonlinear solutions and the solid lines are the spatial collective modes. As v_R is increased through c_s the hydrodynamic spatial collective mode (red) transitions from downstream to upstream and the long-range behaviour downstream jumps to the longest non-hydrodynamic mode (blue). 75

Figure 4.1 Here we give the roadmap of our construction. In the spirit of effective field theory, we first identify the most general symmetry group applicable for our purposes. For the purpose of this chapter we focus on $\mathbb{R}_t \times \mathrm{ISO}(d) \times \mathrm{U}(1)$. Next we write down all possible kinematic structures compatible with that symmetry, which are then constrained by the fixing redefinition ambiguities present in the construction. Finally the remaining physical quantities are then subject to a dynamical principle, which in the case of hydrodynamics follows simply from conservation of the stress tensor and current. From the most general and therefore least constrained structure we also recover more highly symmetric previously known examples as limiting cases as shown in the leftmost box. 81

Figure 5.1 Sketch of a planar flow in a channel. We distinguish three cases: (a) general Couette flow with a pressure gradient, (b) Couette flow, (c) Poiseuille flow. 105

Figure 5.2 Real (a) and imaginary (b) part of the velocity profile solutions of the Couette flow with pressure gradient, for various values of R. $\tilde{v}_1$ is given by lines colored in shades of red, $\tilde{v}_2$ in green-yellow, and $\tilde{v}_3$ in blue. In all cases we've fixed $\tilde{U} = 2$, and $\tilde{G} = -10$. 107

Figure 5.3 Couette flow with pressure gradient, comparison of $\tilde{v}_1$ with the numerical solution, for various values of $R > 0$. The analytical and numerical solutions are in agreement for a wide range of values of R and $\tilde{G}$. In all cases we've fixed $\tilde{U} = 2$. In (a) we fixed $\tilde{G} = -10$, while in (b) we fixed $R = 1$. 107

Figure 5.4 Real and imaginary parts of the velocity profiles $\tilde{v}_1$ (a), $\tilde{v}_2$ (b), and $\tilde{v}_3$ (c). Real parts are given by full lines, imaginary by dashed ones. We can see that if $R\tilde{G}^2 < -128/9$ there is no solution which is real and satisfies the no-slip boundary conditions. 110

Figure 5.5 Real (a) and imaginary (b) part of the velocity profile solutions of the Poiseuille flow, for various values of R. $\tilde{v}_1$ is given by lines colored in shades of red, $\tilde{v}_2$ in green-yellow, and $\tilde{v}_3$ in blue. In all cases we've fixed $\tilde{G} = -10$. 110
Figure 5.6 Poiseuille flow comparison of $\tilde{v}_1$ with the numerical solution (blue dashed lines) and the Galilean-invariant solution (green dotted lines), for various values of $R > 0$, and $\tilde{v}_2$ for $R\tilde{G} < -128/9$. The analytical and numerical solutions are in agreement for a wide range of values of R and $\tilde{G}$. In (a) and (c) we fixed $\tilde{G} = -1$, while in (b) we fixed $R = 1$, and in (d) $R = -1$. 111
Figure 5.7 Real (a) and imaginary (b) part of the velocity profile solutions of the 3D Poiseuille flow, for various values of R. $\tilde{v}_{z,1}$ is given by lines colored in shades of red, $\tilde{v}_{z,2}$ in green-yellow, and $\tilde{v}_{z,3}$ in blue. In all cases we fixed $\tilde{G} = -10$. 112
Figure 5.8 3D plot of $\tilde{v}_{1,z}$ for $R = 10$ and $\tilde{G} = -10$. 112
Figure 5.9 Real and imaginary parts of the velocity profiles $\tilde{v}_1$ (a), $\tilde{v}_2$ (b), and $\tilde{v}_3$ (c) of the planar Couette flow. Real parts are given by full lines, imaginary by dashed ones. We can see that if $-2 \leq R\tilde{U}^2 < 0$ there are three real solutions, however none of them satisfy the boundary conditions, except for $\tilde{v}_3$ at $R\tilde{U}^2 = -1/2$. Note that for $R\tilde{U} \to -\infty$ we find a purely real solution that satisfies the boundary conditions (see (b)). 114
Figure 5.10 Real (a) and imaginary (b) part of the velocity profile solutions of the Couette flow, for various values of R. $\tilde{v}_1$ is given by lines colored in shades of red, $\tilde{v}_2$ in green-yellow, and $\tilde{v}_3$ in blue. In all cases we've fixed $\tilde{U} = 1$. 114
Figure 5.11 Couette flow comparison of $\tilde{v}_1$ with the numerical solution (blue dashed line) and the Galilean-invariant case (green dotted line), for various values of $R > 0$. The analytical and numerical solutions are in agreement for a wide range of values of R. The Galilean-invariant solution is in great agreement for very small values of R. In all cases we've fixed $\tilde{U} = 1$. 115
Figure 5.12 A sketch of the Taylor-Couette flow. 116
Figure 5.13 Comparison of the velocity profiles in our case vs. standard Galilean hydrodynamics. We can see that, unlike conventional hydrodynamics, the velocity profile depends on the value of η in our case. Here we used $\gamma_8 = \gamma_{13} = 1$, and for the boundary conditions $v_\phi(R_1 = 1) = 15$, and $v_\phi(R_2 = 5) = 20$. 116
Figure 5.14 Velocity profile of the Taylor-Couette flow for various values of the ratio R and T. In all cases we used $\epsilon = 1$, and for the boundary conditions $\tilde{v}(\tilde{R}_1 = 0) = 1$, and $\tilde{v}(\tilde{R}_2 = 1) = 10$. In (a) we fixed $T = 1$, and in (b) $R = 1$. 118

Figure 5.15 A comparison of the zeroth-order result (red line), corresponding to the eigenvalue of a mode that is unstable at zeroth-order $\lambda_0 = (0.0000130641 - i\,0.269367)$, and the first-order result obtained by increasing R and setting $\alpha_1 = 0$. . . 121

LIST OF TABLES

Table 2.1 An overview of all the different one-derivative terms of the hydrodynamic variables we can write down, with respect to the symmetries of a relativistic system. The terms in square brackets are the terms we eliminate using the equations of motion at zeroth order. Here d is the number of spatial dimensions. 25

Table 4.1 An overview of all the different one-derivative terms of the thermodynamic variables we can write down, with respect to the symmetries of the system. The parentheses around the indices denote a symmetric tensor, since $T^i_{\ j} = T^j_{\ i}$. The terms in square brackets are the terms we eliminate using the equations of motion at zeroth order. Here $\sigma_{ij} = \partial_i v^j + \partial_j v^i - \delta^i_{\ j} \frac{2}{d} \partial_k v^k$ is the shear tensor and d is the number of spatial dimensions. Note that we do not decompose the vectors into components transverse to the velocity, since we are also interested in situations where $v^i = 0$. 83

ACRONYMS

AdS Anti-de Sitter space

BTZ black hole solution for (2+1)-dimensional gravity with a negative cosmological constant, named after Maximo Bañados, Claudio Teitelboim, and Jorge Zanelli

CFT Conformal field theory

FG Fefferman-Graham coordinates

ISO(d) group of isometries of a Euclidean space of dimension d

ODE Ordinary differential equation

PDE Partial differential equation

QNM Quasinormal mode

SCM Spatial collective mode

SYM Supersymmetric Yang-Mills theory

RÉSUMÉ

Les phénomènes hydrodynamiques semblent omniprésents dans l'univers. Qu'il s'agisse de décrire la manière dont l'eau s'écoule dans un tuyau ou les disques d'accrétion ou le plasma quark-gluon, l'hydrodynamique fournit une description effective et à longue longueur d'onde des systèmes classiques et quantiques. Dans cette thèse, on utilise une perspective de l'holographie, ou plus précisément de la correspondance AdS/CFT.

Nous commençons par étudier les caractéristiques spatiales universelles de certains états stationnaires hors équilibre correspondant à des écoulements de fluides fortement corrélés sur des obstacles. Cela nous permet de prédire caractéristiques spatiales universelles des systèmes éloignés de l'équilibre. Nous identifions les modes collectifs spatiaux du système de nombreux corps fortement couplés. En holographie, ceux-ci peuvent être considérés comme des analogues spatiaux des modes quasi-normaux, qui sont responsables des aspects universels de la relaxation des systèmes dépendant du temps. Ces modes peuvent être d'origine hydrodynamique ou non-hydrodynamique. Nous trouvons des transitions intéressantes entre les régimes oscillatoires et amortis et considérons les exposants critiques associés à ceux-ci. Les longueurs de décroissance des modes hydrodynamiques sont fixées par η/s, le rapport de la viscosité de cisaillement sur la densité d'entropie, ce qui pourrait fournir une nouvelle avenue pour mesurer expérimentalement ce rapport. Nous fournirons également une explication de la méthode numérique, mais donnerons des exemples analytiques de ces modes. Des exemples analytiques peuvent être trouvés dans la limite de haute dimension de la théorie du *bulk*, mais également en trois dimensions.

Motivés par notre étude des modes collectifs spatiaux, nous avons voulu trouver un analogue non-relativiste. Pour ce faire, nous voulions mieux comprendre non seulement l'hydrodynamique non-relativiste, mais l'hydrodynamique en l'absence de symétrie de *boost*. Nous construisons donc la théorie hydrodynamique générale du premier ordre, invariante sous les translations temporelles, le groupe euclidien des transformations spatiales et préservant le nombre de particules, c'est-à-dire avec symétrie $\mathbb{R}_t \times \mathrm{ISO}(d) \times \mathrm{U}(1)$. Ces théories sont importantes dans un certain nombre de situations, de l'hydrodynamique du graphène au comportement de flocage des oiseaux et au mouvement d'organismes autopropulsés. À partir de cette construction générale, nous sommes capables de dériver des cas spéciaux avec une symétrie plus élevée en prenant la limite appropriée, telle que l'hydrodynamique relativiste (c'est-à-dire l'hydrodynamique invariante sous les *boosts* de Lorentz).

Enfin, nous allons essayer d'appliquer notre modèle d'hydrodynamique aux configurations d'écoulement. Nous le faisons afin d'avoir une meilleure compréhension des nouveaux coefficients de transport qui surviennent dans les relations constitutives de fluides sans symétries de *boost*. Notre motivation est également d'essayer d'étudier des configurations d'écoulement qui pourraient être un jour testées expérimentalement. Nous étudions les écoulements de Poiseuille, Couette

et Taylor-Couette, avec l'hypothèse supplémentaire que les écoulements sont incompressibles et trouvons des écarts intéressants par rapport à l'hydrodynamique galiléenne conventionnelle. Nous dérivons également un analogue de l'équation d'Orr-Sommerfeld et testons l'instabilité de l'écoulement de Poiseuille.

SUMMARY AND OUTLINE

Hydrodynamic phenomena seem to be ubiquitous in the universe. Whether it is describing how water flows in a pipe or the accretion discs or quark-gluon plasma, hydrodynamics provides an effective, long-wavelength description of both classical and quantum systems. In this thesis our point of view starts from that of holography, or more precisely, AdS/CFT correspondence.

We start by studying the universal spatial features of certain non-equilibrium steady states corresponding to flows of strongly correlated fluids over obstacles. This allows us to predict universal spatial features of far-from-equilibrium systems. We identify spatial collective modes of the strongly coupled many body system. In holography, these can be thought of as spatial analogues of quasinormal modes, which are responsible for universal aspects of relaxation of time-dependent systems. These modes can be both hydrodynamical or non-hydrodynamical in origin. We find interesting transitions between oscillatory and damped regimes and consider critical exponents associated with these. The decay lengths of the hydrodynamic modes is set by η/s, the ratio of shear viscosity over entropy density, which might provide a new avenue of experimentally measuring this ratio. We shall also provide an explanation of the numerical method, but give analytic examples of these modes. Analytic examples can be found in the large-dimension limit of the bulk theory, but in three dimensions as well.

Motivated by our study of spatial collective modes, we wanted to find a non-relativistic analogue. In order to do so we wanted to understand better not just non-relativistic hydrodynamics, but hydrodynamics in absence of any boost symmetry. We therefore construct the general first-order hydrodynamic theory invariant under time translations, the Euclidean group of spatial transformations and preserving particle number, that is with symmetry $\mathbb{R}_t \times \mathrm{ISO}(d) \times \mathrm{U}(1)$. Such theories are important in a number of situations, from hydrodynamics of graphene to flocking behaviour of birds and motion of self-propelled organisms. From this general construction, we are able to derive special cases with higher symmetry by taking the appropriate limit, such as relativistic hydrodynamics (i.e. hydrodynamics invariant under Lorentz boosts).

Finally, we shall try and apply our non-boost invariant model of hydrodynamics to concrete flow configurations. We do so in order to have a better understanding of the novel transport coefficients that arise in the constitutive relations of non-boost invariant fluids. Our motivation is also to try and study flow configurations that might be one day experimentally tested. We study the Poiseuille, Couette and Taylor-Couette flows, with the additional assumption that the flows are incompressible and find interesting deviations from conventional, Galilean-invariant hydrodynamics. We also derive an analogue of the Orr-Sommerfeld equation and test the instability of the Poiseuille flow.

OUTLINE OF THE THESIS

The outline of this thesis is as follows - we start with the introduction. In Chapter 1 we give a brief summary of holography as we shall employ it. First we introduce certain prerequisites - elements of conformal field theory and basic notions of AdS spacetimes. Then we shall review the AdS/CFT correspondence as it was first conjectured in [1], and describe the holographic dictionary and the GKPW formula [2, 3]. Next, in Chapter 2 we familiarize the Reader with hydrodynamics. We start with a conventional presentation of non-relativistic hydrodynamics, based on [4]. We then proceed to do a similar, but more modern presentation of relativistic hydrodynamics, based on [5]. In particular this more modern presentation, where we identify the relevant symmetries of the system and write down the terms that enter the derivative expansion, and thus, the constitutive relations, will be relevant for our research. We conclude this chapter by giving a brief description of a more modern and manifestly covariant formulation of non-relativistic hydrodynamics that employs Newton-Cartan geometry [6, 7].

We then go onto the "meat and bones" of this thesis. Chapter 3 is based on [8], which itself expands on the work presented in [9]. In this chapter we describe spatial collective modes (abbreviated as SCM), identify non-hydynamical ones and hydrodynamical ones, provide a description of the numerical method that we use and give analytic examples as well. In the appendices we provide additional details on the equations of state that we use (Appendix A) and on extracting the holographic stress tensor (Appendix B). We continue with Chapter 4, which is based on [10]. In this chapter we present a construction of the general first-order hydrodynamic theory without boost symmetries. Finally, we conclude with Chapter 5 in which we present novel results on applying the non-boost invariant hydrodynamics to specific flow configurations that are standard in conventional hydrodynamic literature. These results have not yet been published.

Part I

INTRODUCTION

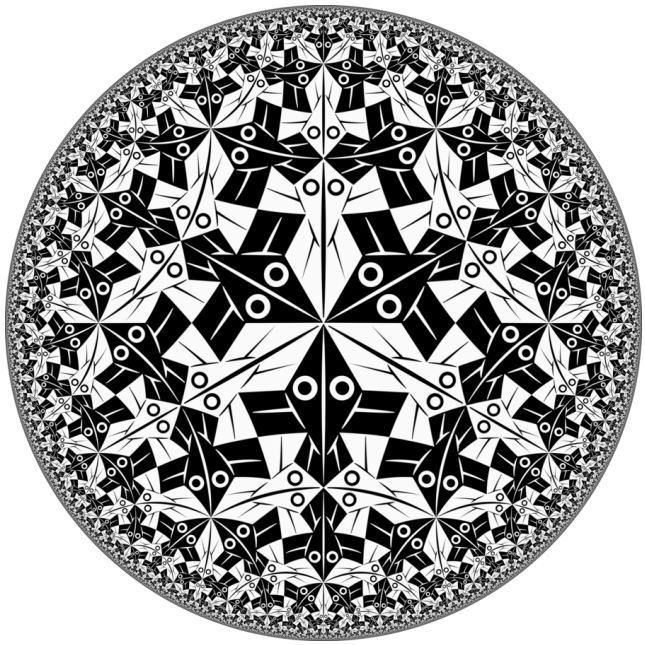

M. C. Escher, *Circle Limit I*

1

HOLOGRAPHY

The Reader hoping to find in this chapter a guide to creating holograms and wooing their friends will sadly be disappointed. However, we hope that the topic will prove to be equally, if not more, interesting. Holography, much like its namesake, deals with objects in higher dimensions being "recorded" on an object of lower spacetime dimension. In our case, there is a *duality* between a theory of gravity in $d+1$ dimensions and a strongly interacting quantum field theory in d spacetime dimension. Holography in this context is also known as *AdS/CFT correspondence*, or *gauge/gravity duality*. It is one of the major developments in theoretical physics in the last several decades, especially in our endeavours to understand quantum gravity, and is a field of active research to this day. The applications of this approach present an interesting interface of high-energy physics and condensed matter theory. We note however that holography is not just restricted to anti-de Sitter spacetimes or conformal field theories. In fact, the story of holography has its roots in black hole thermodynamics. Bekenstein [11, 12] and Hawking [13] showed that the entropy of a black hole is given by

$$S_{BH} = \frac{k_B c^3}{G_N \hbar} \frac{A}{4}, \tag{1.1}$$

where c is the speed of light, k_B the Boltzmann constant, $\hbar$ the Planck constant, G_N Newton's constant, and A the area of the black hole horizon. Already here one can see, in the relationship between the entropy and the area of a black hole horizon, a glimpse of holography. Gerard 't Hooft first formulated the *holographic principle* in [14], and Susskind further discussed it in [15]. It states that the information stored in a spatial volume V in d dimensions is encoded in its boundary area A in $d-1$ dimensions, measured in units of the Planck area ℓ_p^{d-1}. This is motivated by the Bekenstein bound, which applies to systems where there is at most one degree of freedom per Planck area.

In this chapter we aim to give a brief overview of what AdS/CFT correspondence is, since it is relevant for the contents of the research in this thesis, especially Chapter 3. We note that we will not go too much into the technical details. Over the years there has been a plethora of reviews and books on this topic [16–21].

1.1 ELEMENTS OF CONFORMAL SYMMETRY

Since they are half the name, CFTs are an important concept in understanding the AdS/CFT correspondence. We follow mostly the presentation of [19, 22]. A conformal field theory (CFT) consists of fields that transform covariantly under conformal coordinate transformations. Conformal transformations leave angles locally invariant. Let us consider flat d-dimensional spacetime with metric $g_{\mu\nu} =$

$\eta_{\mu\nu} = \text{diag}(-1, 1, \ldots, 1)$ and line element $ds^2 = g_{\mu\nu} dx^\mu dx^\nu$. We can define a differentiable map ϕ as a conformal transformation if

$$\phi : \quad g_{\mu\nu}(x) \to g'_{\mu\nu}(x') = \Lambda(x) g_{\mu\nu}(x). \tag{1.2}$$

Under a coordinate transformation the metric tensor transforms as

$$x \to x' \quad \Longrightarrow \quad g_{\rho\sigma} \to g'_{\mu\nu}(x') = \frac{\partial x'^\rho}{\partial x^\mu} \frac{\partial x'^\sigma}{\partial x^\nu} g_{\mu\nu}(x). \tag{1.3}$$

Therefore, conformal transformations of the flat metric obey

$$\eta_{\rho\sigma} \frac{\partial x'^\rho}{\partial x^\mu} \frac{\partial x'^\sigma}{\partial x^\nu} = \Lambda(x) \eta_{\mu\nu}, \tag{1.4}$$

where $\Lambda(x)$ is called the scale factor. If $\Lambda(x) = 1$, we find the Poincaré group, whereas if $\Lambda(x)$ is a constant, this corresponds to global scale transformations. If we now consider infinitesimal coordinate transformations to first order in $\epsilon(x) \ll 1$:

$$x'^\mu = x^\mu + \epsilon^\mu(x) + \mathcal{O}(\epsilon^2), \tag{1.5}$$

we find the conformal Killing equation

$$\partial_\mu \epsilon_\nu + \partial_\nu \epsilon_\mu = 2\sigma(x) \eta_{\mu\nu}, \qquad \sigma(x) = \frac{1}{d} \partial \cdot \epsilon. \tag{1.6}$$

We also find that the scale factor for this infinitesimal coordinate transformation is

$$\Lambda(x) = 1 + \frac{2}{d} \partial \cdot \epsilon + \mathcal{O}(\epsilon^2). \tag{1.7}$$

In $d = 2$ dimensions, this reduces to the Cauchy-Riemann equations, which are solved by any holomorphic function. This implies that in $d = 2$, conformal symmetry is infinite dimensional and thus leads to an infinite number of conserved quantities. In $d > 2$, however, conformal symmetry is finite dimensional. The conformal Killing vector $\epsilon_\mu(x)$ is at most quadratic in x. This can be seen from the conformal Killing equation (1.6), from which we can derive

$$(d-1) \Box (\partial \cdot \epsilon) = 0. \tag{1.8}$$

The solutions to the conformal Killing equation can be written as

$$\epsilon^\mu(x) = a^\mu + \omega^\mu{}_\nu x^\nu + \lambda x^\mu + b^\mu x^2 - 2(b \cdot x) x^\mu, \tag{1.9}$$

$$\omega_{\mu\nu} = -\omega_{\nu\mu}, \tag{1.10}$$

$$\sigma(x) = \lambda - 2b \cdot x. \tag{1.11}$$

It contains translations (of zeroth order in x^μ), rotations (linear in x^μ) and scale transformations (quadratic in x^μ). The constant vector a_μ corresponds to an infinitesimal translation, and the corresponding generator is the momentum operator $P_\mu = -i\partial_\mu$. The antisymmetric term $\omega_{\mu\nu}$ corresponds to infinitesimal Lorentz transformations $x'^\mu = (\delta^\mu{}_\nu + \omega^\mu{}_\nu) x^\nu$, and the generator of these transformations is given by $L_{\mu\nu} = i(x_\mu \partial_\nu - x_\nu \partial_\mu)$. The scalar term λ corresponds to infinitesimal scale transformations $x'^\mu = (1 + \lambda) x^\mu$, and its corresponding generator is

$D = -ix^\mu\partial_\mu$. Finally, the quadratic term corresponds to infinitesimal special conformal transformations, whose infinitesimal form is

$$x'^\mu = x^\mu + 2(x\cdot b)x^\mu - (x^2)b^\mu. \tag{1.12}$$

The corresponding generator is $K_\mu = -i(2x_\mu x^\nu\partial_\nu - (x^2)\partial_\mu)$. The finite transformation associated with this generator is

$$x'^\mu = \frac{x^\mu - (x\cdot x)b^\mu}{1-2(b\cdot x)+(b\cdot b)(x\cdot x)}. \tag{1.13}$$

There are a total of

$$\begin{aligned}1 \text{ dilatation } + d \text{ translations } + d \text{ special conformal } + \frac{d(d+1)}{2} \text{ rotations}\\ = \frac{(d+1)(d+2)}{2} \text{ generators.}\end{aligned}$$

We can see that the associated conformal algebra consists of the Poincaré algebra supplemented by a few other relations that involve commutators with D and K_μ

$$[D,\, P_\mu] = iP_\mu \tag{1.14}$$
$$[D,\, K_\mu] = -iK_\mu \tag{1.15}$$
$$[D,\, L_{\mu\nu}] = 0 \tag{1.16}$$
$$[K_\mu,\, K_\nu] = 0 \tag{1.17}$$
$$[K_\mu,\, P_\nu] = 2i(\eta_{\mu\nu}D - L_{\mu\nu}) \tag{1.18}$$
$$[K_\rho,\, L_{\mu\nu}] = i(\eta_{\rho\mu}K_\nu - \eta_{\rho\nu}K_\mu) \tag{1.19}$$
$$[P_\rho,\, L_{\mu\nu}] = i(\eta_{\rho\mu}P_\nu - \eta_{\rho\nu}P_\mu) \tag{1.20}$$
$$[L_{\mu\nu},\, L_{\rho\sigma}] = i(\eta_{\nu\rho}L_{\mu\sigma} + \eta_{\mu\sigma}L_{\nu\rho} - \eta_{\mu\rho}L_{\nu\sigma} - \eta_{\nu\sigma}L_{\mu\rho}) \tag{1.21}$$

In Euclidean signature, the symmetry group generated by these transformations is $SO(1,d+1)$, while in Lorentzian signature it is $SO(2,d)$. Oftentimes it is referred to as *the conformal group*.

For the representations we postulate

$$[D,\, \phi(0)] = -i\Delta\phi(0) \tag{1.22}$$

for any field $\phi(x)$. This implies

$$\phi(x) \to \phi'(x') = \lambda^{-\Delta}\phi(x) \tag{1.23}$$

for $x \to x' = \lambda x$. Δ is the scaling dimension of the field ϕ. For an infinitesimal transformation this gives

$$\delta_D\phi \equiv [D,\, \phi(x)] = -i\Delta\phi(x) - ix^\mu\partial_\mu\phi(x), \tag{1.24}$$

with similar relation for the other conformal transformations $\delta_P\phi$, $\delta_L\phi$, $\delta_K\phi$.

For organising the representations, it is useful to define the *quasiprimary* fields which satisfy

$$[K_\mu, \phi(0)] = 0. \tag{1.25}$$

This defines the fields of lowest scaling dimension in an irreducible representation of the conformal algebra. All other fields in this multiplet, the conformal *descendents* of ϕ, are obtained by acting with P_μ on the quasiprimary fields.

Often, we are interested in calculating n-point correlation functions of fields. As it turns out, conformal invariance imposes certain constraints on the form of the correlation function. For example, let's consider the 2-point function

$$\langle \phi_1(x_1)\phi_2(x_2)\rangle = \frac{1}{Z}\int \mathcal{D}\Phi_i \phi_1(x_1)\phi_2(x_2)e^{-S[\Phi_i]}, \tag{1.26}$$

where Φ_i denotes the set of all fields in the theory, S is the conformally invariant action, and ϕ_1, ϕ_2 are quasiprimary fields. Assuming the action and the integration measure are conformally invariant, this correlation function transforms as

$$\langle \phi_1(x_1)\phi_2(x_2)\rangle = \left|\frac{\partial x'}{\partial x}\right|^{\Delta_1/d}_{x=x_1}\left|\frac{\partial x'}{\partial x}\right|^{\Delta_2/d}_{x=x_2}\langle \phi_1(x_1')\phi_2(x_2')\rangle. \tag{1.27}$$

Conformal symmetry constrains the form of the 2-point function to be

$$\langle \phi_1(x_1)\phi_2(x_2)\rangle = \begin{cases} \frac{c}{(x_1-x_2)^{2\Delta}}, & \text{if} \quad \Delta_1=\Delta_2=\Delta, \\ 0, & \text{otherwise.}\end{cases} \tag{1.28}$$

Similarily, invariance under rotations, translations, dilatations and special conformal transformations force the 3-point function to be of the form

$$\langle \phi_1(x_1)\phi_2(x_2)\phi_3(x_3)\rangle = \frac{\lambda_{123}}{x_{12}^{\Delta_1+\Delta_2-\Delta_3}x_{23}^{\Delta_2+\Delta_3-\Delta_1}x_{13}^{\Delta_3+\Delta_1-\Delta_2}}, \tag{1.29}$$

where $x_{ij}\equiv|x_i-x_j|$, and λ_{123} are non-trivial parameters (*structure constants*). The 4-point function is not fixed by conformal symmetry because we can construct two independent conformal invariant cross-ratios

$$u \equiv \left(\frac{x_{12}x_{34}}{x_{13}x_{24}}\right)^2, \quad \text{and} \quad v\equiv\left(\frac{x_{14}x_{23}}{x_{13}x_{24}}\right)^2. \tag{1.30}$$

The general form of the 4-point function is given by

$$\langle \phi_1(x_1)\phi_2(x_2)\phi_3(x_3)\phi_4(x_4)\rangle = \frac{\mathcal{A}(u,v)}{(x_{13}^2x_{24}^2)^\Delta}. \tag{1.31}$$

For fields with spin, the conformal transformation acts also on the spacetime indices and reads

$$\delta_\epsilon \mathcal{O}(x) = -\mathcal{L}_\epsilon \mathcal{O}(x), \quad \mathcal{L}_\epsilon \equiv \epsilon\cdot\partial_x + \frac{\Delta}{d}\partial\cdot\epsilon - \frac{i}{2}\partial^{[\mu}\epsilon^{\nu]}L_{\mu\nu}, \tag{1.32}$$

for an operator $\mathcal{O}(x)$ of arbitrary spin. For these operators, the conformal correlation functions are more involved. However, conformal symmetry still fixes the two- and three-point functions up to a small number of independent contributions [19].

1.2 ANTI-DE SITTER SPACES

Anti-de Sitter spaces are the other half of the name, so it might be a good idea to say a few words about them as well. Named after Willem de Sitter (1872-1934), (anti-)de Sitter spaces are the simplest solutions of the Einstein equations with a non-vanishing cosmological constant $\Lambda \neq 0$. They are maximally symmetric Lorentzian manifolds with constant curvature, in particular anti-de Sitter spaces have *negative* constant curvature (whereas de Sitter spaces have positive curvature). Thus they are the curved counterparts of the flat $\Lambda = 0$ Minkowski spacetime. In order to study them in more detail, let us start by embedding a $(d+1)$-dimensional AdS space into $(d+2)$-dimensional flat Minkowski spacetime

$$ds^2 = -dX_0^2 - dX_{d+1}^2 + \sum dX_i^2. \tag{1.33}$$

Anti-de Sitter space in $d+1$ dimensions is then defined as the hypersurface satisfying

$$X_0^2 + X_{d+1}^2 - \sum X_i^2 = L^2, \tag{1.34}$$

where L is referred to as the *AdS radius*. This embedding equation can be solved in terms of $d+1$ independent coordinates in several different ways. The group $SO(2,d)$ is the group of isometries of AdS_{d+1}. As we have seen before, this is also the symmetry group of a d-dimensional CFT.

The first set of coordinates that we mention, that can solve this equation, are referred to as *global coordinates*. We can solve the embedding constraint by choosing the coordinates

$$X^0 = L\cosh\rho\cos\tau, \tag{1.35}$$

$$X^{d+1} = L\cosh\rho\sin\tau, \tag{1.36}$$

$$X^i = L\Omega_i\sinh\rho, \qquad i = 1,\dots,d \tag{1.37}$$

where Ω_i are the angular coordinates that satisfy $\sum_i \Omega_i^2 = 1$, i.e. parametrize a $d-1$ sphere. The induced metric on the hyperboloid then is of the form

$$ds^2 = L^2\left(-\cosh\rho^2 d\tau^2 + d\rho^2 + \sinh\rho^2 d\Omega_{d-1}^2\right), \tag{1.38}$$

with $0 \leq \rho < \infty$ and $-\infty < \tau < \infty$. One could also choose τ to be an angular variable with period 2π, $\tau \in [0, 2\pi]$. However, in that case we would find closed timelike curves, which would present problems for causality in this space. That is why we "unwrap" or decompactify the τ coordinate in the global coordinates, i.e. we take $-\infty < \tau < \infty$, with no identifications. This is known as the *universal cover* of AdS space.

We can also solve the embedding equation by choosing

$$X_0 = \frac{1}{2r}\left[1 + r^2(L^2 + x_i^2 - t^2)\right] \tag{1.39}$$

$$X_d = \frac{1}{2r}\left[1 - r^2(L^2 - x_i^2 - t^2)\right] \tag{1.40}$$

$$X_i = Lrx_i \tag{1.41}$$

$$X_{d+1} = Lrt \tag{1.42}$$

Now the induced metric on the hyperboloid becomes

$$\begin{aligned} ds^2 &= L^2 \left[\frac{dr^2}{r^2} + r^2 \left(-dt^2 + dx_i^2 \right) \right] \\ &= L^2 \left[\frac{dr^2}{r^2} + r^2 \eta_{\alpha\beta} dx^\alpha dx^\beta \right] \\ &= \frac{L^2}{z^2} \left[dz^2 + \eta_{\alpha\beta} dx^\alpha dx^\beta \right] \qquad \left(r = \frac{L^2}{z} \right) \end{aligned} \tag{1.43}$$

These are known as the *Poincaré coordinates*. They cover only half of the AdS hyperboloid (often called the *Poincaré patch*), since $r > 0$, but it is often very useful to consider, as it corresponds to studying the boundary field theory simply on flat Minkowski space. The boundary in these coordinates is located at $r \to \infty$ (or alternatively $z \to 0$). Using the z coordinate, we may note that there is a coordinate singularity at the boundary but the space remains regular since the curvature remains finite. The Ricci scalar and the cosmological constant, as previously noted, for AdS space are both negative

$$R = -\frac{d(d+1)}{L^2}, \qquad \Lambda = -\frac{d(d-1)}{2L^2}. \tag{1.44}$$

1.3 ADS/CFT CORRESPONDENCE

AdS/CFT correspondence was first conjectured by Juan Maldacena in his seminal paper in 1997 [1]. This conjecture states that a four-dimensional CFT, $\mathcal{N} = 4$ super Yang-Mills (SYM) theory with gauge group $SU(N)$ is dynamically equivalent to type IIB superstring theory on $AdS_5 \times S^5$. We can match their symmetries, spectra and correlation functions. Although the conjecture has not been proven to this day, there have been many tests that have convinced researchers of its general validity, and since then there have been other dual pairs proposed and explored.

Let us describe the gist of the argument. We consider a large number N of Dp branes stacked on top of each other. Dp branes are objects in string theory with p spatial dimensions. A D0 brane describes a point particle, a D1 brane describes an extended string, a D2 brane describes a membrane, etc. Thus a Dp brane describes a physical object, a system that can have low energy excitations, and these low energy excitations can be described in two limits. In Maldacena's case, we look at D3 branes within type IIB string theory. D3 branes are dynamical objects, characterized by the string tension

$$T_3 \sim \frac{1}{\ell_s^4} \frac{1}{g_s}, \tag{1.45}$$

where ℓ_s is the string length, defined as $\ell_s = \sqrt{\alpha'}$, and g_s is the string coupling constant.

At weak 't Hooft coupling

$$\lambda \equiv 4\pi g_s N \ll 1, \tag{1.46}$$

the gravitational effects of D3 branes are negligible. The branes live on flat 10-dimensional space, and we have open strings ending on the D-branes, and closed strings propagating freely in the bulk. In the opposite regime, at strong coupling

$$\lambda \equiv 4\pi g_s N \gg 1, \tag{1.47}$$

D3 branes gravitate very strongly, curve the spacetime substantially and collapse to form extremal black 3-branes, with geometry [1, 16]

$$ds^2 = f(r)^{-1/2}\eta_{\mu\nu}dx^\mu dx^\nu + f(r)^{1/2}(dr^2 + r^2 d\Omega_5^2), \qquad f(r) = 1 + \frac{L^4}{r^4}, \tag{1.48}$$

where $L^4 \equiv 4\pi g_s N \ell_s^4$ is a parameter with dimension of length, the coordinates $x^\mu = (t, \mathbf{x})$ are along the D3 brane worldvolume, and $d\Omega_5^2$ is the metric of a unit 5-sphere. The radial coordinate r is the radius of the remaining, transverse directions (with respect to the worldvolume) which contain the 5-sphere as well.

Apparently there seems to be no overlap between these two regimes, however if we decouple the brane theory from gravity, things change. This we can do by looking at the low energy limit. The low energy degrees of freedom in the first case are strings stretching between pairs of D3 branes. The lightest string states are massless, and there are N^2 of them, since they can begin and end on any of the N D3 branes. At the lowest energy scales, these N^2 massless strings are described by $\mathcal{N} = 4$ super Yang-Mills theory. This field theory has a Lagrangian that can be schematically written as

$$\mathcal{L} \sim \frac{1}{g_{YM}^2}\mathrm{tr}\left(F^2 + (\nabla\Phi)^2 + i\bar{\Psi}\not{D}\Psi + i\bar{\Psi}[\Phi,\Psi] - [\Phi,\Phi]^2\right). \tag{1.49}$$

where F is a $SU(N)$ field strength coupled to bosonic fields Φ and fermionic fields Ψ, all in the adjoint representation. All of these fields are $N \times N$ matrices. The coupling can be rewritten in terms of N and λ, $1/g_{YM}^2 = N/\lambda$, and λ is the 't Hooft coupling.

In the other limit, the low energy excitations are those occur in the region near the horizon of the black brane, the so-called near-horizon geometry, $r \ll L$. In this limit, the near horizon geometry is $AdS_5 \times S^5$, with metric

$$ds^2 = \frac{r^2}{L^2}\eta_{\mu\nu}dx^\mu dx^\nu + L^2\frac{dr^2}{r^2} + L^2 d\Omega_5^2 \tag{1.50}$$

The AdS radius L can be related to two fundamental scales in string theory, the string length ℓ_s, and the Planck length ℓ_P via

$$L = \lambda^{1/4}\ell_s = (4\pi N)^{1/4}\ell_p. \tag{1.51}$$

An excitation with energy E measured by an observer at infinity has energy E_p at a point p, located at radial coordinate position r_p, given by $E = E_p\sqrt{-g_{tt}}$, so we find

$$E = f^{-1/4}E_p \sim \frac{r}{L}E_p. \tag{1.52}$$

A finite energy excitation $E_p \neq 0$ will be seen to have lower and lower energy at the boundary as the point p is brought closer and closer to the horizon at

$r = 0$. In the low-energy limit we find two kinds of excitations: massless type IIB supergravity excitations in the asymptotically flat region near infinity, and any kind of excitations in the near-horizon region, which due to the redshift effect also appears massless to a boundary observer. These two types are decoupled from one another.

To summarize, the low energy limit gives two points of view on the D3 brane system. When $g_s N \gg 1$ it is described by a 10-dimensional string theory with just closed strings in $AdS_5 \times S^5$, and when $g_s N \ll 1$ it is described by a 4-dimensional $\mathcal{N} = 4$ SYM $SU(N)$ gauge theory. The gauge theory is, however, well-defined at any coupling, so we can conjecture that this description applies even when $g_s N$ is large, that is in the same regime where we have the closed string description. Maldacena's conjecture boils down then to that type IIB string theory on $AdS_5 \times S^5$ is precisely the strong coupling description of large N $\mathcal{N} = 4$ super Yang-Mills theory. Both sides describe the same physics. We should also note that when we talk about string theory on $AdS_5 \times S^5$, we mean string theory on spacetime that is asymptotically $AdS_5 \times S^5$, as we can still have all kinds of processes in the interior, e.g. gravitons, D-branes, black holes, etc.

There have been other proposed dual pairs of classical gravitational theories and quantum field theories, for example the duality between the 2+1 dimensional ABJM theory, a Chern-Simons theory, and M-theory on $AdS_4 \times S^7/\mathbb{Z}_k$.

1.3.1 *GKPW formula and the holographic dictionary*

Usually in quantum field theory we are interested in calculating the generating functional, n-point functions, of operators in the theory

$$Z_{QFT} \equiv \left\langle \exp\left(\int d^d x \phi_0(x) \mathcal{O}(x) + \dots \right) \right\rangle_{\text{QFT}}. \tag{1.53}$$

In Euclidean signature, the AdS/CFT conjecture is summarized by the so-called GKPW formula (named after Gubser, Klebanov, Polyakov [2] and Witten [3] who first proposed it), a proposed relation between the gravity partition function in AdS_{d+1} and the generating functional for the connected field theory correlation functions :

$$\boxed{Z_{\text{string}}\left[\Phi(x,r)|_{r\to\infty} = \phi_0(x)\right] = \left\langle \exp\left(\int d^4 x \phi_0(x) \mathcal{O}(x) \right) \right\rangle_{\text{CFT}}} \tag{1.54}$$

This relation states that the string or (super)gravity partition function where the bulk fields approach specific functions at the boundary, is equal to the CFT path integral where we insert a source ϕ_0 for an operator $\mathcal{O}$. ϕ_0 is an arbitrary function that specifies the boundary value of the bulk field Φ. In other words, a generic bulk field Φ, sources a dual operator on the CFT side, and there is a one-to-one correspondence between each field propagating in AdS space and an operator in the field theory. In this way we build a kind of *holographic dictionary*. In order to make things solvable, we take another limit - the limit of classical gravity in which all graviton loops are suppressed, $L \gg \ell_P$. Hence,

$L^4/\ell_P^4 \sim (g_s\alpha'^2 N)/(g_s\alpha'^2) = N \ll 1$. The GKPW formula (1.54) then implies that classical gravity in AdS spacetime gives us access to the strongly coupled QFT with a large number of colours, $N_c \ll 1$,

$$\lim_{\lambda,N\to\infty} Z_{\text{string}}\left[\phi(x,r)|_{r\to\infty} = \phi_0(x)\right] = \exp\left(-S_{\text{grav}}\left[\phi_0\right]\right). \tag{1.55}$$

A natural question arises - how do we know which bulk field matches to which field theory operator? In general this is a subtle question, but we can give some simpler examples that are determined by symmetry. The simplest example is that of a scalar field in the bulk $\phi(x,z)$ that sources a scalar operator $\mathcal{O}(x)$ in the boundary field theory. Fermionic fields in the bulk map into fermionic operators in the boundary. The most important bulk field is the metric g_{AB} and the corresponding QFT operator is the energy-momentum tensor $T^{\mu\nu}$. Thus, the boundary value of the bulk metric (or, more precisely, the induced metric on the boundary) acts as a source for the energy-momentum tensor in the dual field theory. Moreover, diffeomorphism invariance in the bulk will ensure conservation of the energy and momentum currents $\partial_\mu T^{\mu\nu}$. Likewise, vector fields will map into vector operators, and the most important of those are gauge fields in the bulk A_A^a, which correspond to currents J_a^μ in the dual field theory. Again, gauge symmetry in the bulk will imply conservation of the boundary current $\partial_\mu J^\mu$.

Taking functional derivatives of the gravity partition function with respect to its boundary values, we can calculate Euclidean n-point functions

$$\langle \mathcal{O}(x_1)\dots\mathcal{O}(x_n)\rangle = \left.\frac{\delta^n S^E_{\text{on-shell}}}{\delta\phi_{(0)}(x_1)\dots\delta\phi_{(0)}(x_n)}\right|_{\phi_{(0)}=0}. \tag{1.56}$$

An essential aspect of AdS/CFT is the IR/UV correspondence [23, 24]. The extra radial dimension r is related to the energy scale of the field theory. It is often said that the radial dimension geometrizes the renormalization group - processes close to the boundary correspond to high energy physics in the dual QFT, while dynamics deep in the bulk describes low-energy physics in the dual QFT. Therefore, the near-boundary and the deep bulk regions correspond to the UV and IR regimes of the dual field theory, respectively. This statement can be motivated from various points of view. The divergence of the metric tensor near AdS infinity corresponds to the UV divergence of the field theory, whereas the IR is controlled by the black hole thermodynamics. If we slice the bulk along the radial direction and integrate the slices out by starting from the boundary, we can show that this corresponds to the Wilsonian integration of high-momentum modes in the boundary field theory.

2

HYDRODYNAMICS

Examples of hydrodynamic phenomena are everywhere around us, from the mundane, everyday experiences, such as a river flowing or water flowing in a pipe, even bird flocking, to the more distant and exotic, such as gravitational fluctuations of black holes, accretion discs around stars or quark-gluon plasma - the scope of hydrodynamics is far and wide. It is also a very old topic of research - already in the 3rd century B.C. Archimedes stated his principle, and over 260 years ago Euler discovered the fundamental equations governing the flow of an ideal fluid, yet this topic is still far from complete and to this day provides new applications and avenues of research.

Hydrodynamics (or, in this context, fluid dynamics) studies the motion of fluids and the phenomena that it deals with are macroscopic phenomena. Thus, in hydrodynamics one considers a fluid to be continuous. In addition to that, we are not restricted to merely classical systems, but we can apply hydrodynamics to quantum many-body systems as well. Naturally, we know today that all matter is built out of more elementary units. Depending on the resolution we are talking about, we are interested in elementary particles, or atoms, or molecules, etc. However, in hydrodynamics we do "coarse-graining" in the sense that any small volume of the fluid of interest is made out of a great number of elementary units (e.g. atoms, molecules, birds, etc.). What "coarse-graining" means then, is that we average physical quantities, such as particle and energy density or velocity, over volumes or distances much greater than the spacing between elementary units. In this sense "coarse-graining" is much like zooming out of a part of a grainy, pixelated picture and seeing that it forms a sensible whole. At great distances even discrete systems appear continuous. Therefore, hydrodynamics is an effective long-distance description of a system.

Symmetries will play an important role in the following chapters. Following Noether's theorem, if there are continuous symmetries in the system, there are corresponding conserved quantities (conserved currents). The fundamental equations of hydrodynamics express conservation laws.

2.1 NON-RELATIVISTIC HYDRODYNAMICS

Let's start with non-relativistic hydrodynamics, i.e. hydrodynamics that is invariant under Galilei transformations. This is a well-known subject with many references and textbooks [4, 25–29]. In what follows we give a brief overview of the fundamental equations and concepts that describe a non-relativisitic fluid. In our considerations, we restrict ourselves to one-component fluids (i.e. one species of particles), that are parity-invariant. We will try to give a more conventional presentation of the topic, basing most of the section on [4]. There is a more modern interpretation of non-relativistic hydrodynamics, especially from the point of view

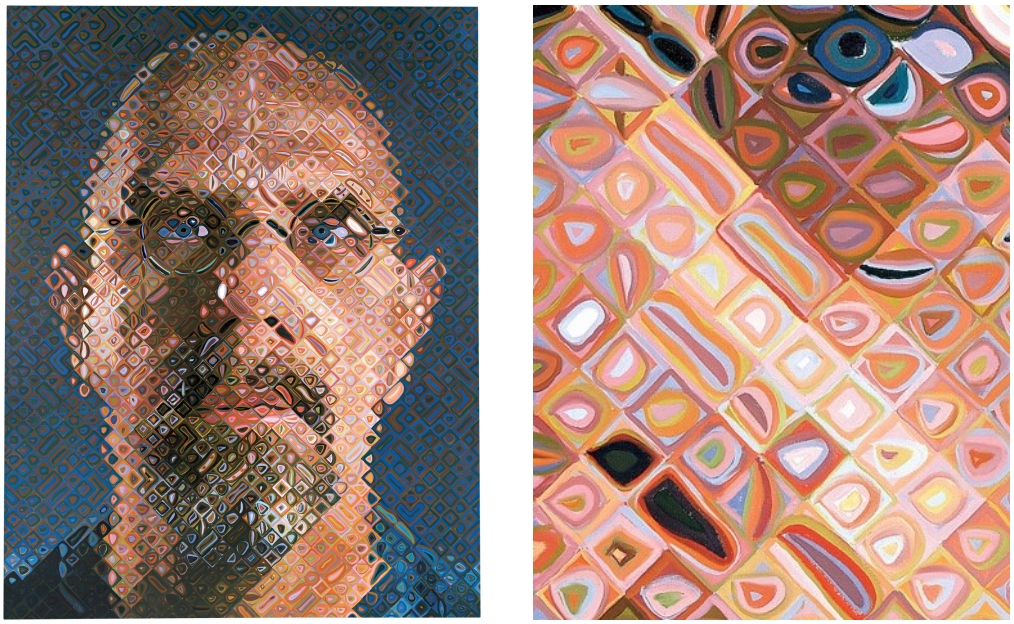

Figure 2.1: Chuck Close, *Self-Portrait* (2000-2001), oil on canvas. This large painting is divided into numerous elements, each, when viewed close-up (no pun intended), has it's own distinct features, colors, even patterns. However, when viewed from afar ("coarse-graining" in a sense) they constitute a different whole, an almost continuous, realistic portrait.

of gravity and field theories on a curved background, which we will briefly revisit in one of the following sections.

In non-relativistic hydrodynamics we have conservation of particle number (or mass) and conservation of momentum. Let's derive these equations.

2.1.1 *Ideal fluids*

We start with the conservation of mass. The total mass contained in some volume V of the fluid is given by $\int_V \rho(t,x)d^dx$, where ρ is the local fluid density (i.e. mass per unit volume). Now, the flow of mass out of this volume in unit time is given by

$$\int_{\partial V} \rho(t,x)\mathbf{v}\cdot d\mathbf{S}, \tag{2.1}$$

where $\mathbf{v}(t,x)$ is the local fluid velocity and $d\mathbf{S}$ is an infinitesimal area element on the boundary surface of the volume V. By convention one thinks of it as a vector pointing along the outward normal. The integral is taken over the entire closed surface that surrounds V. At the same time, this outflow of mass results in the decrease of the total mass that is contained in V

$$-\frac{\partial}{\partial t}\int_V \rho(t,x)d^dx. \tag{2.2}$$

Since mass is conserved in non-relativistic hydrodynamics, we have

$$\frac{\partial}{\partial t}\int_V \rho(t,x)d^dx = -\int_{\partial V} \rho(t,x)\mathbf{v}\cdot d\mathbf{S}. \tag{2.3}$$

Applying Gauss' theorem, we transform the surface integral to a volume integral

$$\int_{\partial V} \rho(t,x)\mathbf{v}\cdot d\mathbf{S} = \int_V \partial_i\left(\rho v_i\right) d^d x, \tag{2.4}$$

which gives us

$$\int_V \left[\partial_t\rho + \partial_i\left(\rho v_i\right)\right] d^d x = 0. \tag{2.5}$$

However, since this must be true for any volume, we must have

$$\boxed{\partial_t\rho + \partial_i(\rho v_i) = 0.} \tag{2.6}$$

Thus, conservation of particle number or mass is given by the well-known *continuity equation*. Using similar arguments we can derive the equation that describes conservation of momentum. Again, we consider some volume of the fluid and look at how momentum changes when it is under the influence of a force. The total force acting on V is given by

$$-\int_{\partial V} p\, d\mathbf{S} \tag{2.7}$$

taken over the boundary surface of the volume. We can transform it in a volume integral, and find

$$-\int_{\partial V} p\, d\mathbf{S} = -\int_V \partial_i p\, d^d x. \tag{2.8}$$

We can recognize $-\partial_i p$ as the force density acting on the fluid. Using Newton's second law, we can write the equation of motion for a fluid element

$$\rho\frac{dv_i}{dt} = -\partial_i p. \tag{2.9}$$

The $\frac{d\mathbf{v}}{dt}$ that appears here is not the rate of change of the fluid velocity at a fixed point in space but the rate of change of the velocity of a given fluid particle as it moves about in space. This is called the *material derivative*, and it is given by

$$\frac{dv_i}{dt} = \partial_t v_i + v_k\partial_k v_i. \tag{2.10}$$

Making use of this fact, we find

$$\partial_t v_i + v_k\partial_k v_i = -\frac{1}{\rho}\partial_i p. \tag{2.11}$$

This is known as *Euler's equation*, named after Leonhard Euler (1707-1783) who first obtained it in 1755. It represents the equation of motion of an ideal fluid. We can also take into account external forces acting on the fluid element (e.g. gravity or, in the case of a charged fluid, external electromagnetic forces). In that case Euler's equation becomes

$$\partial_t v_i + v_k\partial_k v_i = -\frac{1}{\rho}\partial_i p + \frac{1}{\rho}f_i, \tag{2.12}$$

where f_i is the external force density (i.e. force per unit volume). We can rewrite Euler's equation in the form of a conservation equation. With the help of the equation of continuity, we write the temporal derivative of the momentum density ρv_i as

$$\partial_t(\rho v_i) = \rho\partial_t v_i + v_i\partial_t\rho = -\rho\left(v_j\partial_j\right)v_i - \partial_i p - v_i\partial_j\left(\rho v_j\right) = -\partial_j\left(\delta_{ij}p + \rho v_i v_j\right), \tag{2.13}$$

where δ_{ij} is the Kronecker delta. Putting the pieces together, we find the momentum conservation law

$$\boxed{\partial_t\left(\rho v_i\right) = -\partial_j\Pi_{ij}, \quad \Pi_{ij} = p\delta_{ij} + \rho v_i v_j.} \tag{2.14}$$

Π_{ij} is a symmetrical, rank 2 tensor called the *momentum flux density tensor*.

We now have $d+2$ unknown functions ρ, p and $\mathbf{v}$ (d components for d spatial dimensions), but $d+1$ equations. This would imply we are missing an equation. The missing piece is the equilibrium equation of state which provides a relation between p and ρ. However, this depends on the nature of the fluid and often introduces another parameter in the picture, such as entropy. The missing equation can be taken to be entropy conservation

$$\boxed{\partial_t s + \partial_i\left(s v_i\right) = 0,} \tag{2.15}$$

where s is the entropy density (entropy per unit volume).

Finally, let's look at how energy of a fluid element varies with time. A fluid element has energy

$$\frac{\rho v^2}{2} + \epsilon, \tag{2.16}$$

where the first term is the kinetic energy density, and the second one is the internal energy density. With the help of thermodynamic relations

$$dw = Tds + dp, \quad w \text{ is enthalpy per unit volume:} \quad w = \epsilon + p, \tag{2.17}$$

$$d\epsilon = Tds - pdV, \tag{2.18}$$

and conservation of entropy (2.15), we can write down the law of conservation of energy as

$$\boxed{\partial_t\left(\frac{\rho v^2}{2} + \epsilon\right) + \partial_i\left[\left(\frac{\rho v^2}{2} + w\right)v_i\right] = 0.} \tag{2.19}$$

The above equations, along with the equation of state which relates p, ϵ and ρ, are all the necessary equations to describe an ideal non-relativistic fluid. If we have a non-homogeneous fluid, e.g. a mixture of different fluids, this set of equations needs to be expanded to reflect that each of these fluids has a conserved particle number [4]:

$$\partial_t n_K + \partial_i\left(n_K v_i\right) = 0, \tag{2.20}$$

where K denotes the species of the particles in question.

2.1.2 *Incompressible, irrotational and steady flows*

One situation in which the equations of hydrodynamics are simplified are *steady flows*. Steady flows are flows in which the velocity of the fluid is independent of time, at any point in the fluid

$$\frac{\partial v_i}{\partial t} = 0 \tag{2.21}$$

Thus, velocity is a function of only the coordinates. Steady flows represent equilibrium states of the fluid [29] - the individual elements that make up the fluid are moving, but in such a way that another element takes their place so that the overall state of the fluid does not change in time.

Another situation which is useful for purposes of calculations is when the density ρ is assumed constant throughout the fluid, independent of p. Since it is constant, there is no compression or expansion of the fluid. We call this an *incompressible fluid*. For incompressible fluids the relevant equations of hydrodynamics (such as Navier-Stokes equations and equation of continuity) are simplified, especially in the case of dissipative fluids which we will discuss later on. For constant ρ, conservation of mass (2.6) becomes

$$\partial_i v_i = 0. \tag{2.22}$$

This equation is also used as a definition of an *incompressible flow*. The difference between an incompressible fluid and an incompressible flow is that for an incompressible flow we define the material derivative of the density to be zero, but ρ itself need not be constant:

$$\frac{d\rho}{dt} = \partial_t \rho + v_i \partial_i \rho = 0. \tag{2.23}$$

Using the equation of continuity, we have

$$\frac{d\rho}{dt} = -\rho \partial_i v_i = 0. \tag{2.24}$$

Hence, (2.22) is the equivalent condition.

We define the vorticity of the fluid flow as

$$\boldsymbol{\omega} = \nabla \times \mathbf{v}. \tag{2.25}$$

If the vorticity is zero in all space for a fluid flow, we call it an *irrotational flow*. Furthermore, if there exists a scalar field such that the fluid velocity is its gradient

$$\mathbf{v} = \nabla \phi, \tag{2.26}$$

such a fluid flow is, by definition, irrotational. In such instances we call ϕ the *velocity potential*. This is why these flows are also called *potential flows*. If a flow is both potential and incompressible, one finds that the velocity potential has to satisfy Laplace's equation

$$\nabla^2 \phi = 0. \tag{2.27}$$

2.1.3 *Dissipative fluids*

So far our discussion did not include effects of energy dissipation, which is a result of the thermodynamic irreversibility of the fluid motion due to *internal friction* and *thermal conduction*. Simply put, different layers of the fluid rub against each other and in the process transfer some of the energy of the collective motion to heat. This is a form of internal friction called *viscosity*. An illustrative example of the importance of dissipation would be sound waves propagating in air - if we ignore viscosity, the sound waves we derive from ideal hydrodynamics would propagate indefinitely, without dampening. We know that this is not true from our everyday experience.

To better understand how we can account for viscous effects let us look at momentum flow across a small surface. Conservation of momentum tells us that

$$\partial_t (\rho v_i) = -\partial_j \Pi_{ij}, \quad \Pi_{ij} = p\delta_{ij} + \rho v_i v_j. \tag{2.28}$$

We need to insert an additional term in this relation in order to account for the irreversible transfer of momentum due to friction. We write

$$\Pi_{ij} = p\delta_{ij} + \rho v_i v_j - \sigma'_{ij} = -\sigma_{ij} + \rho v_i v_j. \tag{2.29}$$

σ_{ij} is called the stress tensor, and it is responsible for momentum transfer not directly due to the mass of the fluid. σ'_{ij} is known as the viscous stress tensor. To write its general form we note that processes of internal friction occur when different parts of the fluid move at different velocities. Hence, it should depend on v_i and its spatial derivatives. It is often assumed that these gradients are small enough that we can only keep the first derivatives. Furthermore, it must vanish for constant velocity, so σ'_{ij} needs to depend on the derivatives $\partial_i v_j$ of the velocity. In general, we can decompose such a rank 2 tensor into a part proportional to the identity, a symmetric, traceless part and an antisymmetric part

$$\sigma'_{ij} \longrightarrow a \cdot \delta_{ij}\partial_k v_k + b \cdot \left(\partial_i v_j - \partial_j v_i - \frac{2}{d}\partial_k v_k\right) + c \cdot \left(\partial_i v_j - \partial_j v_i\right). \tag{2.30}$$

We also note that this tensor must vanish for a fluid that is rotating uniformly, since there is no friction between different layers of the fluid in this case. For a fluid in uniform rotation $\mathbf{v} = \boldsymbol{\Omega} \times \mathbf{r}$, where $\boldsymbol{\Omega}$ is the angular velocity, the derivative $\partial_i v_j$ is antisymmetric. Consequently, we only keep the symmetric combinations. Finally, the viscous stress tensor can be written as

$$\sigma'_{ij} = \eta\left(\partial_i v_j + \partial_j v_i - \frac{2}{d}\partial_k v_k\right) - \zeta\delta_{ij}\partial_k v_k. \tag{2.31}$$

η and ζ are called *transport coefficients*. η is known as *shear viscosity* and ζ as *bulk viscosity* (sometimes called *second viscosity*). In general they both depend on thermodynamic variables, e.g. temperature T and chemical potential μ, though often in the literature they are considered to be constants. Transport coefficients can be considered as input parameters - since hydrodynamics is an effective theory, they cannot be evaluated within hydrodynamics, but rather from the underlying microscopic theory [5]. We also have to note that, although this simple model of

viscous stress is empirically valid for many fluids, there are cases where it fails. For example, fluids with elaborate molecular structure or asymmetrical shape of molecules, where the length in one direction is comparable to the free mean path for collisions. Such fluids are called *non-Newtonian* [28, 29].

In general, dissipative corrections in fluid dynamics are formulated as a derivative expansion. As the power of the derivative goes higher, the term itself gets smaller, so that one-derivative terms are smaller than zero-derivative ones, two-derivative terms are smaller than one-derivative ones, etc. This is based on the assumption that we are describing a system *near thermal equilibrium*, and the deviations from this thermal equilibrium are assumed to be small. This is akin to the approach found in effective field theory [5], the cutoff now being a characteristic mean free path λ_{mfp}. The requirement of small gradients now translates into the requirement that the mean free path in the fluid is smaller than the system size, $\lambda_{\text{mfp}} \ll L$. Thus, when the size of the system L is shorter than λ_{mfp} hydrodynamics ceases to be a sensible description.

Having seen how viscosity affects momentum transfer, we can modify Euler's equation. We get

$$\rho(\partial_t + v_j\partial_j)v_i = -\partial_i p + \partial_j\left[\eta\left(\partial_i v_j + \partial_j v_i - \frac{2}{d}\delta_{ij}\partial_k v_k\right)\right] + \partial_i\left(\zeta\partial_k v_k\right) + f_i. \tag{2.32}$$

If we regard η and ζ to be constants, we have

$$\rho(\partial_t + v_j\partial_j)v_i = -\partial_i p + \eta\partial^2 v_i + \left(\zeta + \frac{d-2}{d}\eta\right)\partial_i\partial_j v_j. \tag{2.33}$$

This is the *Navier-Stokes equation* named after Claude-Louis Navier (1785-1836) and George Gabriel Stokes (1819-1903). They represent the equations of motion of a viscous fluid.

For an incompressible fluid Navier-Stokes equation becomes much simpler, since $\partial_i v_i = 0$. Dividing by ρ, we find

$$\partial_t v_i + v_j\partial_j v_i = -\frac{1}{\rho}\partial_i p + \frac{\eta}{\rho}\partial^2 v_i + f_i. \tag{2.34}$$

The viscosity of an incompressible fluid is described by only one coefficient, η. The ratio

$$\nu = \frac{\eta}{\rho} \tag{2.35}$$

is often called *kinematic viscosity*.

We can write the incompressible Navier-Stokes equation in a dimensionless form. Such a procedure can give us insight into the relative importance of various terms in the equation. First, we define dimensionless variables[1]

$$\tilde{x}_i = \frac{x_i}{L}, \quad \tilde{t} = \frac{t}{L/V}, \quad \tilde{v}_i = \frac{v_i}{V}, \quad \tilde{p} = \frac{p}{\rho V^2}, \quad \tilde{\partial}_i = L\partial_i, \quad \tilde{\partial}_{\tilde{t}} = \frac{V}{L}\partial_t \tag{2.36}$$

where L and V are the scale factors for the spatial characteristic length and characteristic velocity of the flow, respectively. For example, if we consider a flow past a sphere or radius R which tends at infinity to a constant velocity U, we could define the characteristic length to be $L = R$ and the velocity $V = U$. Inserting these, the incompressible Navier-Stokes equation (ignoring external forces) then becomes

$$\tilde{\partial}_{\tilde{t}}\tilde{v}_i + \tilde{v}_j\tilde{\partial}_j\tilde{v}_i = -\tilde{\partial}_i\tilde{p} + \frac{1}{Re}\tilde{\partial}^2\tilde{v}_i, \quad Re = \frac{\rho VL}{\eta}, \tag{2.37}$$

where we have defined a dimensionless parameter Re, known as the Reynolds number. Large Reynolds number corresponds to nearly ideal fluid flow, whereas for small Reynolds number dissipation is dominant. We can interpret the Reynolds number as a measure of importance of the nonlinear convective term $v_j\partial_j v_i$, versus the viscosity term $\frac{\eta}{\rho}\partial^2 v_i$. Velocity profiles obtained by solving this equation are then given by a function of the form

$$\mathbf{v} = V\mathbf{f}\left(\frac{\mathbf{x}}{L}, Re\right). \tag{2.38}$$

If we have two incompressible flows of the same type (e.g. flow past spheres with different radii) and with the same Reynolds number, then they are described by the same function. In other words, these flows are similar (this is called *the law of similarity*). Many flows at large values of the Reynolds number become turbulent.

The other dissipative effect that occurs in viscous fluids is thermal conduction. If the temperature is not constant throughout the volume of the fluid, there can be another mode of transferring energy - transfer of heat or thermal conduction. Thermal conduction accounts for the transfer of internal energy in collisions and interactions of constituent particles of the fluid (e.g. molecules) from points of higher temperature to points of lower temperature. Recall that for an ideal fluid, the conservation of energy is given by equation (2.19). For viscous fluids energy is still conserved, but the equation that describes it is modified - we need to account for the flux due to processes of internal friction. This we can write as a vector $\sigma'_{ij}v_j$. The other term we need to add is the heat flux density due to thermal conduction, denoted by a vector q_i. In cases where the temperature gradient is not large, we can write this vector as an expansion in powers of the temperature gradient. Taking only the first derivative, we can describe q_i by Fourier's law

$$q_i = \kappa\partial_i T, \tag{2.39}$$

where κ is another transport coefficient, called *thermal conductivity*.

1 The choice of L/U for scale of time, and of ρU^2 for pressure is appropriate for flows where the non-linear terms dominate, i.e. high-velocity flows. For flows where viscous effects are dominant we can use $\tilde{t} = \frac{\eta}{\rho L^2}t$ and $\tilde{p} = \frac{L}{\eta U}p$ [27].

Now that we have a description for thermal conduction, we can modify the law of conservation of energy for a dissipative non-relativistic fluid. The total energy current (or energy flux density) is given by

$$j_i^\epsilon = \left(w + \frac{\rho v^2}{2}\right) v_i - \sigma'_{ij} v_j - \kappa \partial_i T. \tag{2.40}$$

Consequently conservation of energy is now described by the following equation

$$\boxed{\partial_t \left(w + \frac{\rho v^2}{2}\right) - \partial_i j_i^\epsilon = 0.} \tag{2.41}$$

We have completed the set of fundamental equations of dissipative non-relativistic hydrodynamics.

2.2 RELATIVISTIC HYDRODYNAMICS

Now let's turn our attention to relativistic hydrodynamics. We recommend to the Reader a very nice review of relativistic hydrodynamics [5], which serves as the basis of this section and that goes in greater depth. The systems we inspect here will be symmetric under spacetime translations, rotations and Lorentz boosts. There can also be an additional symmetry - e.g. a conserved $U(1)$ number, such as baryon number. Furthermore, we assume the systems in questions are symmetric under parity, for simplicity. As before, conservation laws will play an important role in the hydrodynamic description of a relativistic system. Spacetime translation symmetry is associated with the conservation of the energy-momentum tensor $T^{\mu\nu}$:

$$\partial_\mu T^{\mu\nu} = 0. \tag{2.42}$$

If the system in question is in d spatial dimensions, there are $d+1$ components of the equation above. Symmetry under rotations and Lorentz boosts is associated with the conservation of currents $\mathcal{M}^{\mu\nu\lambda} = x^\mu T^{\nu\lambda} - x^\nu T^{\mu\lambda}$, which are identically conserved due to the conservation of the energy-momentum tensor:

$$\partial_\lambda \mathcal{M}^{\mu\nu\lambda} = 0. \tag{2.43}$$

As previously stated, there can be additional symmetries in the system. One of the more relevant and physically interesting is a global $U(1)$ symmetry which is associated with charge conservation:

$$\partial_\mu J^\mu = 0. \tag{2.44}$$

The charge conservation equation contains only one component. In total, if we are in d spatial dimensions, we have $d+2$ equations coming from (2.42) and (2.44), while there are $(d+1)(d+2)/2$ components of $T^{\mu\nu}$ and $d+1$ components of J^μ. We build the energy-momentum tensor and charge current out of hydrodynamic variables (also known as *fields*): a local temperature $T(x)$, a local chemical potential $\mu(x)$ and a local fluid velocity $\mathbf{v}(x)$. In total, there are $d+2$ of these fields.

The energy-momentum tensor and the charge current can be decomposed, using a timelike vector u^μ, into components that are transverse and longitudinal with respect to u^μ. This decomposition can be written as [5, 30]

$$T^{\mu\nu} = \mathcal{E} u^\mu u^\nu + \mathcal{P}\Delta^{\mu\nu} + (q^\mu u^\nu + q^\nu u^\mu) + t^{\mu\nu}, \tag{2.45}$$

$$J^\mu = \mathcal{N} u^\mu + j^\mu, \tag{2.46}$$

where we have used the projector $\Delta^{\mu\nu} \equiv \eta^{\mu\nu} + u^\mu u^\nu$, and $\eta_{\mu\nu} = \mathrm{diag}(-1, 1, \ldots, 1)$ is the flat-space Minkowski metric. $\mathcal{E}$, $\mathcal{P}$ and $\mathcal{N}$ are scalars, while q^μ and j^μ are transverse vectors, i.e. $u_\mu q^\mu = u_\mu j^\mu = 0$. $t^{\mu\nu}$ is a transverse, symmetric and traceless tensor. We can write these coefficients explicitly, in terms of u^μ, $T^{\mu\nu}$ and J^μ:

$$\mathcal{E} = u_\mu u_\nu T^{\mu\nu}, \quad \mathcal{P} = \frac{1}{d}\Delta_{\mu\nu} T^{\mu\nu}, \quad \mathcal{N} = -u_\mu J^\mu, \tag{2.47}$$

$$q_\mu = -\Delta_{\mu\alpha} u_\beta T^{\alpha\beta}, \quad j_\mu = \Delta_{\mu\nu} J^\nu, \tag{2.48}$$

$$t_{\mu\nu} = \frac{1}{2}\left(\Delta_{\mu\alpha}\Delta_{\nu\beta} + \Delta_{\nu\alpha}\Delta_{\mu\beta} - \frac{2}{d}\Delta_{\mu\nu}\Delta_{\alpha\beta}\right) T^{\alpha\beta}. \tag{2.49}$$

(2.45) are identities, they are valid locally for any symmetric tensor $T^{\mu\nu}(x)$ and any vector $J^\mu(x)$, given a timelike $u^\mu(x)$ [5]. What will make this decomposition specific for our purposes is that we will use hydrodynamic variables u_μ, T, and μ to express the coefficients $\mathcal{E}$, $\mathcal{P}$, $\mathcal{N}$, q^μ, j^μ, and $t^{\mu\nu}$. The expressions we get in this way for $T^{\mu\nu}$ and J^μ are called *constitutive relations*.

Constitutive relations in hydrodynamics are written in a derivative expansion. The terms that enter the expansion are powers of derivatives of the hydrodynamic variables

$$T^{\mu\nu} = T^{\mu\nu}_{(0)} + \Pi^{\mu\nu}_{(1)} + \Pi^{\mu\nu}_{(2)} + \ldots, \tag{2.50}$$

$$J^\mu = J^\mu_{(0)} + J^\mu_{(1)} + J^\mu_{(2)} + \ldots, \tag{2.51}$$

where the number in the bracket denotes the derivative order of the correction. If we take into account only the zeroth-order terms (i.e. the non-derivative terms), we find what is known as ideal hydrodynamics, with many applications in astrophysics and cosmology. If in addition to these, one takes into account the one-derivative terms, we get conventional dissipative (or viscous) hydrodynamics.

2.2.1 *Zeroth-order hydrodynamics*

Just as we did with non-relativistic case, let's start with ideal hydrodynamics. We take no derivative terms into account, which means that q^μ, j^μ and $t^{\mu\nu}$ in (2.45) are zero, since they can be only composed of derivatives of the hydrodynamic variables. The coefficients $\mathcal{E}$, $\mathcal{P}$, and $\mathcal{N}$ are then functions of T and μ. In order to get a better understanding of these coefficients, let's look at what happens in static equilibrium, in the local rest frame. In static equilibrium the energy-momentum tensor is given by

$$T^{\mu\nu} = \mathrm{diag}(\epsilon, p, \ldots, p), \tag{2.52}$$

where ϵ is the equilibrium energy density and p is the equilibrium pressure. Similarly, the $U(1)$ current is given by

$$J^\mu = (n, \mathbf{0}), \tag{2.53}$$

where n is the equilibrium charge density. Now, if we have a fluid which is moving with constant velocity u^μ, we can perform a corresponding Lorentz boost and find the energy-momentum tensor and current

$$T^{\mu\nu} = \epsilon u^\mu u^\nu + p\Delta^{\mu\nu}, \tag{2.54}$$
$$J^\mu = n u^\mu, \tag{2.55}$$

These expressions are quite similar to (2.45). In fact, what we do in ideal hydrodynamics is to promote ϵ, p, n and u^μ to slowly varying fields and match $\mathcal{E}(x) = \epsilon(x)$, $\mathcal{P} = p(x)$, and $\mathcal{N}(x) = n(x)$ [5]. In this way we find a physical interpretation for the coefficients in (2.45) - we can identify $\mathcal{E}(x)$ with the local energy density, $\mathcal{P}(x)$ with the local pressure, $\mathcal{N}(x)$ with the local charge density, and u^μ with the local fluid velocity. Let us recall that the equilibrium equation of state - in this case $p(T, \mu)$, provides the relationship between p and the other hydrodynamic fields - the energy density ϵ, charge density n and entropy density s. We can find these as

$$\epsilon = -p + Ts + \mu n \tag{2.56}$$
$$n = \frac{\partial p}{\partial \mu} \tag{2.57}$$
$$s = \frac{\partial p}{\partial T} \tag{2.58}$$

This equilibrium relation needs to be provided by an explicit calculation in the underlying equilibrium quantum system [31]. Furthermore, using (2.56) along with the Gibbs-Duhem relation $dp = sdT + nd\mu$ and the conservation equations (2.42), (2.44), we find

$$\partial_\mu (s u^\mu) = 0. \tag{2.59}$$

This is equation is interpreted as the conservation of entropy current su^μ, meaning that locally the entropy does not increase in ideal hydrodynamics [5].

2.2.2 *First-order hydrodynamics*

Let us now move on to the next step where we take into account terms in the derivative expansion up to one derivative of the hydrodynamic variables. This seemingly simple step, however, hides an important, yet subtle notion that the hydrodynamic fields - local temperature $T(x)$, local chemical potential $\mu(x)$ and local fluid velocity $u^\mu(x)$ - are not uniquely defined out of equilibrium [5]. We can define many local temperatures or chemical potentials or velocities that differ from each other by gradients of the hydrodynamic variables, yet tend to the same

equilibrium value, when those gradients tend to zero. To put it in mathematical terms, we can express the coefficients in the decomposition (2.45) as

$$\mathcal{E} = \epsilon(T,\mu) + f_{\mathcal{E}}(\partial T, \partial\mu, \partial u), \tag{2.60}$$
$$\mathcal{P} = p(T,\mu) + f_{\mathcal{P}}(\partial T, \partial\mu, \partial u), \tag{2.61}$$
$$\mathcal{N} = n(T,\mu) + f_{\mathcal{N}}(\partial T, \partial\mu, \partial u), \tag{2.62}$$

where ϵ, p, and n are equilibrium values and are determined by the equation of state, while $f_{\mathcal{E}}$, $f_{\mathcal{P}}$, and $f_{\mathcal{N}}$ are the out-of-equilibrium gradient corrections. These corrections depend on the definitions of local temperature, local chemical potential and local fluid velocity. Herein enters an important concept in hydrodynamics - field redefinitions. We can, in fact, redefine the hydrodynamic variables (or fields) in any way we wish as long as the energy-momentum tensor and $U(1)$ current remain unchanged under these redefinitions. The reason for this is that local temperature $T(x)$, local chemical potential $\mu(x)$ and local fluid velocity $u^\mu(x)$ have no fundamental, microscopic definition out of equilibrium. They are simply auxiliary parameters that we use to parametrize quantities that do have a microscopic definition - the energy-momentum tensor $T^{\mu\nu}$ and the $U(1)$ current J^μ. This is why, in hydrodynamics, redefinitions of the hydrodynamic fields are often called a *choice of frame* [5, 32]. We can consider such a redefinition

$$T(x) \to T'(x) = T(x) + \delta T(x), \tag{2.63}$$
$$\mu(x) \to \mu'(x) = \mu(x) + \delta\mu(x), \tag{2.64}$$
$$u^\mu(x) \to u'^\mu(x) = u^\mu(x) + \delta u^\mu(x), \tag{2.65}$$

where $\delta T(x)$, $\delta\mu(x)$, and $\delta u^\mu(x)$ are composed of first-order derivatives of the hydrodynamic variables. Using (2.47) we can see how the coefficients change with respect to this redefinition, up to first order in derivatives:

$$\delta\mathcal{E} = 0, \quad \delta\mathcal{P} = 0, \quad \delta\mathcal{N} = 0, \tag{2.66}$$
$$\delta q_\mu = -(\mathcal{E}+\mathcal{P})\delta u_\mu, \quad \delta j_\mu = -\mathcal{N}\delta u_\mu, \tag{2.67}$$
$$\delta t_{\mu\nu} = 0. \tag{2.68}$$

Here we have used several things - $T^{\mu\nu}$ and J^μ remain invariant under these field redefinitions, q^μ, j^μ, and $t^{\mu\nu}$ are quantities that are first order in derivatives, as well as that δu^μ is transverse, i.e. $u_\mu \delta u^\mu = 0$. This is because we normalized it to be $u^2 = -1$.

Now, the choice of frame boils down to choosing a particular δu_μ. Canonically, in the literature, there are two most often used choices. One is that we choose δu_μ such that $j_\mu = 0$. This choice was adopted by Carl Eckart in [30], thus it is often called the *Eckart frame*. We can also choose δu_μ such that $q_\mu = 0$. This was adopted by Lev Landau and Evgeny Lifshitz in [4], so it's often called the *Landau frame*. This is the frame choice we will pick, not just in this chapter, but in the rest of the thesis as well. The Landau frame implies no energy flow in the local rest frame of the fluid [5].

scalars	$\left[u^\lambda \partial_\lambda T\right],\ \left[u^\lambda \partial_\lambda \mu\right],\ \partial_\lambda u^\lambda$
vectors	$\Delta^{\mu\nu}\partial_\nu T,\ \Delta^{\mu\nu}\partial_\nu \mu,\ \left[\Delta^{\mu\nu}\left(u^\lambda \partial_\lambda u_\nu\right)\right]$
tensors	$\sigma^{\mu\nu} \equiv \Delta^{\mu\alpha}\Delta^{\nu\beta}\left(\partial_\alpha u_\beta + \partial_\beta u_\alpha - \frac{2}{d}\eta_{\alpha\beta}\partial_\lambda u^\lambda\right)$

Table 2.1: An overview of all the different one-derivative terms of the hydrodynamic variables we can write down, with respect to the symmetries of a relativistic system. The terms in square brackets are the terms we eliminate using the equations of motion at zeroth order. Here d is the number of spatial dimensions.

Notice that eq. (2.66) essentially tells us that

$$\epsilon(T,\mu) + f_\mathcal{E}(\partial T, \partial\mu, \partial u) = \epsilon(T',\mu') + f'_\mathcal{E}(\partial T', \partial\mu', \partial u'), \tag{2.69}$$
$$p(T,\mu) + f_\mathcal{P}(\partial T, \partial\mu, \partial u) = p(T',\mu') + f'_\mathcal{P}(\partial T', \partial\mu', \partial u'), \tag{2.70}$$
$$n(T,\mu) + f_\mathcal{N}(\partial T, \partial\mu, \partial u) = n(T',\mu') + f'_\mathcal{N}(\partial T', \partial\mu', \partial u'), \tag{2.71}$$

which implies

$$f'_\mathcal{E} = f_\mathcal{E} - \left(\frac{\partial\epsilon}{\partial T}\right)_\mu \delta T - \left(\frac{\partial\epsilon}{\partial\mu}\right)_T \delta\mu, \tag{2.72}$$
$$f'_\mathcal{P} = f_\mathcal{P} - \left(\frac{\partial p}{\partial T}\right)_\mu \delta T - \left(\frac{\partial p}{\partial\mu}\right)_T \delta\mu, \tag{2.73}$$
$$f'_\mathcal{N} = f_\mathcal{N} - \left(\frac{\partial n}{\partial T}\right)_\mu \delta T - \left(\frac{\partial n}{\partial\mu}\right)_T \delta\mu. \tag{2.74}$$

Therefore, we can use the field redefinitions (2.69) to set two of the three functions $f'_\mathcal{E}$, $f'_\mathcal{P}$, and $f'_\mathcal{N}$ to zero. By convention with most of the literature, we set $f'_\mathcal{E}$ and $f'_\mathcal{N}$ to be zero, which means that we redefine T and μ such that $\mathcal{E} = \epsilon$ and $\mathcal{N} = n$[5].

What remains are the coefficients $\mathcal{P}$, j^μ and $t^{\mu\nu}$. These we need to express in terms of derivatives of hydrodynamic variables, up to first order. In order to do that we need to know what are all of the possible terms we can write in this expansion. We are limited by the symmetries of the system - all of the terms that appear in the expansion need to obey spacetime translation, rotation and Lorentz boost symmetry. $\mathcal{P}$ is a scalar, so let's think of all the scalar terms we can build out of one-derivatives of T, μ, and u^μ, that also obey the required symmetries. Similarly, for j^μ and $t^{\mu\nu}$ we think of transverse vectors and transverse traceless symmetric tensors we can construct in this way. The kinematic structures we can write are given in table 2.1. Using this, we can write the scalar coefficient, $\mathcal{P}$ in a derivative expansion as

$$\mathcal{P} = p + c_1 u^\lambda \partial_\lambda T + c_2 u^\lambda \partial_\lambda \mu + c_3 \partial_\lambda u^\lambda + O(\partial^2). \tag{2.75}$$

Here p is the thermodynamic pressure in the local rest frame of the fluid, c_i are coefficients, and $O(\partial^2)$ stands for terms that are second-order in derivatives or quadratic in one-derivatives.

There still exists a redundancy here - namely, we can use the zeroth-order equations of motion (i.e. equations of ideal hydrodynamics)

$$\partial_\mu T^{\mu\nu}_{(0)} = 0, \tag{2.76}$$

$$\partial_\mu J^{\mu}_{(0)} = 0, \tag{2.77}$$

to get rid of some derivative terms we have written in the table, or to be more exact, to re-express them in terms of remaining tensor structures. Let's look at the scalar terms first. We have two scalar equations,

$$u_\mu \partial_\nu T^{\mu\nu}_{(0)} = 0, \tag{2.78}$$

$$\partial_\mu J^{\mu}_{(0)} = 0, \tag{2.79}$$

which provide us two relations between the three one-derivative scalar terms in table 2.1. By convention, we use these two equations to express $u^\lambda \partial_\lambda T$ and $u^\lambda \partial_\lambda \mu$ in terms of $\partial_\lambda u^\lambda$ [5]. Now the derivative expansion for $\mathcal{P}$ looks like this

$$\mathcal{P} = p - \zeta \partial_\lambda u^\lambda + O(\partial^2). \tag{2.80}$$

Here ζ is a physical *transport coefficient* which can be determined from the microscopic theory. In particular, ζ is called *bulk viscosity*.

A similar procedure is applied to j^μ. We have one transverse vector zeroth-order equation

$$\Delta_{\lambda\nu} \partial_\mu T^{\mu\nu}_{(0)} = 0, \tag{2.81}$$

which we can use to eliminate one of the three vector terms in table 2.1. Again, by convention, we choose to eliminate $\Delta^{\mu\nu}\left(u^\lambda \partial_\lambda u_\nu\right)$, and the derivative expansion for j^μ becomes

$$j^\mu = -\sigma T \Delta^{\mu\nu} \partial_\nu \left(\frac{\mu}{T}\right) + \chi_T \Delta^{\mu\nu} \partial_\nu T + O(\partial^2). \tag{2.82}$$

Now σ and χ_T are transport coefficients. σ is called *charge conductivity*. Since $\sigma^{\mu\nu}$ is the only transverse traceless symmetric tensor, we can immediately write the derivative expansion

$$t^{\mu\nu} = -\eta \sigma^{\mu\nu} + O(\partial^2), \tag{2.83}$$

where η is a transport coefficient, called shear viscosity. Finally, putting all of these things together, we can write the constitutive relations of first-order relativistic hydrodynamics in the Landau frame as:

$$T^{\mu\nu} = \epsilon u^\mu u^\nu + p \Delta^{\mu\nu} - \eta \sigma^{\mu\nu} - \zeta \Delta^{\mu\nu} \partial_\lambda u^\lambda + O(\partial^2), \tag{2.84}$$

$$J^\mu = n u^\mu - \sigma T \Delta^{\mu\nu} \partial_\nu \left(\mu / T\right) + \chi_T \Delta^{\mu\nu} \partial_\nu T + O(\partial^2). \tag{2.85}$$

There are in total 4 transport coefficients - η, ζ, σ and χ_T. However, there will be further constraints on these coefficients coming from the entropy current. But

before that, let us for the sake of comparison and completeness, look at the constitutive relations in the Eckart frame

$$T^{\mu\nu} = \epsilon u^\mu u^\nu + p\Delta^{\mu\nu} + (q^\mu u^\nu + q^\nu u^\mu) - \eta\sigma^{\mu\nu} - \zeta\Delta^{\mu\nu}\partial_\lambda u^\lambda + O(\partial^2), \tag{2.86}$$

$$J^\mu = nu^\mu + O(\partial^2), \tag{2.87}$$

where

$$q^\mu = (\sigma T\Delta^{\mu\nu}\partial\,(\mu/T) - \chi_T\Delta^{\mu\nu}\partial_\nu T)\,\frac{\epsilon + p}{n} + O(\partial^2). \tag{2.88}$$

We see that, despite using a different frame choice, we still find the same 4 transport coefficients as in the Landau frame. One can also often in the literature find the expression for q^μ written as

$$q^\mu = -\kappa\Delta^{\mu\nu}\left(Tu^\lambda\partial_\lambda u_\nu + \partial_\nu T\right) - \chi_T\,(\Delta^{\mu\nu}\partial_\nu T)\,\frac{\epsilon + p}{n} + O(\partial^2), \tag{2.89}$$

where κ is called *heat conductivity*. One can express κ in terms of σ as

$$\kappa = \sigma\left(\frac{\epsilon + p}{n}\right)^2\frac{1}{T}. \tag{2.90}$$

We get (2.89) by using the zeroth-order EOM to re-express $\Delta^{\mu\nu}\partial_\nu\mu$ in terms of $\Delta^{\mu\nu}\partial_\nu T$ and $\Delta^{\mu\nu}\left(u^\lambda\partial_\lambda u_\nu\right)$. Note that from eq. (2.86) with $\chi_T = 0$, we find eq. (2.32) and (2.41) in the non-relativistic limit [5].

2.2.3 *Entropy current*

Now, let's turn our attention to one last element of this theory - the entropy current. In thermal equilibrium, if we have a relativistic fluid moving with constant u^μ, we can define the entropy current as $S^\mu = su^\mu$, where s is the entropy density of the system. We have already seen that for ideal fluids (zeroth-order hydrodynamics) $\partial_\mu S^\mu = 0$. In first-order hydrodynamics it is natural to assume we can modify this current in the following way

$$S^\mu = su^\mu + (\text{gradient corrections}), \tag{2.91}$$

where the gradient corrections are built out of derivatives of T, μ and u^μ, similar to what we had with the constitutive relations. These gradient corrections vanish in equilibrium. The entropy current defined in this way is not unique but demanding that

$$\partial_\mu S^\mu \geq 0 \tag{2.92}$$

can provide constraints on the transport coefficients . We can derive an expression for S^μ by writing down a covariant version of the Euler thermodynamic relation $Ts = p + \epsilon - \mu n$ [33]

$$TS^\mu = pu^\mu - T^{\mu\nu}u_\nu - \mu J^\mu. \tag{2.93}$$

Using the decomposition of the energy-momentum tensor and the current (2.45) we can write S^μ as

$$S^\mu = \left[s + \frac{1}{T}(\mathcal{E} - \epsilon) - \frac{\mu}{T}(\mathcal{N} - n) \right] u^\mu + \frac{1}{T} q^\mu - \frac{\mu}{T} j^\mu \tag{2.94}$$

where the coefficients $\mathcal{E}$, $\mathcal{N}$, q^μ and j^μ were defined in (2.47). This expression for the entropy current is invariant under frame transformations and simplifies whether we choose the Landau frame or the Eckart frame (since we have then for both frames $\mathcal{E} = \epsilon$, $\mathcal{N} = n$, as well as $q^\mu = 0$ or $j^\mu = 0$, respectively). One important result of this entropy current analysis is that, once we have made our frame choice, the positivity of entropy production (2.92) gives certain restrictions on the transport coefficients. Concretely

$$\eta \geq 0, \quad \zeta \geq 0, \quad \sigma \geq 0, \quad \chi_T = 0. \tag{2.95}$$

The canonical form (2.94) of the entropy current and the constraints (2.95) arise by demanding the positivity of entropy production in curved spacetime, $\nabla_\mu S^\mu = 0$, as seen in [32]. These same conditions (2.95) can be obtained in the linear response theory, without reference to an entropy current [5].

2.3 NON-RELATIVISTIC HYDRODYNAMICS REVISITED: NEWTON-CARTAN

There is a more modern approach towards non-relativistic, Galilean-invariant hydrodynamics by way of coupling Galilean-invariant field theories to a curved background, described by Newton-Cartan geometry. With this approach one can systematically build the constitutive relations, and recast them in a manifestly covariant way, not unlike what one does in relativistic hydrodynamics. In this section we shall try to summarize, as compactly as we can, the salient points of this theory, following mostly [6, 7]. We encourage the Reader to read these and other references, e.g. [34–41], that go into far more detail, applications and other aspects, than we will here.

2.3.1 *Elements of Newton-Cartan geometry*

The starting point is the notion of Newton-Cartan geometry. We can equip a smooth $(d+1)$-dimensional manifold $\mathcal{M}$ with tensor data $(n_\mu, h_{\mu\nu}, A_\mu)$, where A_μ is a $U(1)$ gauge field which couples to the particle number current, n_μ is a nowhere-vanishing one-form which effectively defines a local time direction, and $h_{\mu\nu}$ is a symmetric rank-d tensor, the so-called "spatial co-metric". One also demands that

$$\gamma_{\mu\nu} = n_\mu n_\nu + h_{\mu\nu}, \qquad \gamma = \det(\gamma_{\mu\nu}), \tag{2.96}$$

is positive definite and invertible. We denote the inverse of $\gamma_{\mu\nu}$ as $\gamma^{\mu\nu}$. We can obtain the contravariant data $(v^\mu, h^{\mu\nu})$ via

$$v^\mu = \gamma^{\mu\nu} n_\nu, \qquad h^{\mu\nu} = \gamma^{\mu\nu} - v^\mu v^\nu \tag{2.97}$$

which satisfy

$$n \cdot v = 1, \quad h^{\mu\nu} n_\nu = 0, \quad h_{\mu\nu} v^\nu = 0, \quad h_{\mu\rho} h^{\nu\rho} = P^\nu_\mu = \delta^\nu_\mu - v^\nu n_\mu. \tag{2.98}$$

Because there is no underlying metric, we need to distinguish between tensors with upper (covariant) and lower (contravariant) indices, even though in some cases indices are raised using $h^{\mu\nu}$.

A Galilean-invariant theory that is placed on $\mathcal{M}$ should be coupled to the Newton-Cartan data in such a way that it is invariant under reparametrization of coordinates, $U(1)$ gauge transformations, and Milne boosts. Milne boost invariance is a key requirement, since it imposes a local version of Galilean boost invariance. Under Milne boosts, the background fields transform as

$$h_{\mu\nu} \to h_{\mu\nu} - (n_\mu \psi_\nu + n_\nu \psi_\mu) + n_\mu n_\nu \psi^2, \quad A_\mu \to A_\mu + \psi_\mu - \frac{1}{2} n_\mu \psi^2, \tag{2.99}$$

where ψ_μ is an arbitrary one-form satisfying $v^\mu \psi_\mu = 0$, and $\psi^2 = \psi_\mu \psi^\mu = \psi_\mu \psi_\nu h^{\mu\nu}$. The upper index data transforms as

$$v^\mu \to v^\mu + \psi^\mu, \tag{2.100}$$

while $h^{\mu\nu}$ is invariant. We can also uniquely define a covariant derivative, which acts on a $(1,1)$ tensor $\mathfrak{T}$ as

$$D_\mu \mathfrak{T}^\nu{}_\rho = \partial_\mu \mathfrak{T}^\nu{}_\rho + \Gamma^\nu{}_{\sigma\mu} \mathfrak{T}^\sigma{}_\rho - \Gamma^\sigma{}_{\rho\mu} \mathfrak{T}^\nu{}_\sigma. \tag{2.101}$$

To make this choice unique, we demand that

$$D_\mu n_\nu = 0, \qquad D_\mu h^{\nu\rho} = 0, \tag{2.102}$$

and that the torsion is completely temporal

$$T^\mu{}_{\nu\rho} \equiv \Gamma^\mu{}_{\nu\rho} - \Gamma^\mu_{\rho\nu}, \qquad h_{\mu\nu} T^\sigma{}_{\nu\rho} = 0. \tag{2.103}$$

The unique connection that satisfies these conditions is given by [6, 7]

$$\Gamma^\mu{}_{\nu\rho} = v^\mu \partial_\rho n_\nu + \frac{1}{2} h^{\mu\sigma} \left(\partial_\nu h_{\rho\sigma} + \partial_\rho h_{\nu\sigma} - \partial_\sigma h_{\nu\rho} \right) + h^{\mu\sigma} n_{(\nu} F_{\rho)\sigma}, \tag{2.104}$$

$$T^\mu{}_{\nu\rho} = v^\mu F^n_{\rho\nu}, \tag{2.105}$$

where $F_{\mu\nu}$ is the field strength of A_μ

$$F_{\mu\nu} = \partial_\mu A_\nu - \partial_\nu A_\mu, \tag{2.106}$$

and

$$F^n_{\mu\nu} = \partial_\mu n_\nu - \partial_\nu n_\mu. \tag{2.107}$$

One can derive Ward identities arising from the symmetries listed above by varying the generating functional W of correlation functions ($W = -i \ln \mathcal{Z}$, where $\mathcal{Z}$ is the partition function)

$$\delta W = \int d^{d+1}x \sqrt{\gamma} \left\{ \delta A_\mu \, J^\mu - \delta n \, \mathcal{E}^\mu - \delta \bar{v}^\mu \, \mathcal{P}_\mu - \frac{1}{2} \delta \bar{h}^{\mu\nu} \, T_{\mu\nu} \right\}. \tag{2.108}$$

with respect to the background fields. Here J^μ is the particle number current, $\mathcal{P}_\mu$ is the momentum density current, $\mathcal{E}^\mu$ is the energy current and $T_{\mu\nu}$ the spatial stress tensor. Invariance under Milne boosts leads to

$$\mathcal{P}_\mu = h_{\mu\nu} J^\nu \tag{2.109}$$

which tells us that momentum is equal to particle number current. The Ward identities corresponding to invariance under $U(1)$ gauge transformations and coordinate reparametrizations can be written as

$$(D_\nu - \mathcal{G}_\nu) \, \mathcal{E}^\mu = \mathcal{G}_\mu \mathcal{E}^\mu - h_{\rho(\mu} D_{\nu)} v^\rho \mathcal{T}^{\mu\nu}, \tag{2.110}$$

$$(D_\nu - \mathcal{G}_\nu) \, \mathcal{T}^{\mu\nu} = - \, (F^n)^\mu{}_\nu \, \mathcal{E}^\nu, \tag{2.111}$$

where

$$\mathcal{G}_\mu \equiv T^\nu{}_{\mu\nu} = -F^n_{\mu\nu} v^\nu. \tag{2.112}$$

For vectors, $(D_\nu - \mathcal{G}_\nu)$ represents the usual divergence with a volume element $\sqrt{\gamma}$

$$(D_\nu - \mathcal{G}_\nu) \mathfrak{v}^\mu = \frac{1}{\sqrt{\gamma}} \partial_\mu \left(\sqrt{\gamma} \mathfrak{v}^\mu \right). \tag{2.113}$$

Here $\mathcal{T}^{\mu\nu}$ represents the Milne-invariant spacetime stress tensor, defined as

$$\mathcal{T}^{\mu\nu} \equiv T^{\mu\nu} + \mathcal{P}^\mu v^\nu + \mathcal{P}^\nu v^\mu + v^\mu v^\nu n_\rho J^\rho. \tag{2.114}$$

On the other hand, the energy current $\mathcal{E}^\mu$ is not invariant under Milne boosts, the reason being that the underlying Newton-Cartan data, connections A_μ and $\Gamma^\mu_{\nu\rho}$, are not invariant under Milne boosts. This can be ameliorated by equiping the spacetime with a Milne-invariant vector field u^μ which is timelike everywhere, meaning $n_\mu u^\mu > 0$. As it turns out, we can use the fluid velocity u^μ_G as our Milne-invariant vector field. We normalize it so that $u^\mu_G n_\mu = 1$. We can also define its lower index counterpart as

$$u_{G\,\mu} = h_{\mu\nu} u^\nu_G, \qquad u^2_G = u_{G\,\mu} u^\mu_G. \tag{2.115}$$

Using these ingredients we can construct the Milne-invariant versions $\tilde{h}_{\mu\nu}$, $\tilde{A}_\mu$ and $\tilde{P}^\mu_\nu$, as well as define a Milne and $U(1)$ gauge invariant connection $\tilde{\Gamma}^\lambda_{\mu\nu}$ that is compatible with Newton-Cartan data.

2.3.2 *Hydrodynamics*

Let's now look at fluid dynamics. The program for constructing nth order hydrodynamics is simple - first we write down the most general constitutive relations

for $\mathcal{T}^{\mu\nu}$ and $\tilde{\mathcal{E}}^{\mu}$ with tensors containing up to n derivatives of the fluid variables and background fields. Secondly, we demand the existence of the entropy current. Much like before, to write the first-order hydrodynamic constitutive relations we encounter field redefinitions and choice of frame. But here, for brevity's sake, we only look at the zeroth order.

We build constitutive relations, the spacetime stress tensor $\mathcal{T}^{\mu\nu}$ and energy current $\mathcal{E}^{\mu}$, in terms of (T, μ, u^{μ}) of the background fields $(n_{\mu}, h_{\mu\nu}, A_{\mu})$, and their gradients. The Ward identities then give us the equations of motion for the fluid. The constitutive relations for $\mathcal{T}^{\mu\nu}$ and $\mathcal{E}^{\mu}$ need to be expressed in terms of $U(1)$-invariant contravariant symmetric tensors and vectors, respectively. $\mathcal{T}^{\mu\nu}$ is already Milne-invariant, but $\mathcal{E}^{\mu}$ is not. So we separate it into a manifestly Milne-invariant part $\tilde{\mathcal{E}}^{\mu}$, and a part constructed algebraically from $\mathcal{T}^{\mu\nu}$ and the fluid data:

$$\mathcal{E}^{\mu} = \tilde{\mathcal{E}}^{\mu} + \left(u_{G\,\nu} - \frac{1}{2} n_{\nu} u_{G}^{2} \right) \mathcal{T}^{\mu\nu}. \tag{2.116}$$

Finally, the constitutive relations for Galilean-invariant fluids at zeroth order in the derivative expansion (i.e. ideal fluids) are given by

$$\mathcal{T}^{\mu\nu} = P h^{\mu\nu} + \rho u_{G}^{\mu} u_{G}^{\nu}, \tag{2.117}$$

$$\tilde{\mathcal{E}}^{\mu} = \epsilon u_{G}^{\mu}, \tag{2.118}$$

where P is the pressure, ρ is the particle number density, and ϵ is the energy density. These are all now Milne-invariant functions of the Milne-invariant temperature T, and chemical potential μ. Specializing to flat space and repackaging things a bit, one can see that we reproduce the familiar constitutive relations for non-relativistic fluids

$$J^{0} = \rho, \qquad J^{i} = \rho u_{G}^{i}, \tag{2.119}$$

$$\mathcal{E}^{0} = \epsilon + \frac{1}{2}\rho u^{2}, \qquad \mathcal{E}^{i} = \left(\epsilon + P + \frac{1}{2}\rho u_{G}^{2} \right) u_{G}^{i}, \tag{2.120}$$

$$\mathcal{P}_{i} = \rho u_{G\,i}, \qquad T_{ij} = P\delta_{ij} + \rho u_{G\,i} u_{G\,j}. \tag{2.121}$$

Part II

THE SHOWCASE

Karen Gunderson, *Silver Dusk*

3

OVERCOMING OBSTACLES IN NONEQUILIBRIUM HOLOGRAPHY

3.1 INTRODUCTION

Holographic duality duality as a tool for applications to strongly coupled field theories is most effective whenever one is able to identify universal quantities or mechanisms which do not depend on the precise details of the bulk theory employed, as encoded for example in the couplings appearing in the bulk action, but instead relies on universal gravitational physics, such as that associated with black hole horizons. A striking example of this universality, namely the universal ringdown of deformed horizons, has taught us a great deal about the thermalization of strongly coupled field theories with holographic duals. Linear infalling perturbations of black hole horizons in the bulk are characterized by a set of complex-frequency modes, the so-called quasinormal modes (QNM) [42–45]. Physically admissible modes must satisfy regularity at the future horizon and decay (usually exponentially) as a function of time. These modes are ubiquitous in our exploration of strongly coupled quantum matter via holographic duality, not least because they manifest themselves as non-analytic features in field-theory correlation functions, most commonly as poles in retarded correlation functions. By studying the dispersion relations of these poles, that is by calculating their complex frequencies $\omega(k) \in \mathbb{C}$ as a function of real momentum, much can be deduced about the relaxation dynamics of the dual field theories, including all the information about the hydrodynamic effective description of the system, that is transport coefficients, dispersion relations, and so forth.

In this chapter we study a similarly universal set of modes, which govern the behavior of non-equilibrium steady states of strongly coupled field theories with holographic duals. These modes reverse the relationship of frequency and momentum described above. In other words we shall be interested in the analytic properties of correlation functions in the complex momentum plane, $k(\omega) \in \mathbb{C}$, as a function of real frequency. As will be described in detail below, these modes, which we term stationary collective modes (SCM), are generically independent and distinct from QNM. However, as we shall see, for relativistic field theories, they can be related to QNM via a procedure involving Lorentz transformations and analytic continuation.

The physical significance of these modes is broad and universal[1]. In this work, as in [9], our main interest is in spatial features of non-equilibrium quantum matter, but like QNM, these modes crop up in many places, and in fact variants have already been encountered in [48–54]. Suppose a strongly coupled field theory with a holographic dual is set up to flow across an obstacle, as might be achieved, for

1 Nontrivial predictions for nonequilibrium behavior based on equilibrium modes also are at the heart of the Kibble-Zurek mechanism [46, 47]. This analogy was pointed out previously in [9].

example, by applying a thermal gradient or an electric field. Suppose furthermore that this flow is disrupted by some obstacle, in other words that translation invariance along the flow is broken. In this case the system will arrange itself in such a way that there exists an asymptotic flow velocity, $\mathbf{v}_L$, far from the obstacle and 'to the left' and a generally different asymptotic flow velocity, $\mathbf{v}_R$, far from the obstacle and 'to the right'. See Figure 3.1 for an illustration. In between these asymptotic regions the flow will be complicated and strongly non-linear. Nevertheless, as we show, the spatial approach towards the asymptotic regions can be universally characterized using non-analytic features of correlation functions in the complex momentum plane. Holographically these correspond to linear modes of the perturbed black hole which are both regular at the future horizon and which decay appropriately as one of the asymptotic spatial regions is approached. These modes are what we call spatial collective modes (SCM), as they correspond to collective excitations governing the spacelike relaxation of the strongly coupled theory.

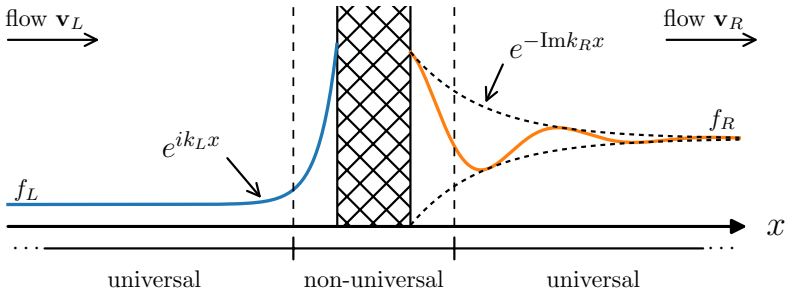

Figure 3.1: Schematic illustration of the nonequilibrium steady state corresponding to flow across an obstacle. Far to the left ($x \to -\infty$) and far to the right ($x \to +\infty$) the flow returns to a steady, homogeneous flow, different on each side. In the vicinity of the obstacle (hatched region) the flow is nonlinearly deformed. Connecting these two regions are a set of spatial collective modes which describe the exponential (and sometimes oscillatory) spatial relaxation back to equilibrium.

In situations where the underlying theory enjoys a boost invariance, an alternative point of view on these types of steady states is provided by transforming into the frame where the fluid on the upstream side of the obstacle is at rest. In this frame, then, the physical picture is one of dragging a co-dimension one obstacle through a fluid at rest, building up a bow wave in front and leaving a wake behind, whose spatial and temporal profiles are precisely what is captured universally by the SCM described in this chapter. A fixed position in the fluid at rest experiences modes which grow exponentially with time until the obstacle arrives (the bow wave), and then decay exponentially in time after the obstacle recedes (the wake). This alternative point of view is schematically depicted in Figure 3.2.

We give the definition of these SCM in full generality, underlining their universal appeal, but we also find it instructive to illustrate this fact by exhibiting these modes in a number of interesting contexts, both analytically and numerically. Two such contexts in which we have in fact analytical control over the spectrum of SCM is the three-dimensional BTZ black hole, as well as the Schwarzschild black brane in a large number of dimensions $d \to \infty$. In both cases we find that the SCM are purely decaying, in other words that their defining complex momenta are in fact purely imaginary. This is not a general feature of such modes, and we go on

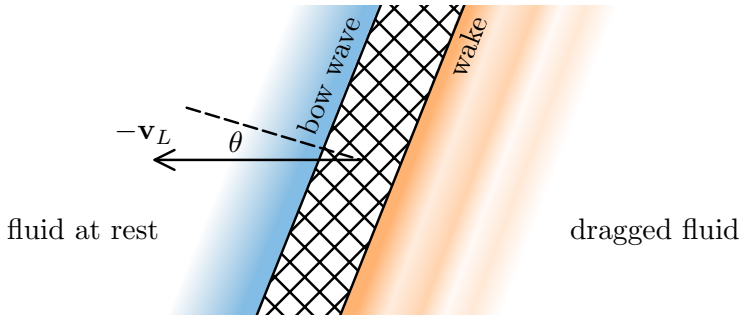

Figure 3.2: Schematic illustration of the nonequilibrium steady state of the type depicted in Figure 3.1 in a boosted frame where the upstream fluid is at rest (here we have allowed for a fluid flow incident angle θ). This corresponds to the time-dependent process of dragging a co-dimension one obstacle (hatched region) through a fluid at rest. As in Figure 3.1 the fluid returns to a steady homogeneous flow far from the obstacle, and the spatial collective modes describe this process, indicated here by the spatial profiles of a bow wave and a wake.

to demonstrate that oscillatory decaying modes which also have a non-vanishing real part of the complex momentum in fact exist. We find the requisite modes in certain regimes of the dual field theory at non-zero charge density, that is in a state that is dual to a bulk Reissner-Nordström black brane.

A second major focus of this chapter is a more detailed treatment of the numerical construction of non-equilibrium steady states dual to four-dimensional black branes with non-Killing horizons. Pursuing holographic insights into the physics of nonequilibrium steady states has proven to be a fruitful endeavour, as evidenced for example in [55–68], which all underline the efficiency of the holographic approach to far-from-equilibrium physics by elegantly exposing fascinating features such as emerging effective temperatures, non-equilibrium fluctuation relations, which are highly non-trivial to derive from a microscopic approach based on field theory methods. Holography serves both to reformulate the underlying non-equilibrium problem in terms of a well-posed system of partial differential equations, suitable for numerical solution, as well as to expose mechanisms and universal features through analytical insight. In this work we strive to combine both numerical and analytical insights into a quite general picture of the kind of situation described in [9], namely stationary flows over obstacles, first introduced in [67] and termed 'stationary quenches'.

These solutions were employed and briefly described in [9], and we wish to supply a more detailed treatment of both the properties of these intriguing solutions as well as the numerical methods employed in their construction as full non-linear solutions to the bulk Einstein equations. The method is a variant of the Einstein DeTurck method of [69] that applies to situations in which the generators of the bulk horizon are not Killing fields. This is essential for the non-equilibrium steady states we wish to construct, as these have broken translation invariance in the direction of the flow as mentioned above. We will also present a three dimensional example, based on the Janus solution of [70], where both the non-linear and the linear analysis can be carried out fully analytically, beautifully confirming our proposal of SCM in detail, that is we are able to exhibit exactly the dominant modes governing the spatial relaxation towards the left and right asymptotic regions. In

fact, we demonstrate that the black Janus solution itself should be viewed as a back-reacted version of the entire tower of SCM of the three dimensional ('BTZ') black hole, which we also construct analytically. Once this is appreciated, the spectrum of SCM can in fact be recovered as an inverse Laplace transform of the non-linear solution and is seen to coincide precisely with the aforementioned tower of SCM of the three-dimensional black hole.

The large array of examples we present in this chapter underscore the ubiquity of the modes proposed and defined in [9], and we conclude with an outline of further contexts and situations were they have promising applications. In particular as emphasised in [9] some of the dominant modes decay universally with a length proportional to η/s, presenting new opportunities to experimentally determine this ratio for strongly interacting many body systems.

The structure of this chapter is as follows. In section 3.2 we give a definition of SCM from a purely field theoretic perspective focusing on translation symmetry breaking, followed by a simple example drawn from hydrodynamic diffusion. We then work out the complete theory of SCM in charged hydrodynamics before doing the same in bulk Einstein-Maxwell theory. The remainder of section 3.2 serves to illustrate the general definitions with a host of examples, notably a fully analytic treatment in the large-dimension limit of the bulk, as well as the three-dimensional case. In the latter we have constructed a fully non-linear examples, based on the black Janus solution, and we dedicate section 3.3 to a detailed study of this illuminating example. Section 3.4 is dedicated to a detailed description of the numerical method employed in constructing examples of non-linear steady states where an analytical treatment is not possible. The final section, 3.5 recaps the most salient features of our analysis and gives an outlook of some interesting future directions. Certain technical details throughout are relegated to two appendices to avoid overly complicating the main thrust of the chapter.

3.2 UNIVERSAL MODES IN GRAVITY AND HYDRODYNAMICS

Our first task will be to characterise the modes which play the central role in this chapter. These modes achieve for breaking spatial translations what quasinormal modes achieve for the breaking of time-translations.

When a system is perturbed by adding a time dependent source, one can extract universal features of the late-time decay by studying certain modes in the complex frequency plane, the quasinormal modes (QNM). This is to be contrasted with our nonequilibrium steady states, where the system is perturbed along a distinguished spatial direction. Then its universal spatial relaxation at large distances from the disturbance is given by stationary collective modes (SCM), to be defined below.

3.2.1 *Definition of stationary collective modes*

Let us commence with a seemingly standard discussion, namely the evaluation of expectation values of operators in the interaction ('Dyson') representation of a

quantum field theory. Let us suppose we have the four-momentum vector P^μ of the undeformed theory, such that a Heisenberg picture operator is given by

$$\Phi(x^\mu) = e^{-iP_\mu x^\mu}\Phi e^{iP_\mu x^\mu}\,. \tag{3.1}$$

Correspondingly we have the Heisenberg equation of motion for the evolution operator

$$\partial_\mu\Phi(x) = i\left[P_\mu,\Phi\right] \qquad \Leftrightarrow \qquad \frac{\partial U(x,x_0)}{\partial x^\mu} = iP_\mu U(x,x_0) \tag{3.2}$$

Usually in quantum field theory, one takes the zero component of this equation to define the time evolution of the system in question, and interprets the spatial components as giving the momentum of the system governed by its Hamiltonian evolution. For reasons that will become clear, we continue with the covariant treatment for the time being. We then have the formal solution

$$U(x,x_0) = \mathrm{P}\exp\left(i\int_{x_0}^{x} P_\mu dx'^\mu\right) \tag{3.3}$$

in terms of the path-ordered exponential function, in the sense that one should interpret the integral as being a long a parametric curve $x^\mu(s)$ with $x^\mu(s_i) = x_0^\mu$ and $x^\mu(s_f) = x^\mu$ and the operators appearing being ordered in increasing order with respect to the parameter s. Say we now deform the theory by adding a term

$$U(x,x_0) \to U^{\text{Heis.}}(x,x_0) = \mathrm{P}\exp\left(i\int_{x_0}^{x} (P_\mu + p_\mu)dx'^\mu\right)\,, \tag{3.4}$$

where we have emphasized that we naturally obtain the evolution operator of the deformed theory in the Heisenberg picture. It is then customary to switch to the 'interaction' representation, where states evolve according to the undeformed theory, i.e. with respect to U, while operators evolve according to

$$\Phi(x^\mu) = U^{\dagger\text{int}}(x,x_0)\Phi(x_0)U^{\text{int}}(x,x_0) \qquad \text{with} \qquad U^{\text{int}}(x,x_0) = \mathrm{P}\exp\left(i\int_{x_0}^{x} p_\mu dx'^\mu\right)\,, \tag{3.5}$$

where the x^μ dependence of p_μ itself is governed only by the undeformed evolution operator $U(x,x_0)$. This construction is particularly useful if we are interested in evaluating the influence of a perturbation on expectation values of the system. Let us examine this for our operator Φ above, with respect to the deformation p_μ. We have

$$\begin{aligned}\langle\Phi(x)\rangle &= \left\langle \mathrm{P}\exp\left(-i\int_{x_0}^{x} p_\mu dx'^\mu\right)\Phi\,\mathrm{P}\exp\left(i\int_{x_0}^{x} p_\mu dx^\mu\right)\right\rangle \\ &= \langle\Phi(x)\rangle_0 - i\int_{x_0}^{x}\left\langle\left[\Phi(x),p_\mu(x')\right]\right\rangle_0 dx'^\mu + \cdots\end{aligned} \tag{3.6}$$

up to first order in the deformation. The subscript '0' on the correlator indicates that the expectation value is to be evaluated in the undeformed state. We will now describe a familiar example, where one adds an explicitly time-dependent term to the Hamiltonian of the system, before turning to the less familiar example that is the focus of this work.

BROKEN TIME TRANSLATIONS

The familiar case usually involves the choice $p^\mu = h(t)\delta^{\mu 0}$, which leads to the well-known result

$$\begin{aligned} \delta \langle \Phi(t,\mathbf{x}) \rangle &= i \int_{-\infty}^{t} \langle \left[\Phi(t,\mathbf{x}), h(t') \right] \rangle_0 \, dt' \\ &= \int_{-\infty}^{\infty} F(t') G_R(t-t', \mathbf{x}-\mathbf{x}') dt' d\mathbf{x}' \end{aligned} \tag{3.7}$$

where in the second line we have specialised to an $h(t)$ given by an external source $h(t) = \int F(t)\Phi(t,\mathbf{x})d\mathbf{x}$, and we have introduced the retarded correlation function

$$G_R(t-t', \mathbf{x}-\mathbf{x}') := i\theta(t-t') \left\langle \left[\Phi(t,\mathbf{x}) \, , \Phi(t',\mathbf{x}') \right] \right\rangle_0 \tag{3.8}$$

The presence of the Heaviside function, which simply came from extending the integration range to $(-\infty, \infty)$, has the important consequence that the Fourier transform $\hat{G}_R(\omega, \mathbf{k})$ is analytic in the upper-half complex frequency plane, but may contain poles or branch cuts in the lower half plane.

Let us conclude this section by remarking that a system with the deformed Hamiltonian $H = H_0 + h(t)$ does not conserve energy, while momentum remains a conserved quantity

$$[H, E] \neq 0, \qquad \text{while} \qquad [H, P_i] = 0, \tag{3.9}$$

which is a direct consequence of the Heisenberg equations of motion (3.2) applied to the deformed Hamiltonian.

BROKEN SPATIAL TRANSLATIONS

We now consider situations in which translation invariance is explicitly broken along a special direction $\mathbf{s}$, while it remains intact along the remaining spatial directions, $\mathbf{x}^\parallel$. Let us define some coordinates by writing $\mathbf{x} = (\mathbf{x}\cdot\hat{\mathbf{s}}, \mathbf{x}^\parallel) = (x, \mathbf{x}^\parallel)$. Let us thus examine the choice of deformation $p^\mu = p(x)s^\mu$, for some spacelike vector $s^\mu = (0, \hat{\mathbf{s}})$, along which we assume spatial homogeneity to be broken, while all other directions remain homogeneous[2]. A particular example of such a situation is given by the type of non-equilibrium steady states mentioned in the introduction, where we consider the stationary states of an interacting quantum fluid flowing over an obstacle, the obstacle being evidently the origin of the breaking of spa-

2 An alternative picture of this situation may be given as follows: let us, for argument's sake, consider adding a term $\int F(x')\phi(t,x',\mathbf{x}^\parallel)dx'd\mathbf{x}^\parallel$ to the Hamiltonian. Here x' is the special direction along which translation invariance is broken. Then the exponent of the evolution operator (3.1) formally gets a new contribution of the form

$$Ht - \mathbf{P}\cdot\mathbf{x} \to Ht - \mathbf{P}\cdot\mathbf{x} + \int_{-\infty}^{t} F(x')\phi(t',x',\mathbf{x}^\parallel)dx d\mathbf{x}^\parallel dt' \, .$$

Since we are interested in steady states, we may safely take the $t \to \infty$ limit. We now specialize to a source $F(x') = \Theta(x-x')f(x')$. At this point, it becomes more natural to actually think of the deformation as pertaining to the momentum operator, so that

$$\mathbf{P}\cdot\mathbf{x} \to \mathbf{P}\cdot\mathbf{x} - \int_{-\infty}^{x} p(x')dx'$$

with $p(x') := \int F(t,x',\mathbf{x}^\parallel)\phi(t,x',\mathbf{x}^\parallel)dtd\mathbf{x}^\parallel$. This is precisely the spacelike case treated above.

tial translations. This also explains the 'parallel' superscript which refers to the directions which are unbroken, i.e. parallel to the obstacle. This gives[3]

$$\begin{aligned}\delta\langle\Phi(t,\mathbf{x})\rangle &= -i\int_{-\infty}^{\mathbf{x}\cdot\hat{\mathbf{s}}}\left\langle\left[\Phi(t,\mathbf{x}),p(x')\right]\right\rangle_0 s_\mu dx'^\mu \\ &= -i\int_{-\infty}^{x}\left\langle\left[\Phi(t,\mathbf{x}),p(x')\right]\right\rangle_0 dx' \\ &= \int_{-\infty}^{\infty}F(x')G^{[\searrow]}(t-t',x-x',\mathbf{x}^{\parallel}-\mathbf{x}^{\parallel\prime}\|)dt'd\mathbf{x}'\,. \end{aligned} \tag{3.10}$$

In the first line the upper limit of the integral instructs us to integrate along the direction s^μ up to the spatial position $\mathbf{x}\cdot\hat{\mathbf{s}}$ of the operator we are interested in measuring. In the second line we have introduced the parametrization $s_\mu dx^\mu = dx$ and written the limits on the integral accordingly. The source $F(x)$ now depends only on the spatial direction x. Finally, in the last step we have written the deformation as $p(x) = \int F(\mathbf{x}\cdot\hat{\mathbf{s}})\Phi(t,\mathbf{x})dtd\mathbf{x}^{\parallel}$, and introduced the 'decay to the right' correlator

$$G^{[\searrow]}(x-x') = -i\theta(x-x')\left\langle\left[\Phi(t,\mathbf{x})\,,\Phi(t',\mathbf{x}')\right]\right\rangle_0 \tag{3.11}$$

where we have suppressed the dependence with respect to $t-t'$ and the remaining spatial directions for simplicity. At first sight this looks very unfamiliar, taking the form of a 'retarded' correlation function with respect to some spatial direction. We now explain why such a definition is useful.

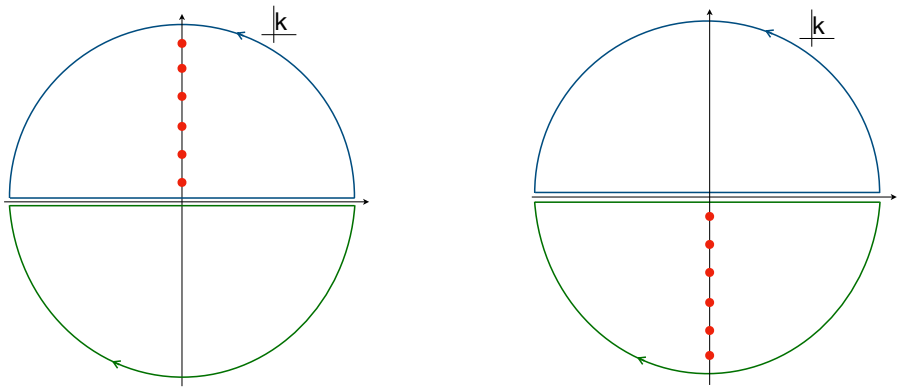

Figure 3.3: (color figure) poles of the Fourier transform of the 'decay to the right' correlation function, $\hat{G}^{[\searrow]}(k)$, and of the 'decay to the left' correlation function, $\hat{G}^{[\swarrow]}(k)$, in this order, and as defined in the text. The blue contour corresponds to the region to the right of the obstacle, and the green contour to the left.

We first note that the Fourier transform of this object with respect to the special direction

$$\hat{G}^{[\searrow]}(k) := \int\frac{dx}{2\pi}G^{[\searrow]}(x)e^{-ikx} \tag{3.12}$$

is analytic in the lower half complex k plane, but may show non-analytic features, such a poles and branch cuts in the upper half complex k plane. This corresponds to the situation illustrated in Figure 3.3 and gives rise to modes that are decaying in the positive x direction. In other words, there is an obstacle breaking spatial

3 By assumption our system is in a steady state with respect to the undeformed Hamiltonian. Therefore the entire time dependence, comes from the undeformed part of the Hamiltonian.

homogeneity in the special direction, and we enquire about the spatial profile of the expectation value of Φ to the right of the obstacle. The relevant physical solutions contributing to this quantity are therefore modes which have regular, i.e. decaying, behavior as we approach the right asymptotic region $x \to +\infty$, while they are unconstrained as $x \to -\infty$.

The analytic structure discussed here parallels what is found in the $\omega \to 0$ limit of [49], and we refer the reader to this work for an insightful discussion. Illustrating further the ubiquity of SCM, these authors study modes at complex momentum in the context of equilibrium attenuation lengths of a holographic plasma, while our present work emphasizes the relevance of SCM to non-equilibrium properties of stationary states.

The analogously defined correlator

$$G^{[\swarrow]}(x - x') = i\theta(x' - x) \left\langle \left[\Phi(t, \mathbf{x}) \, , \Phi(t', \mathbf{x}')\right] \right\rangle_0 \tag{3.13}$$

instead involves only excitations which are regular as the left asymptotic region $x \to -\infty$ is approached, while being unconstrained for $x \to +\infty$. The corresponding Fourier transform

$$\hat{G}^{[\swarrow]}(k) := \int \frac{dx}{2\pi} G^{[\swarrow]}(x) e^{-ikx} \tag{3.14}$$

is analytic in the upper half complex k plane, while allowing for non-trivial structure in the lower half complex plane, illustrated in Figure 3.3. In a further analogy to the previous subsection, the system described here conserves energy, but does not conserve momentum

$$[H, E] = 0, \qquad \text{while} \qquad [H, P_i] \neq 0 \, . \tag{3.15}$$

Without anticipating too much of our discussion in section 3.2.5 below, let us briefly remark that these modes can be computed from a simple holographic prescription. There SCM are found by studying linear modes around a finite-v black brane background, which are regular at the future horizon as well as regular for $x \to \infty$ for $G^{[\searrow]}(k)$ or regular as $x \to -\infty$ for $G^{[\swarrow]}(k)$, where x is the distinguished direction along which translational symmetry is broken.

We will now illustrate our definitions in various different situations. We will start by a simple example, namely the hydrodynamic theory of diffusion. We will then work out the general description within a charged relativistic hydrodynamic effective theory before moving on to holography in a number of different contexts. The latter remains the focus of this chapter, so we aim on giving a clear prescription of how to compute these modes in theories with holographic duals.

3.2.2 *A simple hydrodynamic example*

Let us furnish the definition above with a simple example. Consider a diffusive linear fluctuation, $n(t, \mathbf{x})$, obeying the equation

$$\left(u^\mu \partial_\mu - D\Delta^{\mu\nu}\partial_\mu \partial_\nu\right) n(t, \mathbf{x}) = 0, \tag{3.16}$$

with diffusion constant $D \geq 0$ where u^μ is unit-normed, timelike and future directed, which we may parameterise by a $(d-1)$-velocity, $u^\mu = \gamma(1, \mathbf{v})^\mu$, where $\gamma = (1 - \mathbf{v}\cdot\mathbf{v})^{-1/2}$. The projector orthogonal to u^μ is given by $\Delta^{\mu\nu} = \eta^{\mu\nu} + u^\mu u^\nu$. With the choice $\mathbf{v} = \mathbf{0}$ (3.16) reduces to the diffusion equation. A defining feature of the modes we are interested in is the absence of temporal growth or decay since we are seeking the late time behaviour of a system, and this may be either steady or time-oscillatory. A second defining feature of the collective modes is unbounded growth in one spatial direction. This is so that the mode can grow in order to match on to a source, such as an obstacle. Let us therefore single out the coordinate $x = \mathbf{x}\cdot\hat{\mathbf{s}}$ (see above), in which we permit unbounded growth, and we denote all other spatial directions by $\mathbf{x}_\parallel$ in which we do not. For convenience we can decompose in Fourier modes in t and $\mathbf{x}_\parallel$,

$$n(t, x, \mathbf{x}_\parallel) = \int \frac{d\omega d^{d-1}k_\parallel}{(2\pi)^d} \hat{n}(x, \omega, \mathbf{k}_\parallel) e^{i\mathbf{k}_\parallel\cdot\mathbf{x}_\parallel - i\omega t}, \tag{3.17}$$

and then the desired stationarity / temporal regularity condition is expressed by $\mathrm{Im}\omega = 0$ and the desired spatial regularity condition is expressed by $\mathrm{Im}\mathbf{k}_\parallel = 0$, whilst $\hat{n}(x, \omega, \mathbf{k}_\parallel)$ may be unbounded in x. We make no restriction on $\mathbf{v}$ in general, but for the sake of simplicity in this example we restrict to flows which satisfy $\mathbf{v}_\parallel \cdot \mathbf{k}_\parallel = 0$. Solutions to (3.16) are then given by,

$$\hat{n}(x, \omega, \mathbf{k}_\parallel) = A_+ e^{\alpha_+ x} + A_- e^{\alpha_- x} \tag{3.18}$$

where

$$\alpha_\pm = \frac{1}{2\gamma D}\left(v \mp \sqrt{v^2 + 4D^2k_\parallel^2 - \frac{4Di\omega}{\gamma}}\right) + vi\omega. \tag{3.19}$$

With the given conditions on $D, k_\parallel, \omega$ one can prove that $\mathrm{Re}\alpha_+ \leq 0$ when $v \geq 0$ and so the associated mode (with coefficient A_+) does not diverge as $x \to +\infty$. Thus this mode describes decay in the downstream direction. Similarly the α_- mode describes decay in the upstream direction.

In the notation of section 3.2.1, the α_- mode would appear as a pole in $\hat{G}^{[\swarrow]}(k)$, while the α_+ mode would appear as a pole in $\hat{G}^{]\searrow]}(k)$.

We note that $\mathbf{k}_\parallel \neq 0$ cannot induce a nonzero $\mathrm{Im}\alpha_-$ at $\omega = 0$, but such oscillations are seen if $\omega \neq 0$ – a source that is oscillating in time leaves an imprinted pattern on both the upstream and downstream sides of the flow, with a wavelength set by the velocity of the flow itself.

Finally, let us remark that a similar hydrodynamic analysis for the timelike case would appear to give rise to modes that appear as poles both in the retarded and the advanced correlation function. This is actually not the case, as the diffusive nature of the hydrodynamic equation dictates a direction of time and therefore selects one or the other of the retarded or advanced correlation function depending on the sign of D. In other words, one cannot run the diffusion equation backwards in time without un-physically changing the sign of the diffusion constant. There is an interesting link with analyticity and causality underpinning this behavior, which we further elaborate in the discussion section.

3.2.3 *Charged hydrodynamics*

Although we are mostly concerned with two and three dimensional field theories, the analysis is easily performed in d space-time dimensions. As usual in hydrodynamics we begin by writing down the stress tensor and current in a derivative expansion

$$T_{\mu\nu} = T^{(0)}_{\mu\nu} + \Pi^{(1)}_{\mu\nu} + O(\partial)^2, \tag{3.20}$$

$$J_\mu = J^{(0)}_\mu + J^{(1)}_\mu + O(\partial)^2 \tag{3.21}$$

where, up to first order, we have the Landau frame expressions

$$T^{(0)}_{\mu\nu} = \varepsilon u_\mu u_\nu + p\Delta_{\mu\nu}, \tag{3.22}$$

$$\Pi^{(1)}_{\mu\nu} = -\eta\sigma_{\mu\nu} - \zeta\Delta_{\mu\nu}\partial\cdot u, \tag{3.23}$$

$$J^{(0)}_\mu = nu_\mu, \tag{3.24}$$

$$J^{(1)}_\mu = -\sigma T\Delta_\mu{}^\nu\partial_\nu\left(\frac{\mu}{T}\right). \tag{3.25}$$

Here the shear tensor is given by

$$\sigma_{\mu\nu} = 2\Delta_\mu{}^\rho\Delta_\nu{}^\sigma\left(\partial_{(\rho}u_{\sigma)} - \frac{1}{d-1}\eta_{\rho\sigma}\partial\cdot u\right), \tag{3.26}$$

where ε is the energy density, p is the pressure, u^μ is a timelike unit-normalised d-velocity field while n is the charge density. The tensor $\Delta^{\mu\nu} = \eta^{\mu\nu} + u^\mu u^\nu$ projects orthogonally to u^μ. The quantities η and ζ are the shear and bulk viscosities, and σ is the charge conductivity. The energy-stress tensor and the current are subject to conservation equations:

$$\partial_\mu T^{\mu\nu} = 0, \tag{3.27}$$

$$\partial_\mu J^\mu = 0. \tag{3.28}$$

These conservation laws give rise to $d+1$ equations for the $d+2$ unknowns contained in u^μ, ε, p, n. Consequently, this system of equations still needs to be closed by specifying an equation of state $p(T,\mu)$. This equation of state depends on the physical system under consideration, but for the majority of this chapter we are interested in holographic field theories, which are conformal in the UV. The required general conformal equation of state, and the specific example of the conformal equation of state for the Reissner-Nordström solution can be found in appendix A together with its associated transport coefficients.

In order to find the collective modes, we solve the conservation equations for linear perturbations about a long-range stationary state characterised by ε, p, n and

a $(d-1)$ velocity $\mathbf{v}$, such that $u^\mu = \gamma(1,\mathbf{v})$ where $\gamma = \frac{1}{\sqrt{1-\mathbf{v}\cdot\mathbf{v}}}$. We then consider time-independent perturbations of the form

$$\varepsilon\left(x^\mu\right) = \varepsilon + \delta\varepsilon\, e^{ik_\sigma x^\sigma}, \tag{3.29}$$
$$p\left(x^\mu\right) = p + \delta p\, e^{ik_\sigma x^\sigma}, \tag{3.30}$$
$$n\left(x^\mu\right) = n + \delta n\, e^{ik_\sigma x^\sigma}, \tag{3.31}$$
$$u^\mu\left(x^\mu\right) = u^\mu + \delta u^\mu\, e^{ik_\sigma x^\sigma}. \tag{3.32}$$

The modes we are interested in are time independent in the laboratory frame, namely the frame in which we have a steady state, that is they have $k_\mu = (0,\mathbf{k})$ in the frame where $u^\mu = \gamma(1,\mathbf{v})$. Inserting these perturbations into the energy-stress tensor, we find

$$\delta T^{\mu\nu}_{(0)} = \left(u^\mu u^\nu \delta\varepsilon + \Delta^{\mu\nu}\delta p + 2(\varepsilon+p)u^{(\mu}\delta u^{\nu)}\right) e^{ik_\sigma x^\sigma}, \tag{3.33}$$
$$\delta\Pi^{\mu\nu}_{(1)} = \left(-2\eta\Delta^{\rho(\mu}\delta u^{\nu)} + \left(\frac{2\eta}{d-1} - \zeta\right)\Delta^{\mu\nu}\delta u^\rho\right) ik_\rho e^{ik_\sigma x^\sigma}. \tag{3.34}$$

The conservation equations (3.27) then give

$$ik_\mu \delta T^{\mu\nu}_{(0)} + ik_\mu \delta\Pi^{\mu\nu}_{(1)} + O(k^3) = 0, \tag{3.35}$$
$$ik_\mu J^\mu_{(0)} + ik_\mu J^\mu_{(1)} + O(k^3) = 0\,. \tag{3.36}$$

Finally let us use the equation of state to define the suceptibilities

$$\alpha_1 = \left(\frac{\partial\mu}{\partial\varepsilon}\right)_n - \frac{\mu}{T}\left(\frac{\partial T}{\partial\varepsilon}\right)_n, \quad \alpha_2 = \left(\frac{\partial\mu}{\partial n}\right)_\varepsilon - \frac{\mu}{T}\left(\frac{\partial T}{\partial n}\right)_\varepsilon \tag{3.37}$$

and

$$\beta_1 = \left(\frac{\partial p}{\partial\varepsilon}\right)_n, \quad \beta_2 = \left(\frac{\partial p}{\partial n}\right)_\varepsilon. \tag{3.38}$$

We now have all formulae and definitions in place to determine our SCM. Once an equation of state is specific these quantities can be found explicitly, see for example A for the case of the conformal equation of state in d dimensions. In the following, it is most convenient to split the analysis into different channels, according to whether the velocity field perturbation is transverse or longitudinal with respect to the momentum.

3.2.3.1 *Transverse channel*

We start with the transverse channel, that is velocity field perturbations δu, such that $k\cdot\delta u = 0$. We find

$$(k\cdot u)\delta n - i\sigma\Delta_{k^2}\left(\alpha_1\delta\varepsilon + \alpha_2\delta n\right) = 0 \tag{3.39}$$
$$(k\cdot u)u^\nu\delta\varepsilon + k_\mu\Delta^{\mu\nu}\left(\beta_1\delta\varepsilon + \beta_2\delta n\right) + (\varepsilon+p)\,(k\cdot u)\delta u^\nu - i\eta\Delta_{k^2}\delta u^\nu = 0 \tag{3.40}$$

where here and below we use the shorthand

$$\Delta_{k^2} = k_\mu k_\nu \Delta^{\mu\nu}\,. \tag{3.41}$$

Let us first examine the case when $k \cdot u = 0$, i.e. when the momentum of the perturbation, in addition to being transverse to δu, is also transverse to the background flow velocity. First we note that the stress-tensor conservation, contracted with u gives the relation

$$(k \cdot u)\delta\varepsilon = -(\varepsilon + p)k \cdot \delta u \tag{3.42}$$

i.e. that $k \cdot u = 0$ implies that the perturbation is transverse $k \cdot \delta u = 0$. Assuming this is the case, the charge conservation equation gives

$$\delta n = -\frac{\alpha_1}{\alpha_2}\delta\varepsilon \tag{3.43}$$

which when plugged back into the stress tensor conservation tells us that

$$\delta u^\mu = \frac{\alpha_2\beta_1 - \alpha_1\beta_2}{i\eta\alpha_2}\frac{k^\mu}{k^2}\delta\varepsilon\,. \tag{3.44}$$

However, this contradicts our assumption that δu is normal to k, implying that our system of equations has no solution unless the quantity in the numerator above vanishes. As we will see below, this combination of susceptibilities is related to the charge diffusion constant, which is generically non-zero. We conclude that no non-trivial mode for $k \cdot u = 0$ exists. We may thus proceed with our analysis, assuming $k \cdot u \neq 0$.

In order to make further progress, we start by projecting Eq. (3.40) onto u^μ, keeping in mind that the normalization condition on the flow velocity implies that $u \cdot \delta u = 0$. We immediately find that $\delta\varepsilon = 0$. Projecting (3.40) onto k, we discover in addition that $\delta n = 0$. Notice that this follows from the fact that $\Delta_k^2 \neq 0$, since both contributing terms are positive definite for our choice of k^μ in the lab frame. We are thus left with the nontrivial condition

$$\left[(\varepsilon + p)(k \cdot u) - i\eta\Delta_{k^2}\right]\delta u^\mu = 0 \tag{3.45}$$

Writing

$$u^\mu = \gamma(1, \mathbf{v})\,, \qquad k^\mu = (0, \mathbf{k})^\mu\,, \tag{3.46}$$

so that $\mathbf{v} \cdot \mathbf{k} = vk\cos\theta$, we conclude that there is a non-trivial transverse mode with dispersion relation

$$(\varepsilon + p)\frac{kv\cos\theta}{\sqrt{1 - v^2}} - i\eta k^2\frac{1 - (v\sin\theta)^2}{1 - v^2} + O(k^3) = 0. \tag{3.47}$$

for which

$$\delta\varepsilon = \delta n = 0\,, \qquad \delta u^\mu \neq 0\,, \qquad (\text{with} \quad k \cdot \delta u = 0)\,. \tag{3.48}$$

This concludes our analysis of the transverse channel. Let us now turn to the longitudinal channel.

3.2.3.2 *Longitudinal channel*

A longitudinal perturbation satisfies $\delta u^\mu = \delta u_L \Delta^{\mu\nu}k_\nu/k$, where $k = \sqrt{k_\mu k^\nu}$ is the norm of the spacelike momentum. As we argued above, without loss of generality we can take $k \cdot u \neq 0$ in the longitudinal channel and we do so from now on. There

are three independent modes in this channel, which we determine as follows. We first substitute the form of δu_L into the dynamical equations (3.35). These then take the form of a scalar equation (the current conservation equation) and a vector equation (the stress tensor conservation equation). We may use the equation of state to eliminate δp from these, and finally project the vector equation first onto k_μ and then onto u_μ. This results in the following system of three linear equations

$$\begin{pmatrix} k\cdot u & 0 & (\varepsilon+p)\frac{\Delta_k^2}{k} \\ -i\sigma\Delta_k^2\alpha_1 & k\cdot u - i\sigma\Delta_k^2\alpha_2 & n\frac{\Delta_k^2}{k} \\ \frac{\Delta_k^2}{k}\beta_1 & \frac{\Delta_k^2}{k}\beta_2 & \frac{\Delta_k^2(\varepsilon+p)}{k^2}\left(k\cdot u - i\Delta_k^2\gamma_s\right) \end{pmatrix} \begin{pmatrix} \delta\varepsilon \\ \delta n \\ \delta u_L \end{pmatrix} + \begin{pmatrix} 0 \\ O(k)^3 \\ O(k)^3 \end{pmatrix} = 0\,, \tag{3.49}$$

expanded in small momentum k and where we have defined

$$\gamma_s \equiv \frac{\frac{d-2}{d-1}2\eta+\zeta}{\varepsilon+p}. \tag{3.50}$$

Note that the first of these equations corresponds to the conservation of energy and is exact in k. The second of these is the charge conservation equation and is correct to second order in k with order k^3 terms truncated. The remaining equation is correct to second order in k. A physical mode, that is a hydrodynamic SCM, corresponds to a non-trivial solution of this linear equation, in other words an eigenmode with eigenvalue zero. Each eigenvalue is a polynomial in k and the vanishing of this polynomial gives the dispersion relation of a non-trivial longitudinal SCM admitted by the system of equations (3.27).

We shall now explicitly construct the eigenvalues and associated eigenmodes for the system (3.49), working order-by-order in k. Specifically, denoting the matrix multiplying $(\delta\varepsilon, \delta n, \delta u_L)^{\mathrm{T}}$ in (3.49) by M, we wish to solve,

$$M\cdot V_I = \lambda_I V_I \tag{3.51}$$

where $I = 1,2,3$ labels the eigenmode. As in the transverse channel we have $\mathbf{v}\cdot\mathbf{k} = vk\cos\theta$. Next we expand as follows in powers of k,

$$\begin{aligned} M &= M^{(1)}k + M^{(2)}k^2 + O(k)^3 && (3.52)\\ V_I &= V_I^{(0)} + V_I^{(1)}k + O(k)^2 && (3.53)\\ \lambda_I &= \lambda_I^{(1)}k + \lambda_I^{(2)}k^2 + O(k)^3 && (3.54)\\ v\to v_I &= v_I^{(0)} + v_I^{(1)}k + O(k)^2 && (3.55) \end{aligned}$$

Then we solve the eigenmode equation (3.51), where at each order setting $\lambda_I^{(n)} = 0$ determines $v_I^{(n-1)}$ for the mode in question labelled by I. Note that in the results that follow we have fixed a freedom to shift $V_I^{(1)}$ by a multiple of $V_I^{(0)}$, and we have done so simply by looking for the most compact presentation.

At $\mathcal{O}(k)$ we have the following eigenmode problem,

$$M^{(1)}\cdot V_I^{(0)} = \lambda_I^{(1)} V_I^{(0)} \tag{3.56}$$

which we solve directly to obtain V_I^0 and $\lambda_I^{(1)}$. Each solution to this leading order problem picks a different physical mode, with $\lambda_I^{(1)} = 0$ corresponding to the leading order part of its dispersion relation. In the following we shall treat each in turn, denoting $c_\theta \equiv \cos\theta$ and $s_\theta \equiv \sin\theta$, for compactness.

DIFFUSIVE MODE

In this case the fluctuations, up to first order in the momentum expansion, have dispersion relation and eigenmodes, given by

$$v = i\frac{D_{\alpha\beta}}{c_\theta}k + O(k)^2 \tag{3.57}$$

$$\{\delta\varepsilon, \delta n, \delta u_L\}^{(0)} = \{-\beta_2, \beta_1, 0\} \tag{3.58}$$

$$\{\delta\varepsilon, \delta n, \delta u_L\}^{(1)} = \left\{0, 0, i\beta_2\frac{D_{\alpha\beta}}{\varepsilon + p}\right\} \tag{3.59}$$

Where we have defined a diffusion constant and the speed of sound,

$$D_{\alpha\beta} = \sigma\frac{\alpha_2\beta_1 - \alpha_1\beta_2}{c_s^2}\,, \qquad c_s^2 \equiv \beta_1 + \frac{n}{\varepsilon + p}\beta_2\,. \tag{3.60}$$

We may think of this mode as primarily accounting for charge density perturbations since, for example, in a conformal theory ($\beta_2 = 0$, see appendix A) it consists solely of δn, even at nonzero background velocities. In more general theories, we still have a diffusive (purely imaginary) dispersion relation for charge fluctuations, which are, however, coupled to non-trivial energy and velocity fluctuations.

SOUND-LIKE MODES

For sound-like modes the fluctuations, up to first order in the momentum expansion, take the form

$$v = \pm v_0 + i\Gamma\frac{\left(1 - s_\theta^2 v_0^2\right)^2}{2c_\theta}\gamma_0 k + O(k)^2 \tag{3.61}$$

$$\{\delta\varepsilon, \delta n, \delta u_L\}^{(0)} = \left\{\left(1 - s_\theta^2 v_0^2\right)\gamma_0^2(\varepsilon + p), \left(1 - s_\theta^2 v_0^2\right)\gamma_0^2 n, \mp c_\theta\gamma_0 v_0\right\} \tag{3.62}$$

$$\{\delta\varepsilon, \delta n, \delta u_L\}^{(1)} = \gamma_0^3\left(1 - s_\theta^2 v_0^2\right)\left\{0, \pm ic_\theta v_0\frac{\Gamma - \gamma_s}{\beta_2(\varepsilon + p)}, -\frac{i}{2}\gamma_0\left(1 - (1 + c_\theta^2)v_0^2\right)\Gamma\right\} \tag{3.63}$$

where we have introduced a second diffusion constant

$$\Gamma \equiv \gamma_s + \frac{\sigma\beta_2\left(\alpha_1 + \frac{n}{\varepsilon+p}\alpha_2\right)}{c_s^2}, \tag{3.64}$$

and where $\gamma_0 = \frac{1}{\sqrt{1 - v_0^2}}$ for a speed of sound modified by the angle of incidence,

$$v_0 = \frac{c_s}{\sqrt{c_s^2 s_\theta^2 + c_\theta^2}}. \tag{3.65}$$

Note that this mode does not contain any δn component for neutral backgrounds $\mu = n = 0$.

Let us now further explain why we used the terminology *diffusive* and *sound like* for our SCM, which will also show that Γ is related to conventional sound attenuation.

RELATION TO CONVENTIONAL HYDRODYNAMIC MODES

Our SCM in the laboratory frame are defined to have vanishing imaginary part of the frequency and appear for complex values of momentum. For simplicity we here restrict to zero frequency. More generally one can also consider SCM with nonzero frequency similar to the equilibrium modes studied in [49]. Due to the underlying Lorentz symmetry it is possible, at least formally, to transform these modes back into the rest frame of the fluid. There they can be analytically continued into modes which satisfy dispersion relations, more conventionally associated with hydrodynamic modes, or in the gravity case, hydrodynamic quasinormal modes. In this way the diffusive SCM is related to ordinary charge diffusion in the fluid rest frame where this mode obeys the dispersion relation $\omega = -iD_{\alpha\beta}q^2$. Similarly the sound-like SCM is related via boost and analytic continuation to a standard sound mode with dispersion relation $\omega = \pm c_s q - i\frac{\Gamma}{2}q^2$. We emphasize once more that this procedure relies on the Lorentz symmetry of the underlying theory, as well as analytic continuation, and will fail for a non-relativistic theory. In general, i.e. in the absence for Lorentz symmetry, the SCM considered in this chapter, are physically distinct from and independent of quasinormal modes.

3.2.4 *Neutral hydrodynamics*

Here we review briefly the special case of a neutral fluid, which was previously discussed in [9]. In the present context the results of [9] can be recovered simply as the limit of zero charge density, $n \to 0$, of the charged case. For completeness we repeat the salient equations here. [9] did not consider charge density fluctuations, as there was no bulk gauge field. In that case, only the sound-like mode arises, whose dispersion relation indeed corresponds to the $n \to 0$ limit of (3.61).

3.2.4.1 *Transverse channel*

The analysis for the transverse mode proceeds as for the charged case above, resulting in the un-modified transverse mode dispersion relation

$$(\varepsilon + p)\frac{kv\cos\theta}{\sqrt{1-v^2}} - i\eta k^2 \frac{1-(v\sin\theta)^2}{1-v^2} + O(k^3) = 0\,, \tag{3.66}$$

which was given previously in [9].

3.2.4.2 *Longitudinal channel*

DIFFUSIVE MODE

We again have a diffusive mode with dispersion relation $v = i\frac{D_{\alpha\beta}}{c_\theta}k + O(k)^2$, and mode structure

$$\{\delta\varepsilon, \delta n, \delta u_L\}^{(0)} = \{-\beta_2, \beta_1, 0\} \tag{3.67}$$

$$\{\delta\varepsilon, \delta n, \delta u_L\}^{(1)} = \left\{0, 0, i\beta_2 \frac{D_{\alpha\beta}}{\varepsilon + p}\right\}. \tag{3.68}$$

The constant $D_{\alpha\beta}$ is defined as before, and the speed of sound reduces to $c_s^2 \equiv \beta_1$. This mode is primarily a charge diffusion mode, and was consequently not considered in the analysis of the neutral fluid in [9].

SOUND-LIKE MODES

Finally, we have the sound mode with dispersion relation $v = \pm v_0 + i\Gamma\frac{\left(1-s_\theta^2 v_0^2\right)^2}{2c_\theta}\gamma_0 k + O(k)^2$ and mode structure

$$\{\delta\varepsilon, \delta n, \delta u_L\}^{(0)} = \left\{\left(1 - s_\theta^2 v_0^2\right)\gamma_0^2(\varepsilon + p), 0, \mp c_\theta \gamma_0 v_0\right\} \tag{3.69}$$

$$\{\delta\varepsilon, \delta n, \delta u_L\}^{(1)} = \gamma_0^3\left(1 - s_\theta^2 v_0^2\right)\left\{0, 0, -\frac{i}{2}\gamma_0\left(1 - (1 + c_\theta^2)v_0^2\right)\Gamma\right\} \tag{3.70}$$

We can solve the dispersion relation for k to obtain

$$k = -i\frac{\varepsilon + p}{\frac{d-2}{d-1}\eta + \frac{1}{2}\zeta}\frac{\sqrt{1 - v_0^2}\cos\theta}{(1 - (v_0\sin\theta)^2)^2}(v \mp v_0) + O(k)^2 \tag{3.71}$$

which is the form given in [9]. We shall now move on to a different arena in which we can characterise our SCM in a detailed fashion, namely holography. Since this is a microscopic theory going beyond the hydrodynamic limit, we will also be able to illustrate SCM that are not captured by a hydrodynamic effective theory.

3.2.5 *Reissner-Nordström AdS*

Since we would like to compute modes pertaining to steady states of a finite-temperature finite charge system, the appropriate bulk theory is Einstein-Maxwell. We start from such a theory in the bulk in the conventions of [71]

$$S_{\text{bulk}} = \int d^{d+1}x\sqrt{-g}\left[\frac{1}{2\kappa^2}\left(R + \frac{d(d-1)}{L^2}\right) - \frac{1}{4\tilde{g}^2}F^2\right]. \tag{3.72}$$

Here $\tilde{g}$ is the Maxwell coupling and $\kappa = 8\pi G_N$. The relevant background is the Reissner-Nordström black hole in AdS, with line element given by

$$ds^2 = \frac{L^2}{z^2}\left(-f(z)dt^2 + \frac{dz^2}{f(z)} + dx^i dx^i\right), \tag{3.73}$$

where L is the AdS radius and

$$f(z) = 1 - \left(1 + \frac{z_h^2 \mu^2}{\tilde{\gamma}^2}\right)\left(\frac{z}{z_h}\right)^d + \frac{z_h^2 \mu^2}{\tilde{\gamma}^2}\left(\frac{z}{z_h}\right)^{2(d-1)}. \tag{3.74}$$

In the expression for $f(z)$ we have introduced the dimension-dependent constant $\tilde{\gamma}$, defined as

$$\tilde{\gamma}^2 = \frac{(d-1)\tilde{g}^2 L^2}{(d-2)\kappa^2}. \tag{3.75}$$

In these coordinates the conformal boundary is located at $z = 0$, and we denote the position of the horizon by z_h. The scalar potential is nontrivial and given by

$$A_t = \mu\left[1 - \left(\frac{z}{z_h}\right)^{d-2}\right], \tag{3.76}$$

and the Hawking temperature by the expression

$$T = \frac{1}{4\pi z_h}\left(d - \frac{(d-2)z_h^2\mu^2}{\tilde{\gamma}^2}\right). \tag{3.77}$$

Now, we boost along the planar horizon direction by u_μ. Writing the boosted metric in ingoing Eddington-Finkelstein coordinates we have

$$ds^2_{\text{boosted}} = \frac{L^2}{z^2}\left(-f(z)(u_\mu dx^\mu)^2 + 2u_\mu dx^\mu dz + \Delta_{\mu\nu}dx^\mu dx^\nu\right), \tag{3.78}$$

where

$$\Delta_{\mu\nu} = \eta_{\mu\nu} + u_\mu u_\nu \quad \text{and} \quad u_\mu = \frac{1}{\sqrt{1-\mathbf{v}^2}}(1, \mathbf{v}). \tag{3.79}$$

The Greek indices μ, ν refer to boundary coordinates, i.e. $\mu, \nu = v, x, y$, while the Latin indices encompass all of the coordinates. To construct the spatial collective modes from the bulk perspective, we linearly perturb the metric. We take the following ansatz for the perturbations

$$\delta g_{ab}(z, x^\mu)dx^a dx^b = h_{\mu\nu}(z)e^{ik_\sigma x^\sigma}dx^\mu dx^\nu, \tag{3.80}$$

$$\delta A_a(z, x^\mu)dx^a = H_\mu(z)e^{ik_\sigma x^\sigma}dx^\mu. \tag{3.81}$$

There are no perturbations that involve the radial direction z by our choice of axial gauge.

For sake of specificity in the calculations, which we eventually perform numerically, we boost the metric in the x-direction

$$\mathbf{v} = (0, v_x, 0) \tag{3.82}$$

The perturbations (3.80) give rise to a set of coupled ODEs in z in the Einstein and Maxwell equations. It is most convenient to organise them into a transverse and longitudinal channel with respect to the obstacle[4]. The h_{xy}, h_{vy} and H_y belong

4 For a detailed covariant treatment of this decomposition, for a general incident angle, see the Supplementary Material of [9]

to the transverse channel, whereas h_{vv}, h_{xx}, h_{yy} and H_v, H_x belong to the longitudinal channel. The two channels cannot mix and thus form two sets of mutually decoupled linear differential equations.

We must also specify boundary conditions. In analogy with a similar procedure for calculating black hole quasinormal modes, we require regularity on the future event horizon, and in addition regularity in one of the two asymptotic directions [9]. For a detailed discussion, the Reader may refer back to section 3.2.1.

We have not been able to solve the equations analytically[5]. We therefore solve these ODEs numerically, utilizing a double-sided shooting method. We specify input boundary and horizon data and then integrate the equations on one side from the boundary, and on the other from the horizon to a common mid-point. In order to have a solution the numerical values obtained by integrating from both sides must match at the mid-point for the functions and whenever a component equation is of second order, also their first derivatives. This is achieved by finding suitable values of the input data via a Newton-Raphson routine. The routine changes the values we initially specify incrementally, until the mid-point solutions are a match up to a certain precision we specify. In our case, for most solutions, the threshold for an acceptable solution was chosen such that the absolute value of the difference at the mid-point was less than 10^{-8}.

In the concrete calculations we report on below, we choose $d = 3$, that is we work in AdS_4 and to simplify things further, we choose $L = z_h = 1$ and units in which $\tilde{g}^2 = 2\kappa^2 = 1$.

3.2.5.1 *Transverse channel*

The ODEs in the transverse channel are given by the following expressions,

$$ik_x\gamma h_{vy} + \mu v\gamma H_y + \frac{(f-1)v\gamma^2}{z^2}\left(z^2 h_{vy}\right)' + \frac{1+(f-1)\gamma^2}{z^2}\left(z^2 h_{xy}\right)' = 0, \quad (3.83)$$

$$\mu\gamma\left(z^2(h_{vy}+vh_{xy})\right)' + k_x^2\gamma^2 H_y + 2ik_x v\gamma H_y' - \left(fH_y'\right)' = 0, \quad (3.84)$$

$$\frac{ik_x\mu v\gamma^2}{f}H_y + \mu\gamma H_y' + \frac{k_x^2\gamma^2}{f}h_{vy} + \frac{2ik_x v\gamma}{zf}\left(zh_{vy}\right)' + \frac{f}{f'}\frac{v\gamma^2}{z^2}\left(z^2(h_{xy}+vh_{vy})\right)' + \frac{1}{z^3}\left(z^2(h_{vy}-zh_{vy}')\right)' = 0. \quad (3.85)$$

where f is the metric function defined in (3.74), and primes denote derivatives with respect to z. Just like the QNM case, our holographic model UV completes the hydrodynamic analysis given above. In other words, we expect to find modes corresponding to the hydrodynamic poles we exhibited above, as well as an infinite tower of additional non-hydrodynamic modes which are specific to the holographic model we analyse. More specifically, in the transverse channel, we expect to find the hydrodynamic shear diffusion mode calculated in section 3.2.3.1, given by the dispersion relation

$$k = -i\frac{\epsilon+p}{\eta}v\cos\theta + O(k^2)\,, \quad (3.86)$$

5 Although, see section 3.2.7 for the AdS_3 case, where analytical solutions can in fact be obtained.

as well as a tower of higher non-hydrodynamic modes. In fact we will see a fascinating interplay of hydrodynamic poles and non-hydrodynamic poles, which gives rise to a rich analytic structure in the complex momentum plane recently observed in [72]. Such an analytic continuation suggests a path for a definition of QNMs in terms of hydrodynamic resummations, as indeed has been already explored in [73] for the Müller-Israel-Stewart theory [74, 75]. The neutral case ($\mu = 0$) has been reported previously in [9] and so we are mostly interested in the behavior of these modes at finite chemical potential μ.

In Figure 3.4 we plot the spectrum of spatial collective modes, as a function of asymptotic flow velocity, for values of $\mu = 1$ (left panel) and $\mu = 1.5$ (right panel). We show the imaginary part of the complex momentum k in suitable units along the vertical axis as a function of asymptotic flow velocity v along the horizontal axis. The red dashed line represents the dispersion relation given by hydrodynamics (3.86). It can be seen that indeed one of the modes we find numerically corresponds to hydrodynamic shear diffusion in the low k limit, while there exist, as expected, higher non-hydro poles. It is of particular interest to notice the pole collisions that take place between the hydrodynamical mode and a non-hydrodynamical mode for a critical value of the background flow velocity $v = v_{\text{critical}}$ as indicated by turquoise diamonds in Figure 3.4: initially the poles have purely imaginary momentum k (shown in orange), while, at the critical velocity v_{critical}, the poles collide with the resulting mode (shown in blue) acquiring a real part of k.

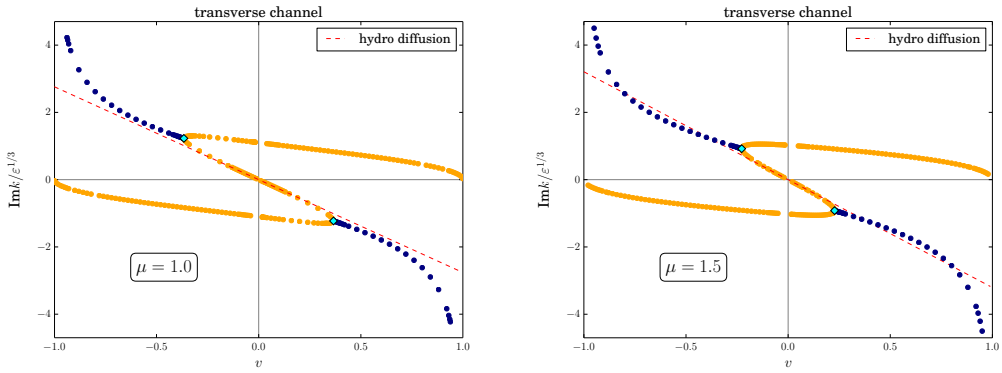

Figure 3.4: (color figure) Spectrum of SCMs in the transverse channel for values of $\mu = 1.0$ (left panel) and $\mu = 1.5$ (right panel). The motion of the imaginary part of the complex momentum is shown as a function of background velocity. Parts of the spectrum where the mode is purely imaginary are shown in orange, while blue dots correspond to the parts where the mode has non-trivial imaginary and real parts. These behaviors transition into each other at the collision points indicated by turquoise diamonds. The red dashed line shows the SCM as predicted in our charged hydrodynamic effective theory.

This pole collision is the SCM analog of similar QNM collisions, encountered previously in in [76–79]. The relevance to nonequilibrium phase transitions, as is also the case here, was first noted in [77]. Accordingly we find that the vanishing of the real part as one approaches the critical point follows a power law

$$\mathrm{Re}\, k = A\ (v_{\text{critical}} - v)^{\alpha} \tag{3.87}$$

where A is a proportionality coefficient, v_{critical} is the critical velocity at which the transition occurs, and α is the critical exponent. We can numerically extract from this relation the value of the critical exponent α. By defining $f(v) = (\operatorname{Re} k)^2$ one can see that the following function

$$\alpha(v) = \frac{1}{2}\left[1 - \frac{f''(v)\, f(v)}{(f'(v))^2}\right]^{-1}, \tag{3.88}$$

where a prime denotes a derivative with respect to v, gives the critical exponent α in (3.87) when evaluated at the critical velocity, i.e. $\alpha = \alpha(v_c)$. We use this relation to plot the behaviour of the critical exponent. By plotting the behaviour of this combination of derivatives for the range of velocities at which there exists a real part of the momentum (see Figure 3.5), one can see that it converges to $\frac{1}{2}$ as we approach the critical velocity. This corresponds to the value of the critical exponent one might expect from a mean-field theory of this transition.

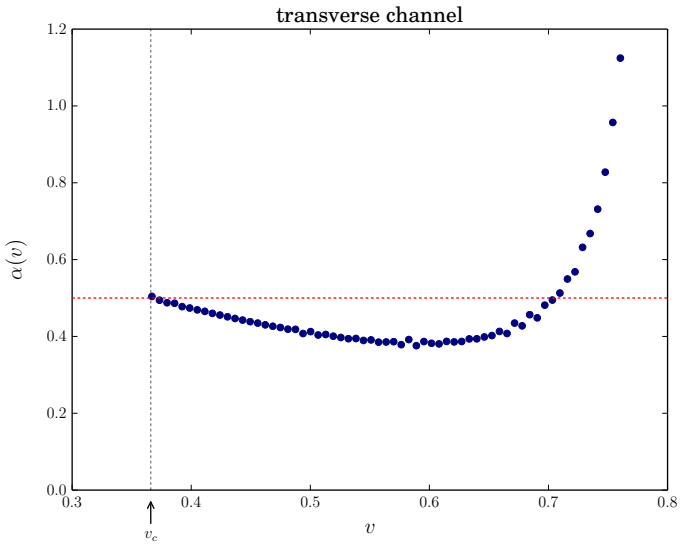

Figure 3.5: The critical exponent in the transverse channel for $\mu = 1.0$, exhibited by the function $\alpha(v)$ defined in (3.88). It can be seen that the mean-field value of $\alpha = 1/2$ is approached at the critical velocity, v_c.

We also analyzed how the critical velocity depends on the dimensionless ratio μ/T. The results are shown in Figure 3.6. One can see that for very low μ/T (the high-temperature limit) the critical velocity approaches values nearing 1.

3.2.5.2 *Longitudinal channel*

The perturbation equations in the longitudinal channel are unwieldy and unenlightening, so we do not give them here. We repeat a similar analysis as in the transverse case, mutatis mutandis.

From the hydrodynamic analysis in section 3.2.3.2, in the longitudinal channel we expect to find hydrodynamic sound modes

$$k = -i\frac{2\cos\theta}{\Gamma(1-\sin^2\theta v_0^2)^2\gamma_0}(v \mp v_0) + O(k^2), \tag{3.89}$$

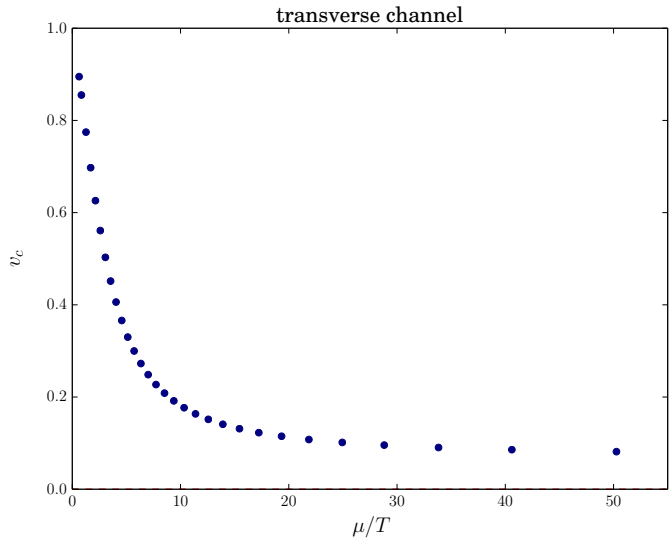

Figure 3.6: Behaviour of the critical velocity for flows of a holographic plasma at finite charge density as a function of μ/T, above which the transverse channel SCM wavevector develops a real part, and the spatial relaxation becomes oscillatory. For specific values of μ/T these transitions are shown by the turquoise diamonds in Figure 3.4.

as well as a charge diffusion mode

$$k = -i\frac{\cos\theta}{D_{\alpha\beta}}v + O(k^2). \tag{3.90}$$

The numerical spectrum of bulk SCMs in the longitudinal channel for $\mu = 1.0$ and $\mu = 1.5$ is given in Figure 3.7. The modes we calculate show good agreement with hydrodynamics (3.89) and (3.90) in the regime of small k, as required by hydrodynamics, and these are shown in Figure 3.7 as the green and red dashed lines, respectively. As in the transverse case, we can again observe a pole collision at a certain critical velocity, indicated in Figure 3.7 by yellow and turquoise diamonds. In the case indicated by the turquoise diamond the two sound and charge diffusion poles collide, after which the resulting pole has a non-zero value of Re k. Both these poles are visible within a hydrodynamical analysis, and their point of collision appears to be well approximated by the extrapolation of their first-order in hydrodynamics dispersion relation as we discuss below. Within a purely hydrodynamical analysis, however, one does not observe the actual collision, the two modes remaining distinct through the would-be collision point. The yellow diamond corresponds to a collision between the hydrodynamic sound mode and a non-hydro SCM, which shows oscillatory behavior for small flow velocities, i.e. $v < v_c$, contrasting with the behavior of the collision between the two hydrodynamical modes marked in turquoise.

As shown in Figure 3.8, the value of the critical exponent again converges to 0.5 as one approaches the critical velocity. This is in agreement with what we found in the transverse channel and, again, with expectations from mean-field theory. The numerical error in the computation of the expression (3.88) becomes more

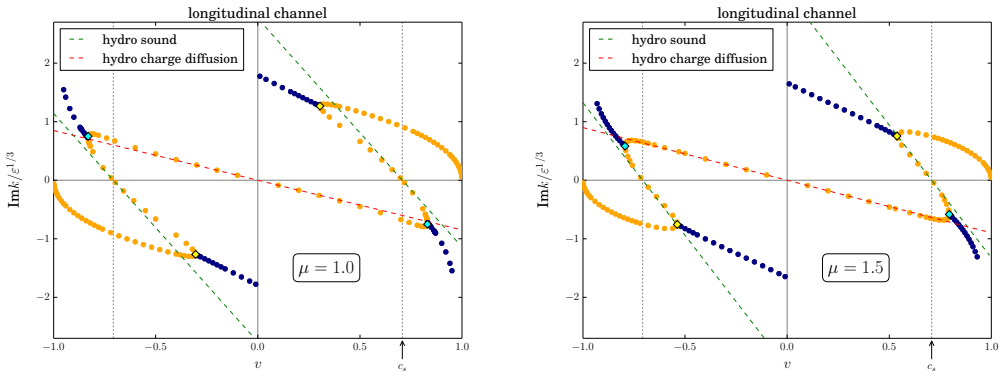

Figure 3.7: (color figure) Spectrum of SCMs in the longitudinal channel for values of $\mu = 1.0$ (left panel) and $\mu = 1.5$ (right panel). As before purely imaginary-k poles are shown in orange, while poles with both imaginary and real parts are shown in blue. In the longitudinal channel there are two kinds of pole collisions, where these behaviors transition into one another, one indicated by turquoise diamonds, and the other by yellow diamonds. Green and yellow lines show the predictions on the basis of our hydrodynamic effective theory.

pronounced as we go further away from the critical point, as evidenced by the noisier data.

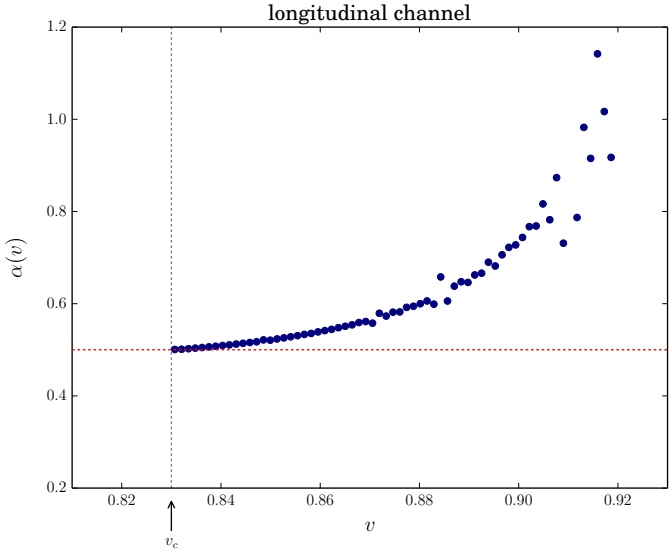

Figure 3.8: The critical exponent in the longitudinal channel for $\mu = 1.0$, as exhibited by the function $\alpha(v)$ defined in (3.88). As for the analogous transition in the transverse channel Figure 3.5, the value mean-field value $\alpha = 1/2$ is approached at the critical velocity, v_c.

Likewise, the dependence of the critical velocity on μ/T (Figure 3.9) is rather similar to the transverse case. In Figure 3.9 we also show a hydrodynamic estimate for this collision obtained simply by equating the analytic expressions for $k(v)$ for the one of the sound modes (3.89) with the diffusion mode (3.90), at normal incidence,

$$v_c^{\text{hydro.}} = \pm \frac{v_0}{1 - \frac{\Gamma \gamma_0}{2 D_{\alpha\beta}}}. \tag{3.91}$$

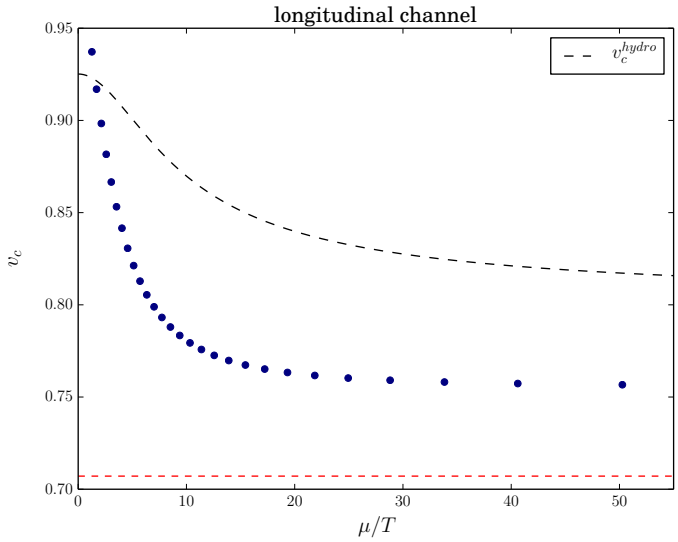

Figure 3.9: Behaviour of the critical velocity for flows of a holographic plasma at finite charge density as a function of μ/T, above which the longitudinal channel SCM wavevector develops a real part and the spatial relaxation becomes oscillatory. For specific values of μ/T these transitions are shown by the turquoise diamonds in Figure 3.7. The dashed line indicates the hydrodynamic estimate for this collision point, $v_c^{\text{hydro.}}$ given in (3.91).

3.2.6 *Spatial Collective Modes in a large number of dimensions*

In order to gain further analytic insight into the spectrum of SCMs in holographic models, we turn our attention to large-d general relativity [80–82]. In this approach one gains a small parameter, $1/d$, and an associated increase in analytic control. In this limit the set of quasinormal modes is partitioned by the scaling of their frequencies with d. In particular, there is one family of light modes with $\omega = \mathcal{O}(d^0)$ and $q = \mathcal{O}(d^{1/2})$, whose dispersion relations can be constructed analytically. These modes will be the focus of this section.

The dispersion relations for the light modes in AdS were given in [83] at charge neutrality, order-by-order in powers of $1/d$. In order to compute the corresponding SCM dispersion relations we simply perform a Lorentz boost to introduce a background velocity v, which transforms the frequency and wavenumber (ω, q) of [83] to a perturbation with zero frequency and wavenumber $k(v)$ which we analytically continue into the complex plane. Restricting for simplicity to the case where q, v, k are all in the x direction, the Lorentz transformation relates them as follows,

$$\omega = -\gamma v k, \quad q = \gamma k. \tag{3.92}$$

From these relations and the large-d scaling of ω, q we immediately see that we should treat $v = \mathcal{O}(\omega/q) = \mathcal{O}(d^{-1/2})$, which is in keeping with the scaling of the speed of sound for a conformal theory, $c_s = \mathcal{O}(d^{-1/2})$. We further conclude that $\gamma = \mathcal{O}(d^0)$ and thus $k = \mathcal{O}(d^{1/2})$. Based on these scalings, let us define the order d^0 quantities:

$$\bar{k} \equiv \frac{k}{\sqrt{d}}, \qquad \bar{v} \equiv \sqrt{d} v, \tag{3.93}$$

Our goal is to now find $\bar{k}(\bar{v})$ order-by-order in d^{-1} from the dispersion relations given in [83]. This can be achieved by replacing ω, q using (3.92) then converting to barred quantities (3.93). We then expand

$$\bar{k}(\bar{v}) = \sum_{i=0}^{\infty} \frac{\bar{k}_i(\bar{v})}{d^i}, \tag{3.94}$$

and solve for the coefficients $\bar{k}_i(\bar{v})$ in the $1/d$ Taylor expansion of the dispersion relation.

3.2.6.1 *Transverse channel*

The dispersion relation is given by [83][6]

$$\omega = -i\bar{q}^2\left(1 + \frac{1}{d^2}2\zeta(2)\bar{q}^2 - \frac{1}{d^3}4\zeta(3)\left(\bar{q}^2 + \bar{q}^4\right) + \frac{1}{d^4}8\zeta(4)\left(\bar{q}^2 + 7\bar{q}^4 + \bar{q}^6\right) + O(d)^{-5}\right) \tag{3.95}$$

where we have introduced the order d^0 quantity, $\bar{q} \equiv q/\sqrt{d}$. At leading order in the conversion to SCMs we find the following choice,

$$\bar{k}_0(\bar{k}_0 + i\bar{v}) = 0. \tag{3.96}$$

Choosing $\bar{k}_0 = 0$ results in a trivial $\bar{k}$, and so this is a zero mode shifting the moduli of the equilibrium state. For the second root of (3.96) we obtain a non-trivial mode, whose wavenumber $\bar{k}(\bar{v})$ can be written in a reasonably compact way by identifying an overall factor of $\gamma = \frac{1}{\sqrt{1-\bar{v}^2/d}}$,

$$\frac{i\gamma}{\bar{v}}\bar{k} = 1 + 2\bar{v}^2\frac{\zeta(2)}{d^2} - 4\bar{v}^2(1-\bar{v}^2)\frac{\zeta(3)}{d^3} + 2\bar{v}^2(4 - 13\bar{v}^2 + 4\bar{v}^4)\frac{\zeta(4)}{d^4} + \mathcal{O}(d^{-5}). \tag{3.97}$$

From this expression we conclude that $\mathrm{Re}\bar{k} = \mathcal{O}(d^{-5})$.

6 In the notation of [83] $\bar{q} = \hat{k}_{\text{there}}$ and $d = D_{\text{there}} - 1$.

3.2.6.2 *Longitudinal channel*

The dispersion relation is given by [83]

$$\begin{aligned}\omega = \; & -i\bar{q}^2\Bigg[\; 1-\frac{1}{d}-\frac{1}{d^2}\left(1-\frac{\pi^2}{3}\bar{q}^2\right)-\frac{1}{d^3}\left(1+\left(\frac{4\pi^2}{3}+8\zeta(3)\right)\bar{q}^2+4\zeta(3)\bar{q}^4\right)\\ & -\frac{1}{d^4}\left(1+\left(\frac{\pi^2}{3}-\frac{\pi^4}{9}-16\zeta(3)\right)\bar{q}^2-\left(\frac{31\pi^4}{45}+36\zeta(3)\right)\bar{q}^4-\frac{4\pi^4}{45}\bar{q}^6\right)\Bigg]\\ & \pm\bar{q}\Bigg[\; 1+\frac{1}{d}\left(\frac{1}{2}+\bar{q}^2\right)+\frac{1}{d^2}\left(\frac{3}{8}+\left(\frac{\pi^2}{3}-\frac{1}{2}\right)\bar{q}^2-\frac{1}{2}\bar{q}^4\right)\\ & +\frac{1}{d^3}\left(\frac{5}{16}-\left(\frac{9}{8}+\frac{\pi^2}{6}+4\zeta(3)\right)\bar{q}^2+\left(\frac{3}{4}+\pi^2-2\zeta(3)\right)\bar{q}^4+\frac{1}{2}\bar{q}^6\right)\\ & +\frac{1}{d^4}\left(\frac{35}{128}-\left(\frac{25}{16}+\frac{3\pi^2}{8}-\frac{4\pi^4}{45}-2\zeta(3)\right)\bar{q}^2+\left(\frac{13}{16}-\frac{3\pi^2}{2}+\frac{29\pi^4}{45}-5\zeta(3)\right)\bar{q}^4\right.\\ & \left.-\left(\frac{5}{4}+\frac{5\pi^2}{6}-\frac{\pi^4}{15}+22\zeta(3)\right)\bar{q}^6-\frac{5}{8}\bar{q}^8\right)\Bigg]+\mathcal{O}(d^{-5})\end{aligned} \tag{3.98}$$

Similarly at order d^0 we find

$$i\bar{k}_0\left(\bar{k}_0+i(\bar{v}\pm 1)\right)=0 \tag{3.99}$$

The choice $\bar{k}_0$ leads to a zero-mode, whilst the other root leads to,

$$\begin{aligned}i\gamma\bar{k} \;=\; & (\bar{v}\pm 1)+\frac{1}{d}\left[-\bar{v}\pm\left(\frac{1}{2}-\bar{v}^2\right)\right]+\frac{1}{d^2}\left[\pm\left(\frac{7}{8}+\frac{\bar{v}^2}{2}-\frac{\bar{v}^4}{2}\right)+\left(2\bar{v}\pm 4\bar{v}^2+2\bar{v}^3\right)\zeta(2)\right]\\ & +\frac{1}{d^3}\left[\pm\left(\frac{25}{16}-\frac{3\bar{v}^2}{8}+\frac{3\bar{v}^4}{4}-\frac{\bar{v}^6}{2}\right)+\left(2\bar{v}-8\bar{v}^3\mp 2\left(\bar{v}^2+2\bar{v}^4\right)\right)\zeta(2)\right.\\ & \left.+\left(-4\bar{v}+24\bar{v}^3+4\bar{v}^5\pm\left(-2+8\bar{v}^2+18\bar{v}^4\right)\right)\zeta(3)\right]\\ & +\frac{1}{d^4}\left[\pm\left(\frac{363}{128}-\frac{11\bar{v}^2}{16}-\frac{7\bar{v}^4}{16}+\frac{5\bar{v}^6}{4}-\frac{5\bar{v}^8}{8}\right)+\left(4\bar{v}+2\bar{v}^3\pm\left(\frac{3\bar{v}^2}{2}+6\bar{v}^4-2\bar{v}^6\right)\right)\zeta(2)\right.\\ & +\left(-4\bar{v}-16\bar{v}^3-36\bar{v}^5\pm\left(-5+10\bar{v}^2-55\bar{v}^4-6\bar{v}^6\right)\right)\zeta(3)\\ & \left.+\left(-34\bar{v}-98\bar{v}^3+100\bar{v}^5+8\bar{v}^7\pm\left(-112\bar{v}^2+38\bar{v}^4+50\bar{v}^6\right)\right)\zeta(4)\right]+O(d)^{-5}.\end{aligned} \tag{3.100}$$

Once more, from this expression we conclude that $\mathrm{Re}\bar{k}=\mathcal{O}(d^{-5})$. We expect that $\mathrm{Re}\bar{k}=0$ continues to all perturbative orders in $1/d$.

3.2.7 *BTZ black hole*

An example in which we can find the exact SCM analytically [9] and without any approximation is the three-dimensional BTZ black hole, dual to the thermal ensemble of a two-dimensional relativistic CFT. We follow the conventions of [84].

In particular we will study modes of a probe scalar field, $\phi(t,\rho,\varphi) \sim \Phi(\rho)e^{-i\omega t+iq\varphi}$, of mass m in the background

$$ds^2 = -\frac{\rho^2-\rho_+^2}{\ell^2}dt^2 + \rho^2 d\varphi^2 + \frac{\ell^2}{\rho^2-\rho_+^2}d\rho^2. \tag{3.101}$$

This background has Hawking temperatures $T = \frac{\rho_+}{2\pi\ell^2}$ which are related to its mass M as

$$M = \frac{\pi^2\ell^2}{4G_N}T^2. \tag{3.102}$$

The strategy here is to exploit the Lorentz invariance of the underlying CFT_2 to construct the SCM from the known spectrum of quasinormal modes [84–86]. For a scalar field ϕ, dual to an operator $\mathcal{O}$ of dimension $\Delta = 1+\sqrt{1+m^2\ell^2}$, the quasinormal modes occur in two integer series, [84]

$$\omega_n^{(\pm)} = \pm q - 4\pi i T\left(\frac{\Delta}{2}+n\right), \qquad n\in\mathbb{Z}^*. \tag{3.103}$$

We are, as before, interested in purely spatial modes at complex momentum in a frame where the fluid has a finite background velocity. The four-momentum of such a mode is thus given by $k^\mu_{\text{lab}} = (0,k)^\mu$ in the lab frame. We can then boost to the fluid rest frame to obtain

$$\omega = -\gamma v k\,, \qquad q = \gamma k\,. \tag{3.104}$$

Plugging these values into equation (3.103) and solving for k, we find two series of purely imaginary SCM at

$$k_\pm = i\frac{4\pi T}{\gamma\,(v\pm 1)}\left(\frac{\Delta}{2}+n\right). \tag{3.105}$$

We show the resulting SCM spectrum in Figure 3.10.

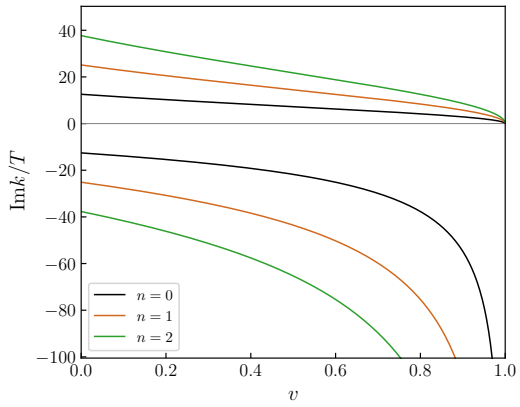

Figure 3.10: (color figure) First three modes of the spectrum of SCM of a neutral CFT_2 at temperature T, as deduced from the mode spectrum of the boosted BTZ solution. The positive branches correspond to k_+ modes, while the negative branches correspond to k_- modes.

Let us note that in this case there is an intuitive explanation in terms of the relativistic Doppler shift. The prefactor on the right-hand side of (3.105), namely $\frac{T}{\gamma(v\pm 1)}$, can be interpreted as the Doppler shifted temperature

$$T^{\text{Doppler}} = \sqrt{\frac{v\pm 1}{v\mp 1}}\, T \tag{3.106}$$

experienced by an observer in relative motion measuring a black-body spectrum, or equivalently the black-body spectrum with respect to a Doppler shifted wavelength if the observer instead chooses to interpret the spectrum keeping the temperature constant. This simple relationship between the quasinormal modes and SCM is special to the BTZ case. As one can easily verify, it depends crucially on the fact that ω depends only linearly on momentum, while any non-linear correction term would spoil this simple relationship. We have explicitly confirmed that our higher-dimensional SCM do not follow a functional form that is simply given by a Doppler-shifted temperature. Finally, it is clear that in non-relativistic systems no relationship relying on boost symmetry will be applicable.

Somewhat remarkably, in three dimensions we can actually go further.

3.3 BLACK JANUS: A FULLY NON-LINEAR ANALYTIC EXAMPLE

As we have argued, SCMs describe steady states. But, up to this point, the evidence we presented was numerical [9] (see section 3.4 below for more details on the numerical method employed in that work), due to the difficulty in obtaining analytic solutions describing the requisite non-linear steady states. In fact, analytical backgrounds illustrating the importance of SCM can be obtained. A particularly sharp example of this is provided by the finite T black Janus solution of [70]. This solution describes a finite T defect solution created by turning on a step function for a source of a scalar operator in the field theory. As argued previously, the physics of the SCM is universal and therefore independent of how they are excited, and here that excitation is the spatial variation of the scalar source. In fact, we now show that the black Janus solution may globally be regarded as a self-consistently backreacted sum of infinitely many SCMs. This makes it clear that at large distances from the obstacle, as predicted from our analysis, a single SCM dominates the spatial profile. We will now demonstrate this structure explicitly.

Having this analytic solution will also allow us to take the $T = 0$ limit, where the SCMs coalesce in the complex k-plane and the Janus tail becomes power-law. This emergence of a branch cut from the coalescence of poles is expected to be relevant also in other examples.

The black hole of [70] at temperature T may be written in the following form

$$ds^2 = f(\mu)^2(-\sinh^2(2\pi T p)\, d\tau^2 + dp^2 + d\mu^2), \tag{3.107}$$

$$\phi = \phi(\mu) \tag{3.108}$$

where

$$f(\mu)^{-1} = \frac{\sqrt{1+k}}{2\pi T}\,\mathsf{cd}\left(\frac{2\pi T\mu}{\sqrt{1+\mathsf{m}}},\mathsf{m}\right), \tag{3.109}$$

$$e^{\frac{1}{2}\phi} = \frac{1+\sqrt{k}\,\mathsf{sn}\left(\frac{2\pi T\mu}{\sqrt{1+\mathsf{m}}},\mathsf{m}\right)}{\mathsf{dn}\left(\frac{2\pi T\mu}{\sqrt{1+\mathsf{m}}},\mathsf{m}\right)}, \tag{3.110}$$

where sn, cd and dn are Jacobi elliptic functions and m is the elliptic modulus[7].

This is a solution to the Einstein-massless scalar equations of motion for $d = 2$ with negative cosmological constant [70]. It is described by an angular coordinate μ and a radial coordinate p. The angle is bounded by $|\mu| \leq \mu_0 \equiv \frac{\sqrt{1+\mathsf{m}}}{2\pi T}K(\mathsf{m})$ where K is the complete elliptic integral of the first kind, the limit being saturated on the AdS boundary. The defect itself can be reached by taking $p \to \infty$ at fixed μ. An illustration of the geometry and the coordinates employed is given in Figure 3.11.

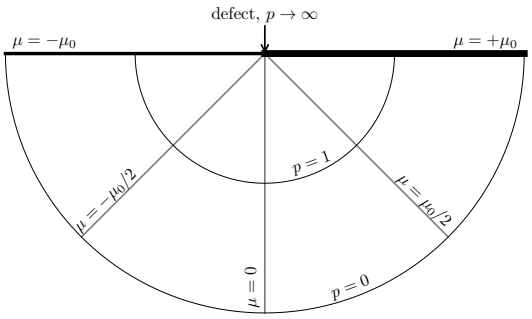

Figure 3.11: Coordinates for the black Janus solution. The defect is located at the origin $p = 0$. We reach the asymptotic regions on either side by taking $p \to \infty$ with angular coordinate $\mu = \pm\mu_0$. In the asymptotic regions the scalar field approaches the limiting value $\phi(\pm\mu_0) = \pm 2\log\left(\frac{1+\sqrt{\mathsf{m}}}{\sqrt{1-\mathsf{m}}}\right)$.

Finally, the solution is parameterised by the elliptic modulus m, which is the parameter that determines the size of the step, i.e. it dictates the value of the scalar field source on either side of the defect, through the relation

$$\phi(\pm\mu_0) = \pm 2\log\left(\frac{1+\sqrt{\mathsf{m}}}{\sqrt{1-\mathsf{m}}}\right). \tag{3.111}$$

3.3.1 *One-point functions*

We first focus our attention on the CFT one-point functions, which we compute by going to Fefferman-Graham coordinates, (t, x, ρ), near the boundary on either

7 This is denoted 'k' in the original references, but we prefer to relabel is 'm' in order to avoid any confusion with the momentum k.

side of the defect, i.e $\mu = \pm\mu_0$. In the new coordinates the boundary is given by $\rho = 0$, and the coordinate transformation is given by

$$\begin{aligned}
\tau &= t + O(\rho)^4 \\
\mu &= \pm\mu_0 + \operatorname{csch}(2\pi T x)\,\rho - \frac{1}{24}(2\pi T)^2 \operatorname{csch}^3(2\pi T x)(5 + 3\cosh(4\pi T x))\,\rho^3 + O(\rho)^4 \\
p &= -\frac{1}{\pi T}\log\left(\pm\tanh(\pi T x)\right) - \pi T \coth(2\pi T x)\operatorname{csch}(2\pi T x)\,\rho^2 + O(\rho)^4
\end{aligned} \tag{3.112}$$

Note that we take $x > 0$ for all $0 \leq p < \infty$ at $\mu = \mu_0$ and similarly $x < 0$ for all $0 \leq p < \infty$ at $\mu = -\mu_0$. We do not consider the defect location $x = 0$ directly. The metric and scalar field in these coordinates are given by the expressions,

$$ds^2 = \frac{d\rho^2}{\rho^2} - \left(\frac{1}{\rho^2} - \frac{(2\pi T)^2}{2}\right)dt^2 + \left(\frac{1}{\rho^2} + \frac{(2\pi T)^2}{2}\right)dx^2 + O(\rho)^2, \tag{3.113}$$

$$\phi = \pm\left(2\log\left(\frac{1+\sqrt{\mathsf{m}}}{\sqrt{1-\mathsf{m}}}\right) - \frac{\sqrt{k}(2\pi T)^2\operatorname{csch}^2(2\pi T x)}{1+k}\rho^2 + O(\rho)^4\right) \tag{3.114}$$

where the upper sign corresponds to the right asymptotic region and the lower sign to the left asymptotic region. There is no $\rho^2 \log\rho$ term since the source is constant on either side of the defect. Going into the bulk, the metric eventually becomes deformed by the scalar backreaction at order ρ^2 as we outline below. From the above results, using holographic renormalisation [87], we find the expectation values

$$\langle T_{ab}\rangle = (2\pi T)^2\delta_{ab} \tag{3.115}$$

$$\langle O_\phi\rangle = \mp 2\frac{\sqrt{\mathsf{m}}(2\pi T)^2}{1+\mathsf{m}}\operatorname{csch}^2(2\pi T x). \tag{3.116}$$

3.3.2 *Extracting the SCM*

We begin our comparison by studying the behaviour of the one-point functions. For this we recall that the spectrum of SCM for a scalar field on BTZ were computed in (3.105). In the present analysis we only need the $v = 0$ cases. Specializing to a massless field, we have $\Delta = 2$, whence

$$k_n^{\pm} = \pm i 4\pi T(1+n). \tag{3.117}$$

Then, we can explicitly see that (3.116) can be expressed as a linear sum of these modes, on either side of the defect. On the $x > 0$ side of the defect we have

$$\langle O_\phi\rangle = \sum_{n=0}^{\infty} A_n^+ e^{ik_n^+ x} \qquad \text{with} \qquad A_n^+ = -\frac{8\sqrt{\mathsf{m}}(2\pi T)^2}{1+\mathsf{m}}(n+1), \tag{3.118}$$

and on the $x < 0$ side of the defect we have,

$$\langle O_\phi\rangle = \sum_{n=0}^{\infty} A_n^- e^{ik_n^- x} \qquad \text{with} \qquad A_n^- = \frac{8\sqrt{\mathsf{m}}(2\pi T)^2}{1+\mathsf{m}}(n+1). \tag{3.119}$$

For large distances from the obstacle one readily sees that the solution falls off exponentially in either direction with a characteristic length scale $k_0^- = 4\pi T$ to the left and $|k_0^+| = 4\pi T$ to the right, in other words according to the dominant SCM in either sector.

The above one-point functions combined with metric and scalar boundary conditions are sufficient to determine the full bulk solution. Thus, the one-point functions tell us that the bulk black Janus solution is simply the result of summing infinitely many SCMs and matching at a defect boundary condition. It may be tempting to then conclude that the full bulk metric is a linear sum of SCMs, in the way that the one-point functions are. However this is only true asymptotically, near the AdS boundary. Specifically, up to and including stress-tensor and expectation-value order in the small ρ expansion there is no trace of backreaction of the modes. However, moving to higher powers in ρ one encounters non-linear backreaction, (presented here for the $x > 0$ side)

$$\delta(ds^2) = -\left(\frac{A_0^+}{16}\right)^2 \operatorname{csch}^4(2\pi T x)\,(dt^2 + dx^2)\rho^2 + O(\rho)^4\,, \tag{3.120}$$

where $\delta(ds^2)$ is the difference between the linearized and the fully backreacted metric, e.g. $\delta(ds^2) = ds^2 - (ds^2)_{\text{lin}}$. Subsequently, at even higher powers of ρ, the scalar modes can interact with each other resulting in non-linear adjustments to the ϕ profile,

$$\delta\phi = -\frac{2}{3}\left(\frac{A_0^+}{16}\right)^3 \operatorname{csch}^6(2\pi T x)\,\rho^6 + O(\rho)^8\,, \tag{3.121}$$

with the δ notation defined as an obvious extension of the above. Thus we regard the black Janus solution as a self-consistently backreacted solution resulting from the linear sum of infinitely many BTZ SCMs.

3.3.2.1 *Zero-temperature limit and analytical structure*

Finally, we would like to comment on the $T = 0$ limit. Here the expectation value (3.116) becomes power-law in x rather than exponential,

$$\langle O_\phi \rangle = \mp 2\frac{\sqrt{\mathsf{m}}}{1+\mathsf{m}}\frac{1}{x^2}\,, \qquad (T=0), \tag{3.122}$$

and in this limit the SCMs appear to accumulate at the origin (3.117), which becomes in fact a branch point, conforming with the usual intuition of power laws coming from branch cuts.

We can make this precise by writing the expectation value as a Laplace transform

$$\langle O_\phi \rangle = \int_0^\infty A(s) e^{-sx} ds\,. \tag{3.123}$$

Note that we are specialising in the modes to the right of the obstacle, but an analogous formula obviously exists for the modes on the left. We are interested in

the function $A(s)$ which describes the density of SCM in the complex momentum plane. We can calculate this using the usual Bromwich inversion formula

$$A(s) = \frac{1}{2\pi i}\int_{\gamma-i\infty}^{\gamma+i\infty} \langle O_\phi(x)\rangle\, e^{sx} dx\,, \tag{3.124}$$

substituting the form of $\langle O_\phi(x)\rangle$ for black Janus, i.e. Eq. (3.116). We start with the finite-temperature case, which results in a sum of delta functions,

$$A(s) = \sum_{n=0}^{\infty} A_n^+ \delta\left(s - s_n\right)\,, \qquad \text{with} \qquad s_n = 4\pi T(1+n) \tag{3.125}$$

for A_n^+ as defined above. Evidently we have recovered a discrete infinity of modes. Plugging this back into (3.123), we find

$$\langle O_\phi\rangle = \sum_{n=0}^{\infty} A_n^+ e^{-s_n x} = \sum_{n=0}^{\infty} A_n^+ e^{ik_n^+ x}\,. \tag{3.126}$$

In other words, we recover the discrete set of purely imaginary SCM ascending the positive imaginary momentum axis of (3.118) by means of the Laplace transform. Repeating now the same procedure for the zero-temperature expression for $\langle O_\phi(x)\rangle$ we find

$$A(s) = 2\frac{\sqrt{\mathsf{m}}}{1+\mathsf{m}}s\,, \tag{3.127}$$

i.e. a continuum of modes emanating from $s = 0$. This spectral density, translated into the complex k plane, corresponds to a continuum of modes lying on a branch cut along the positive imaginary $k-$axis emanating from a branch point $k = 0$. Let us finally remark that this coincides, as expected, with the naive continuum limit in Eq. (3.117), i.e. taking $T \to 0$, and defining a continuum variable $s = Tn$. This analytic structure is illustrated in Figure 3.12.

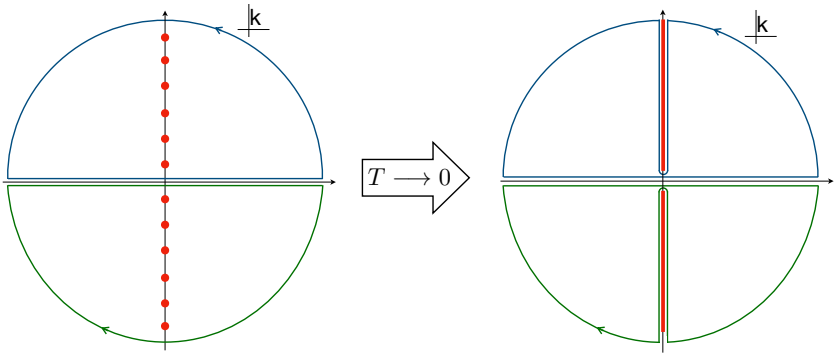

Figure 3.12: (color figure) Analytic structure in the complex momentum plane for the black Janus solution. At finite temperature we have two sectors of SCM along the positive and negative imaginary axis (we summarize all poles, that is both those of $G^{[\searrow]}(k)$ and $G^{[\swarrow]}(k)$ in the same figure). In the $T \to 0$ limit these condense into a continuum in the form of two branch cuts along positive and negative imaginary axes. This continuum, for example, manifests itself as a power-law decay at large distances (3.122) or as a discontinuity in the spectral representation of the two point function.

3.4 NONLINEAR SOLUTIONS: STEADY STATES WITHOUT KILLING HORIZONS

In [9], two of the authors of the material presented in this chapter constructed a class of non-equilibrium steady states, and pointed out the relevance of SCM to their spatial asymptotic behavior. In this section, we give more details about the numerical aspects of the construction.

In what follows we will construct a holographic example of a nonlinear non-equilibrium steady state. Our goal is twofold: on the one hand we wish to demonstrate the role played by the spatial collective modes that have been explored in this chapter, and on the other, we wish to supply more detail on the actual numerical construction employed to obtain the fully non-linear solutions. Specifically we will demonstrate that the approach to equilibrium at long distances is governed by the SCM.

We construct non-Killing black brane solutions corresponding to flow-past-obstacle steady states in the dual field theory. Solutions of this type, stationary quenches[8], have been constructed before, [67]. Indeed our results for this section draw on the methods introduced in [67]. Here we shall elaborate on the numerical techniques we used, which extend those of [67] to include transverse velocity and supersonic asymptotic flow velocities. This extension is necessary so that we may compare to our transverse and supersonic collective modes.

3.4.1 *Numerical method*

One way to understand the method is to consider a steady state formed by waiting for a time-dependent process to settle down. This is an inefficient way to access the steady state, and offers little control over which steady state is reached, since the resulting steady state at late times will have its moduli governed by the chosen initial conditions. Specifically, the moduli are a set of numbers which label the flowing solutions, and so for instance dictate the left and right asymptotic energy densities, velocities and incident angles. Instead, one may *skip to the end* and look directly for the stationary solution. In this case there are no initial conditions to determine which solution is obtained, and so the moduli must be fixed by other means. In this work the moduli are conveniently fixed by imposing additional boundary conditions at points behind the future event horizon, following [67]. We find that three boundary conditions are required to fix three moduli, which we think of as an asymptotic flow velocity, an asymptotic energy density and an asymptotic incident angle, and we go into some detail on these choices below.

We denote our bulk metric as g_{ab} with $a, b = 0, \ldots, 3$ and boundary directions labelled by $\mu, \nu = 0, \ldots, 2$. To keep things as simple as possible we use the boundary metric itself, $\gamma_{\mu\nu}$ in order to produce an obstacle,

$$\gamma_{\mu\nu} = \eta_{\mu\nu} + s_{\mu\nu}(x), \tag{3.128}$$

which depends non-trivially only on one boundary direction, x. As is apparent from the rest of this chapter, the interesting spatial behavior we observe is ex-

8 Other interesting discussions and constructions of non-Killing black holes are provided by [68, 88–92]. Nonlinear solutions with time-dependent horizons have been studied earlier, for example in the work of [93].

pected to be fully universal [9] and would manifest itself in many other ways of introducing an obstacle. Our present choice of obstacle as a boundary metric deformation allows us to consider a minimal bulk theory of pure gravity in AdS_4, with no matter fields required. To deal with the usual gauge issues we adopt the Einstein-DeTurck or 'generalised harmonic' equations [69, 94, 95], and we recommend these references for further details. Briefly, one introduces a reference metric $\bar{g}_{ab}$ and a vector $\xi^a = g^{bc}\left(\Gamma^a_{bc} - \bar{\Gamma}^a_{bc}\right)$ and modifies the equations of motion,

$$R_{ab} - \nabla_{(a}\xi_{b)} + 3g_{ab} = 0. \tag{3.129}$$

To define our reference metric we first introduce Schwarzschild-AdS_4 boosted by a 2-velocity $\boldsymbol{\beta}$ with corresponding 3-vector $u^\mu = \frac{1}{\sqrt{1-\delta_{ij}\beta^i\beta^j}}(1, \boldsymbol{\beta})$, written in ingoing Eddington-Finkelstein coordinates,

$$ds^2_{Schw.} = \frac{1}{z^2}\left(-f(z)(u_\mu dx^\mu)^2 + 2u_\mu dx^\mu dz + \Delta_{\mu\nu}dx^\mu dx^\nu\right), \tag{3.130}$$

$$f \equiv 1 - \frac{z^3}{z_h^3} \tag{3.131}$$

where $\Delta_{\mu\nu} \equiv \eta_{\mu\nu} + u_\mu u_\nu$. This metric also introduces the holographic coordinate z chosen such that the conformal boundary is defined by the double-pole at $z = 0$. We choose our reference metric to be this solution manually adjusted to match the boundary metric choice (3.128) in the following way,

$$\bar{ds}^2 = ds^2_{Schw.} + z^{-2}s_{\mu\nu}(x)dx^\mu dx^\nu, \tag{3.132}$$

which is not a metric which solves the Einstein equations in general. We ensure that the source components are orthogonal to u^μ,

$$s_{\mu\nu} = \Delta_\mu^{\ \rho}\Delta_\nu^{\ \sigma}\mathcal{S}_{\rho\sigma}. \tag{3.133}$$

In this way u^μ is still unit-norm, $\gamma_{\mu\nu}u^\mu u^\nu = -1$, despite the presence of the obstacle, $s_{\mu\nu}(x)$. For concreteness we adopt a particularly simple choice of source,

$$s_{\mu\nu} = \mathcal{S}_{\mu\nu} = s(x)n_\mu n_\nu \tag{3.134}$$

where $n_\mu = \left(\beta_x^2 + \beta_y^2\right)^{-1/2}(0, -\beta_y, \beta_x)$ with a Gaussian choice

$$s(x) = Ae^{-Bx^2} \tag{3.135}$$

and free parameters A, B. At this point we also introduce the angle of incidence parameter in the reference metric as,

$$\tan\theta = \beta^y/\beta^x. \tag{3.136}$$

We emphasise that β^i, z_h and θ are simply reference metric parameters, and do not directly correspond to a final velocity, energy density or angle of incidence in the resulting solution.

Finally, we find it convenient to factor out the leading divergence in the bulk metric, defining instead h_{ab} through,

$$h_{ab}(z,x) \equiv z^2 g_{ab}(z,x). \tag{3.137}$$

3.4.1.1 *Implementation details*

To aid the construction of flows that are infinitely extended and inhomogeneous in the x direction, we compactify using a coordinate ρ,

$$x = \frac{\rho/\ell}{1-\rho^2} \tag{3.138}$$

with $\rho \in [-1,1]$. The other non-trivial direction is labelled by the holographic coordinate $z \in [0, z_{max}]$ with the conformal boundary of AdS at $z = 0$ and the set $z = z_{max}$ should be entirely behind the future event horizon of the solution, $\mathcal{H}^+$. The parameter ℓ allows us to adjust the overall scale of the grid relative to the characteristic size of the inhomogeneities. In practice, typical choices of ℓ are $\mathcal{O}(1)$ in our simulations. Finally there is no dependence in the remaining two directions, t, y. The resulting domain is shown in Figure 3.13.

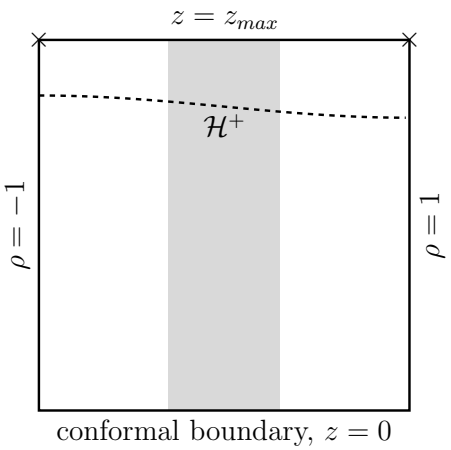

Figure 3.13: A sketch of the domain used for the numerical construction of holographic non-equilibrium steady states. The spatial field theory direction is compactified using coordinate ρ as defined in (3.138). The '$\times$'s mark the points where boundary conditions are imposed to fix moduli of the solution. The gray filled region schematically indicates the presence of the obstacle, in the sense that far to the left or to the right the bulk is described by an equilibrium solution with spatial collective modes.

We use Dirichlet boundary conditions to fix h_{ab} to be the conformal boundary metric (3.128) at $z = 0$ for all ρ. As discussed we must also introduce data which fix the moduli of the solution, as in [67]. This is introduced as additional Dirichlet data behind the horizon in the corners of the grid, at $z = z_{max}, \rho = \pm 1$ for some metric components. Roughly speaking we have three moduli fixing boundary conditions

because we have three solution moduli: an energy density, a velocity and an angle of incidence for the flow. Specifically, at these points we set $h_{ab} = z^2 \bar{g}_{ab}$ as follows:

asymptotic v	upstream corner	downstream corner
subsonic	h_{tt}, h_{ty}	h_{tz}
supersonic	h_{tt}, h_{ty}, h_{tz}	–

.

Whilst the above choices work well in practise, in the sense that the numerical method converges to a solution to the Einstein equations, we do not have a rigorous understanding of why these particular choices work where certain others do not. For instance, the choice we arrived at for the supersonic case amounts to a specification of all three moduli in the upstream asymptotic region; it would be interesting to understand the connection to the character of the corresponding problem in fluid dynamics. Finally we impose Neumann boundary conditions on all fields along the remaining points of the $\rho = \pm 1$ edges. The remaining points at $z = z_{max}$ are left free to obey the equations of motion.

We utilise a regularly spaced discretisation of ρ, z with N_ρ, N_z grid points respectively, taking $N_\rho = 4N_z$. We adopt sixth-order finite difference approximations of the derivative operators. The resulting system of equations is solved iteratively using the Newton method. The Jacobian is computed numerically, utilising a second-order centre-difference stencil for taking derivatives of the equations, which is slower to compute but results in considerably better convergence of the Newton method than the first-order finite difference. Computing the Jacobian can be sped up by restricting the difference computation to only the affected areas, i.e. roughly speaking in a stencil-sized box around the varied grid point. The resulting sparse linear system is then solved directly using the LU-factorisation algorithm provided by `UMFPACK`[96].

The initial guess for the Newton method is taken to be the reference metric, together with a low amplitude (A) source. Once obtained we use small A solutions as initial guess metrics for larger A solutions. In all cases we find it is convenient to start at low resolutions (typically $N_\rho = 80, N_z = 20$), and then use sixth-order-interpolated versions of these as solution guesses for higher resolutions. The interpolated guess converges in one or two Newton steps to a solution. In this fashion we have obtained solutions up to $N_\rho = 520, N_z = 130$, limited ultimately here by the memory required for the direct linear solver, but a resolution that is more than sufficient for our requirements.

For a selection of representative solutions (examples (a), (b) and (c) defined later in section 3.4.2) we have carried out convergence tests, looking at the approach to the continuum limit of the vector ξ^a. This is shown in Figure 3.14 demonstrating results consistent with fourth-order convergence.

3.4.2 *Results*

With solutions obtained our next task is to interpret the results from the CFT perspective. Our first task is to read off the one-point function of the CFT stress

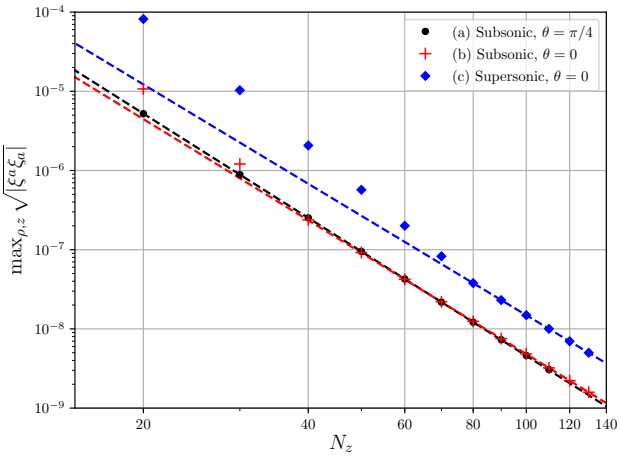

Figure 3.14: Convergence tests of the numerical method for non-Killing black branes describing NESS. We show the approach to the continuum limit of the ξ^a vector, whose maximum value on the numerical grid approaches zero as a power law with order (a) 4.4, (b) 4.2, (c) 4.2.

tensor, $\langle T_{\mu\nu} \rangle$, from the bulk solutions. The details of this calculation are set out in appendix B, and we quote the main result here for convenience,

$$\langle T_{\mu\nu} \rangle = \frac{1}{2}\partial_z^3 h_{\mu\nu}\big|_{z=0} + \frac{\gamma_{\mu\nu}}{z_h^3} + V_{\mu\nu} \tag{3.139}$$

where $V_{\mu\nu}$ is a known term which vanishes outside the obstacle. With $\langle T_{\mu\nu} \rangle$ in hand, we solve the following eigenvalue problem at each point x along the flow,

$$\langle T^{\mu}{}_{\nu} \rangle U^{\nu} = -\epsilon U^{\mu} \qquad \gamma_{\mu\nu} U^{\mu} U^{\nu} = -1, \tag{3.140}$$

and define the local flow velocities

$$v^x \equiv \frac{U^x}{U^t}, \qquad v^y \equiv \frac{U^y}{U^t}. \tag{3.141}$$

Note that it is not always possible to solve (3.140) within the obstacle region where the flow becomes strongly non-linear. For illustrative purposes we restrict our attention to three different points in moduli space,

a) Subsonic flow at non-zero angle of incidence. The parameters used are, $z_h = 0.975, \beta_x = 0.15, \beta_y = 0.15, A = 1.0, B = 3.0, \ell = 0.5$. The corresponding ε, v^x, v^y are shown in Figure 3.15.

b) Subsonic flow at zero angle of incidence, $\theta = 0$. The parameters used are, $z_h = 0.975, \beta_x = 0.6, \beta_y = 0.0, A = 0.1, B = 2.9618, \ell = 0.5$. The corresponding ε, v^x are shown in Figure 3.16.

c) Supersonic flow at zero angle of incidence, $\theta = 0$. The parameters used are, $z_h = 0.975, \beta_x = 0.8, \beta_y = 0.0, A = 0.1, B = 3.0, \ell = 0.5$. The corresponding ε, v^x are shown in Figure 3.17.

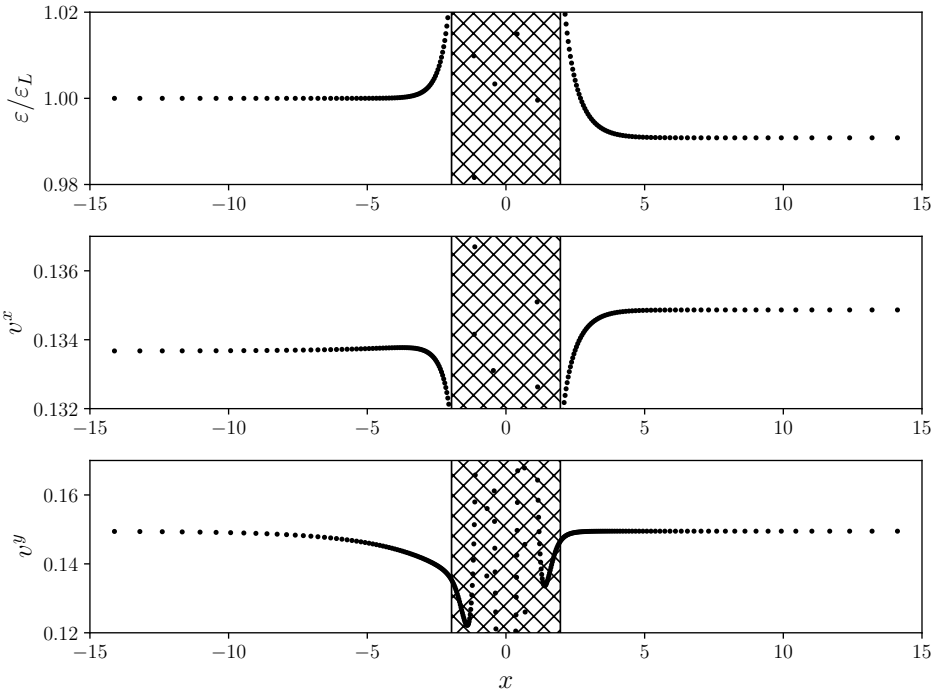

Figure 3.15: Flow profiles for solution (a): subsonic-to-subsonic non-equilibrium steady flow at incidence parameter $\theta = \pi/4$. In this case the fluid is rarefied, refracted and sped up by the obstacle. Note that $v^y_L = v^y_R$. The tails visible in these spatial profiles are the spatial collective modes.

The imprint of the spatial collective modes is already apparent in the flow profiles of Figure 3.15, Figure 3.16, and Figure 3.17. To demonstrate this more clearly we take derivatives of the data in order to extract the decay length and compare it to the modes of section 3.2.5, given the specific asymptotic equilibrium approached. Specifically, for some quantity f we define,

$$\kappa_f(x) \equiv -\frac{1}{\varepsilon^{1/3}} \frac{\partial_x^2 f}{\partial_x f}. \tag{3.142}$$

Then, if the asymptotic functional form of f is given by $f = C + A_k e^{-\mathrm{Im}k\, x}$, the asymptotic value of κ_f will be the wavenumber itself, $\mathrm{Im}k/\varepsilon^{1/3} = \lim_{x\to\pm\infty} \kappa_f(x)$. A comparison is shown for the solution (a) in Figure 3.18, illustrating the existence of these modes in the flow profile, including a mode which is of non-hydrodynamic origin.

Next, we perform a similar analysis in order to investigate the asymptotic behaviour of solutions (b) and (c). In moving from (b) to (c) we move from subsonic to supersonic flows and we expect to see the non-equilibrium phase transition due to a complex-k mode crossing the real axis. To illustrate this more clearly, we restrict to the downstream side and subtract the asymptotic value. Then on a log-linear plot, the slope will give the appropriate spatial collective mode. This is shown together with the leading pole structure in the complex-k plane for downstream (b) and downstream (c), in Figure 3.19.

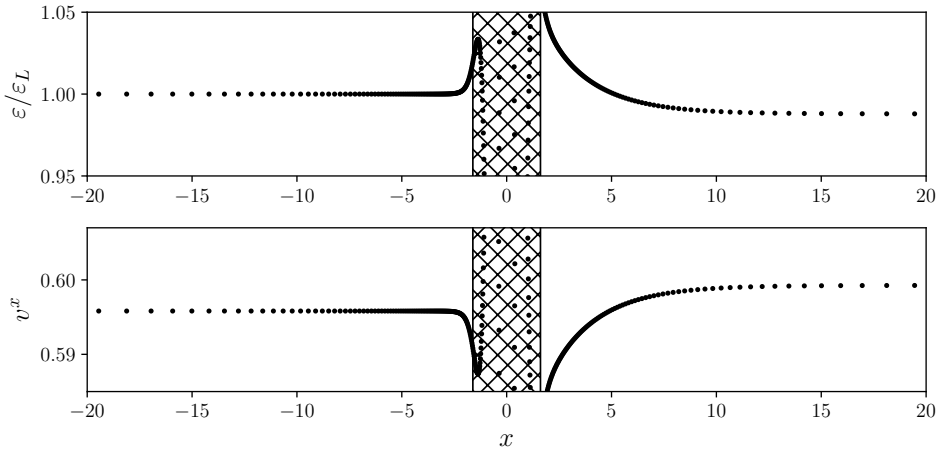

Figure 3.16: Flow profiles for solution (b): subsonic-to-subsonic non-equilibrium steady flow at normal incidence. Here the fluid is rarefied and sped up by the obstacle. The tails visible in these spatial profiles are the spatial collective modes.

3.5 SUMMARY AND DISCUSSION

Before moving to discuss open issues and future work, let us pause to briefly recapitulate the salient features of this work. In [9] two of us proposed a universal description of a class of nonequilibrium steady states, motivated by holographic duality. This description relies on a set of modes, the spatial collective modes (SCM), defined in the complex momentum plane, which are spacelike cousins of quasinormal modes, used to describe universal equilibration dynamics in holography for systems excited by an explicit time-dependent perturbation. The SCM, instead, describe the spatial relaxation of nonequilibrium steady states, and are excited by spatial inhomogeneities. The behavior away from the source is universal in the sense that it depends only on the theory and the asymptotic configuration that is approached but not on the details of the inhomogeneities.

In section 3.2.1 we gave a description of these modes from the point of view of the boundary field theory, where they appear notably as poles of correlation functions in the complex momentum plane. We then embarked on a range of calculations in order to illustrate SCM, in various interesting contexts. The most complete understanding, unsurprisingly, is obtained in holography. We explicitly construct non-linear solutions (based on the methods described in [67]) by forcing the strongly coupled fluid dual to Einstein gravity over an obstacle, modelled by sourcing the boundary metric, and match the asymptotic spatial behavior of such steady state solutions to the leading SCM appearing in the complex momentum plane of the relevant two-point functions. As we have pointed out these are defined by boundary conditions which are regular at the horizon and in one of the nontrivial spatial directions. We have considered the SCM in a variety of systems and have given a general numerical recipe for their calculation. There are a number of contexts where we can determine the spectrum of modes analytically, notably three-dimensional holography (the BTZ black hole) and the large-D limit of [83]. An interesting feature of all cases we considered is that the SCM were always purely imaginary for a neutral fluid, but could acquire non-zero real parts,

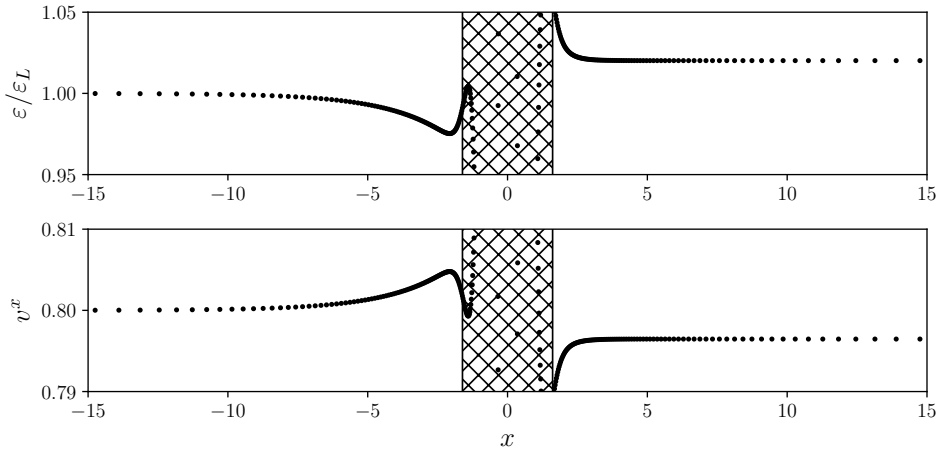

Figure 3.17: Flow profiles for solution (c): supersonic-to-supersonic non-equilibrium steady flow at normal incidence. Here the fluid is compressed and slowed through its encounter with the obstacle. The tails visible in these spatial profiles are the spatial collective modes.

that is represent damped oscillatory behaviour, at finite chemical potential. We pointed out that there are interesting critical phenomena at the points where pure decay transitions into damped oscillations, producing nonequilibrium phase transitions of the same flavor as those first described in [77]. Due to the ubiquity of SCM as well as QNM we expect to find examples of such transitions recurring in many more contexts, and indeed we remark that similar phenomena have already appeared in [76, 79]. Each of these transitions can be reduced to either a pole collision or an exchange of dominance between poles. In the former case, the vanishing of the real part of the mode proceeds with a critical exponent $1/2$. It would be of interest to develop a general mean-field treatment of these phenomena, in the spirit of the theory of dynamic critical phenomena of [97].

A particularly well controlled case arises for three dimensions, where we already pointed out that we can construct the full spectrum of SCM analytically. As it turns out, in this case we were able to find a full non-linear example analytically, namely the black Janus solution of [70] and we point out that its spatial relaxation on either side of the obstacle is precisely given by the leading SCM. In fact one can go further and show that the entire black Janus solution can be re-expressed as a sum over the full spectrum of SCM of the BTZ black hole, which start out as a linear superposition in the boundary, and construct the in-filling bulk solution as a non-linear backreacted version of the tower of modes. This is reviewed in detail in section 3.3 where we also point out that one can reconstruct the spectrum SCM via an inverse Laplace transform of the boundary expectation values of fields in the black Janus solution of [70].

A subset of the SCM appearing this work can be constructed using a hydrodynamic effective theory, with decay lengths depending on hydrodynamic transport coefficients, such as η/s and various diffusion constants. Interestingly we also exhibited cases where the hydrodynamic effective theory does not capture the leading behavior in one or the other asymptotic direction, and we see direct manifestations of higher SCM, as well as interesting phase transitions between

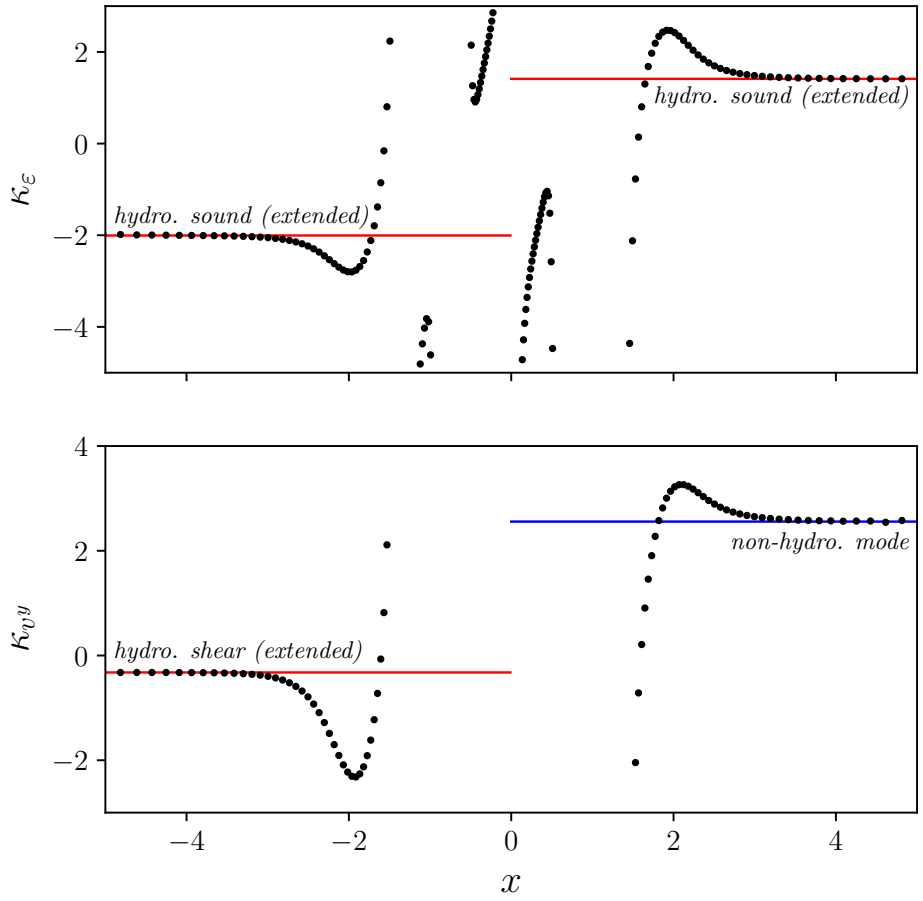

Figure 3.18: Comparing the asymptotics of solution (a) to the spatial collective modes appropriate to each asymptotic equilibrium region. The points are given by derivatives of the spatial profiles of solution (a), according to the definition (3.142). The spatial collective modes are shown by the coloured solid lines. Note that a non-hydrodynamic mode is excited in the transverse channel on the downstream side.

hydrodynamic and non-hydrodynamic fall-offs. The steady state thus encodes in a time independent way the hydrodynamic transport coefficients, which may be read off from the spatial decay properties of certain modes excited by the obstacle. In particular the shear SCM decays with length proportional to η/s and is thus a direct probe of the shear viscosity to entropy density ratio of whatever strongly-coupled fluid is set up in such a steady state. Experimental evidence for strongly coupled electron flow has been seen in $PdCoO_2$ [98] and graphene [99]. In [9] we have estimated these decay lengths for graphene at charge neutrality as well as $\mathcal{N} = 4$ SYM, and we give a few more details about these analyses here[9]. For the transverse mode in first order neutral hydrodynamics the dispersion relation is given by (3.66), leading to a decay length for a flow v at normal incidence to the obstacle ($\theta = 0$),

$$|\mathrm{Im}k|^{-1} = \frac{\eta}{s}\frac{c^2}{vT}, \tag{3.143}$$

9 We thank an anonymous referee of [9] for encouraging us to produce such an estimate.

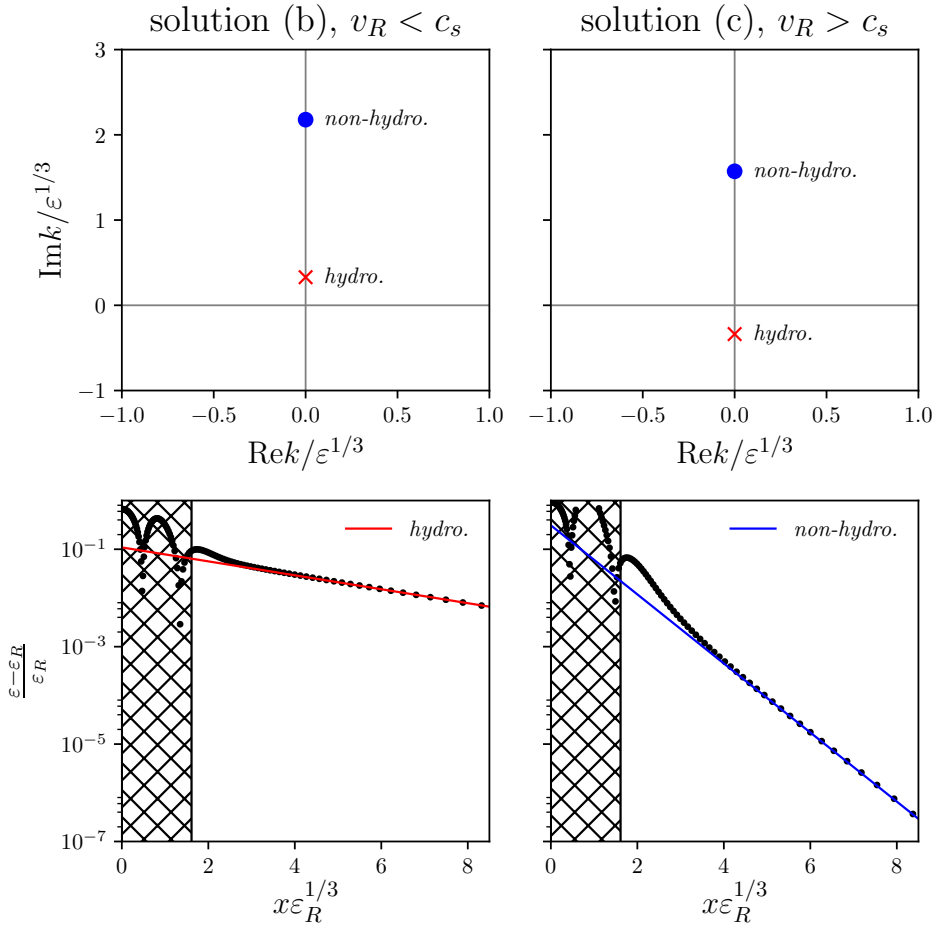

Figure 3.19: Matching the downstream asymptotics of the subsonic flow solution (b) (left column) and the supersonic flow solution (c) (right column) to spatial collective modes. Upper panels show the leading pole structure in the complex-k plane as computed in [9] in the neutral case of relevance here, and in section 3.2.5 with finite charge density. Lower panels show the asymptotic behaviour of ε using log-linear axes. The black dots are the nonlinear solutions and the solid lines are the spatial collective modes. As v_R is increased through c_s the hydrodynamic spatial collective mode (red) transitions from downstream to upstream and the long-range behaviour downstream jumps to the longest non-hydrodynamic mode (blue).

where we have re-introduced the speed of light, c. To estimate this length for graphene we utilise a number of existing results in the literature. Firstly, we introduce the Fermi velocity via $c = v_F$ which we take to be $v_F = 10^6 m/s$ as in the experimental results of [100]. Next we utilise the value for η/s computed in kinetic theory in [101], i.e. we take $\eta/s \simeq 0.00815 \left(\log T_\Lambda/T\right)^2 \frac{\hbar}{k_B}$ with UV cutoff $T_\Lambda = 8.34 \times 10^4 K$. Finally we must provide v and T for the experiment of interest. For flow velocities at around $v \simeq 10^4 m/s$ as in the setup of [102] we obtain $|\mathrm{Im}k|^{-1} \simeq 0.7 \mu m$ at standard temperature, whilst the experiments of [103] obtain much higher velocities $v \simeq 3 \times 10^5 m/s$ giving rise to $|\mathrm{Im}k|^{-1} = 15nm$ at $T \simeq 400K$. For comparison we may consider the strongly interacting $\mathcal{N} = 4$ SYM plasma with $c = 3 \times 10^8 m/s$, under the same conditions, finding $|\mathrm{Im}k|^{-1} \simeq 2cm$ and

$|\mathrm{Im}k|^{-1} \simeq 0.4mm$ in each case. The main difference between the decay lengths in the two theories arises from the quadratic scaling with the speed of light in (3.143), rather than the minor differences in η/s.

Let us now move on to a discussion of interesting open issues as well as promising directions for future work. Throughout this work we have emphasized parallels between the SCM here and their timelike cousins, the QNM. Let us now address some important differences. An important conceptual point concerns the issue of causality. From our construction one may get the impression that there really exists a notion of a 'spatially retarded' correlation function as defined in 3.2.1, in complete analogy to the temporally retarded, i.e. causal, one. This is not so, and our construction should be seen more as a convenience in order to exhibit a particular set of modes in the field-theory, essentially by defining correlation functions that are analytic in either the upper or lower half complex k plane. Note that in the QNM context, for a stable system, the analyticity in the complex ω plane really is dictated by causality; a system reacts to a disturbance after the quench is applied, and does not have a way of 'knowing' that it will be perturbed before it actually gets hit. In other words, only modes decaying towards the future are physically relevant and therefore only retarded correlation functions enter the discussion. By contrast, for the 'spatial quench' considered here, the system does exhibit both modes that decay toward positive x as well as negative x (although these modes are generically different from one another). This becomes clear if we consider such a steady state as something that is formed at late times via a time dependent process, since in this case all parts of the system have had causal contact with one another regardless of the flow velocity. Thus, even though for much of the discussion we can think of the SCM as being spacelike analogs of QNM with the special direction x being treated like time, fundamentally the equations both of the dual gravity and the field theory are hyperbolic with respect to the time coordinate t and thus the above causal restrictions apply.

The distinction between QNM and SCM is particularly salient for non-relativistic theories, where we cannot define one as an analytic continuation of a boosted version of the other. Note that this was the way we constructed the tower of SCM in three dimensions. In looking for SCM about an asymptotic state with flow velocity v we instead boosted into a frame where the fluid was at rest and solved the QNM dispersion relation for the boosted values of the frequency and momentum (3.104). The resulting mode necessarily had complex momentum k, and could also have been constructed directly by solving the perturbation equations in the lab frame where the fluid has finite velocity v. In other words, in the relativistic context we can consider the dispersion relations of linear modes as being defined on a $\mathbb{C}^2$ spanned by both complex ω and complex k and SCM and QNM are merely two different slices (real k and real ω respectively) of the more general situation. This will not be true in the non-relativistic context, which illustrates that generically the two really describe two different classes of physical phenomena. For this reason it would be enlightening to explore our construction of SCM in non-relativistic theories, perhaps starting from a hydrodynamic effective treatment and then moving on to a model with non-relativistic holography.

Other future directions of interest relate to decreasing the amount of symmetry in the steady state, either by increasing the co-dimension of the obstacle, or by adding spatial inhomogeneities along the direction(s) of the obstacle. In the most

general setups one will likely have to confront the issue of heating and whether a parametrically large steady state region (both in space and time) can be established [104, 105].

Finally it will be important to study issue of time dependence, both in the sense of establishing the steady state from an initial equilibrium state, say by gradually switching on the obstacle, and in the sense of stability to perturbations of the steady state itself (this latter question has already been considered for steady states in ideal hydrodynamics by [106]).

4

HYDRODYNAMICS WITHOUT BOOSTS

4.1 INTRODUCTION

Any system that finds itself in a state of local thermodynamic equilibrium, is thought to evolve to its global equilibrium state, described by universal long-wavelength, long time-scale hydrodynamics, respecting positivity of entropy production. The universal theory governing this dynamics, corresponds to the relaxation of all conserved quantities of a given system, and can be adapted to particular physical situations of interest by specifying an equation of state, as well as the functional form and value in equilibrium of a specified set of transport coefficients [4].

Hydrodynamics is an extremely successful practical example of the philosophy of effective field theory. Its equations are formulated by arranging terms in ascending order of derivatives, truncating at a specified order in this expansion[1]. The possible terms that may appear in this expansion are restricted by the symmetries as well as the usual rules of effective field theories, in such a way as to reduce an a-priori redundant set of transport coefficients to a smaller, purely physical subset. The fewer symmetries one requires, the more general the resulting framework, and the larger the number of allowed transport coefficients. From this one may recover previously known, more symmetric versions by taking appropriate limits.

The main impetus to develop the general theory, apart from being structurally interesting, is of course that situations arise in which the least symmetric theory is the only one applicable. For example, in order to clarify the distinction between ordinary quasi-normal modes and the spatial collective modes of [8, 9] one should look to non-boost invariant systems. A non-relativistic hydrodynamic theory without Galilean invariance is furthermore needed to describe the electron fluid of graphene at finite carrier density [107, 108]. Another area where such examples are relevant is biophysics. Consider, for example, the case of a system of a large number of *self-propelled* organisms such as birds, moving through a *fixed medium*, such as the air. A coarse grained description of such a collection of self-propelled "particles" in terms of fluid dynamics will be translation invariant, but not invariant under any form of boosts. For a perspective of applying non boost-invariant hydrodynamics to flocking behavior of birds, the reader may want to consult [109]. Applications to the theory of active matter are discussed in [110–112]. It should be noted that our results are not directly applicable to the settings discussed in references [109–112] as these involve translation-breaking terms visible at the level of the equations of motions already at ideal order, as well as non-conservation terms on the right hand side. Such effects could be systematically studied by further breaking the symmetries of our setup to allow for broken translations, and by turning on appropriate sources.

1 For a clear review of this procedure in a relativistic system, see [5]

In the spirit of proceeding from the most general to the more specific, in this chapter we formulate the complete first-order theory of hydrodynamics invariant under time translations $\mathbb{R}_t$, the Euclidean group of spatial symmetries $\mathrm{ISO}(d)$ and containing a conserved charge or particle number leading to the total symmetry group $\mathbb{R}_t \times \mathrm{ISO}(d) \times \mathrm{U}(1)$. Such a theory does not possess any form of boost symmetry, be it of non-relativistic Galilean or relativistic Lorentz form. We also explain how to recover previously known examples of Galilean-invariant, Lifshitz-invariant and relativistically invariant hydrodynamics as a limiting procedure. In all these the number of transport coefficients is reduced, sometimes drastically.

We approach this theory from the non-relativistic, non-boost invariant side, but it is also interesting and informative to ask the opposite question: if we were to start with a relativistically invariant theory, what different patterns of symmetry breaking and what kind of non-relativistic and non-boost invariant structures can possibly arise? This was answered for equilibrium configurations in [113], where the resulting states can be classified according to eight different symmetry-breaking patterns, according to how the remaining generators of Poincaré are twisted with internal symmetries. In their language we are developing the hydrodynamics of a"type-I framid", which breaks full Poincaré invariance down to only translations and rotations without any internal symmetry twist, in other words to $\mathbb{R}_t \times \mathrm{ISO}(d) \times G_{\text{internal}}$. We will exclusively focus on the case where the internal symmetry is $\mathrm{U}(1)$. As was already noted in [113] this pattern of symmetry breaking is closely related to Einstein-Aether theory [114] and can be seen as the breaking of Poincaré invariance induced by a time-like expectation value of a vector operator.

The authors of [115–117] analyse linearised hydrodynamic fluctuations at first order in the derivative expansion for fluid flows at rest with respect to the preferred reference frame. As our analysis in the following shows, the more general case of arbitrary velocity with respect to the preferred reference frame, forces one to introduce a larger number of additional transport coefficient and thus exhibits new physics associated with these.

4.2 NON-BOOST-INVARIANT HYDRODYNAMICS

Figure 4.1 gives a conceptual overview of the procedure we follow in order to construct the general non boost-invariant hydrodynamic theory at first dissipative order. The challenge in this construction lies in the large number of allowed tensor structures (45 in the general setting) and transport coefficients (29 in the general setting[2]) and so it is essential to ensure one includes all terms and to be calculationally as efficient as possible. Hydrodynamics, being defined as a gradient expansion, contains the usual field redefinition ambiguities inherent in effective field theory constructions. At first order – the highest order to we explore in this work – one may adjust the coefficients of a certain subset of tensor structures, by a) using the zeroth-order equations of motion and b) by redefining the zeroth-order hydrodynamic variables (temperature, velocity and chemical potential) by first-order shifts. This means that not all coefficients appearing at first order are

2 This count includes both dissipative and non-dissipative transport coefficients at first order. Eliminating the latter class reduces the count further to 20.

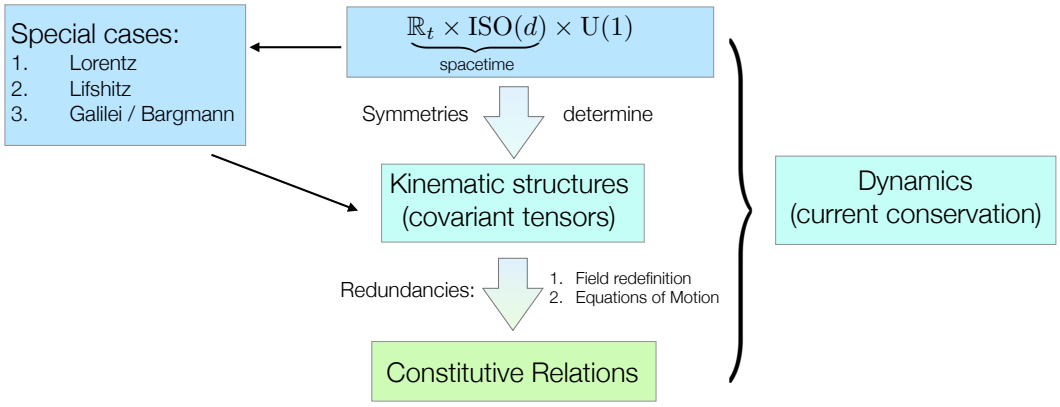

Figure 4.1: Here we give the roadmap of our construction. In the spirit of effective field theory, we first identify the most general symmetry group applicable for our purposes. For the purpose of this chapter we focus on $\mathbb{R}_t \times \mathrm{ISO}(d) \times \mathrm{U}(1)$. Next we write down all possible kinematic structures compatible with that symmetry, which are then constrained by the fixing redefinition ambiguities present in the construction. Finally the remaining physical quantities are then subject to a dynamical principle, which in the case of hydrodynamics follows simply from conservation of the stress tensor and current. From the most general and therefore least constrained structure we also recover more highly symmetric previously known examples as limiting cases as shown in the leftmost box.

physical transport coefficients and our goal becomes to isolate only those that are. Once all equations of motion have been imposed, the remaining ambiguities are those associated to shifts of the hydrodynamic variables. In a boost-invariant setting these ambiguities are typically fixed by a choice of hydrodynamic frame, such as Landau frame. Here, in the non boost-invariant setting, we demonstrate similarly that all remaining ambiguities are fixed by an appropriate frame choice. It is encouraging that the resulting theory, in all limiting cases, reduces to the previously known constructions with the right number of transport coefficients and tensor structures.

4.2.1 *The ideal fluid*

We being our construction of the general first-order hydrodynamics theory with symmetry $\mathbb{R}_t \times \mathrm{ISO}(d) \times \mathrm{U}(1)$ by writing the constitutive relations up to first order in derivatives. This task is facilitated by the work of [115, 116], who wrote down, in the first instance, the constitutive relations for an *ideal* fluid in this symmetry class. These authors write the constitutive relations in the laboratory frame where the fluid has velocity v^i:

$$T^{(0)0}{}_0 = -\mathcal{E}, \quad T^{(0)0}{}_j = \rho v^j, \quad T^{(0)i}{}_0 = -(\mathcal{E}+P)v^i, \quad T^{(0)i}{}_j = P\delta^i_j + \rho v^i v^j. \tag{4.1}$$

$$J^{(0)0} = n, \quad J^{(0)i} = n v^i \tag{4.2}$$

In these expressions $\mathcal{E}$ and P are the energy density and pressure, n is the particle density or charge density (depending on the chosen interpretation of the $\mathrm{U}(1)$ symmetry), while ρ is the "kinetic mass density" [115]. This additional thermody-

namic function is generically different from the mass density due to the absence of a boost symmetry and must therefore be included independently in all boost-non-invariant cases. In total we thus have the thermodynamic functions $\mathcal{E}, P, n$ and ρ, which are arbitrary functions of the thermodynamic variables, namely the temperature $T(t, x^i)$, the square of the velocity field $v^2(t, x^i)$ and the chemical potential $\mu(t, x^i)$. A related quantity that we will sometimes find convenient is the internal energy $\tilde{\mathcal{E}} := \mathcal{E} - \rho v^2$. The principal interest of this chapter is to extend this to the dissipative level, more precisely to first order in the hydrodynamic expansion, keeping arbitrary the velocity with respect to the preferred reference frame, v^i. A linear analysis in v^i around $v^i = 0$ is performed in [116], giving the hydrodynamic modes in the preferred frame.

4.2.2 *Dissipative corrections*

The goal of this section is to write down the general constitutive relations for stress tensor and current at first order in derivatives with respect to the hydrodynamical variables. Keeping with common notation in the literature we write

$$T^{\mu}{}_{\nu} = T^{(0)\mu}{}_{\nu} + \Pi^{\mu}{}_{\nu}, \tag{4.3}$$

$$J^{\mu} = J^{(0)\mu} + \Pi^{\mu}, \tag{4.4}$$

where $\Pi^{\mu}{}_{\nu}$ and Π^{μ} contain terms of first-order or higher in derivatives of the hydrodynamic variables. These contain the dissipative terms (in addition to several non-dissipative transport coefficients which we will discuss in detail).

As has been outlined above, there is a large degree of redundancy to be fixed, which stems from the way hydrodynamics is arranged as an expansion in derivatives. The ambiguity is usually fixed by making use of a particular 'frame' (e.g. Landau frame). We will ultimately make such a choice as well, but not before systematically exploring precisely what ambiguity is present in the general non boost-invariant hydrodynamic theory, and that our choice of frame consistently fixes the ambiguity. A loose, but helpful, analogy here is the construction of a putative new gauge theory, where one would be interested to demonstrate that a particular gauge condition actually fixes the full redundancy.

Let us therefore now discuss in more detail what sort of redundancies arise in the construction.

4.2.2.1 *Field redefinitions*

The first class of redundancy we need to take into account comes from the fact that shifts of the form

$$\begin{aligned} T(t, x^i) &\longrightarrow T(t, x^i) + \delta T(t, x^i), \\ v^i(t, x^i) &\longrightarrow v^i(t, x^i) + \delta v^i(t, x^i), \\ \mu(t, x^i) &\longrightarrow \mu(t, x^i) + \delta\mu(t, x^i), \end{aligned} \tag{4.5}$$

where the $\delta T(t, x^i)$ etc. are of first order in derivatives, do not affect the ideal part of the theory, but do introduce shifts at first order. Physically this means that we may consider a family of redefinitions of the hydrodynamic variables

scalars	$\left[v^k\partial_k T\right],\ v^k\partial_k v^2,\ v^k\partial_k \frac{\mu}{T},\ \left[\partial_t T\right],\ \partial_t v^2,\ \left[\partial_t \frac{\mu}{T}\right],\ \partial_k v^k$
vectors	$\left[\partial_i T\right],\ \partial_i v^2,\ \partial_i \frac{\mu}{T},\ \partial_t v^i,\ v^k\partial_k v^i,\ v^i\cdot$ (scalars)
tensors	$\sigma_{ij},\ v^{(i}\cdot$ (vectors)$^{j)},\ \delta^i_j\cdot$ (scalars)

Table 4.1: An overview of all the different one-derivative terms of the thermodynamic variables we can write down, with respect to the symmetries of the system. The parentheses around the indices denote a symmetric tensor, since $T^i_{\ j} = T^j_{\ i}$. The terms in square brackets are the terms we eliminate using the equations of motion at zeroth order. Here $\sigma_{ij} = \partial_i v^j + \partial_j v^i - \delta^i_j \frac{2}{d}\partial_k v^k$ is the shear tensor and d is the number of spatial dimensions. Note that we do not decompose the vectors into components transverse to the velocity, since we are also interested in situations where $v^i = 0$.

$T(t,x^i), v^i(t,x^i), \mu(t,x^i)$ by gradient terms which all agree in equilibrium, when those gradient terms vanish. Such a redefinition, by the chain rule, also causes shifts of the thermodynamic functions $\mathcal{E}, P, \rho, n$.

The second kind of ambiguity arises since, when working to first order in the gradient expansion, one may always use the zeroth-order equations of motion in order to simplify the expressions appearing at first order.

4.2.2.2 *Tensor structures and equations of motion ambiguity*

Concretely this is done by using the equations to express certain tensor structures in terms of the remaining ones. The most efficient way to implement this, is by first enumerating all possible tensor structures allowed by the symmetries at first order and then eliminating a convenient set using the zeroth order equations of motion. This then results in a smaller effective set of tensor structures, which are then still subject to the field redefinition ambiguity mentioned above. However, it is considerably simpler to apply the latter to the reduced effective set of tensor structures, which is the procedure we will follow. Indicated in table 4.1 are all the allowed tensor structures at first order, classified by their content under the ISO(d) symmetry. In this work we focus solely on parity-preserving transport. Note it is natural to consider further decomposing the vectors listed in 4.1 into scalars (by contracting with v^i) and pieces transverse to the velocity (by using a projector $P^{ij} = \delta^{ij} - v^i v^j/v^2$). However, we opt not to take this step since such a decomposition fails to be well-defined for $v^i = 0$. This is to be contrasted with the relativistic case where one may always decompose with respect to u^μ.

Note that the same tensor structure can appear multiple times in different currents. For example, the scalars are counted seven times, because they contribute five times to the stress tensor, and two times to the U(1) current. To be more precise, they appear once in J^0 and once in J^i, where they are multiplied by v^i to form a vector. Similarly they contribute to different index structures in the stress tensor multiplied by appropriate combinations of the v^i and δ^{ij}.

Having thus defined the full set of tensor structures, we use the equations of motion at the ideal fluid level,

$$\partial_\mu T^{(0)\mu}{}_0 = 0, \tag{4.6}$$
$$\partial_\mu T^{(0)\mu}{}_j = 0, \tag{4.7}$$
$$\partial_\mu J^{(0)\mu} = 0, \tag{4.8}$$

to eliminate as many first-order structures as possible. We have of course a large amount of freedom to choose which ones to eliminate. We go with the customary selection of eliminating $\partial_i T, \partial_t T$ and $\partial_t \frac{\mu}{T}$. This gives us the desired reduced set of physical tensor structures, in which to expand our field-redefinitions.

We now have all the ingredients necessary to write down and constrain the first-order stress tensor and current.

4.2.2.3 *First-order constitutive relations and choice of frame*

Expanded in our reduced basis of tensor structures (see table 4.1), the field redefinitions now take the form

$$\delta T \longrightarrow a_1 v^k \partial_k v^2 + a_2 v^k \partial_k \frac{\mu}{T} + a_3 \partial_t v^2 + a_4 \partial_k v^k \tag{4.9}$$
$$\delta \mu \longrightarrow a_5 v^k \partial_k v^2 + a_6 v^k \partial_k \frac{\mu}{T} + a_7 \partial_t v^2 + a_8 \partial_k v^k \tag{4.10}$$
$$\begin{aligned}\delta v^i \longrightarrow\ & a_9 \partial_i v^2 + a_{10} \partial_i \frac{\mu}{T} + a_{11} \partial_t v^i + a_{12} v^k \partial_k v^i + \\ & + v^i \left(a_{13} v^k \partial_k v^2 + a_{14} v^k \partial_k \frac{\mu}{T} + a_{15} \partial_t v^2 + a_{16} \partial_k v^k \right)\end{aligned} \tag{4.11}$$

with free coefficients $\{a_i\}_{i=1}^{16}$. These redefinition ambiguities see themselves confronted with the most general first order stress tensor, again expanded in the reduced basis of tensor structures

$$\Pi^0_0 = c_1 v^k \partial_k v^2 + c_2 v^k \partial_k \frac{\mu}{T} + c_3 \partial_t v^2 + c_4 \partial_k v^k \tag{4.12}$$
$$\begin{aligned}\Pi^0_j = & c_5 \partial_j v^2 + c_6 \partial_j \frac{\mu}{T} + c_7 \partial_t v^j + c_8 v^k \partial_k v^j + \\ & + v^j \left(c_9 v^k \partial_k v^2 + c_{10} v^k \partial_k \frac{\mu}{T} + c_{11} \partial_t v^2 + c_{12} \partial_k v^k \right)\end{aligned} \tag{4.13}$$
$$\begin{aligned}\Pi^i_0 = & c_{13} \partial_i v^2 + c_{14} \partial_i \frac{\mu}{T} + c_{15} \partial_t v^i + c_{16} v^k \partial_k v^i + \\ & + v^i \left(c_{17} v^k \partial_k v^2 + c_{18} v^k \partial_k \frac{\mu}{T} + c_{19} \partial_t v^2 + c_{20} \partial_k v^k \right)\end{aligned} \tag{4.14}$$
$$\begin{aligned}\Pi^i_j = & c_{21} \sigma_{ij} + c_{22} \left(v^i \partial_j v^2 + v^j \partial_i v^2 \right) + c_{23} \left(v^i \partial_j \frac{\mu}{T} + v^j \partial_i \frac{\mu}{T} \right) \\ & + c_{24} \left(v^i \partial_t v^j + v^j \partial_t v^i \right) + c_{25} \left(v^i v^k \partial_k v^j + v^j v^k \partial_k v^i \right) \\ & + v^i v^j \left(c_{26} v^k \partial_k v^2 + c_{27} v^k \partial_k \frac{\mu}{T} + c_{28} \partial_t v^2 + c_{29} \partial_k v^k \right) \\ & + \delta^i_j \left(c_{30} v^k \partial_k v^2 + c_{31} v^k \partial_k \frac{\mu}{T} + c_{32} \partial_t v^2 + c_{33} \partial_k v^k \right)\end{aligned} \tag{4.15}$$

containing the set $\{c_i\}_{i=1}^{33}$ of unconstrained coefficients. To this we add the current

$$\Pi^0 = c_{34} v^k \partial_k v^2 + c_{35} v^k \partial_k \frac{\mu}{T} + c_{36} \partial_t v^2 + c_{37} \partial_k v^k \tag{4.16}$$

$$\Pi^i = c_{38} \partial_i v^2 + c_{39} \partial_i \frac{\mu}{T} + c_{40} \partial_t v^i + c_{41} v^k \partial_k v^i + \\ + v^i \left(c_{42} v^k \partial_k v^2 + c_{43} v^k \partial_k \frac{\mu}{T} + c_{44} \partial_t v^2 + c_{45} \partial_k v^k \right) \tag{4.17}$$

which carries the set $\{c_i\}_{i=34}^{45}$ of unconstrained coefficients, which, using the ambiguities above get whittled down to 29 remaining physical transport coefficients. Imposing that non-dissipative contributions vanish may further reduce this number and we return to this point in our analysis of the entropy current. This is still a somewhat large number, but in the following we will develop more intuition for their physical meaning by considering limiting cases with more symmetries.

Implementing the zeroth-order shifts results in

$$T^\mu{}_\nu = T^{(0)\mu}{}_\nu + \underbrace{\delta \left(T^{(0)\mu}{}_\nu \right) + \Pi^\mu{}_\nu \left(\{c_i\} \right)}_{= \Pi^\mu{}_\nu (\{\tilde{c}_i\})} \tag{4.18}$$

$$J^\mu = J^{(0)\mu} + \underbrace{\delta \left(J^{(0)\mu} \right) + \Pi^\mu \left(\{c_i\} \right)}_{= \Pi^\mu (\{\tilde{c}_i\})}, \tag{4.19}$$

in other words we may think of the field redefinitions as acting on the first-order stress tensor and current by moving in the space of coefficients

$$c_i \to \tilde{c}_i = c_i + M_{ij} a^j , \tag{4.20}$$

where the coefficients M_{ij} form the elements of a 45×16 matrix.

The structure we just exposed means that the ambiguities of the first-order stress tensor and current can be understood as a linear, α-dependent trajectory in the space of coefficients $\{c_i\}$. Any two stress tensors lying on the same trajectory through this space are physically equivalent (and similarly for the current), and so our next goal is to put conditions on the first-order stress tensor and current that fix the ambiguity. In other words, we would like to select one representative for each orbit through the space of $\{c_i\}$. We will now demonstrate that the natural generalization of what is usually called the Landau frame supplies a sufficient number of conditions on the first-order quantities to fully fix their form. The Landau frame conditions appropriate to our symmetry class were given in [116] and read

$$T^\mu{}_\nu u^\nu = -\tilde{\mathcal{E}} u^\mu \Longrightarrow \begin{cases} \mu = 0 : & T^0{}_0 + T^0{}_j v^j = -\tilde{\mathcal{E}} \\ \mu = i : & T^i{}_0 + T^i{}_j v^j = -\tilde{\mathcal{E}} v^i \end{cases} \tag{4.21}$$

The eigenvector u^μ is parametrized as $u^\mu = u^0 (1, v^i)$, where u^0 is a function of thermodynamic variables and is not fixed. The frame condition for the $U(1)$ current can be taken as [115]

$$\bar{u}_\mu J^\mu = -\frac{1}{u^0} n. \tag{4.22}$$

In fact u^0 is not the only freedom that enters in the choice of frame. Due to the lack of a metric structure to lower the index on u^μ, the corresponding object with index down, $\bar{u}_\mu$, is again for us to choose. We shall employ the same choice as [115], namely we take $\bar{u}_\mu$, such that

$$u^\mu \bar{u}_\mu = -c^2\,, \qquad \text{with} \qquad \bar{u}_\mu = \frac{1}{u^0}(-c^2 - Bv^2, Bv^i) \tag{4.23}$$

parametrized in terms of v^i and the free function B, which may in general depend on the thermodynamic variables. The parameters B, c^2 and u^0 are all free choices giving different hydrodynamic frames, that is for each choice of B, c^2, u^0 there is a corresponding Landau frame. However, we retain them explicitly in our construction, as this facilitates our later analysis of limiting cases. In certain more highly symmetric situations these parameters are naturally chosen by the requirement that the frame condition is constructed in accordance with the symmetries at hand. For example for a Lorentz invariant fluid $(u^0)^2 = B = \frac{1}{1-v^2/c^2}$, while a Galilean invariant fluid has $B = 0$ and $u^0 = 1$.

Fixing the frame will reduce the number of coefficients we have in the constitutive relations. Initially, we had 45 different coefficients $\{c_i\}$ in (4.12) - (4.17). The Landau frame conditions, (4.21) and (4.22), give us 16 constraints, resulting in 29 physical transport coefficients. In practice, we solve the Landau conditions by requiring all the coefficients that multiply different tensor structures in different components of $\Pi^\mu{}_\nu$ and J^μ to vanish. These coefficients are functions of c_i and a_i, and we solve the resulting 16 equations for $a_1, \ldots, a_{16}$. Having done that, the new coefficients are functions of only c_i and we can explicitly see that there are only 29 different coefficients. These we have relabelled as detailed below, and each are functions of T, v^2, μ. This brings us to our main result for the constitutive relations at first order.

Stress tensor

$$
\begin{aligned}
\Pi^0_0 &= \gamma_2 v^k \partial_k v^2 + \left(\gamma_1 v^2 + \tfrac{\bar{\pi}}{2}\right) \partial_t v^2 + \gamma_3 v^2 \partial_k v^k + (\gamma_4 v^2 - T(\bar{\alpha} + \bar{\gamma})) v^k \partial_k \tfrac{\mu}{T} \\
\Pi^0_j &= \gamma_5 \partial_j v^2 + \gamma_6 v^k \partial_k v^j + T(\bar{\alpha} + \bar{\gamma}) \partial_j \tfrac{\mu}{T} - \bar{\pi} \partial_t v^j \\
&\quad - v^j \left(\tfrac{1}{2v^2}(2\gamma_2 + 2\gamma_5 + \gamma_6) v^k \partial_k v^2 - \gamma_4 v^k \partial_k \tfrac{\mu}{T} - \gamma_1 \partial_t v^2 - \gamma_3 \partial_k v^k\right) \\
\Pi^i_0 &= \left(\gamma_8 v^2 + \tfrac{\bar{\eta}}{2}\right) \partial_i v^2 + \left(\gamma_{13} v^2 + \bar{\eta}\right) v^k \partial_k v^i + \gamma_7 v^2 \partial_t v^i + \gamma_{14} v^2 \partial_i \tfrac{\mu}{T} \\
&\quad + v^i \left(\gamma_9 v^k \partial_k v^2 + \gamma_{10} \partial_t v^2 + \left(\gamma_{11} v^2 + \bar{\zeta} - \tfrac{2\bar{\eta}}{d}\right) \partial_k v^k + \gamma_{12} v^k \partial_k \tfrac{\mu}{T}\right) \\
\Pi^i_j &= \delta^i_j \left(\gamma_{15} v^k \partial_k v^2 + \gamma_{17} v^k \partial_k \tfrac{\mu}{T} + \gamma_{16} \partial_t v^2 - \bar{\zeta} \partial_k v^k\right) - \bar{\eta} \sigma_{ij} \\
&\quad - \gamma_8 \left(v^i \partial_j v^2 + v^j \partial_i v^2\right) - \gamma_{14} \left(v^i \partial_j \tfrac{\mu}{T} + v^j \partial_i \tfrac{\mu}{T}\right) \\
&\quad - \gamma_7 \left(v^i \partial_t v^j + v^j \partial_t v^i\right) - \gamma_{13} \left(v^i v^k \partial_k v^j + v^j v^k \partial_k v^i\right) \\
&\quad + \tfrac{v^i v^j}{v^2} \left(\left(\tfrac{1}{2}\gamma_{13} - \gamma_{15} + \gamma_8 - \gamma_9\right) v^k \partial_k v^2 - (\gamma_{12} - \gamma_{14} + \gamma_{17}) v^k \partial_k \tfrac{\mu}{T}\right. \\
&\quad \left. - (\gamma_{10} + \gamma_{16} - \tfrac{1}{2}\gamma_7) \partial_t v^2 - \gamma_{11} v^2 \partial_k v^k\right)
\end{aligned}
$$

U(1) current

$$
\begin{aligned}
\Pi^0 &= \tfrac{B}{c^2 + B v^2} \left(\gamma_{19} v^k \partial_k v^2 + \tfrac{1}{2}(\bar{\alpha} + 2v^2 \gamma_{18} - \bar{\gamma}) \partial_t v^2 + \gamma_{20} v^2 \partial_k v^k + (\gamma_{21} v^2 - T\bar{\sigma}) v^k \partial_k \tfrac{\mu}{T}\right) \\
\Pi^i &= \gamma_{22} \partial_i v^2 + \gamma_{23} v^k \partial_k v^i - T\bar{\sigma} \partial_i \tfrac{\mu}{T} + (\bar{\alpha} - \bar{\gamma}) \partial_t v^i \\
&\quad + v^i \left(\tfrac{1}{2v^2}(2\gamma_{19} - 2\gamma_{22} - \gamma_{23}) v^k \partial_k v^2 + \gamma_{21} v^k \partial_k \tfrac{\mu}{T} + \gamma_{18} \partial_t v^2 + \gamma_{20} \partial_k v^k\right)
\end{aligned}
$$

Transport coefficients

$\bar{\eta}, \bar{\zeta}, \bar{\sigma}, \bar{\alpha}, \bar{\gamma}, \bar{\pi}, \quad \gamma_1, \ldots, \gamma_{23}$ (each a function of T, v^2, μ)

(4.24)

Note that 29 transport coefficients is the count before the constraints of positivity of entropy current have been applied. The transport coefficients $\bar{\eta}, \bar{\zeta}, \bar{\sigma}, \bar{\alpha}, \bar{\gamma}, \bar{\pi}$ become those utilised in [116] in a linear perturbation analysis around a uniform zero-velocity background, i.e. $\eta_0, \zeta_0, \sigma_0, \alpha_0, \gamma_0, \pi_0$, respectively, but otherwise differ as here they are functions of v^2 too. We will see that imposing boost symmetry, be it Lorentz, or Galilean, significantly reduces the number of transport coefficients. Imposing Lifshitz symmetry will constrain the functional form of the transport coefficients as well as reduce their number (though not as significantly as boost symmetry).

4.2.3 *Entropy current*

One of the physical requirements of any theory of hydrodynamics is its adherence to the second law, namely the positivity of entropy production. At equilib-

rium one can readily identify a unique entropy current, however at first order in the hydrodynamic expansion there can be several ambiguities. Nevertheless, as is well-known, the process of defining the most general entropy current and demanding that its divergence is non-negative can still lead to definitive constraints on transport coefficients. We shall elucidate this in what follows.

The procedure outlined above is straightforward; we wish to construct the most general expression for the entropy current S^μ consistent with the symmetries at hand, up to first derivative order, and then ensure that $\partial_\mu S^\mu \geq 0$. The entropy current at ideal order is then given by $S^\mu = sv^\mu + O(\partial)$ where $v^\mu \equiv (1, v^i)^\mu$. One can verify that with this definition, $\partial_\mu S^\mu = 0 + O(\partial)^2$, ensuring there is no entropy production at this hydrodynamic order.

In order to construct the most general first order contribution to S^μ consistent with symmetries, it is convenient to split S^μ into two contributions, a canonical part, and a non-canonical part,

$$S^\mu = S^\mu_{\text{can}} + S^\mu_{\text{non}}. \tag{4.25}$$

We shall begin with the canonical part. Consider the expression for the entropy density,

$$\begin{aligned} Ts &= \varepsilon - \rho v^2 + P - \mu n && (4.26)\\ \implies Tsv^\mu &= -T^{(0)\mu}{}_\nu v^\nu + Pv^\mu - \mu J^{(0)\mu}. && (4.27) \end{aligned}$$

Inspired by (4.27) we now define S^μ_{can} which, by construction, differs from sv^μ by terms that are at least first order in derivatives,

$$TS^\mu_{\text{can}} \equiv -T^\mu{}_\nu v^\nu + Pv^\mu - \mu J^\mu, \tag{4.28}$$

whose divergence is easily evaluated,

$$\partial_\mu S^\mu_{\text{can}} = -\Pi^\mu{}_\nu \partial_\mu \frac{v^\nu}{T} - \Pi^\mu \partial_\mu \frac{\mu}{T} \tag{4.29}$$

and crucially depends only on products of first derivatives; there are no explicit second derivative terms. What remains in order to construct S^μ proper is the non-canonical part, which is simply the most general set of terms consistent with the symmetries at hand. In other words, the construction of S^μ_{non} parallels our enumeration of the possible terms allowed in the constitutive relations:

$$\begin{aligned} S^0_{\text{non}} &= \tilde{c}_1 v^k \partial_k v^2 + \tilde{c}_2 v^k \partial_k \frac{\mu}{T} + \tilde{c}_3 \partial_t v^2 + \tilde{c}_4 \partial_k v^k, && (4.30)\\ S^i_{\text{non}} &= \tilde{c}_5 \partial_i v^2 + \tilde{c}_6 \partial_i \frac{\mu}{T} + \tilde{c}_7 \partial_t v^i + \tilde{c}_8 v^k \partial_k v^i + \\ &\quad + v^i \left(\tilde{c}_9 v^k \partial_k v^2 + \tilde{c}_{10} v^k \partial_k \frac{\mu}{T} + \tilde{c}_{11} \partial_t v^2 + \tilde{c}_{12} \partial_k v^k \right). && (4.31) \end{aligned}$$

There are two types of contribution to $\partial_\mu S^\mu$: there are products of first derivatives (as is the case for $\partial_\mu S^\mu_{\text{can}}$), and there are second derivative terms. Our first task is to use the equations of motion to maximally reduce the number of terms that can appear, and we do so here by eliminating all terms that contain one or more time derivatives. We then require that the coefficients of the remaining second

derivative terms vanish, since they do not have a definite sign. This results in equality-type constraints (as opposed to inequality-type) that fix 8 out of the 12 coefficients in the definition of S^μ_{non},

$$\begin{array}{l|l|l|l} \tilde{c}_5 = 0 & \tilde{c}_6 = 0 & \tilde{c}_{10} = \tilde{c}_2 & \tilde{c}_3 = m_1\tilde{c}_2 \\ \tilde{c}_4 + \tilde{c}_7 = m_2\tilde{c}_2 & \tilde{c}_8 + \tilde{c}_{12} = m_3\tilde{c}_2 & \tilde{c}_9 = m_4\tilde{c}_2 & \tilde{c}_1 + \tilde{c}_{11} = (m_1+m_2)\tilde{c}_2 \end{array} \tag{4.32}$$

where $m_{1,2,3,4}$ are constants of proportionality determined completely by the equation of state.[3] After imposing these conditions $\partial_\mu S^\mu$ is then quadratic in derivatives, taking the general form,

$$\partial_\mu S^\mu = \begin{pmatrix} \partial_i T \\ \partial_i \mu \\ \partial_i v_j \end{pmatrix}^{\mathrm{T}} \begin{pmatrix} T_{ik} & A_{ik} & B_{ikl} \\ A_{ki} & M_{ik} & C_{ikl} \\ B_{kij} & C_{kij} & V_{ijkl} \end{pmatrix} \begin{pmatrix} \partial_k T \\ \partial_k \mu \\ \partial_k v_l \end{pmatrix} \tag{4.33}$$

where the components of the matrix are given by all possible index contractions,

$$T_{ik} = b_0\delta_{ik} + b_1 v_i v_k \tag{4.34}$$
$$A_{ik} = b_2\delta_{ik} + b_3 v_i v_k \tag{4.35}$$
$$M_{ik} = b_4\delta_{ik} + b_5 v_i v_k \tag{4.36}$$
$$B_{ikl} = b_6 v_i\delta_{kl} + b_7 v_i v_k v_l + b_8\delta_{ik}v_l + b_9\delta_{il}v_k \tag{4.37}$$
$$C_{ikl} = b_{10} v_i\delta_{kl} + b_{11} v_i v_k v_l + b_{12}\delta_{ik}v_l + b_{13}\delta_{il}v_k \tag{4.38}$$
$$\begin{aligned} V_{ijkl} = {} & b_{14}\delta_{ik}\delta_{jl} + b_{15}\delta_{il}\delta_{jk} + b_{16}\delta_{ij}\delta_{kl} + b_{17} v_i v_j v_k v_l \\ & b_{18}(v_i v_j\delta_{kl} + v_k v_l\delta_{ij}) + b_{19}(v_i v_l\delta_{jk} + v_j v_k\delta_{il}) + \\ & b_{20} v_i v_k\delta_{jl} + b_{21} v_j v_l\delta_{ik}. \end{aligned} \tag{4.39}$$

We have computed each of these b_I coefficients explicitly, and in general they depend on the transport coefficients, the remaining redundancies in the definition of S^μ_{non} (i.e. the $\tilde{c}$) plus equation of state data.[4] For example, some of the more compact expressions we have encountered are,

$$b_{14} = \frac{\bar{\eta}}{T} \tag{4.40}$$
$$b_{15} = \tilde{c}_8 + \frac{\bar{\eta}}{T} \tag{4.41}$$
$$b_{20} = \frac{\bar{\pi} + \gamma_6 - \gamma_7 + \gamma_{13}}{T} \tag{4.42}$$
$$\frac{b_{21}}{4} - \frac{b_{19}}{2} + \frac{b_{20}}{4} = -\frac{1}{2}\frac{\partial \tilde{c}_3}{\partial v^2}. \tag{4.43}$$

So far, we have ensured that second derivative terms vanish, and computed the resulting quadratic form explicitly (4.33). We note that there are 22 coefficients appearing in the quadratic form but there are a total of 29 transport coefficients, and so we expect there to be non-dissipative combinations of transport coefficients which we will enumerate in the next section 4.2.3.1.

3 These coefficients are provided in a companion notebook to the paper [10].
4 These coefficients are provided in a companion notebook to the paper [10].

We also expect an additional class of equality-type constraints on transport coefficients. These usually arise in considerations of couplings to background fields, and by imposing time-reversal covariance in the form of Onsager reciprocal relations. In some cases these may be related to the non-dissipative contributions we discuss below.

Finally, the physical requirement of the second law $\partial_\mu S^\mu \geq 0$ requires that the quadratic form (4.33) be non-negative for all fluid configurations. These result in inequality-type constraints. As many of the coefficients appearing in (4.33) are of considerable length, we will not present an exhaustive analysis of these inequalities. However in section 4.2.3.2 we present a complete analysis of the inequalities that can be extracted by studying shear-type perturbations of uniform flow.

4.2.3.1 *Non-dissipative transport coefficients*

There are linearly independent combinations of transport coefficients that do not enter $\partial_\mu S^\mu$. Such terms are therefore responsible for effects which are nonuniform and non-dissipative, and thus potentially interesting physical effects in their own right. Moreover a theory constructed from such terms alone contains an additional conserved current, S^μ, and may therefore not be subject to the usual difficulties in constructing Lagrangian descriptions of hydrodynamics (see, for example, [118]). On the other hand, there may be physical requirements which dictate that such terms vanish. For example, constraints on such terms arise in the study of hydrostatic partition functions [119, 120]. To explore these terms in detail, in this section we enumerate the constraints that must be placed on the general theory to remove all non-dissipative contributions.

We begin by decomposing the currents appearing in $\partial_\mu S^\mu_{\text{can}}$, (4.29), into dissipative and non-dissipative pieces,

$$\Pi^\mu{}_\nu = (\Pi_{\text{D}})^\mu{}_\nu + (\Pi_{\text{ND}})^\mu{}_\nu, \tag{4.44}$$

$$\Pi^\mu = (\Pi_{\text{D}})^\mu + (\Pi_{\text{ND}})^\mu, \tag{4.45}$$

where the non-dissipative pieces (ND) do not enter $\partial_\mu S^\mu$ by definition, and the dissipative pieces (D) are here assumed to take the form,

$$\partial_\mu S^\mu = -(\Pi_{\text{D}})^\mu{}_\nu \partial_\mu \frac{v^\nu}{T} - (\Pi_{\text{D}})^\mu \partial_\mu \frac{\mu}{T}. \tag{4.46}$$

There are two classes of such non-dissipative transport coefficients.

The first class are those which arise directly in $\partial_\mu S^\mu_{\text{non}}$, as these manifestly do not enter (4.46). These, as we have already seen, are constructed from the remaining coefficients in the constitutive relation for S^μ_{non} after second-derivative constraints are imposed, namely (4.32), and are given by $\tilde{c}_1, \tilde{c}_2, \tilde{c}_4, \tilde{c}_8$. There can be additional equality-type constraints that result from considering new second-derivative terms that arise when background fields are turned on, as was demonstrated in the Lorentz invariant case [32]. Having recognised these terms as non-dissipative, for this section we now set $\tilde{c}_1 = \tilde{c}_2 = \tilde{c}_4 = \tilde{c}_8 = 0$ and the remaining entropy current is purely of canonical form.

We now turn to the second class of non-dissipative transport coefficients. Having imposed the vanishing of the first class of coefficients, there are 29 transport

coefficients remaining (those appearing in the constitutive relations for $\Pi^\mu{}_\nu$ and Π^μ) but only 22 independent terms in the quadratic form (the b_i) (4.33). Thus there are additional independent linear combinations of transport coefficients that are non-dissipative. We can now count how many such non-dissipative transport coefficients there are. Denoting a general transport coefficient as t_I, we can define a linear map $\mathcal{M}$ from the space of transport coefficients to the space of quadratic-form coefficients,

$$b_i = \mathcal{M}_{iJ} t_J, \tag{4.47}$$

where $\mathcal{M}$ is a 22×29 rectangular matrix. We are interested in how many linearly independent vectors there are in the vector space of transport coefficients that do not contribute to b_i. By direct computation we find that the rank of $\mathcal{M}$ is 20 and the dimension of its null space is 9. Thus we conclude that there is a vector space of dimension 20 spanned by dissipative transport coefficients (the image of $\mathcal{M}$), and a vector space of dimension 9 spanned by non-dissipative transport coefficients (the null space of $\mathcal{M}$). The linearly independent non-dissipative coefficients are as follows;

$$\gamma_{23} + \frac{\gamma_{22}}{2} + T\gamma_{14} - T\gamma_{12}, \tag{4.48}$$

$$\gamma_{18} + 2T\gamma_4 + 2v^2\bar{\gamma}, \tag{4.49}$$

$$\gamma_{16} - \gamma_2 + 2\gamma_3, \tag{4.50}$$

$$\gamma_{15} + 2\gamma_{11} - \gamma_9, \tag{4.51}$$

$$\gamma_{10} - \gamma_2, \tag{4.52}$$

$$\gamma_7 + \gamma_6 + \frac{\gamma_5}{2} - \frac{\gamma_2}{2}, \tag{4.53}$$

$$\gamma_{20} - \frac{c^2 T}{c^2 + Bv^2}(\gamma_{17} - \gamma_{12}) + 2Q_2 v^2(\gamma_{11} + \gamma_3) + Q_1 v^2 \bar{\zeta}, \tag{4.54}$$

$$\gamma_{19} + \frac{c^2 T}{c^2 + Bv^2} 2\gamma_{12} + 2Q_1\gamma_{11} + 2Q_2 v^2(\gamma_9 + \gamma_2), \tag{4.55}$$

$$\frac{BT}{c^2 + Bv^2}\gamma_4 - Q_1\gamma_3 - Q_2(\gamma_2 v^2 + \gamma_1) + \bar{\gamma}, \tag{4.56}$$

where we have defined the following thermodynamic quantities,

$$Q_1 \equiv \frac{B}{c^2 + Bv^2} \frac{P_\mu(TP_{TT} + \mu P_{T\mu}) - P_T(TP_{T\mu} + \mu P_{\mu\mu})}{T(P_{T\mu}^2 - P_{TT}P_{\mu\mu})}, \tag{4.57}$$

$$Q_2 \equiv \frac{B}{c^2 + Bv^2} \frac{P_{v^2\mu}(TP_{TT} + \mu P_{T\mu}) - P_{Tv^2}(TP_{T\mu} + \mu P_{\mu\mu})}{T(P_{T\mu}^2 - P_{TT}P_{\mu\mu})}, \tag{4.58}$$

where $P_\mu \equiv \partial_\mu P$, $P_{v^2\mu} \equiv \partial_{v^2}\partial_\mu P$ and similarly for other derivatives. The orthogonal complement of this space of transport coefficients is purely dissipative, and an analysis of a theory where these are set to zero would be interesting to study further. One simple example is to set $\gamma_{10} = -\gamma_2$ and then set all other transport coefficients to zero. This theory has $\Pi^\mu = 0$ while,

$$\Pi^0{}_0 = \gamma_2 v^k \partial_k v^2, \quad \Pi^i{}_0 = -\gamma_2 v^i \partial_t v^2, \quad \Pi^0{}_j = -\gamma_2 \frac{v^j v^k \partial_k v^2}{v^2}, \quad \Pi^i{}_j = \gamma_2 \frac{v^i v^j \partial_t v^2}{v^2} \tag{4.59}$$

and is non-dissipative as is easily verified by evaluating the quadratic form.

As a cautionary remark, the above procedure has to be repeated in cases where additional linear constraints are imposed, such as those arising due to enhanced symmetry. The calculation of the null space should be performed only after additional constraints have been imposed. The reason is that non-dissipative terms in the general theory may not respect those symmetries and consequently contribute to dissipative transport in the more symmetrical theory. On the other hand, once the dissipative terms have been computed as the orthogonal complement of (4.48)-(4.56), then one may assess whether or not dissipative terms in a more symmetrical theory are zero, simply evaluating them on the particular transport coefficients of the theory in question. This is the same as computing the quadratic form coefficients.

Before concluding, we can check our non-dissipative constraints for perturbations around $v^i = 0$ flows. In this case, the dimension of the null space is much higher, since there are many fewer terms that can appear in the quadratic form. In particular, the null space is enlarged to include all γ_I as independent basis vectors. Hence setting all these to zero, leaves a single constraint in (4.48)-(4.56), namely $\bar{\gamma}(T, v^2 = 0, \mu) = \gamma_0(T, \mu) = 0$. This constraint was also found in [116] but based on imposing Onsager reciprocity. The connection between Onsager reciprocity and non-dissipative coefficients is manifest when the antisymmetric components of the conductivity matrix are linearly independent of all other contributions. However the interaction between strictly dissipative coefficients, strictly non-dissipative coefficients and those coefficients which are required to vanish due to Onsager reciprocity is not clear in this most general case. In order to understand the role of Onsager and the requirements of microscopic time reversal invariance we would need to conduct an analysis of modes and associated Green's functions along the lines of [5], which we postpone to future work.

In summary, if we require that all non-dissipative contributions vanish (these are given in (4.48)-(4.56)), the number of transport coefficients appearing in the stress tensor and U(1) current is reduced from 29 to 20.

4.2.3.2 *Example: shear modes and shear viscosity*

Consider the fluid configuration corresponding to a shear-type velocity perturbation around uniform flow,

$$T(t, \vec{x}) = \bar{T}, \qquad \mu(t, \vec{x}) = \bar{\mu}, \qquad v^i = \bar{v}^i + \delta v^i(t, k \cdot \vec{x}) \tag{4.60}$$

where k^i is a spatial wavevector and $k \cdot \delta v = \bar{v} \cdot \delta v = 0$. For this perturbation the only contributions to the quadratic form (4.33) at second order in the perturbation are,

$$\begin{aligned} \partial_\mu S^\mu &= b_{14}(T, v^2, \mu)\partial_i v^j \partial_i v^j + b_{20}(T, v^2, \mu) v^j v^k \partial_j v^i \partial_k v^i & (4.61)\\ &= (b_{14}(\bar{T}, \bar{v}^2, \bar{\mu})k^2 + b_{20}(\bar{T}, \bar{v}^2, \bar{\mu})(k \cdot \bar{v})^2)(\partial_2 \delta v^i)^2 & (4.62)\\ &= \left(b_{14}(\bar{T}, \bar{v}^2, \bar{\mu}) + \bar{v}^2 b_{20}(\bar{T}, \bar{v}^2, \bar{\mu})(\cos\theta)^2\right) k^2 (\partial_2 \delta v^i)^2. & (4.63) \end{aligned}$$

where θ is the angle between k and $\bar{v}$ and ∂_2 denotes derivative with respect to the second argument of the function δv^i. Hence for perturbations satisfying $\theta = \pi/2$, positivity of entropy production requires

$$b_{14}(T, v^2, \mu) \geq 0. \tag{4.64}$$

Positive b_{14} allows b_{20} to take on negative values, with $\partial_\mu S^\mu$ minimised at $\theta = 0$, hence we also require

$$b_{14}(T, v^2, \mu) + v^2 b_{20}(T, v^2, \mu) \geq 0. \tag{4.65}$$

In terms of transport coefficients listed above, (4.40) and (4.42), these constraints become

$$\boxed{\begin{aligned} &\bar{\eta} \geq 0, \\ &\bar{\eta} + v^2(\bar{\pi} + \gamma_6 - \gamma_7 + \gamma_{13}) \geq 0. \end{aligned}} \tag{4.66}$$

We will show that these constraints coincide with those arising out of the requirement of dynamical stability. Finally, we shall see later in section 4.3.1 that for theories with Lorentz boost invariance the two constraints (4.66) coincide, becoming $\eta \geq 0$ where η is the usual shear viscosity transport coefficient of relativistic hydrodynamics. Additionally it coincides with the conclusion of $\eta_0 \geq 0$ reached in [116] where $\eta_0 = \lim_{v^2 \to 0} \bar{\eta}$.

4.2.4 *Hydrodynamic shear mode*

In this section we consider hydrodynamic modes, that is, perturbations of a background uniform flow that satisfy the hydrodynamic conservation equations. They describe how small departures from uniformity relax over time (quasinormal modes), or how they decay spatially in the context of non-equilibrium steady states (spatial collective modes). We consider a background temperature $\bar{T}$ chemical potential $\bar{\mu}$ and velocity $\bar{v}^i$, and consider the equations of motion resulting from the general first order constitutive relation (4.24). Specifically we focus on the shear-type perturbation (4.60) in Fourier space, $\delta v^i(t, k \cdot \vec{x}) = e^{-i\omega t + ik\cdot\vec{x}} \delta v^i$. Such perturbations are also hydrodynamic modes provided a dispersion relation $\omega(k^i)$ is satisfied. To linear order in amplitude, and to first hydrodynamic order, the constitutive relations are perturbed as follows,

$$\delta T^0{}_j = e^{-i\omega t + ik\cdot\vec{x}} \left(\rho + ik\cdot\bar{v}\gamma_6 + i\omega\bar{\pi}\right)\delta v^j, \tag{4.67}$$

$$\delta T^i{}_j = e^{-i\omega t + ik\cdot\vec{x}} \Big((\rho - ik\cdot\bar{v}\gamma_{13} + i\omega\gamma_7)(\bar{v}^i\delta v^j + \bar{v}^j\delta v^i) - i\bar{\eta}(k^i\delta v^j + k^j\delta v^i)\Big) \tag{4.68}$$

and the equations of motion thus give rise to the following dispersion relation, as a Taylor series in gradients,

$$i\rho(k\cdot\bar{v} - \omega) + (\bar{\pi}\omega^2 + (\gamma_6 - \gamma_7)k\cdot\bar{v}\omega + \bar{\eta}k^2 + (k\cdot\bar{v})^2\gamma_{13}) + O(\omega, k)^3 = 0. \tag{4.69}$$

There are two roots of this polynomial, $\omega(k)$, however one root $\omega = i\rho/\bar{\pi} + O(k)$ is not consistent with the hydrodynamic gradient expansion and we discard it. The other root is,

$$\omega(k^i) = k\cdot\bar{v} - i\frac{\bar{\eta}k^2 + (\bar{\pi} + \gamma_6 - \gamma_7 + \gamma_{13})(k\cdot\bar{v})^2}{\rho} + O(k)^3. \tag{4.70}$$

We observe that this hydrodynamic mode is stable, with a frequency in the lower-half complex plane, provided the conditions derived from positivity of entropy production are met, (4.66). Therefore the conditions of dynamical stability and positivity of entropy production coincide here. We also note that all combinations of transport coefficients entering here are in the orthogonal complement of the purely non-dissipative sector (4.48)-(4.56) and so in a theory with only non-dissipative terms these $O(k)^2$ pieces vanish.

So far we considered the requirements according to $\omega \in \mathbb{C}$ with $k \in \mathbb{R}^d$. Of recent physical interest are modes with complex momenta; spatial collective modes which can obtained from this dispersion relation by fixing $\omega = 0$ (or more generally, $\omega \in \mathbb{R}$) and continuing to complex momenta $k \in \mathbb{C}^d$, yielding a dispersion relation of the form $k^i(\bar{v}^j)$ describing how decay lengths in stationary systems depend on background velocity [8, 9].

From (4.70) we can see that the mode is purely diffusive if we move to a coordinate system that comoves with the fluid at velocity $\bar{v}$, but as the explicit $\bar{v}^2$ dependence makes clear, the different $\bar{v}$ frames are physically inequivalent as expected due to the lack of boost invariance. We can see a particular combination of the 29 transport coefficients enter this dispersion relation; it would be interesting to analyse the physical consequences of the other new transport coefficients through studying hydrodynamic modes in other sectors: sound and charge diffusion.

4.3 SPECIAL CASES

4.3.1 *Lorentz boosts*

Theories admitting Lorentz invariance are a special case of our general $\mathbb{R}_t \times \mathrm{ISO}(d) \times \mathrm{U}(1)$ construction, enlarging the number of symmetries. Imposing such additional symmetry requirements on our constitutive relations (4.24) severely constrains the allowed form of the 29 transport coefficients. In this section we will calculate these 29 coefficients for a Lorentz invariant theory, and show how they are completely determined by only 4 free functions of two variables. This is further reduced to 3 after imposing positivity entropy production. These are of course the well-known transport coefficients of first order relativistic hydrodynamics.

A Lorentz boost by a velocity $c\beta^i$, with respect to the speed of light c, is achieved by the following coordinate transformation,

$$t \to t + \frac{\beta_i x^i}{c}, \quad x^i \to x^i + \beta^i c t, \tag{4.71}$$

working to linear order in β^i, the velocity transforms as

$$v^i \to v^i + c\beta^i - \frac{\beta \cdot v}{c} v^i. \tag{4.72}$$

In addition, as we shall see, we also require that the following quantities are invariant in order that we have a non-trivial equation of state,

$$\tilde{T} \equiv \gamma T, \qquad \tilde{\mu} \equiv \gamma \mu \tag{4.73}$$

where we have introduced the Lorentz factor $\gamma \equiv \left(1 - v^2/c^2\right)^{-1/2}$, and which completes the transformation rules for all hydrodynamic variables,

$$T \to T - \frac{\beta \cdot v}{c} T, \qquad \mu \to \mu - \frac{\beta \cdot v}{c} \mu. \tag{4.74}$$

We require that the stress tensor and U(1) current transform as Lorentz tensors under the above linearised transformations, for any boost parameter β^i. This gives rise to a set of equations that must be satisfied, leading to constraints on both the thermodynamic variables and the transport coefficients. In more detail, recall that all thermodynamic variables and transport coefficients are functions of T, v^2, μ, and so performing the above boost (4.71) – which affects the hydrodynamic variables through (4.72) and (4.74) – leads to a Taylor expansion of the transport coefficients to order β^i. Thus, demanding the correct transformation rule under any linear boost parameter β^i results in a set of partial differential equations for the transport coefficients in terms of T, v^2, μ, the solutions to which we will set out in the two subsections that now follow.

4.3.1.1 *Ideal hydrodynamic order*

At ideal hydrodynamic order, by demanding that the component $T^{(0)0}{}_j$ transform correctly, we find the following constraint (as a coefficient of the parameter of the boost β^j),

$$\rho c^2 = P + \mathcal{E}. \tag{4.75}$$

This is so far independent of any transformation rules for T, μ, which cannot contribute to the term proportional to β^j. Upon utilising thermodynamic identities this gives the following PDE for the equation of state,

$$\left(\mu \partial_\mu - 2(c^2 - v^2)\partial_{v^2} + T\partial_T\right) P(T, v^2, \mu) = 0 \tag{4.76}$$

with a general solution

$$P = \tilde{P}\left(\gamma T, \gamma \mu\right) = \tilde{P}\left(\tilde{T}, \tilde{\mu}\right). \tag{4.77}$$

where $\tilde{T}, \tilde{\mu}$ are defined in (4.73). All remaining PDEs resulting from demanding Lorentz invariance at ideal order are now solved by (4.77), provided we also ensure that T, μ transform leaving $\tilde{T}, \tilde{\mu}$ invariant, i.e. under the rule (4.74). If we do not, then additional constraints arise on $\tilde{P}$ and prevent us from having a general

function of two independent variables. Furthermore demanding that the frame conditions (4.21) and (4.22) take Lorentz covariant form determines

$$B = \gamma^2, \qquad u^0 = \gamma \tag{4.78}$$

where we have also fixed an arbitrary constant of proportionality in u^0. (4.78) furnishes us with a covariant vector u^μ which we can now use to construct covariant forms of the constitutive relations in the usual way. With (4.77) imposed, we arrive at the following familiar constitutive relations at ideal order,

$$T^{(0)\mu}{}_\nu = \tilde{\mathcal{E}}\frac{u^\mu u_\nu}{c^2} + \tilde{P}\Delta^\mu{}_\nu \tag{4.79}$$

$$J^{(0)\mu} = \tilde{n}u^\mu \tag{4.80}$$

where we have introduced the projector,

$$\Delta^\mu{}_\nu = \delta^\mu_\nu + \frac{1}{c^2}u^\mu u_\nu \tag{4.81}$$

and the thermodynamic relations,

$$\tilde{s} = \partial_{\tilde{T}}\tilde{P}, \tag{4.82}$$

$$\tilde{n} = \partial_{\tilde{\mu}}\tilde{P}, \tag{4.83}$$

$$\tilde{\mathcal{E}} = -\tilde{P} + \tilde{s}\tilde{T} + \tilde{n}\tilde{\mu}. \tag{4.84}$$

4.3.1.2 *First order*

At first order, after solving the multitudinous PDEs, we arrive at the following expressions for the first 6 transport coefficients

$$\bar{\eta}(T, v^2, \mu) = \gamma\,\eta(\tilde{T}, \tilde{\mu}) \tag{4.85}$$

$$\bar{\zeta}(T, v^2, \mu) = \gamma\,\zeta(\tilde{T}, \tilde{\mu}) \tag{4.86}$$

$$\bar{\pi}(T, v^2, \mu) = \frac{\gamma^3 v^2}{c^4}\,\eta(\tilde{T}, \tilde{\mu}) \tag{4.87}$$

$$\bar{\alpha}(T, v^2, \mu) = -\frac{\gamma^2}{2c^2}\tilde{T}\,\chi(\tilde{T}, \tilde{\mu}) \tag{4.88}$$

$$\bar{\gamma}(T, v^2, \mu) = \frac{\gamma^2}{2c^2}\tilde{T}\,\chi(\tilde{T}, \tilde{\mu}) \tag{4.89}$$

$$\bar{\sigma}(T, v^2, \mu) = \gamma\sigma(\tilde{T}, \tilde{\mu}) + \gamma\frac{\tilde{T}\tilde{P}_{\tilde{\mu}}}{\tilde{T}\tilde{P}_{\tilde{T}} + \tilde{\mu}\tilde{P}_{\tilde{\mu}}}\,\chi(\tilde{T}, \tilde{\mu}) \tag{4.90}$$

where $\tilde{P}_{\tilde{\mu}} \equiv \partial_{\tilde{\mu}}\tilde{P}$ and similarly for other derivatives. In solving the equations we have introduced the integration constants $\eta, \zeta, \chi, \sigma$ above, which are each arbitrary functions of $\tilde{T}, \tilde{\mu}$. We shall see that these integration constants serve as the only remaining transport coefficients for a Lorentz invariant theory. The remaining 29 –

6 transport coefficients are given as follows, where we have omitted functional dependence detailed above for brevity.

$$\begin{array}{lll}
\gamma_1 = \frac{\gamma^5}{2c^4}\zeta + \frac{\gamma^5(c^2(d-2)+dv^2)}{2dc^6}\eta & \gamma_2 = \frac{\gamma^5 v^2}{2c^4}\zeta + \frac{\gamma^5(c^2 d - v^2)}{dc^4}\eta & \gamma_3 = \frac{\gamma^3}{c^2}\zeta - \frac{2\gamma^3}{dc^2}\eta \\
\gamma_4 = 0 & \gamma_5 = -\frac{\gamma^3}{2c^2}\eta & \gamma_6 = -\frac{\gamma^3}{c^2}\eta \\
\gamma_7 = \frac{\gamma^3}{c^2}\eta & \gamma_8 = \frac{\gamma^3}{2c^2}\eta & \gamma_9 = \frac{\gamma^5}{2c^2}\zeta + \frac{(d-1)\gamma^5}{dc^2}\eta \\
\gamma_{10} = \frac{\gamma^5}{2c^2}\zeta + \frac{\gamma^5(c^2(d-2)+dv^2)}{2dc^4}\eta & \gamma_{11} = \frac{\gamma^3}{c^2}\zeta - \frac{2\gamma^3}{dc^2}\eta & \gamma_{12} = 0 \\
\gamma_{13} = \frac{\gamma^3}{c^2}\eta & \gamma_{14} = 0 & \gamma_{15} = -\frac{\gamma^3}{2c^2}\zeta + \frac{\gamma^3}{dc^2}\eta \\
\gamma_{16} = -\frac{\gamma^3}{2c^2}\zeta + \frac{\gamma^3}{dc^2}\eta & \gamma_{17} = 0 & \gamma_{18} = -\frac{\tilde{T}\gamma^4}{2c^4}\chi \\
\gamma_{19} = -\frac{\tilde{T}\gamma^4}{2c^2}\chi + \frac{\gamma^4 v^2}{2c^4}\tilde{Q}\left(\sigma + \frac{\tilde{T}\tilde{P}_{\tilde{\mu}}}{\tilde{T}\tilde{P}_{\tilde{T}} + \tilde{\mu}\tilde{P}_{\tilde{\mu}}}\chi\right) & \gamma_{20} = \frac{\gamma^2}{c^2}\tilde{Q}\left(\sigma + \frac{\tilde{T}\tilde{P}_{\tilde{\mu}}}{\tilde{T}\tilde{P}_{\tilde{T}} + \tilde{\mu}\tilde{P}_{\tilde{\mu}}}\chi\right) & + \frac{\gamma^4}{2c^4}\tilde{Q}\left(\sigma + \frac{\tilde{T}\tilde{P}_{\tilde{\mu}}}{\tilde{T}\tilde{P}_{\tilde{T}} + \tilde{\mu}\tilde{P}_{\tilde{\mu}}}\chi\right) \\
\gamma_{21} = 0 & \gamma_{22} = 0 & \gamma_{23} = -\frac{\gamma^2}{c^2}\tilde{T}\chi
\end{array} \tag{4.91}$$

where we have defined the following combination of thermodynamic quantities

$$\tilde{Q} \equiv \frac{-\tilde{P}_{\tilde{\mu}}(\tilde{T}\tilde{P}_{\tilde{T}\tilde{T}} + \tilde{\mu}\tilde{P}_{\tilde{T}\tilde{\mu}}) + \tilde{P}_{\tilde{T}}(\tilde{T}\tilde{P}_{\tilde{T}\tilde{\mu}} + \tilde{\mu}\tilde{P}_{\tilde{\mu}\tilde{\mu}})}{\tilde{T}(\tilde{P}^2_{\tilde{T}\tilde{\mu}} - \tilde{P}_{\tilde{\mu}\tilde{\mu}}\tilde{P}_{\tilde{T}\tilde{T}})}. \tag{4.92}$$

Indeed, once the above relations are imposed, the first order constitutive relations reduce to the familiar form of relativistic hydrodynamics, viz.,

$$\Pi^{\mu}_{\ \nu} = -\eta\Delta^{\mu\alpha}\Delta_{\nu}^{\ \beta}\sigma_{\alpha\beta} - \zeta\Delta^{\mu}_{\ \nu}\partial\cdot u, \quad \text{with} \quad \sigma_{\mu\nu} \equiv \partial_\mu u_\nu + \partial_\nu u_\mu - \frac{2}{d}\eta_{\mu\nu}\partial\cdot u, \tag{4.93}$$

$$\Pi^{\mu} = -\sigma\tilde{T}\Delta^{\mu\nu}\partial_\nu\left(\frac{\tilde{\mu}}{\tilde{T}}\right) + \chi\Delta^{\mu\nu}\partial_\nu\tilde{T}. \tag{4.94}$$

Imposing Lorentz invariance has thus reduced the number of first order transport coefficients from 29 to 4: the shear viscosity η, bulk viscosity ζ, conductivity σ and χ. To reiterate, each of these are arbitrary functions of $\tilde{T}, \tilde{\mu}$ in the usual way.

4.3.1.3 *Entropy current*

With Lorentz invariance imposed, the divergence of the canonical part of the entropy current is given by

$$\partial_\mu S^{\mu}_{\text{can}} = -\Pi^{\mu}_{\ \nu}\partial_\mu\frac{v^\nu}{T} - \Pi^{\mu}\partial_\mu\frac{\mu}{T}, \tag{4.95}$$

$$= -\Pi^{\mu}_{\ \nu}\partial_\mu\frac{u^\nu}{\tilde{T}} - \Pi^{\mu}\partial_\mu\frac{\tilde{\mu}}{\tilde{T}}. \tag{4.96}$$

Imposing that S^μ transform as a Lorentz vector, together with the constraints that $\partial_\mu S^\mu$ contains no explicit second derivative terms constrains the coefficients in the non-canonical entropy current (4.30), (4.31) to take the form

$$\begin{array}{llllll}
\tilde{c}_1 = 0, & \tilde{c}_2 = 0, & \tilde{c}_3 = 0, & \tilde{c}_4 = \alpha/T^2, & \tilde{c}_5 = 0, & \tilde{c}_6 = 0, \\
\tilde{c}_7 = -\alpha/T^2, & \tilde{c}_8 = -\alpha/T^2, & \tilde{c}_9 = 0, & \tilde{c}_{10} = 0, & \tilde{c}_{11} = 0, & \tilde{c}_{12} = \alpha/T^2
\end{array} \tag{4.97}$$

where α is an unconstrained function of $\tilde{T}, \tilde{\mu}$. The non-canonical entropy current then takes the form

$$S^{\mu}_{\text{non}} = \alpha(\tilde{T}, \tilde{\mu}) \left(u^{\mu} \partial \cdot u - u^{\sigma} \partial_{\sigma} u^{\mu} \right), \tag{4.98}$$

and thus an ambiguity has appeared. However, as was shown in [32], placing the theory on a curved background provides additional constraints. In particular new terms $\propto \alpha R_{\mu\nu} u^{\mu} u^{\nu}$ appear in $\partial_{\mu} S^{\mu}$, and since depending on the chosen background curvature this term can take any sign, it forces $\alpha = 0$. Adopting this result the entropy current is given entirely by the canonical piece.

Without loss of generality we now extract positivity constraints by checking the quadratic form for fluctuations around $v^i = 0$. We find,

$$\tilde{T} \partial_{\mu} S^{\mu} = \frac{1}{2} \eta \sigma_{ij} \sigma^{ij} + \zeta (\partial_i v^i)^2 + \sigma \left(\partial_i \tilde{\mu} - \left(\frac{\tilde{\mu}}{\tilde{T}} + \frac{\chi}{2\sigma} \right) \partial_i \tilde{T} \right)^2 - \frac{\chi^2}{4\sigma} (\partial_i \tilde{T})^2, \tag{4.99}$$

and hence imposing $\partial_{\mu} S^{\mu} \geq 0$ enforces

$$\eta \geq 0, \quad \zeta \geq 0, \quad \sigma \geq 0, \quad \chi = 0. \tag{4.100}$$

4.3.2 *Galilean boosts*

Another special case of interest are theories with non-relativistic boost symmetry, extending the symmetry algebra of the system H, P_i, J_{ij}, M for time translations, spatial translations, spatial rotations, and $\mathrm{U}(1)$ respectively, to include a boost generator K_i. A particularly simple example can be reached by starting with a relativistic theory and sending $c \to \infty$, corresponding to a group contraction from $\mathrm{ISO}(1, d) \times \mathrm{U}(1)$. The resulting theory is invariant under so-called *massless* Galilean boosts, for which, most notably,

$$[K_i, P_j] = 0. \tag{4.101}$$

This algebra will be the present focus of this section, which can be reached by contracting the results we have obtained in section 4.3.1. It is important to note that since we also have particle number / charge conservation, this algebra can be centrally extended to the Bargmann algebra [121] (see also [122]), namely,

$$[K_i, P_j] = iM\delta_{ij}, \tag{4.102}$$

where M, as the $\mathrm{U}(1)$ generator, is the centre. This is part of a rich vein of research into non-relativistic boost-invariant hydrodynamics and couplings to gravity via the Newton-Cartan formalism. We will not consider the centrally extended case in this chapter, but simply refer the interested reader to important papers in this hydrodynamic context [7, 115, 116, 123, 124].

The limit $c \to \infty$ for the relativistic boost (4.71), (4.72), (4.74) results in the Galilean boost with parameter $u^i = c\beta^i$,

$$t \to t, \quad x^i \to x^i + u^i t, \quad v^i \to v^i + u^i, \quad T \to T, \quad \mu \to \mu. \tag{4.103}$$

In particular the Lorentz factor $\gamma \to 1$ as $c \to \infty$, and $\tilde{T} = T, \tilde{\mu} = \mu$, with the equation of state $P = \tilde{P}(T, \mu)$. From this we conclude,

$$\rho = 0, \quad \tilde{\mathcal{E}} = \mathcal{E}, \quad \tilde{n} = n, \tag{4.104}$$

and an ideal stress tensor (see also [115])

$$T^{(0)0}{}_0 = -\mathcal{E}, \quad T^{(0)i}{}_0 = -(\mathcal{E} + P)v^i, \quad T^{(0)0}{}_j = 0, \quad T^{(0)i}{}_j = P\delta^i_j \tag{4.105}$$

$$J^{(0)0} = n, \quad J^{(0)i} = nv^i \tag{4.106}$$

where $n, \mathcal{E}, P$ are each functions of T, μ only.

At first hydrodynamic order, recall that in the relativistic case we have 3 transport coefficients remaining after analysis of the entropy current: η, ζ, σ, each a function of $\tilde{T}, \tilde{\mu}$. In the $c \to \infty$ limit, each of these are functions of T, μ. We can choose how each of these transport coefficients scale with c so that they provide finite contributions to the constitutive relations as $c \to \infty$. This is achieved without any additional rescaling,

$$\eta = O(c)^0, \quad \zeta = O(c)^0, \quad \sigma = O(c)^0 \quad \text{as} \quad c \to \infty \tag{4.107}$$

then the 29 transport coefficients of the general theory take on the following values,

$$\bar{\eta} = \eta, \quad \bar{\zeta} = \zeta, \quad \bar{\sigma} = \sigma, \quad \text{others} = 0, \tag{4.108}$$

and the first order constitutive relations (4.24) become

$$\Pi^0_0 = 0, \tag{4.109}$$

$$\Pi^0_j = 0, \tag{4.110}$$

$$\Pi^i_0 = \frac{\eta}{2}\partial_i v^2 + \eta v^k \partial_k v^i + \left(\zeta - \frac{2\eta}{d}\right) v^i \partial_k v^k, \tag{4.111}$$

$$\Pi^i_j = -\zeta \delta^i_j \partial_k v^k - \eta \sigma_{ij}, \tag{4.112}$$

$$\Pi^0 = 0, \tag{4.113}$$

$$\Pi^i = -\sigma T \partial_i \frac{\mu}{T}, \tag{4.114}$$

where η, ζ, σ are arbitrary non-negative functions of T, μ.

4.3.3 *Lifshitz scale invariance*

In this section we compute the form of the 29 transport coefficients for the $\mathbb{R}_t \times \mathrm{ISO}(d) \times \mathrm{U}(1)$ theory in the case where we further restrict to invariance under the inhomogeneous scale transformation

$$t \to \lambda^z t, \quad x^i \to \lambda x^i, \tag{4.115}$$

for some arbitrary dynamical critical exponent z. At first sight, such invariance is merely imposed by restricting all terms in the constitutive relations to have the correct scaling weights. However, the hydrodynamic theory is treated here as an effective description of an underlying microscopic theory with a Ward identity

for scale transformations. This Ward identity imposes further constraints which causes transport coefficients, or linear combinations thereof, to vanish. In the case of scale transformations this point was made clear in [125], where it was shown that conformal invariance leads to vanishing of bulk viscosity. We direct the interested reader to other results on Lifshitz invariant hydrodynamics [126–135].

Let us begin with a discussion of the scaling weights. It is convenient to denote a quantity that scales as λ^{-w} to have scaling weight w. In other words, the scaling weights of t and x^i as presented above, are $w_t = -z$ and $w_{x^i} = -1$ respectively, whilst the scaling weights of the hydrodynamic variables (T, v^i, μ) are,

$$w_T = z, \quad w_{v^i} = z - 1, \quad w_\mu = z. \tag{4.116}$$

In particular, for a transport coefficient $\gamma_I(T, v^2, \mu)$ with scaling weight w_I, it must be an arbitrary function of the scaling invariant combinations $v^2/T^{\frac{2(z-1)}{z}}$ and μ/T, together with an overall factor of T to make up its weight, i.e.

$$\gamma_I(T, v^2, \mu) = T^{\frac{w_I}{z}} \hat{\gamma}_I \left(\frac{v^2}{T^{\frac{2(z-1)}{z}}}, \frac{\mu}{T} \right). \tag{4.117}$$

This is a severe restriction on the functional form of the 29 transport coefficients, albeit not a reduction in their number. The scaling weights for the transport coefficients are as follows,

$$\begin{array}{l|l|l|l|l} w_{\bar{\eta}} = d & w_{\bar{\zeta}} = d & w_{\bar{\alpha}} = d - z & w_{\bar{\gamma}} = d - z & w_{\bar{\sigma}} = d - 2 \\ w_{\gamma_1} = d + 4 - 4z & w_{\gamma_{12}} = d & w_{\gamma_{14}} = d & w_{\gamma_{17}} = d & w_{\gamma_{18}} = d + 2 - 3z \\ w_{\gamma_{19}} = d - z & w_{\gamma_{20}} = d - z & w_{\gamma_{21}} = d - z & w_{\gamma_{22}} = d - z & w_{\gamma_{23}} = d - z \end{array} \tag{4.118}$$

while the weights for the remaining coefficients $(\bar{\pi}, \gamma_2, \gamma_3, \gamma_4, \gamma_5, \gamma_6, \gamma_7, \gamma_8, \gamma_9, \gamma_{10}, \gamma_{11}, \gamma_{13}, \gamma_{15}, \gamma_{16})$ are each $d + 2 - 2z$.

We now turn to the Ward identity, for which we impose the following relation

$$z T^0_{\ 0} + T^i_{\ i} = 0. \tag{4.119}$$

At ideal hydrodynamic order (4.119) corresponds to an appropriate restriction of the equation of state. Namely,

$$dP - z\mathcal{E} + v^2 \rho = 0 \tag{4.120}$$

which implies the following PDE for the equation of state, through standard thermodynamic relations,

$$\left(zT\partial_T + 2(z-1)v^2 \partial_{v^2} + z\mu\partial_\mu - (d+z) \right) P(T, v^2, \mu) = 0. \tag{4.121}$$

The PDE (4.121) has the general solution

$$P = T^{\frac{d+z}{z}} \hat{P} \left(\frac{v^2}{T^{\frac{2(z-1)}{z}}}, \frac{\mu}{T} \right), \tag{4.122}$$

which is of course the expected functional form for the equation of state of a Lifshitz invariant system given the scaling weight of P, i.e. it is of the form (4.117)

with $w_P = d + z$. If we furthermore impose (4.119) at first hydrodynamic order, there are four constraints, as the coefficients of the four possible scalar terms $\{v^k\partial_k v^2, v^k\partial_k \frac{\mu}{T}, \partial_i v^i, \partial_t v^2\}$. These constraints can be expressed as follows,

$$\bar{\zeta} = \frac{(z\gamma_3 - \gamma_{11})v^2}{d}, \tag{4.123}$$

$$\gamma_{15} = \frac{-2z\gamma_2 + 2\gamma_8 + 2\gamma_9 + \gamma_{13}}{2(d-1)}, \tag{4.124}$$

$$\gamma_{16} = \frac{z\bar{\pi} + 2z\gamma_1 v^2 - \gamma_7 - 2\gamma_{10}}{2(d-1)}, \tag{4.125}$$

$$\gamma_{17} = \frac{Tz(\bar{\alpha} + \bar{\gamma}) - z\gamma_4 v^2 + \gamma_{12} + \gamma_{14}}{d-1}. \tag{4.126}$$

To summarise this section, imposing Lifshitz scaling weights and the Ward identity (4.119) reduces the number of transport coefficients from 29 to 25, and moreover places stringent constraints on the functional form of all of them (4.117).

4.4 DISCUSSION

In this chapter we have constructed the first-order hydrodynamic theory describing a fluid in the presence of a preferred reference frame, which possesses no boost invariance, neither Galilean nor Lorentzian. In this frame the theory is rotationally invariant and ISO(d) acts naturally. If we nevertheless boost to a reference frame with boost parameter β^i, the resulting theory will contain explicit dependence on β^i and will no longer be rotationally invariant. Of course ISO(d) is still preserved, however it acts in a less natural way. The symmetry is realised by boosting back into the preferred frame, where rotation invariance is manifest, and then boosting back to the finite β^i frame.

A consequence of this relaxed symmetry group is the appearance of many new transport coefficients. In principle each of these transport coefficients is associated to a distinct physical effect which can be accessed by considering general fluid flows with respect to the preferred reference frame. Some of these are accessible in hydrodynamic modes. Indeed, in section 4.2.4 we computed the shear diffusion mode, which grants independent access to the combinations of transport coefficients $\bar{\eta}$ and $\bar{\pi} + \gamma_6 - \gamma_7 + \gamma_{13}$ through varying the angle of the mode with respect to the background fluid flow. In addition there may be coefficients that are only accessible through nonlinear considerations. We leave a more comprehensive study of the physical effects to a future publication.

We also considered the constraints resulting from imposing the positivity of entropy production for all possible fluid configurations. We constructed the general entropy current to first order in derivatives, and found all constraints that reduce its divergence to a quadratic form.[5] By restricting this quadratic form to shearing perturbations around a general uniform flow we extracted two very simple positivity constraints, (4.66), which coincide with the linear stability requirements for the shear diffusion hydrodynamic mode. Constraints may also more easily be extracted in special cases, such as those enjoying Lorentz boost invariance.

5 This quadratic form is available explicitly in an accompanying notebook to the paper [10].

We also enumerated all independent linear combinations of transport coefficients that are non-dissipative, i.e. that do not contribute to $\partial_\mu S^\mu$. We counted 9 such combinations, listed in (4.48)-(4.56). Understanding the relation between dissipative coefficients, non-dissipative coefficients, requirements of Onsager reciprocity and the constraints arising from hydrostatic partition functions [119, 120], is an interesting problem that deserves further study.

Finally, we note that our constitutive relations contain only parity-invariant terms. Clearly it would be interesting to extend our analysis to include parity non-invariant effects.

5

FLOWS WITHOUT BOOSTS

5.1 INTRODUCTION

Recently, there has been increasing interest in studying hydrodynamics without boost invariance [115–117, 136, 137]. In the previous chapter we constructed such a theory, at first-order in the gradient expansion for parity-invariant fluids on a flat background. The system in our case was invariant under time translations, the Euclidean group of spatial transformations and had a conserved particle number, i.e. with symmetry $\mathbb{R}_t \times \mathrm{ISO}(d) \times \mathrm{U}(1)$. The constitutive relations that we found contained 29 physical transport coefficients, much more than is found in non-relativistic or relativistic hydrodynamics. We would like to understand better the physical interpretation of these new transport coefficients as well as see what are the possible applications of this model, e.g. graphene, cellular membranes, bird flocking etc. One might perhaps experimentally observe these new coefficients in various flow configurations. An example would be how one can experimentally observe hydrodynamic signatures of a Fermi liquid in the flow of an electron fluid through a narrow channel (i.e. a Poiseuille flow), driven by an electric field. There, the velocity profile and the resistance per unit length $\mathcal{R}$ of the channel depend on the viscosity $\bar{\eta}$ of the fluid [108, 138]. Another example might be motor molecules described by the flow of an active polar fluid in the Taylor-Couette geometry [112].

5.2 THE SETUP

We start with the constitutive relations for a non-boost invariant fluid as described in [10, 115, 116]. For an ideal fluid in the laboratory frame where the fluid has velocity v^i the constitutive relations were given in (4.1). For a dissipative fluid, the constitutive relations at first order in derivatives were given in (4.24). To make matters more solvable, we will look at incompressible flows, i.e. $\partial_i v^i = 0$. This is how incompressible flows are defined in conventional, non-relativistic Galilei-invariant hydrodynamics, along with taking the kinetic density ρ being a constant. Let us also take the ratio of chemical potential and temperature μ/T to be constant, as well as take all of the transport coefficients to be constants. To further simplify things, let's also assume the flows to be steady, time-independent. With these assumptions in mind, the conservation of stress-energy tensor

$$\partial_\mu T^\mu{}_\nu = 0 \tag{5.1}$$

gives:

$$\nu = 0: \quad -v^i\partial_i(\varepsilon+P)+\partial_i\left(\gamma_8 v^2+\frac{\bar{\eta}}{2}\right)\partial_i v^2+\left(\gamma_8 v^2+\frac{\bar{\eta}}{2}\right)\partial^2 v^2+\partial_i\left(\gamma_{13}v^2+\bar{\eta}\right)v^k\partial_k v^i$$
$$+\left(\gamma_{13}v^2+\bar{\eta}\right)\partial_i\left(v^k\partial_k v^i\right)+v^i\partial_i\left(\gamma_9 v^k\partial_k v^2\right)=0 \tag{5.2}$$

$$\nu = j: \quad \partial_j P+v^i\partial_i\rho v^j+\rho v^i\partial_i v^j+\partial_j\left[\gamma_{15}v^k\partial_k v^2\right]-\bar{\eta}\partial^2 v^j-\partial_i\bar{\eta}\partial_i v^j$$
$$-\partial_i\left[\gamma_8\left(v^i\partial_j v^2+v^j\partial_i v^2\right)\right]-\partial_i\left[\gamma_{13}\left(v^i v^k\partial_k v^j+v^j v^k\partial_k v^i\right)\right]$$
$$+\frac{1}{v^2}v^i\partial_i v^j(\dots)+\frac{v^j}{v^2}v^i\partial_i(\dots)=0 \tag{5.3}$$

These are our equations of motion, they are our analogue of the Navier-Stokes equations. In what follows we will study the velocity profiles that we calculate, either analytically or numerically, from these equations for various flow configurations. We will look at what happens in a planar 2D flow through a channel (for Poiseuille and Couette flows), as well as a circular flow of a fluid between two concentric cylinders (i.e. Taylor-Couette flow). We will compare our results to those familiar from usual non-relativistic hydrodynamics.

5.3 FLOW IN A 2D CHANNEL

Let's consider a non-boost invariant fluid flowing steadily along a long channel of width W and length L, located in the xy-plane, with the x-axis pointing along the channel. In the limit of an infinitely long channel, the velocity should be independent of x. Thus, we have

$$\mathbf{v} = (v_x(y), 0) \tag{5.4}$$

Depending on the boundary conditions and whether or not there is a pressure gradient present, we can distinguish several situations (depicted in Figure 5.1):

- *Couette flow with pressure gradient*: this is the most general case in which one of the walls is at rest, while the other has velocity U in the direction along the channel (in this case, in the x-direction). We also have a pressure gradient present in the channel. See Figure 5.1 (a).
- *Couette flow*: This case is the same as the previous one, with one difference - there is no pressure gradient in the channel. See Figure 5.1 (b).
- *Poiseuille flow*: In the case of the Poiseuille flow both walls are fixed, and there is a pressure gradient in the channel. See Figure 5.1 (c).

We will start with the general case, and then specialize to the other two cases. The boundary conditions are given by:

$$v_x(0) = 0, \quad v_x(W) = U. \tag{5.5}$$

To find the velocity profile of the general flow, we first turn our attention to the equations of motion. We start from (5.3). For $j = y$:

$$\partial_y P - v_x\partial_x\gamma_8\partial_y v^2 = 0. \tag{5.6}$$

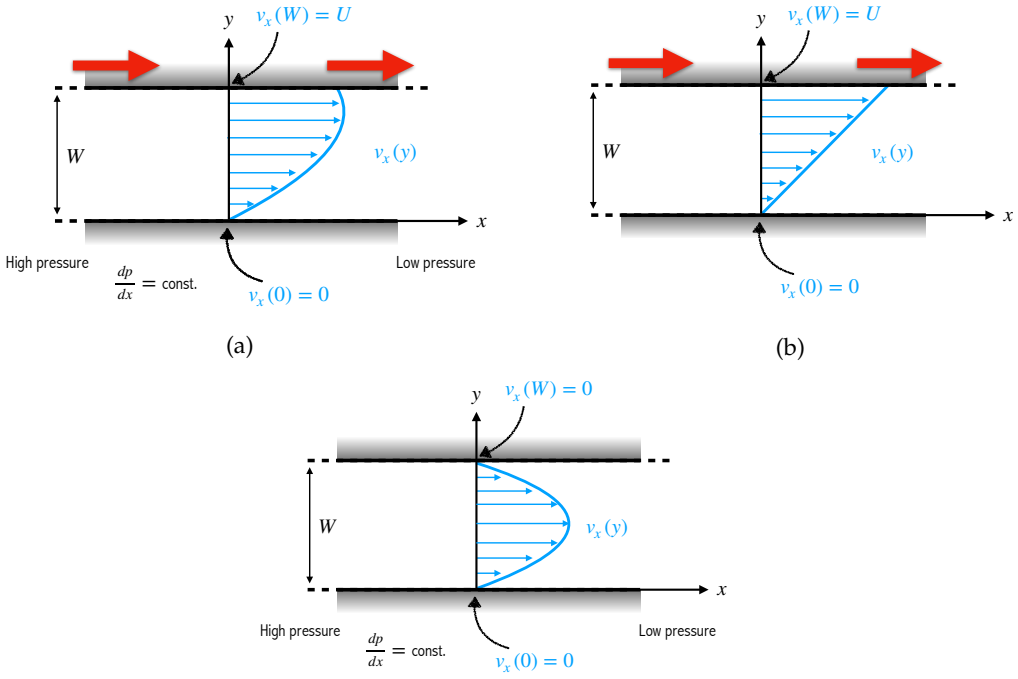

Figure 5.1: Sketch of a planar flow in a channel. We distinguish three cases: (a) general Couette flow with a pressure gradient, (b) Couette flow, (c) Poiseuille flow.

For $j = x$, we have

$$\partial_x P - \bar{\eta}\partial_y^2 v_x - \partial_y v_x \partial_y \bar{\eta} - \partial_y \gamma_8 \partial_y v^2 v_x - \gamma_8 \partial_y v_x \partial_y v^2 - \gamma_8 v_x \partial_y^2 v_x^2 = 0 \tag{5.7}$$

If we assume the transport coefficients to be constants, we have

$$\partial_y P = 0, \tag{5.8}$$

$$\partial_x P - \bar{\eta}\partial_y^2 v_x - \gamma_8 \partial_y v_x \partial_y v_x^2 - \gamma_8 v_x \partial_y^2 v_x^2 = 0. \tag{5.9}$$

From the first equation one can see that the pressure depends only on x. The second equation can be separated into terms that depend only on x and only on y. This can be true only if both sides are constant. Thus, $\partial_x P =$ constant, the pressure is a linear function of the coordinate x along the direction of flow. We can write the pressure gradient as $-|\Delta P|/L$, where L is the length of the channel and $|\Delta P|$ is the magnitude of the pressure difference between the ends of the channel. The pressure is then

$$P(x) = -\frac{|\Delta P|}{L} x, \tag{5.10}$$

and equation (5.9) becomes

$$G - \bar{\eta}\partial_y^2 v_x - \gamma_8 \partial_y v_x \partial_y v_x^2 - \gamma_8 v_x \partial_y^2 v_x^2 = 0, \tag{5.11}$$

where $G \equiv \partial_x P$. We see that there are only two transport coefficients in play here - $\bar{\eta}$, what in the non-relativistic case would correspond to the shear viscosity, and γ_8. From now on we will suppress the subscript x on the velocity and simply write

v. We can write the equation in a dimensionless form, by selecting the following scales

$$y = W\tilde{y}, \quad \partial_y = \frac{1}{W}\partial_{\tilde{y}}, \quad \text{and} \quad v = v_F\tilde{v}, \tag{5.12}$$

where W is the width of the channel, and v_F is some reference (Fermi) velocity. This gives us

$$G - \bar{\eta}\frac{v_F}{W^2}\partial_{\tilde{y}}^2\tilde{v} - \gamma_8\frac{v_F^3}{W^2}\partial_{\tilde{y}}\tilde{v}\,\partial_{\tilde{y}}\tilde{v}^2 - \gamma_8\frac{v_F^3}{W^2}\tilde{v}\,\partial_{\tilde{y}}^2\tilde{v}^2 = 0 \tag{5.13}$$

Now, dividing this equation by $\bar{\eta}v_F/W^2$, we find

$$\frac{GW^2}{\bar{\eta}v_F} - \tilde{v}'' - \frac{\gamma_8 v_F}{\bar{\eta}}\tilde{v}'\left(\tilde{v}'\right)^2 - \frac{\gamma_8 v_F^2}{\bar{\eta}}\tilde{v}(\tilde{v}^2)'' = 0 \tag{5.14}$$

where the primes denote derivatives with respect to $\tilde{y}$. We can define dimensionless quantities

$$\tilde{G} \equiv \frac{GW^2}{\bar{\eta}v_F}, \quad \text{and} \quad R \equiv \frac{\gamma_8 v_F^2}{\bar{\eta}}, \tag{5.15}$$

with R is the dimensionless ratio of γ_8 and $\bar{\eta}$. The dimensionless equation of motion for the Poiseuille flow is

$$\tilde{G} - 4R\tilde{v}(\tilde{v}')^2 - 2R\tilde{v}^2\tilde{v}'' - \tilde{v}'' = 0, \tag{5.16}$$

and the boundary conditions

$$\tilde{v}(0) = 0, \quad \tilde{v}(1) = \tilde{U}. \tag{5.17}$$

We find analytical solutions using Wolfram Mathematica's DSolve function,

$$\tilde{v}_1(\tilde{y}) = -\frac{1}{\delta^{1/3}} + \frac{\delta^{1/2}}{2\,R} \tag{5.18}$$

$$\tilde{v}_2(\tilde{y}) = \frac{(2+2i\sqrt{3})R + (-1+i\sqrt{3})\delta^{2/3}}{4\,R\,\delta^{1/3}} \tag{5.19}$$

$$\tilde{v}_3(\tilde{y}) = \frac{(2-2i\sqrt{3})R + (-1-i\sqrt{3})\delta^{2/3}}{4\,R\,\delta^{1/3}} \tag{5.20}$$

$$\delta = R^2\left[6\tilde{U} + 4R\tilde{U}^3 + 3\tilde{G}(-1+\tilde{y})\right]\tilde{y} + \sqrt{R^3\left[8 + R\left(6\tilde{U} + 4R\tilde{U}^3 + 3\tilde{G}(-1+\tilde{y})\right)^2\tilde{y}^2\right]}$$

Interestingly we find three solutions. We can look at how the real and imaginary parts of these solutions behave when we vary the numerical values of the ratio R. The resulting plots are given in Figure 5.2. Note that $\tilde{v}_1(\tilde{y})$ is a purely real solution for $R > 0$, while the other two solutions are complex conjugates of one another. We can also solve the equation numerically, e.g. using Wolfram Mathematica's NDSolve function. The numerical solution corresponds to the purely real analytical solution $\tilde{v}_1$, eq. (5.18) if $R > 0$, as seen from Figure 5.3. Increasing R seems to flatten and decrease the velocity profile, so we might think of it (and by extension, γ_8) as a some kind of second viscosity.

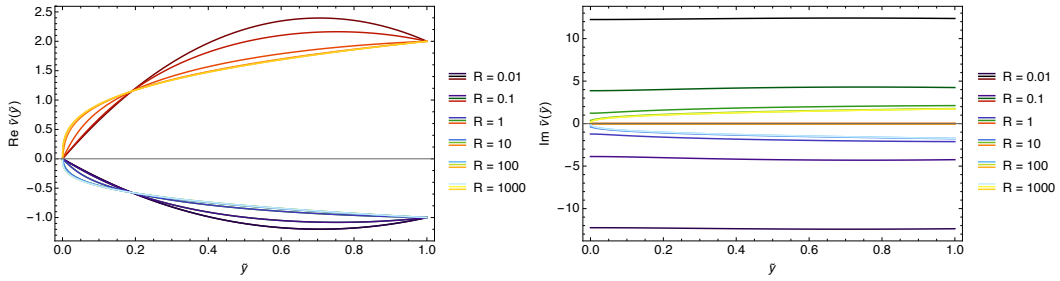

(a) (b)

Figure 5.2: Real (a) and imaginary (b) part of the velocity profile solutions of the Couette flow with pressure gradient, for various values of R. $\tilde{v}_1$ is given by lines colored in shades of red, $\tilde{v}_2$ in green-yellow, and $\tilde{v}_3$ in blue. In all cases we've fixed $\tilde{U} = 2$, and $\tilde{G} = -10$.

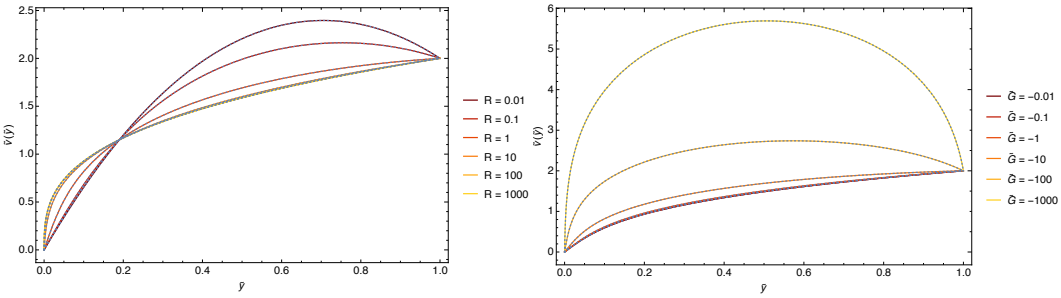

(a) (b)

Figure 5.3: Couette flow with pressure gradient, comparison of $\tilde{v}_1$ with the numerical solution, for various values of $R > 0$. The analytical and numerical solutions are in agreement for a wide range of values of R and $\tilde{G}$. In all cases we've fixed $\tilde{U} = 2$. In (a) we fixed $\tilde{G} = -10$, while in (b) we fixed $R = 1$.

5.3.1 *Flow characterization*

To get a better understanding how these solutions arise, let us rewrite the equation of motion in the following way

$$\tilde{G} - 4R\tilde{v}(\tilde{v}')^2 - 2R\tilde{v}^2\tilde{v}'' - \tilde{v}'' = 0 \tag{5.21}$$

$$\Rightarrow \left(\tilde{v}'(1 + 2R\tilde{v}^2)\right)' - \tilde{G} = 0. \tag{5.22}$$

This can be integrated once with respect to $\tilde{y}$. We arrive at a first order ODE,

$$(1 + 2R\tilde{v}^2)\tilde{v}' = \tilde{G}\tilde{y} + A, \tag{5.23}$$

where A is an integration constant. We can further integrate the left-hand side of the equation with respect to v and the right hand with respect to $\tilde{y}$, and find

$$\tilde{v} + \frac{2}{3}R\tilde{v}^3 = \frac{\tilde{G}}{2}\tilde{y}^2 + A\tilde{y} + B. \tag{5.24}$$

A necessary (but not sufficient) condition for $\tilde{v}(\tilde{y}=0)=0$ is $B=0$. Imposing the other boundary condition $\tilde{v}(1)=\tilde{U}$ gives us

$$A=\tilde{U}\left(1+\frac{2}{3}R\tilde{U}^2\right)-\frac{\tilde{G}}{2} \tag{5.25}$$

Thus the solutions are the roots of the following cubic polynomial

$$\tilde{v}+\frac{2}{3}R\tilde{v}^3-\left[\frac{\tilde{G}}{2}(\tilde{y}-1)+\tilde{U}\left(1+\frac{2}{3}R\tilde{U}^2\right)\right]\tilde{y}=0. \tag{5.26}$$

This cubic has a discriminant

$$\Delta=\frac{1}{3}R\left[-8-R\left(6\tilde{U}+4R\tilde{U}^3+3\tilde{G}(\tilde{y}-1)\right)^2\tilde{y}^2\right]. \tag{5.27}$$

If $\Delta>0$ then there are three real roots, if $\Delta<0$ there is one real root and two complex non-real roots. Note that this is a local condition, for each $\tilde{y}$. $\Delta>0$ can only occur for $R<0$, then the two regions are delineated by $\Delta=0$, i.e.

$$-8-R\left(6\tilde{U}+4R\tilde{U}^3+3\tilde{G}(\tilde{y}-1)\right)^2\tilde{y}^2=0. \tag{5.28}$$

From here we can look at several different cases, namely

- General flow, with both $\tilde{U}\neq 0$ and $\tilde{G}\neq 0$.
- Poiseuille flow, for which $\tilde{U}=0$ and $\tilde{G}\neq 0$.
- Couette flow, for which $\tilde{U}\neq 0$ and $\tilde{G}=0$.

We will inspect the special cases in the following subsections.

5.3.2 *Planar Poiseuille flow*

The dimensionless equation of motion for the Poiseuille flow is

$$\tilde{G}-4R\tilde{v}(\tilde{v}')^2-2R\tilde{v}^2\tilde{v}''-\tilde{v}''=0. \tag{5.29}$$

with the no-slip boundary conditions

$$\tilde{v}(0)=\tilde{v}(1)=0. \tag{5.30}$$

We find again three analytical solutions to this equation using Wolfram Mathematica's DSolve function,

$$\tilde{v}_1(\tilde{y}) = \frac{-2R + \left(2\tilde{G}R^2(-1+\tilde{y})\tilde{y} + \sqrt{R^3\left(8+\tilde{G}^2R(-1+\tilde{y})^2\tilde{y}^2\right)}\right)^{2/3}}{2R\left(2\tilde{G}R^2(-1+\tilde{y})\tilde{y} + \sqrt{R^3\left(8+\tilde{G}^2R(-1+\tilde{y})^2\tilde{y}^2\right)}\right)^{1/3}} \tag{5.31}$$

$$\tilde{v}_2(\tilde{y}) = \frac{2(1-i\sqrt{3})R - i(-i+\sqrt{3})\left(2\tilde{G}R^2(-1+\tilde{y})\tilde{y} + \sqrt{R^3\left(8+\tilde{G}^2R(-1+\tilde{y})^2\tilde{y}^2\right)}\right)^{2/3}}{4R\left(2\tilde{G}R^2(-1+\tilde{y})\tilde{y} + \sqrt{R^3\left(8+\tilde{G}^2R(-1+\tilde{y})^2\tilde{y}^2\right)}\right)^{1/3}} \tag{5.32}$$

$$\tilde{v}_3(\tilde{y}) = \frac{2(1+i\sqrt{3})R + i(i+\sqrt{3})\left(2\tilde{G}R^2(-1+\tilde{y})\tilde{y} + \sqrt{R^3\left(8+\tilde{G}^2R(-1+\tilde{y})^2\tilde{y}^2\right)}\right)^{2/3}}{4R\left(2\tilde{G}R^2(-1+\tilde{y})\tilde{y} + \sqrt{R^3\left(8+\tilde{G}^2R(-1+\tilde{y})^2\tilde{y}^2\right)}\right)^{1/3}} \tag{5.33}$$

Following up on the discussion in the previous section, the discriminant in eq. (5.27) for the Poiseuille case becomes

$$\Delta_{\text{Poiseuille}} = -\frac{R}{3}\left(8 + 9\tilde{G}^2Ry^2(1-\tilde{y})^2\right). \tag{5.34}$$

Since $\Delta_{\text{Poiseuille}} > 0$ can only occur for $R < 0$, the two regions are delineated by $\Delta_{\text{Poiseuille}} = 0$

$$8 + 9\tilde{G}^2R\tilde{y}^2(1-\tilde{y})^2 = 0. \tag{5.35}$$

The smallest $|R|$ for which this can happen in $\tilde{y} \in [0,1]$ is given by $R\tilde{G}^2 = -128/9$. In particular, if $R\tilde{G}^2 < -128/9$ then there is no solution which is real for all $\tilde{y} \in [0,1]$, and satisfies $\tilde{v}(0) = 0$. This can be seen in Figure 5.4. We can look at how the real and imaginary parts of the solutions behave when we vary the numerical values of the ratio R. The resulting plots are given in Figure 5.5. To sum up, when $R > 0$, $\tilde{v}_1(\tilde{y})$ is a purely real solution, while the other two solutions are complex and we don't consider them to be physical. On the other hand, for $-\frac{128}{9} \leq R\tilde{G}^2 < 0$, $\tilde{v}_2$ is purely real, and satisfies the boundary conditions. The other two solutions are also real for those values of $R\tilde{G}^2$, but they do not satisfy the boundary conditions, and we thus consider them unphysical.

We can also solve the equation of motion numerically. The numerical solution corresponds to the purely real analytical solution $\tilde{v}_1$, eq. (5.31) if $R > 0$, and to $\tilde{v}_2$ for $-\frac{128}{9} \leq R\tilde{G}^2 < 0$, as seen from Figure 5.6. In the same dimensionless variables, the non-relativistic, Galilean-invariant solution is given by

$$\tilde{v}_G(\tilde{y}) = \frac{\tilde{G}}{2}\tilde{y}(\tilde{y}-1). \tag{5.36}$$

Unsurprisingly, for very small values of R, $\tilde{v}_1$ and the Galilean-invariant velocity are in great agreement (see Figure 5.6). Both velocity profiles are parabolic, the difference is that as we increase R, the new velocity profile decreases and becomes flattened compared to the non-relativistic one.

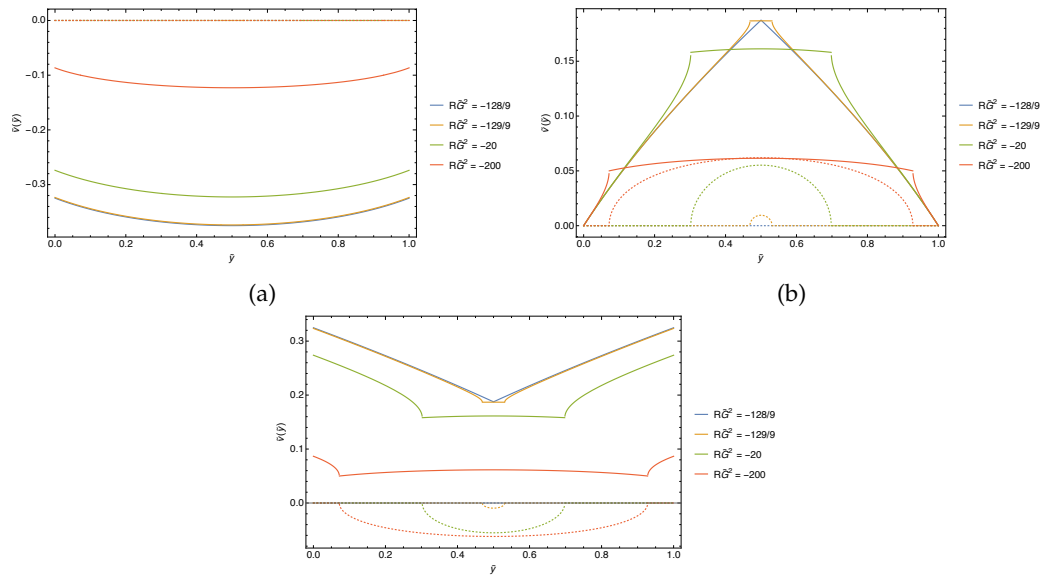

(a) (b)

(c)

Figure 5.4: Real and imaginary parts of the velocity profiles $\tilde{v}_1$ (a), $\tilde{v}_2$ (b), and $\tilde{v}_3$ (c). Real parts are given by full lines, imaginary by dashed ones. We can see that if $R\tilde{G}^2 < -128/9$ there is no solution which is real and satisfies the no-slip boundary conditions.

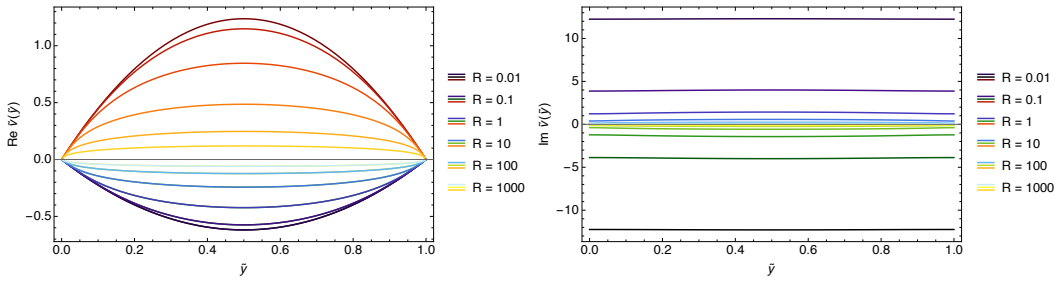

(a) (b)

Figure 5.5: Real (a) and imaginary (b) part of the velocity profile solutions of the Poiseuille flow, for various values of R. $\tilde{v}_1$ is given by lines colored in shades of red, $\tilde{v}_2$ in green-yellow, and $\tilde{v}_3$ in blue. In all cases we've fixed $\tilde{G} = -10$.

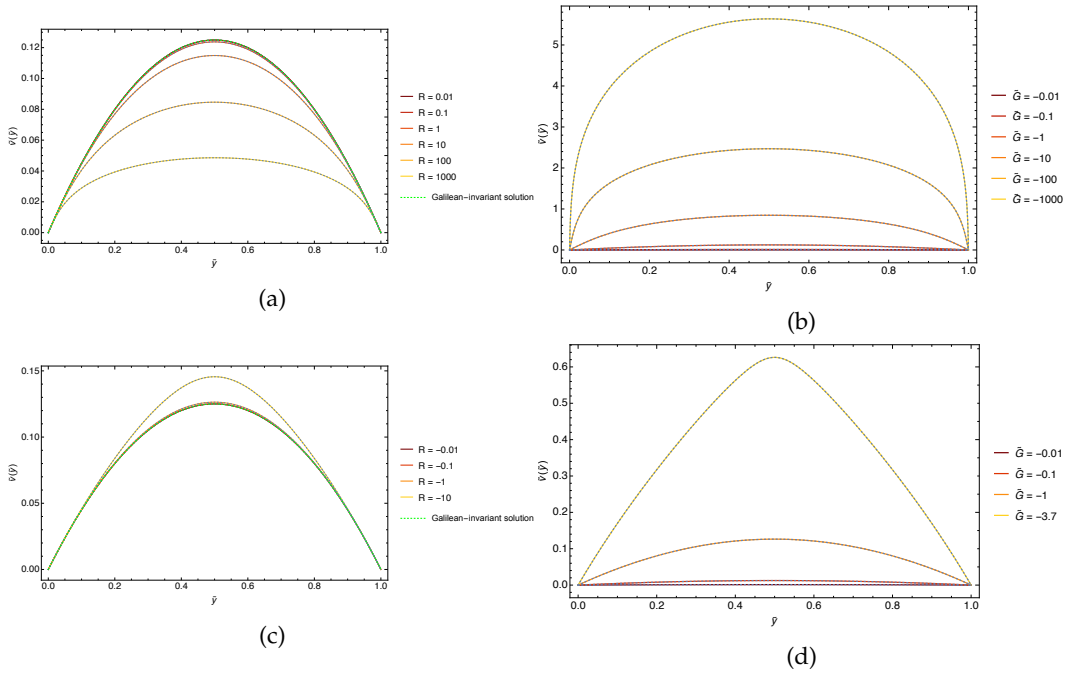

Figure 5.6: Poiseuille flow comparison of $\tilde{v}_1$ with the numerical solution (blue dashed lines) and the Galilean-invariant solution (green dotted lines), for various values of $R > 0$, and $\tilde{v}_2$ for $R\tilde{G} < -128/9$. The analytical and numerical solutions are in agreement for a wide range of values of R and $\tilde{G}$. In (a) and (c) we fixed $\tilde{G} = -1$, while in (b) we fixed $R = 1$, and in (d) $R = -1$.

5.3.3 *3D Poiseuille flow in a pipe*

We can repeat the analysis that we've done for the 2D case, in 3D for a Poiseuille flow in a pipe. Working in cylindrical coordinates, the problem is axisymmetric, with the pipe stretching along the z-direction. As a result, the velocity of the flow is

$$\mathbf{v} = (0, 0, v_z(r)). \tag{5.37}$$

The equation of motion becomes

$$G - \eta\left(\frac{v_z'}{r} + v_z''\right) - 2\gamma_8 v_z (v_z')^2 - \gamma_8\left(\frac{2v_z v_z'}{r} + 2(v_z')^2 + 2v_z v_z''\right) = 0, \tag{5.38}$$

with the boundary condition

$$v_z(r = a) = 0, \tag{5.39}$$

where a is the radius of the pipe, and ticks denote derivatives with respect to r. Similarly in dimensionless variables,

$$\tilde{r} = \frac{r}{a}, \quad \partial_{\tilde{r}} = a\partial_r, \quad \text{and} \quad v_z = v_F \tilde{v}_z, \tag{5.40}$$

the equation of motion and the boundary condition become

$$\tilde{G} - \tilde{v}_z'' - \frac{\tilde{v}_z'}{\tilde{r}} - \frac{2R}{\tilde{r}} v_z \left[2\tilde{r}(\tilde{v}_z')^2 + \tilde{v}_z\left(\tilde{v}_z' + \tilde{r}\tilde{v}_z''\right)\right] = 0, \tag{5.41}$$

$$\tilde{v}_z(\tilde{r}=1) = 0. \tag{5.42}$$

We find three solutions, much like in the previous case

$$\tilde{v}_{z,1} = -\frac{2^{1/3}}{\delta^{1/3}} + \frac{\delta^{1/3}}{2\cdot 2^{1/3} R}, \tag{5.43}$$

$$\tilde{v}_{z,2} = \frac{2^{1/3}\cdot 4\left(1+i\sqrt{3}\right)R + 2^{2/3}\left(-1+i\sqrt{3}\right)\delta^{2/3}}{8R\,\delta^{1/3}}, \tag{5.44}$$

$$\tilde{v}_{z,3} = \frac{2^{1/3}\cdot 4\left(1-i\sqrt{3}\right)R + 2^{2/3}\left(-1-i\sqrt{3}\right)\delta^{2/3}}{8R\,\delta^{1/3}}, \tag{5.45}$$

$$\delta = 3\tilde{G}\left(\tilde{r}^2-1\right)R^2 + \sqrt{R^3\left(32 + 9\tilde{G}^2\left(\tilde{r}^2-1\right)^2 R\right)}. \tag{5.46}$$

In Figure 5.7, we can see the plots of these solutions for different values of $R > 0$, as well as a full 3D surface plot of the velocity profile in Figure 5.8

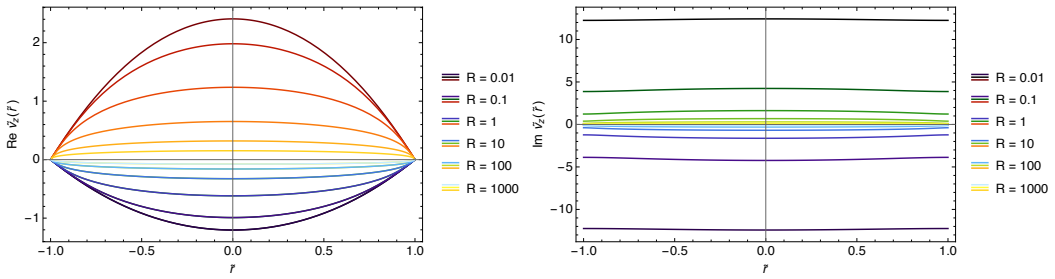

(a) (b)

Figure 5.7: Real (a) and imaginary (b) part of the velocity profile solutions of the 3D Poiseuille flow, for various values of R. $\tilde{v}_{z,1}$ is given by lines colored in shades of red, $\tilde{v}_{z,2}$ in green-yellow, and $\tilde{v}_{z,3}$ in blue. In all cases we fixed $\tilde{G} = -10$.

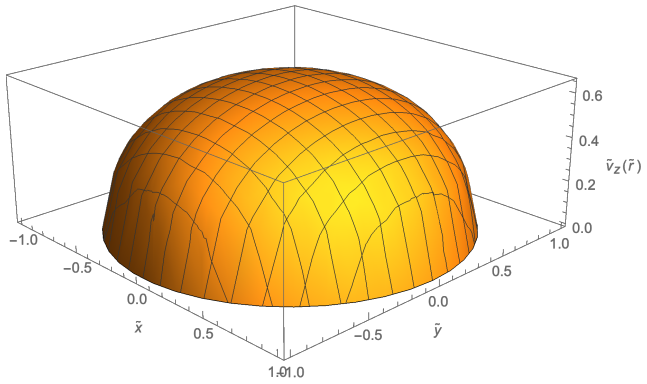

Figure 5.8: 3D plot of $\tilde{v}_{1,z}$ for $R = 10$ and $\tilde{G} = -10$.

5.3.4 *Planar Couette flow*

Similar to the planar Poiseuille flow, we consider a steady flow between two long, parallel plates, width W apart. The difference with respect to the Poiseuille flow is that now only one of the plates is at rest, while the other has velocity U in the direction along the channel. Moreover, we set the pressure gradient $\partial_x P = \partial_y P = 0$. Expressed in dimensionless units, the equation of motion becomes

$$4R\tilde{v}(\tilde{v}')^2 + 2R\tilde{v}^2\tilde{v}'' + \tilde{v}'' = 0, \tag{5.47}$$

with the boundary conditions

$$\tilde{v}(0) = 0, \quad \text{and} \quad \tilde{v}(1) = \tilde{U}. \tag{5.48}$$

Again, we find 3 analytical solutions,

$$\tilde{v}_1(\tilde{y}) = \frac{1}{2^{1/3}\delta^{1/3}} + \frac{\delta^{1/3}}{2^{2/3}R} \tag{5.49}$$

$$\tilde{v}_2(\tilde{y}) = \frac{\left(-\frac{1}{2}\right)^{1/3}}{\delta^{1/3}} + \frac{i(1+\sqrt{3})\delta^{1/3}}{2\cdot 2^{2/3}R} \tag{5.50}$$

$$\tilde{v}_3(\tilde{y}) = \frac{-2(-2)^{2/3}R + 2^{1/3}(-1-i\sqrt{3})\delta^{2/3}}{4R\delta^{1/3}} \tag{5.51}$$

$$\delta = R^2\tilde{U}\left(3+2R\tilde{U}^2\right)\tilde{y} + \sqrt{R^3\left[2+R\tilde{U}^2\left(3+2R\tilde{U}^2\right)^2\tilde{y}^2\right]} \tag{5.52}$$

The discriminant of the cubic (5.27) in this case becomes

$$\Delta_{\text{Couette}} = \frac{4}{3}R\left[-2 - R\tilde{U}^2(3+2R\tilde{U}^2)^2\tilde{y}^2\right] \tag{5.53}$$

Much like in the Poiseuille case, $\Delta_{\text{Couette}} > 0$ only for $R < 0$. Moreover, instead of $R\tilde{G}^2$, the controlling parameter now is $R\tilde{U}^2$. The two regions are delineated by the equation

$$-2 - R\tilde{U}^2(3+2R\tilde{U}^2)^2\tilde{y}^2 = 0. \tag{5.54}$$

In order to have three real solutions in $\tilde{y} \in [0,1]$, we must have $-2 \leq R\tilde{U}^2 < 0$. None of these solutions, except for $\tilde{v}_3$ when $R\tilde{U}^2 = -1/2$, satisfies the boundary conditions, as can be seen from Figure 5.9. Interestingly, if we take the limit $R\tilde{U} \to -\infty$, we recover another real solution, $\tilde{v}_2$, that satisfies the boundary conditions (see Figure 5.9 (b)). Again, when $R > 0$ we have one solution $\tilde{v}_1$ is real, and the other two are complex conjugates. The numerical solution is in agreement with the purely real analytical solution $\tilde{v}_1$ for $R > 0$. The results are given in Figure 5.10 and Figure 5.11. The Galilean-invariant, non-relativistic solution is given by

$$\tilde{v}_G(\tilde{y}) = \tilde{y}. \tag{5.55}$$

Unlike the Poiseuille flow, the velocity profile one finds in standard non-relativistic hydrodynamics can be vastly different from the one we find. A comparison is given in Figure 5.11. They seem to agree quite well for very small values of R,

but as we increase R the new velocity profile seems to increase relative to the non-relativistic one.

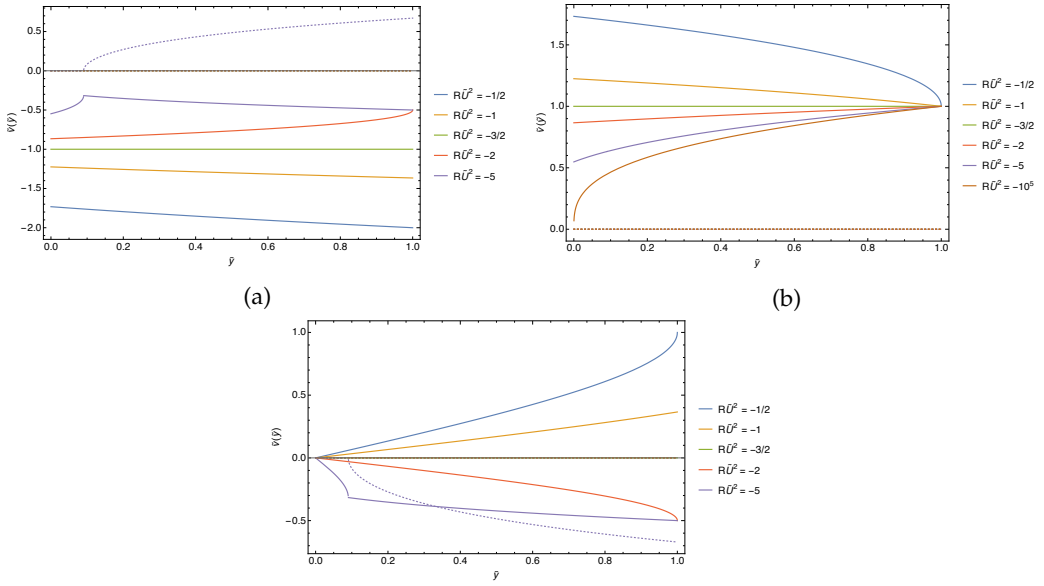

(a) (b)

(c)

Figure 5.9: Real and imaginary parts of the velocity profiles $\tilde{v}_1$ (a), $\tilde{v}_2$ (b), and $\tilde{v}_3$ (c) of the planar Couette flow. Real parts are given by full lines, imaginary by dashed ones. We can see that if $-2 \leq R\tilde{U}^2 < 0$ there are three real solutions, however none of them satisfy the boundary conditions, except for $\tilde{v}_3$ at $R\tilde{U}^2 = -1/2$. Note that for $R\tilde{U} \to -\infty$ we find a purely real solution that satisfies the boundary conditions (see (b)).

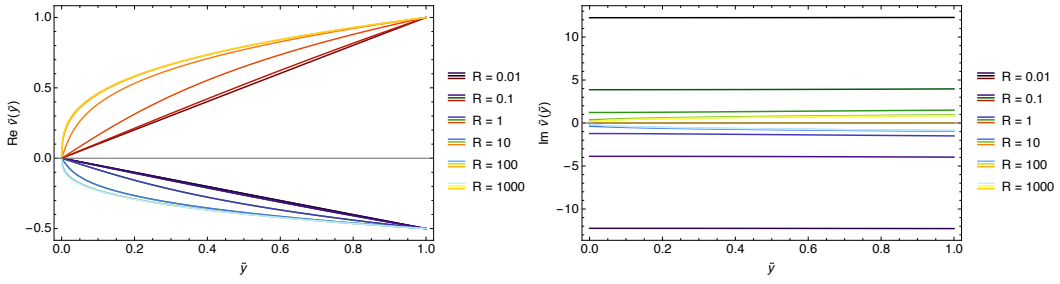

(a) (b)

Figure 5.10: Real (a) and imaginary (b) part of the velocity profile solutions of the Couette flow, for various values of R. $\tilde{v}_1$ is given by lines colored in shades of red, $\tilde{v}_2$ in green-yellow, and $\tilde{v}_3$ in blue. In all cases we've fixed $\tilde{U} = 1$.

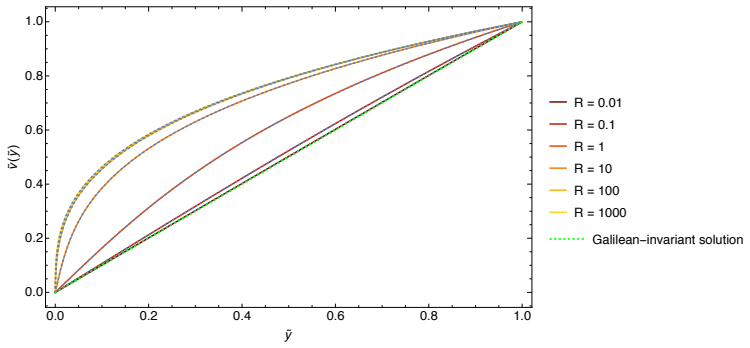

Figure 5.11: Couette flow comparison of $\tilde{v}_1$ with the numerical solution (blue dashed line) and the Galilean-invariant case (green dotted line), for various values of $R > 0$. The analytical and numerical solutions are in agreement for a wide range of values of R. The Galilean-invariant solution is in great agreement for very small values of R. In all cases we've fixed $\tilde{U} = 1$.

5.4 TAYLOR-COUETTE FLOW

One can also consider the motion of a fluid trapped between two infinite rotating coaxial cylinders. The cylinders have radii R_1, R_2 (where $R_2 > R_1$) and rotate about their axis with angular velocities ω_1, ω_2 respectively. A sketch of the geometry of the problem is given in Figure 5.12. This problem can be solved in cylindrical polar coordinates, with the z-axis along the axis of the cylinders. From the symmetry of the problem one can look for a solution with

$$\mathbf{v} = (0, v_\phi(r), 0). \tag{5.56}$$

At the surface of the cylinders, the fluid the velocity needs to be equal to the velocity of the corresponding cylinder. This defines our boundary conditions

$$v_\phi(R_1) = R_1\omega_1, \quad \text{and} \quad v_\phi(R_2) = R_2\omega_2. \tag{5.57}$$

We take the same assumptions as before (i.e. incompressible flow, etc.) and from (5.3) find the following equations

$$\frac{dp}{dr} - \frac{\rho v_\phi^2}{r} = 0, \tag{5.58}$$

$$\frac{\bar{\eta}}{r^2}\left[v_\phi - r(v_\phi' + rv_\phi'')\right] + \frac{\gamma_{13}v_\phi^2}{r^2}\left(v_\phi + 3rv_\phi'\right) - \frac{2\gamma_8 v_\phi}{r}\left[rv_\phi' + v_\phi(2v_\phi' + rv_\phi'')\right] = 0, \tag{5.59}$$

where ticks now indicate a derivative with respect to r. Note that we can derive the Navier-Stokes equations for the Galilean-invariant case by simply setting γ_8 and γ_{13} to zero in the equations above. First we solve the second equation (5.59) in order to find the velocity profile. Thus far, we've been unable to solve this equation analytically. We can solve it numerically, using Mathematica's NDSolve. The velocity profile in the Galilean-invariant case is independent of transport coefficients. In

our non-boost invariant model on the other hand, there seems to be a dependence of the velocity profile on $\bar{\eta}$ (see Figure 5.13), as well as on γ_8 and γ_{13}.

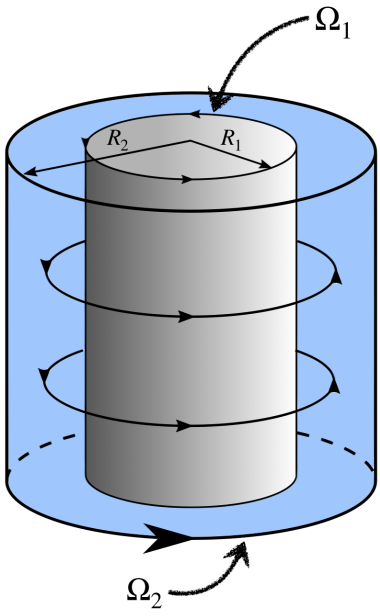

Figure 5.12: A sketch of the Taylor-Couette flow.

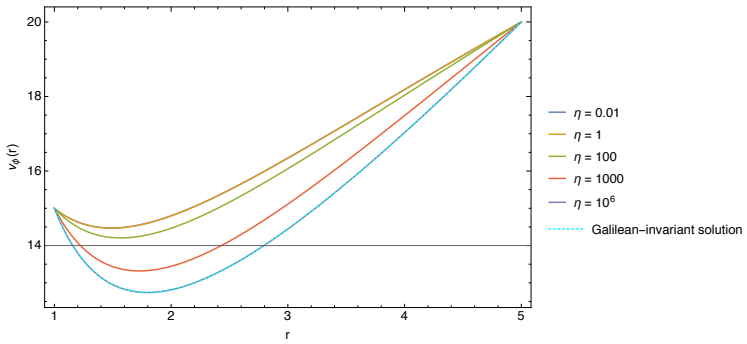

Figure 5.13: Comparison of the velocity profiles in our case vs. standard Galilean hydrodynamics. We can see that, unlike conventional hydrodynamics, the velocity profile depends on the value of η in our case. Here we used $\gamma_8 = \gamma_{13} = 1$, and for the boundary conditions $v_\phi(R_1 = 1) = 15$, and $v_\phi(R_2 = 5) = 20$.

Although unable to find the full analytical solution, we can find perturbative corrections in a double expansion for small γ_8 and γ_{13}. At first order, we find

$$v_\phi(r) = v_\phi^0(r) + \gamma_8 v_\phi^{1,\gamma_8}(r) + \gamma_{13} v_\phi^{1,\gamma_{13}}(r) + O(\gamma_8^2, \gamma_{13}^2) \tag{5.60}$$

$$v_\phi^0(r) = \frac{R_1^2 R_2^2(\Omega_2 - \Omega_1)}{R_2^2 - R_1^2}\frac{1}{r} + \frac{\Omega_2 R_2^2 - \Omega_1 R_1^2}{R_2^2 - R_1^2} r \tag{5.61}$$

$$\begin{aligned}\gamma_8 v_\phi^{1,\gamma_8}(r) = \frac{1}{2r^3(R_1+R_2)^4\delta_R^4}\frac{\gamma_8}{\bar{\eta}}\Big\{ & 4r^4\delta_{R^2}\delta_\Omega\left(R_1^3 R_2\Omega_1 - R_1 R_2^3\Omega_2\right)^2 \log r \\ & - 4r^2 R_1^4 R_2^2\left(r^2 - R_2^2\right)\delta_{R\Omega}^2\delta_\Omega \log R_1 - 4r^2 R_1^2 R_2^4\left(r^2 - R_1^2\right)\delta_{R\Omega}^2\delta_\Omega \log R_2 \\ & - \left(r^2 - R_1^2\right)\left(r^2 - R_2^2\right)\delta_{R^2}\left((R_1R_2)^4\delta_\Omega^3 - 2r^2\delta_{R\Omega}^3\right)\Big\}\end{aligned} \tag{5.62}$$

$$\begin{aligned}\gamma_{13} v_\phi^{1,\gamma_{13}}(r) = -\frac{1}{4r^3(R_1+R_2)^4\delta_R^4}\frac{\gamma_{13}}{\bar{\eta}}\Big\{ & 12r^4\delta_{R^2}\delta_\Omega\left(R_1^3 R_2\Omega_1 - R_1 R_2^3\Omega_2\right)^2 \log r \\ & + 12r^2 R_1^4 R_2^2\left(r^2 - R_2^2\right)\delta_{R\Omega}^2\delta_\Omega \log R_1 - 12r^2 R_1^2 R_2^4\left(r^2 - R_1^2\right)\delta_{R\Omega}^2\delta_\Omega \log R_2 \\ & + \left(r^2 - R_1^2\right)\left(r^2 - R_2^2\right)\delta_{R^2}\left((R_1R_2)^4\delta_\Omega^3 - 2r^2\delta_{R\Omega}^3\right)\Big\},\end{aligned} \tag{5.63}$$

with the following shorthands

$$\delta_\Omega = \Omega_2 - \Omega_1, \quad \delta_R = R_2 - R_1, \quad \delta_{R^2} = R_2^2 - R_1^2, \quad \delta_{R\Omega} = R_2^2\Omega_2 - R_1^2\Omega_1. \tag{5.64}$$

We can transform the equations of motion into dimensionless form, by introducing dimensionless variables

$$r = (\tilde{r}\delta_R + R_1), \quad \partial_r = \frac{1}{\delta_R}\partial_{\tilde{r}}, \quad v_\phi = v_F\tilde{v}, \tag{5.65}$$

where $\delta_R \equiv R_2 - R_1$ is the difference between the outer and inner radii. With this choice of variables, the dimensionless radial variable $\tilde{r}$ runs from 0 (inner cylinder) to 1 (outer cylinder). Equation (5.59) then becomes

$$\begin{aligned}\tilde{v} - (\tilde{r}+\epsilon)\left(\tilde{v}' + (\tilde{r}+\epsilon)\tilde{v}''\right) - 2R(\tilde{r}+\epsilon)\tilde{v}\left[2(\tilde{r}+\epsilon)(\tilde{v}')^2 + v\left(2\tilde{v}' + (\tilde{r}+\epsilon)\tilde{v}''\right)\right] \\ + T\tilde{v}^2\left[v + (\tilde{r}+\epsilon)\tilde{v}'\right] = 0,\end{aligned} \tag{5.66}$$

where we have two dimensionless quantities acting as transport coefficients

$$R \equiv \frac{\gamma_8 v_F^2}{\eta}, \quad \text{and} \quad T \equiv \frac{\gamma_{13} v_F^2}{\eta}, \tag{5.67}$$

and $\epsilon \equiv R_1/\delta_R$. Results for various values of R and T are given in Figure 5.14. We can see that R and T seem to have inverse effects. For low values of R the velocity profile is concave, for higher values it is convex, whereas for T it is vice versa.

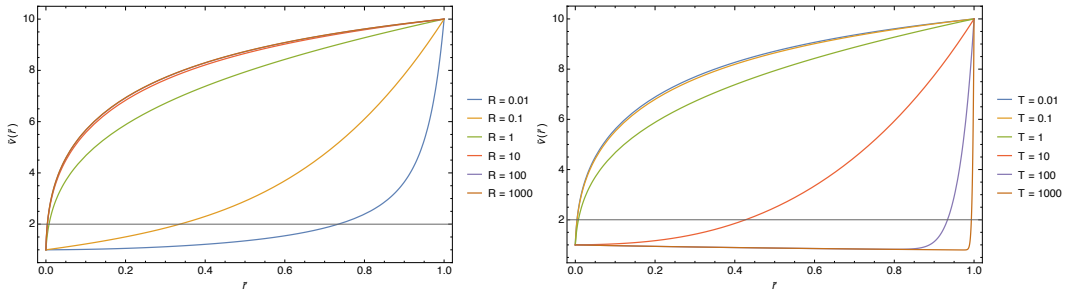

(a) (b)

Figure 5.14: Velocity profile of the Taylor-Couette flow for various values of the ratio R and T. In all cases we used $\epsilon = 1$, and for the boundary conditions $\tilde{v}(\tilde{R}_1 = 0) = 1$, and $\tilde{v}(\tilde{R}_2 = 1) = 10$. In (a) we fixed $T = 1$, and in (b) $R = 1$.

5.5 (IN)STABILITY OF THE POISEUILLE FLOW

Let us consider a small perturbation to the equations of motion (5.1) around the real solution of the 2D Poiseuille flow

$$\mathbf{v}(x,y,t) = \mathbf{V} + \varepsilon\,\mathbf{u} = (V(y) + \varepsilon\,u_x(x,y,t), \varepsilon\,u_y(x,y,t)), \tag{5.68}$$

$$p_{\text{tot}}(x,y,t) = P(x) + \varepsilon\,p(x,y,t), \tag{5.69}$$

where $V(y)$ and $P(x)$ are the solutions of the background 2D Poiseuille flow. To first order in the perturbations (i.e. first order in ε), we find

$$\begin{aligned}
\nu = x: \quad & \partial_x p - (\bar{\pi} + 2\gamma_1 V^2)\partial_t^2 u_x + \rho(u_y V' + \partial_t u_x + V\partial_x u_x) - V'(2(\gamma_2+\gamma_5)\partial_t u_y + 3\gamma_{13} V\partial_x u_y) \\
& + \gamma_8\left[-4u_x(V'^2 + V\,V'') - V'\left(\partial_t u_y + 8V\partial_y u_x - 2V\partial_x u_y\right) - V\left(\partial_{x,t}^2 u_x + 2V\nabla^2 u_x\right)\right] \\
& - \gamma_{13}V^2(\partial_{x,y}^2 u_y + \partial_x^2 u_x) - \bar{\eta}\nabla^2 u_x - 2\gamma_9 V\left(V'\partial_x u_y + V\partial_x^2 u_x\right) \\
& - 2V\left(\gamma_{10} - \gamma_{16} + \gamma_2 + \gamma_6 - \frac{\gamma_7}{2}\right)\partial_{x,t}^2 u_x = 0
\end{aligned} \tag{5.70}$$

$$\begin{aligned}
\nu = y: \quad & \partial_y p + \rho\left(\partial_t u_y + V\partial_x u_y\right) - \bar{\eta}\nabla^2 u_y - \bar{\pi}\partial_t^2 u_y + 2\gamma_5\left(V'\partial_t u_x + V\partial_{y,t}^2 u_x\right) + \gamma_6 V\partial_{x,t}^2 u_y \\
& \gamma_8\left[-4u_y(V'^2 + V\,V'') - V\left(2V'\nabla\cdot u + \partial_{x,t}^2 u_y + 2V\partial_{x,y}^2 u_x\right)\right] \\
& - \gamma_{13}V^2\partial_x^2 u_y + 2\gamma_{16}\left(V'\partial_t u_x + V\partial_{y,t}^2 u_x\right) = 0.
\end{aligned} \tag{5.71}$$

Here, primes denote a derivative with respect to y. Note that this problem is now time-dependent, thus we must account for terms in the constitutive relations that we eliminated before by stating that the flow was steady. In other words, we must bring back time derivative of the velocity terms. We will eliminate u_x and p, by first using the incompressibility of the flow

$$\nabla\cdot u = 0, \tag{5.72}$$

to replace all derivatives of u_x in favor of u_y. Then we differentiate the x-equation (5.70) with respect to x and y, and we differentiate the y-equation (5.71) twice

with respect to x. Finally, we subtract one from the other. We then assume the perturbations are of the form

$$u_y(x,y,t) = A(y)e^{i(kx-\omega t)}, \tag{5.73}$$

where $A(y)$ is a complex function. Inserting this ansatz into the resulting equation, gives us our version of the Orr-Sommerfeld equation

$$\begin{aligned}
&\frac{\bar{\eta}+2\gamma_8 V^2}{\rho}A^{(4)} + \frac{12\gamma_8 V\,V'}{\rho}A^{(3)} + \left\{ i\omega k\left[-iV + \frac{(2\gamma_{10}+2\gamma_2+2\gamma_5+2\gamma_6-\gamma_7+\gamma_8)\omega V}{\rho}\right]\right.\\
&\left. -\frac{\omega^2(\bar{\pi}-2\gamma_1 V^2)}{\rho} - \frac{2k^2\left(\bar{\eta}+(\gamma_{15}+\gamma_9)V^2\right)}{\rho} + \frac{12\gamma_8\left(V'^2+V\,V''\right)}{\rho}\right\}A''\\
&+\left[\frac{k(2\gamma_{10}+2\gamma_6-\gamma_7)\omega V'}{\rho} + \frac{k^2\left(3\gamma_{13}-2(\gamma_{15}+3\gamma_8+\gamma_9)\right)V'\,V}{\rho}\right.\\
&\left. +\frac{4\gamma_1\omega^2 V'\,V}{\rho} + \frac{4\gamma_8(3V'\,V''+V\,V^{(3)})}{\rho}\right]A'\\
&+\left\{k^3\left[iV+\frac{(\gamma_6-\gamma_8)\omega V}{\rho}\right] + \frac{k^4(\bar{\eta}+\gamma_{13}V^2)}{\rho} + k\left[iV'' - \frac{(2\gamma_2+2\gamma_5+\gamma_8)\omega V''}{\rho}\right]\right.\\
&\left. k^2\left[-i\omega + \frac{\bar{\pi}\omega^2}{\rho} + \frac{\left(3\gamma_{13}+2(\gamma_{15}-3\gamma_8+\gamma_9)\right)\left(V'^2+V\,V''\right)}{\rho}\right]\right\}A = 0.
\end{aligned} \tag{5.74}$$

If we were to take a limit where all the new transport coefficients go to zero ($\gamma_i,\ \bar{\pi} \to 0$), we would get the well-known original Orr-Sommerfeld equation

$$\frac{\bar{\eta}}{\rho}A^{(4)} - \left(\lambda + \frac{2\alpha^2\bar{\eta}}{\rho} + i\alpha V\right)A'' + \left(\alpha^2\lambda + \frac{\alpha^4\bar{\eta}}{\rho} + i\alpha\left(\alpha^2 V + V''\right)\right)A = 0, \tag{5.75}$$

where we have used $\alpha \equiv k$ and $\lambda \equiv -i\omega$, which is common in the literature. Furthermore, this equation is subject to boundary conditions

$$A(-h) = A(h) = 0, \tag{5.76}$$
$$A'(-h) = A'(h) = 0, \tag{5.77}$$

where h is the half-width of the channel. This is an eigenvalue problem for λ. If the real part of λ is positive, the perturbation will grow with time. In the usual Orr-Sommerfeld problem, we can test for instability by looking for values of η/ρ, or more commonly, the Reynolds number Re and wave number α, which give eigenvalues λ with positive real part. This problem was solved in the 1970s by Orszag [139], determining that the critical Reynolds number and the critical wave number, at which turbulence sets in, are

$$Re_c^O \approx 5772.22 \qquad \alpha_c^O \approx 1.02056. \tag{5.78}$$

For a planar Poiseuille flow there is a critical set (α_c^O, Re_c^O), and for all values less than these the flow is stable to all two dimensional disturbances that satisfy eq. (5.75).

This problem can be solved using spectral methods. We will try to solve an analogous problem for our case, using a modified code of [140] that implements a spectral collocation method described by [141]. We would like to find corrections to the usual, Galilean case, and see whether turning on new transport coefficient changes the stability picture of the Poiseuille flow. To make matters simpler, we will only account for $\bar{\eta}$ and γ_8, and set all the other, new transport coefficients to zero in (5.74). We can rewrite the resulting equation in dimensionless variables

$$y = h\tilde{y}, \quad V = U_{\max}\tilde{V}, \quad \alpha = \frac{1}{h}\tilde{\alpha}, \quad \lambda = \frac{U_{\max}}{h}\tilde{\lambda}, \tag{5.79}$$

where $U_{\max} = -\frac{Gh^2}{2\bar{\eta}}$ is the maximum velocity of the non-relativistic Poiseuille flow. It corresponds to the velocity at the mid-center of the channel in the Galilean-invariant flow

$$V_{\text{Gal.}}(y) = U_{\max}\left[1 - \left(\frac{y}{h}\right)^2\right]. \tag{5.80}$$

We can use the same quantity to define the Reynolds number and R as

$$Re = \frac{\rho h U_{\max}}{\bar{\eta}}, \quad R = \frac{\gamma_8 U_{\max}^2}{\bar{\eta}}. \tag{5.81}$$

Furthermore, we linearize the equation in R, up to first order

$$\begin{aligned}
&\lambda \to \lambda_0 + R\lambda_1,\\
&A \to A_0 + RA_1,\\
&\alpha \to \alpha_0 + R\alpha_1,\\
&\tilde{V} \to \tilde{V}_0 + R\tilde{V}_1 = (1-y^2) - \frac{2}{3}R(1-y^2)^3,
\end{aligned} \tag{5.82}$$

and find

$$\begin{aligned}
R^0: \quad & \frac{A_0^{(4)}}{Re} - \left(\frac{2\alpha_0^2}{Re} + i\alpha_0 V_0\right)A_0'' + \left(\frac{\alpha_0^4}{Re} + i\alpha_0^3 V_0 + i\alpha_0 V_0''\right)A = \lambda_0\left(A_0'' - \alpha_0^2 A_0\right),\\
R^1: \quad & \frac{2V_0^2}{Re}A_0^{(4)} + \frac{12V_0V_0'}{Re}A_0^{(3)} + \left[-i(\alpha_0 V_1 + \alpha_1 V_0) + \frac{-4\alpha_0\alpha_1 + 12\left((V_0')^2 + V_0V_0''\right)}{Re}\right]A_0''\\
& + \frac{1}{Re}\left[4\left(3V_0'V_0'' + V_0V_0^{(3)}\right) - 6\alpha_0^2 V_0V_0'\right]A_0'\\
& + \left[i\alpha_0^3 V_1 + 3i\alpha_1\alpha_0^2 V_0 + i\alpha_0 V_1'' + \frac{1}{Re}\left(4\alpha_1\alpha_0^3 - 6\alpha_0^2\left((V_0')^2 + V_0V_0''\right)\right)\right]A_0\\
& + \frac{A_1^{(4)}}{Re} - \left(\frac{2\alpha_0^2}{Re} + i\alpha_0 V_0\right)A_1'' + \left(i\alpha_0(V_0'' + \alpha_0^2 V_0) + \frac{\alpha_0^4}{Re}\right)A_1\\
& = \left[A_1'' - \alpha_0^2 A_1 + \left(-2\alpha_1\alpha_0 + \frac{i\alpha_0(V_0'' + \alpha_0^2 V_0)}{Re}\right)A_0 - \frac{i\alpha_0 V_0}{Re}A_0''\right]\lambda_0 + \left(A_0'' - \alpha_0^2 A_0\right)\lambda_1.
\end{aligned} \tag{5.83}$$

The zeroth-order equation reproduces the standard Orr-Sommerfeld equation for this flow. Now we can solve the problem perturbatively and using the spectral collocation method to find corrections λ_1 to the zeroth-order eigenvalues λ_0. The

input parameters of our program are the Reynolds number Re, the zeroth-order wave number α_0, and the first-order correction to it α_1, and the number of collocation points N. We find corrections to the "critical" eigenvalue, for which Re(λ)=0, at $N = 60$ collocation points:

$$(\alpha_c^O, Re_c^O) \implies \lambda_c^O \approx (-3 \cdot 10^{-9} - i\,0.269205) \tag{5.84}$$

$$(\alpha_c^O + R\,\alpha_{1,c},\ Re_c^O) \implies \lambda_c^O + R\,\lambda_{1,c} \approx \lambda_c^O + R\,(2 \cdot 10^{-10} + i\,3188.262), \tag{5.85}$$

and $\alpha_{1,c} = -8321.9$. For an illustrative example, let's look at an unstable mode given by $Re = 5780$, and $\alpha_0 = \alpha_c^O = 1.02056$. Solving the standard Orr-Sommerfeld equation, we find that it's eigenvalue is $\lambda_0 = (0.0000130641 - i\,0.269367)$. The real part is positive, so it is indeed unstable. Now, taking the same parameters in our case and taking $\alpha_1 = 0$, it would seem that the effect of increasing R is that it pushes the critical mode back into "stable territory", as can be seen from Figure 5.15.

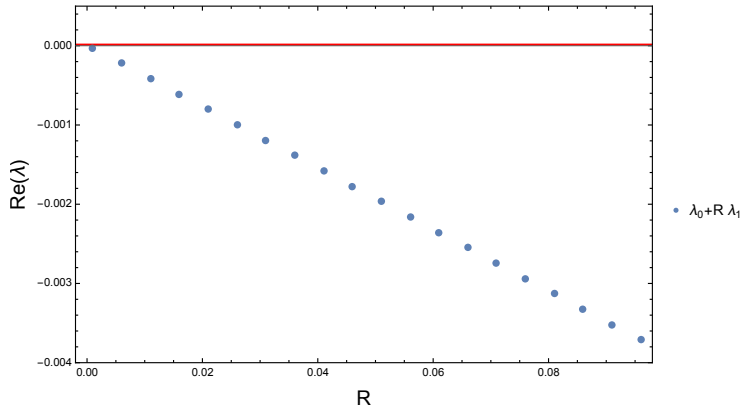

Figure 5.15: A comparison of the zeroth-order result (red line), corresponding to the eigenvalue of a mode that is unstable at zeroth-order $\lambda_0 = (0.0000130641 - i\,0.269367)$, and the first-order result obtained by increasing R and setting $\alpha_1 = 0$.

5.6 DISCUSSION

We have analyzed several flow configurations for a non-boost invariant fluid flow. We looked at a 2D flow through a channel (Poiseuille and Couette flow), a flow through a 3D pipe (Poiseuille flow) and a flow between two concentric, rotating cylinders (Taylor-Couette flow). We found that the flow is characterized by R, the ratio of γ_8 and $\bar{\eta}$. Unlike ordinary Galilean fluids, the velocity profile of non-boost invariant fluids, in this configuration, is not just controlled by the shear viscosity, but also by another transport coefficient that seems to act like a "second" viscosity. Interestingly, solving the equation of motion we find three solutions, which depending on the values of R, the pressure gradient and the boundary conditions, can consist of one real and two complex solutions, or three real solutions. However, in all cases there is only one physical solution - one of the three will satisfy the boundary conditions and be purely real. In the case of Taylor-Couette flow, we were unable to find analytic solutions, but were able to find numerical ones.

Unlike Galilean fluids, the velocity profile here depends on what would in the Galilean case be the shear viscosity, as well as new transport coefficients γ_8 and γ_{13}. In dimensionless variables we define two ratios R (ratio of γ_8 and $\bar{\eta}$), and T (the ratio of γ_{13} and $\bar{\eta}$), which parametrize the velocity profile, and seem to have inverse effects of one another. Finally, we have derived the analogue of the Orr-Sommerfeld equation, and explored the instability of the 2D Poiseuille flow. As a matter of further investigation, it might be interesting to look at other flow configurations from which we might clearly identify the effects of other, new transport coefficients. It might be of interest to test the instability of the Taylor-Couette flow, and see what are the effects of γ_8 and γ_{13} there.

Part III

APPENDIX

A

EQUATIONS OF STATE

A.1 CONFORMAL EQUATION OF STATE

For a conformal system at temperature T and chemical potential μ in d-dimensions we have the following general expression for the equation of state,

$$p(T,\mu) = T^d \Phi\left(\frac{\mu}{T}\right) \tag{A.1}$$

From which follows charge, entropy and energy densities using standard thermodynamic relations,

$$n(T,\mu) \equiv \left(\frac{\partial p}{\partial \mu}\right)_T = T^{d-1}\Phi'\left(\frac{\mu}{T}\right), \tag{A.2}$$

$$s(T,\mu) \equiv \left(\frac{\partial p}{\partial T}\right)_\mu = T^{d-2}\left(dT\Phi\left(\frac{\mu}{T}\right) - \mu\Phi'\left(\frac{\mu}{T}\right)\right), \tag{A.3}$$

$$\epsilon(T,\mu) \equiv -p + Ts + \mu n = (d-1)T^d\Phi\left(\frac{\mu}{T}\right). \tag{A.4}$$

After some manipulations, we may obtain the quantities defined in the hydrodynamic analysis in section 3.2.3,

$$\beta_1 = \frac{1}{d-1}, \tag{A.5}$$

$$\beta_2 = 0, \tag{A.6}$$

$$\alpha_1 = \frac{T^{1-d}\Phi'}{(d-1)(\Phi')^2 - d\Phi\Phi''}. \tag{A.7}$$

$$\alpha_2 = \frac{-dT^{2-d}\Phi}{(d-1)(\Phi')^2 - d\Phi\Phi''}. \tag{A.8}$$

A.2 REISSNER-NORDSTRÖM ADS$_{d+1}$ EQUATION OF STATE

For a strongly coupled fluid holographically dual to a Reissner-Nordström AdS$_{d+1}$ black brane, as a solution to the equations of motion of (3.72) with $2\kappa^2 = \tilde{g}^2 = L = 1$, has the following conformal equation of state,

$$\Phi(X) = R(X)^d\left(1 + \frac{(d-2)X^2}{2(d-1)R(X)^2}\right) \tag{A.9}$$

where R is the positive solution of

$$R^2 - \frac{4\pi}{d}R - \frac{(d-2)^2X^2}{2d(d-1)} = 0. \tag{A.10}$$

Using the above definitions this leads to the expressions,

$$n = (d-2)\mu r_0^{d-2}, \qquad s = 4\pi r_0^{d-1}, \qquad \epsilon = (d-1) r_0^d \left(1 + \frac{d-2}{2(d-1)} \frac{\mu^2}{r_0^2}\right), \quad \text{(A.11)}$$

where $r_0 \equiv TR\left(\frac{\mu}{T}\right)$ gives the coordinate position of the event horizon in a Schwarzschild coordinate system. For completeness we finish this section by providing the associated first order hydrodynamic transport coefficients for this state,

$$\eta = \frac{s}{4\pi}, \qquad \zeta = 0, \qquad \sigma = \left(\frac{sT}{\epsilon + p}\right)^2. \quad \text{(A.12)}$$

where σ was computed in [142].

B

EXTRACTING THE HOLOGRAPHIC STRESS TENSOR

Once we have numerically constructed the NESS, as described in section 3.4.1, we wish to extract the one-point function of the CFT stress tensor. Holographic renormalisation is readily performed in Fefferman-Graham (FG) coordinates, where the one-point function is given by a term in the near-boundary expansion there. However our numerical solutions are not obtained in FG coordinates, rather, they are obtained in coordinates defined by $\xi = 0$. To compute the stress tensor using existing holographic renormalisation results [87] we must find the coordinate map which relates the two.

B.1 NEAR-BOUNDARY SOLUTION IN FG COORDINATES

We seek the near-boundary solution in Fefferman-Graham form so that we may use existing results for holographic renormalisation. Taking z, x^μ to be such coordinates, then by definition $h_{z\mu} = 0$ and $h_{zz} = 1$. Additionally, we compute the following near-boundary expansion of the solutions to (3.129) at $\xi = 0$ as

$$h_{\mu\nu}(z,x) = \eta_{\mu\nu} + s_{\mu\nu}(x) + h^{(2)}_{\mu\nu}(x)z^2 + h^{(3)}_{\mu\nu}(x)z^3 + O(z)^4 \tag{B.1}$$

where the $h^{(2)}_{\mu\nu}$ are given by

$$h^{(2)}_{00}(x) = \frac{\beta_x^2}{\beta_x^2+\beta_y^2}\frac{2(1+s)s'' - (s')^2}{8(1+s)^2} \tag{B.2}$$

$$h^{(2)}_{0i}(x) = 0 \tag{B.3}$$

$$h^{(2)}_{ij}(x) = \frac{\beta_x^2}{\beta_x^2+\beta_y^2}\frac{2(1+s)s'' - (s')^2}{8(1+s)^2}(\eta_{ij} + s_{ij}(x)) \tag{B.4}$$

Aside from constraints imposed by the conformal and diffeomorphism Ward identities, the $h^{(3)}_{\mu\nu}(x)$ are unconstrained, and in holographic renormalisation yield the one-point function of the stress tensor, [87],

$$\langle T_{\mu\nu} \rangle = 3h^{(3)}_{\mu\nu}. \tag{B.5}$$

B.2 CONVERTING FROM FG TO $\xi = 0$ COORDINATE SYSTEM

From the above analysis we have an expression for the CFT stress tensor in terms of data in a FG near-boundary expansion. Let us map from FG to a new set of coordinates near the boundary

$$t \rightarrow t + \sum_{n=1} T_n(x) z^n \tag{B.6}$$

$$x \rightarrow x + \sum_{n=1} X_n(x) z^n \tag{B.7}$$

$$y \rightarrow y + \sum_{n=1} Y_n(x) z^n \tag{B.8}$$

$$z \rightarrow z + \sum_{n=1} Z_n(x) z^{1+n} \tag{B.9}$$

We take the line element in near-boundary FG expansion and apply these coordinate transformations. The resulting near-boundary metric is then used to compute the vector ξ. For the first few couple of orders we find the following choices render $\xi = 0$,

$$T_1 = \gamma, \quad X_1 = \gamma\beta_x, \quad Y_1 = \gamma\beta_y, \quad Z_1 = \frac{\gamma\beta_x s'}{16(1+s)} \tag{B.10}$$

$$T_2 = 0, \quad X_2 = 0, \quad Y_2 = 0, \quad Z_2 = \frac{\gamma^2\beta_x^2(64(1+s)s'' - 57(s')^2}{1024(1+s)^2}. \tag{B.11}$$

We continue in this way to reach the order at which the stress tensor enters, with expressions that are too cumbersome to present here. The resulting metric in $\xi = 0$ coordinates contains the sought after data defined through the FG expansion, i.e. $\langle T_{\mu\nu} \rangle$, and so by identifying where these terms appear allows us to extract the stress tensor from a bulk solution in $\xi = 0$ coordinates. We find,

$$\langle T_{\mu\nu} \rangle = \frac{1}{2}\partial_z^3 h_{\mu\nu}\big|_{z=0} + \frac{\gamma_{\mu\nu}}{z_h^3} + V_{\mu\nu} \tag{B.12}$$

where $V_{\mu\nu}$ vanishes when $s' = s'' = s''' = 0$. Note that this expression depends explicitly on the quantities z_h, β_i which are introduced by the gauge $\xi = 0$ through the reference metric.

BIBLIOGRAPHY

[1] Juan Martin Maldacena. "The Large N limit of superconformal field theories and supergravity." In: *Int. J. Theor. Phys.* 38 (1999), pp. 1113–1133. DOI: 10.1023/A:1026654312961. arXiv: hep-th/9711200.

[2] S.S. Gubser, Igor R. Klebanov, and Alexander M. Polyakov. "Gauge theory correlators from noncritical string theory." In: *Phys. Lett. B* 428 (1998), pp. 105–114. DOI: 10.1016/S0370-2693(98)00377-3. arXiv: hep-th/9802109.

[3] Edward Witten. "Anti-de Sitter space and holography." In: *Adv. Theor. Math. Phys.* 2 (1998), pp. 253–291. DOI: 10.4310/ATMP.1998.v2.n2.a2. arXiv: hep-th/9802150.

[4] Lev D Landau and Evgeny Mikhailovich Lifshitz. "Fluid mechanics." In: *Fluid Mechanics. Second Edition. 1987. Pergamon, Oxford* (1987).

[5] Pavel Kovtun. "Lectures on Hydrodynamic Fluctuations in Relativistic Theories." In: *J. Phys.* A45 (2012), p. 473001. DOI: 10.1088/1751-8113/45/47/473001. arXiv: 1205.5040 [hep-th].

[6] Kristan Jensen. "On the coupling of Galilean-invariant field theories to curved spacetime." In: *SciPost Phys.* 5.1 (2018), p. 011. DOI: 10.21468/SciPostPhys.5.1.011. arXiv: 1408.6855 [hep-th].

[7] Kristan Jensen. "Aspects of hot Galilean field theory." In: *JHEP* 04 (2015), p. 123. DOI: 10.1007/JHEP04(2015)123. arXiv: 1411.7024 [hep-th].

[8] Igor Novak, Julian Sonner, and Benjamin Withers. "Overcoming Obstacles in Nonequilibrium Holography." In: *Phys. Rev.* D98.8 (2018), p. 086023. DOI: 10.1103/PhysRevD.98.086023. arXiv: 1806.08655 [hep-th].

[9] Julian Sonner and Benjamin Withers. "Universal spatial structure of nonequilibrium steady states." In: *Phys. Rev. Lett.* 119.16 (2017), p. 161603. DOI: 10.1103/PhysRevLett.119.161603. arXiv: 1705.01950 [hep-th].

[10] Igor Novak, Julian Sonner, and Benjamin Withers. "Hydrodynamics without boosts." In: *JHEP* 07 (2020), p. 165. DOI: 10.1007/JHEP07(2020)165. arXiv: 1911.02578 [hep-th].

[11] J.D. Bekenstein. "Black holes and the second law." In: *Lett. Nuovo Cim.* 4 (1972), pp. 737–740. DOI: 10.1007/BF02757029.

[12] Jacob D. Bekenstein. "Black holes and entropy." In: *Phys. Rev. D* 7 (1973), pp. 2333–2346. DOI: 10.1103/PhysRevD.7.2333.

[13] S.W. Hawking. "Particle Creation by Black Holes." In: *Commun. Math. Phys.* 43 (1975). Ed. by G.W. Gibbons and S.W. Hawking. [Erratum: Commun.Math.Phys. 46, 206 (1976)], pp. 199–220. DOI: 10.1007/BF02345020.

[14] Gerard 't Hooft. "Dimensional reduction in quantum gravity." In: *Conf. Proc. C* 930308 (1993), pp. 284–296. arXiv: gr-qc/9310026.

[15] Leonard Susskind. "The World as a hologram." In: *J. Math. Phys.* 36 (1995), pp. 6377–6396. DOI: 10.1063/1.531249. arXiv: hep-th/9409089.

[16] Ofer Aharony, Steven S. Gubser, Juan Martin Maldacena, Hirosi Ooguri, and Yaron Oz. "Large N field theories, string theory and gravity." In: *Phys. Rept.* 323 (2000), pp. 183–386. DOI: 10.1016/S0370-1573(99)00083-6. arXiv: hep-th/9905111.

[17] Eric D'Hoker and Daniel Z. Freedman. "Supersymmetric gauge theories and the AdS / CFT correspondence." In: *Theoretical Advanced Study Institute in Elementary Particle Physics (TASI 2001): Strings, Branes and EXTRA Dimensions*. Jan. 2002, pp. 3–158. arXiv: hep-th/0201253.

[18] John McGreevy. "Holographic duality with a view toward many-body physics." In: *Adv. High Energy Phys.* 2010 (2010), p. 723105. DOI: 10.1155/2010/723105. arXiv: 0909.0518 [hep-th].

[19] Martin Ammon and Johanna Erdmenger. *Gauge/gravity duality: Foundations and applications*. Cambridge: Cambridge University Press, Apr. 2015. ISBN: 978-1-107-01034-5, 978-1-316-23594-2.

[20] Horatiu Nastase. *Introduction to the ADS/CFT Correspondence*. Cambridge University Press, Sept. 2015. ISBN: 978-1-107-08585-5, 978-1-316-35530-5.

[21] Sean A. Hartnoll, Andrew Lucas, and Subir Sachdev. "Holographic quantum matter." In: (Dec. 2016). arXiv: 1612.07324 [hep-th].

[22] Joshua D. Qualls. "Lectures on Conformal Field Theory." In: (Nov. 2015). arXiv: 1511.04074 [hep-th].

[23] Leonard Susskind and Edward Witten. "The Holographic bound in anti-de Sitter space." In: (May 1998). arXiv: hep-th/9805114.

[24] Amanda W. Peet and Joseph Polchinski. "UV / IR relations in AdS dynamics." In: *Phys. Rev. D* 59 (1999), p. 065011. DOI: 10.1103/PhysRevD.59.065011. arXiv: hep-th/9809022.

[25] Leo P. Kadanoff and Paul C. Martin. "Hydrodynamic equations and correlation functions." In: *Annals of Physics* 24 (1963), pp. 419 –469. ISSN: 0003-4916. DOI: https://doi.org/10.1016/0003-4916(63)90078-2.

[26] G. K. Batchelor. *An Introduction to Fluid Dynamics*. Cambridge Mathematical Library. Cambridge University Press, 2000. DOI: 10.1017/CBO9780511800955.

[27] E. Guyon, J. P. Hulin, L. Petit, and C. D. Mitescu. *Physical Hydrodynamics*. 2nd ed. Oxford University Press, 2015. ISBN: 9780198702443.

[28] Gregory Falkovich. *Fluid Mechanics*. 2nd ed. Cambridge University Press, 2018. DOI: 10.1017/9781316416600.

[29] S. G. Rajeev. *Fluid mechanics: A Geometrical Point of View*. 1st ed. Oxford University Press, 2018. ISBN: 9780198805021.

[30] Carl Eckart. "The Thermodynamics of irreversible processes. III. Relativistic theory of the simple fluid." In: *Phys. Rev.* 58 (1940), pp. 919–924. DOI: 10.1103/PhysRev.58.919.

[31] Paul Romatschke and Ulrike Romatschke. *Relativistic Fluid Dynamics In and Out of Equilibrium*. Cambridge Monographs on Mathematical Physics. Cambridge University Press, May 2019. ISBN: 978-1-108-48368-1, 978-1-108-75002-8. DOI: 10.1017/9781108651998. arXiv: 1712.05815 [nucl-th].

[32] Jyotirmoy Bhattacharya, Sayantani Bhattacharyya, Shiraz Minwalla, and Amos Yarom. "A Theory of First Order Dissipative Superfluid Dynamics." In: *JHEP* 05 (2014), p. 147. DOI: 10.1007/JHEP05(2014)147. arXiv: 1105.3733 [hep-th].

[33] W. Israel. "Thermodynamics of relativistic systems." In: *Physica A: Statistical Mechanics and its Applications* 106.1 (1981), pp. 204 –214. ISSN: 0378-4371. DOI: https://doi.org/10.1016/0378-4371(81)90220-X. URL: http://www.sciencedirect.com/science/article/pii/037843718190220X.

[34] Dam Thanh Son. "Newton-Cartan Geometry and the Quantum Hall Effect." In: (June 2013). arXiv: 1306.0638 [cond-mat.mes-hall].

[35] Morten H. Christensen, Jelle Hartong, Niels A. Obers, and Blaise Rollier. "Torsional Newton-Cartan Geometry and Lifshitz Holography." In: *Phys. Rev. D* 89 (2014), p. 061901. DOI: 10.1103/PhysRevD.89.061901. arXiv: 1311.4794 [hep-th].

[36] Morten H. Christensen, Jelle Hartong, Niels A. Obers, and Blaise Rollier. "Boundary Stress-Energy Tensor and Newton-Cartan Geometry in Lifshitz Holography." In: *JHEP* 01 (2014), p. 057. DOI: 10.1007/JHEP01(2014)057. arXiv: 1311.6471 [hep-th].

[37] Michael Geracie, Dam Thanh Son, Chaolun Wu, and Shao-Feng Wu. "Spacetime Symmetries of the Quantum Hall Effect." In: *Phys. Rev. D* 91 (2015), p. 045030. DOI: 10.1103/PhysRevD.91.045030. arXiv: 1407.1252 [cond-mat.mes-hall].

[38] Andrey Gromov and Alexander G. Abanov. "Thermal Hall Effect and Geometry with Torsion." In: *Phys. Rev. Lett.* 114 (2015), p. 016802. DOI: 10.1103/PhysRevLett.114.016802. arXiv: 1407.2908 [cond-mat.str-el].

[39] Jelle Hartong and Niels A. Obers. "Hořava-Lifshitz gravity from dynamical Newton-Cartan geometry." In: *JHEP* 07 (2015), p. 155. DOI: 10.1007/JHEP07(2015)155. arXiv: 1504.07461 [hep-th].

[40] Guido Festuccia, Dennis Hansen, Jelle Hartong, and Niels A. Obers. "Torsional Newton-Cartan Geometry from the Noether Procedure." In: *Phys. Rev. D* 94.10 (2016), p. 105023. DOI: 10.1103/PhysRevD.94.105023. arXiv: 1607.01926 [hep-th].

[41] Jay Armas, Jelle Hartong, Emil Have, Bjarke Frost Nielsen, and Niels A. Obers. "Newton-Cartan Submanifolds and Fluid Membranes." In: *Phys. Rev. E* 101.6 (2020), p. 062803. DOI: 10.1103/PhysRevE.101.062803. arXiv: 1912.01613 [hep-th].

[42] C. V. Vishveshwara. "Scattering of Gravitational Radiation by a Schwarzschild Black-hole." In: *Nature* 227 (1970), pp. 936–938. DOI: 10.1038/227936a0.

[43] William H. Press. "Long Wave Trains of Gravitational Waves from a Vibrating Black Hole." In: *Astrophys. J.* 170 (1971), pp. L105–L108. DOI: 10.1086/180849.

[44] Gary T. Horowitz and Veronika E. Hubeny. "Quasinormal Modes of AdS Black Holes and the Approach to Thermal Equilibrium." In: *Phys. Rev.* D62 (2000), p. 024027. DOI: 10.1103/PhysRevD.62.024027. arXiv: hep-th/9909056 [hep-th].

[45] Pavel K. Kovtun and Andrei O. Starinets. "Quasinormal modes and holography." In: *Phys. Rev.* D72 (2005), p. 086009. DOI: 10.1103/PhysRevD.72.086009. arXiv: hep-th/0506184 [hep-th].

[46] T. W. B. Kibble. "Topology of Cosmic Domains and Strings." In: *J. Phys.* A9 (1976), pp. 1387–1398. DOI: 10.1088/0305-4470/9/8/029.

[47] W. H. Zurek. "Cosmological Experiments in Superfluid Helium?" In: *Nature* 317 (1985), pp. 505–508. DOI: 10.1038/317505a0.

[48] Csaba Csaki, Hirosi Ooguri, Yaron Oz, and John Terning. "Glueball mass spectrum from supergravity." In: *JHEP* 01 (1999), p. 017. DOI: 10.1088/1126-6708/1999/01/017. arXiv: hep-th/9806021 [hep-th].

[49] Irene Amado, Carlos Hoyos-Badajoz, Karl Landsteiner, and Sergio Montero. "Absorption lengths in the holographic plasma." In: *JHEP* 09 (2007), p. 057. DOI: 10.1088/1126-6708/2007/09/057. arXiv: 0706.2750 [hep-th].

[50] Kengo Maeda, Makoto Natsuume, and Takashi Okamura. "Universality class of holographic superconductors." In: *Phys. Rev.* D79 (2009), p. 126004. DOI: 10.1103/PhysRevD.79.126004. arXiv: 0904.1914 [hep-th].

[51] Sergei Khlebnikov, Martin Kruczenski, and Georgios Michalogiorgakis. "Shock waves in strongly coupled plasmas." In: *Phys. Rev.* D82 (2010), p. 125003. DOI: 10.1103/PhysRevD.82.125003. arXiv: 1004.3803 [hep-th].

[52] Sergei Khlebnikov, Martin Kruczenski, and Georgios Michalogiorgakis. "Shock Waves in Strongly Coupled Plasmas II." In: *JHEP* 07 (2011), p. 097. DOI: 10.1007/JHEP07(2011)097. arXiv: 1105.1355 [hep-th].

[53] Julian Sonner, Adolfo del Campo, and Wojciech H. Zurek. "Universal far-from-equilibrium Dynamics of a Holographic Superconductor." In: (2014). [Nature Commun.6,7406(2015)]. DOI: 10.1038/ncomms8406. arXiv: 1406.2329 [hep-th].

[54] Mike Blake, Aristomenis Donos, and David Tong. "Holographic Charge Oscillations." In: *JHEP* 04 (2015), p. 019. DOI: 10.1007/JHEP04(2015)019. arXiv: 1412.2003 [hep-th].

[55] Andreas Karch and S. L. Sondhi. "Non-Linear, Finite Frequency Quantum Critical Transport from AdS/CFT." In: *JHEP* 01 (2011), p. 149. DOI: 10.1007/JHEP01(2011)149. arXiv: 1008.4134 [cond-mat.str-el].

[56] Julian Sonner and Andrew G. Green. "Hawking Radiation and Non-Equilibrium Quantum Critical Current Noise." In: *Phys. Rev. Lett.* 109 (2012), p. 091601. DOI: 10.1103/PhysRevLett.109.091601. arXiv: 1203.4908 [cond-mat.str-el].

[57] Arnab Kundu and Sandipan Kundu. "Steady-state Physics, Effective Temperature Dynamics in Holography." In: *Phys. Rev.* D91.4 (2015), p. 046004. DOI: 10.1103/PhysRevD.91.046004. arXiv: 1307.6607 [hep-th].

[58] Shin Nakamura and Hirosi Ooguri. "Out of Equilibrium Temperature from Holography." In: *Phys. Rev.* D88.12 (2013), p. 126003. DOI: 10.1103/PhysRevD.88.126003. arXiv: 1309.4089 [hep-th].

[59] Han-Chih Chang, Andreas Karch, and Amos Yarom. "An Ansatz for One Dimensional Steady State Configurations." In: *J. Stat. Mech.* 1406.6 (2014), P06018. DOI: 10.1088/1742-5468/2014/06/P06018. arXiv: 1311.2590 [hep-th].

[60] M. J. Bhaseen, Benjamin Doyon, Andrew Lucas, and Koenraad Schalm. "Far from Equilibrium Energy Flow in Quantum Critical Systems." In: (2013). [Nature Phys.11,5(2015)]. DOI: 10.1038/nphy$S^3$220. arXiv: 1311.3655 [hep-th].

[61] Irene Amado and Amos Yarom. "Black brane steady states." In: *JHEP* 10 (2015), p. 015. DOI: 10.1007/JHEP10(2015)015. arXiv: 1501.01627 [hep-th].

[62] Arnab Kundu. "Effective Temperature in Steady-state Dynamics from Holography." In: *JHEP* 09 (2015), p. 042. DOI: 10.1007/JHEP09(2015)042. arXiv: 1507.00818 [hep-th].

[63] Michael Spillane and Christopher P. Herzog. "Relativistic Hydrodynamics and Non-Equilibrium Steady States." In: *J. Stat. Mech.* 1610.10 (2016), p. 103208. DOI: 10.1088/1742-5468/2016/10/103208. arXiv: 1512.09071 [hep-th].

[64] Ioannis Bakas, Kostas Skenderis, and Benjamin Withers. "Self-similar equilibration of strongly interacting systems from holography." In: *Phys. Rev.* D93.10 (2016), p. 101902. DOI: 10.1103/PhysRevD.93.101902. arXiv: 1512.09151 [hep-th].

[65] Christopher P. Herzog, Michael Spillane, and Amos Yarom. "The holographic dual of a Riemann problem in a large number of dimensions." In: *JHEP* 08 (2016), p. 120. DOI: 10.1007/JHEP08(2016)120. arXiv: 1605.01404 [hep-th].

[66] Johanna Erdmenger, Daniel Fernandez, Mario Flory, Eugenio Megias, Ann-Kathrin Straub, and Piotr Witkowski. "Time evolution of entanglement for holographic steady state formation." In: *JHEP* 10 (2017), p. 034. DOI: 10.1007/JHEP10(2017)034. arXiv: 1705.04696 [hep-th].

[67] Pau Figueras and Toby Wiseman. "Stationary holographic plasma quenches and numerical methods for non-Killing horizons." In: *Phys. Rev. Lett.* 110 (2013), p. 171602. DOI: 10.1103/PhysRevLett.110.171602. arXiv: 1212.4498 [hep-th].

[68] Sebastian Fischetti, Donald Marolf, and Jorge E. Santos. "AdS flowing black funnels: Stationary AdS black holes with non-Killing horizons and heat transport in the dual CFT." In: *Class. Quant. Grav.* 30 (2013), p. 075001. DOI: 10.1088/0264-9381/30/7/075001. arXiv: 1212.4820 [hep-th].

[69] Matthew Headrick, Sam Kitchen, and Toby Wiseman. "A New approach to static numerical relativity, and its application to Kaluza-Klein black holes." In: *Class. Quant. Grav.* 27 (2010), p. 035002. DOI: 10.1088/0264-9381/27/3/035002. arXiv: 0905.1822 [gr-qc].

[70] Dongsu Bak, Michael Gutperle, and Romuald A. Janik. "Janus Black Holes." In: *JHEP* 10 (2011), p. 056. DOI: 10.1007/JHEP10(2011)056. arXiv: 1109.2736 [hep-th].

[71] Sean A. Hartnoll. "Lectures on holographic methods for condensed matter physics." In: *Class. Quant. Grav.* 26 (2009), p. 224002. DOI: 10.1088/0264-9381/26/22/224002. arXiv: 0903.3246 [hep-th].

[72] Benjamin Withers. "Short-lived modes from hydrodynamic dispersion relations." In: *JHEP* 06 (2018), p. 059. DOI: 10.1007/JHEP06(2018)059. arXiv: 1803.08058 [hep-th].

[73] Michal P. Heller and Michal Spałinski. "Hydrodynamics Beyond the Gradient Expansion: Resurgence and Resummation." In: *Phys. Rev. Lett.* 115.7 (2015), p. 072501. DOI: 10.1103/PhysRevLett.115.072501. arXiv: 1503.07514 [hep-th].

[74] Ingo Müller. "Zum paradoxon der wärmeleitungstheorie." In: *Zeitschrift für Physik* 198.4 (1967), pp. 329–344.

[75] Werner Israel and J. M. Stewart. "Transient relativistic thermodynamics and kinetic theory." In: *Annals of Physics* 118.2 (1979), pp. 341–372.

[76] Daniel K. Brattan and Simon A. Gentle. "Shear channel correlators from hot charged black holes." In: *JHEP* 04 (2011), p. 082. DOI: 10.1007/JHEP04(2011)082. arXiv: 1012.1280 [hep-th].

[77] M. J. Bhaseen, Jerome P. Gauntlett, B. D. Simons, Julian Sonner, and Toby Wiseman. "Holographic Superfluids and the Dynamics of Symmetry Breaking." In: *Phys. Rev. Lett.* 110.1 (2013), p. 015301. DOI: 10.1103/PhysRevLett.110.015301. arXiv: 1207.4194 [hep-th].

[78] Richard A. Davison and Blaise Goutéraux. "Momentum Dissipation and Effective Theories of Coherent and Incoherent Transport." In: *JHEP* 01 (2015), p. 039. DOI: 10.1007/JHEP01(2015)039. arXiv: 1411.1062 [hep-th].

[79] Benjamin Withers. "Nonlinear Conductivity and the Ringdown of Currents in Metallic Holography." In: *JHEP* 10 (2016), p. 008. DOI: 10.1007/JHEP10(2016)008. arXiv: 1606.03457 [hep-th].

[80] Vadim Asnin, Dan Gorbonos, Shahar Hadar, Barak Kol, Michele Levi, and Umpei Miyamoto. "High and Low Dimensions in The Black Hole Negative Mode." In: *Class. Quant. Grav.* 24 (2007), pp. 5527–5540. DOI: 10.1088/0264-9381/24/22/015. arXiv: 0706.1555 [hep-th].

[81] Roberto Emparan, Ryotaku Suzuki, and Kentaro Tanabe. "The large D limit of General Relativity." In: *JHEP* 06 (2013), p. 009. DOI: 10.1007/JHEP06(2013)009. arXiv: 1302.6382 [hep-th].

[82] Roberto Emparan, Daniel Grumiller, and Kentaro Tanabe. "Large-D gravity and low-D strings." In: *Phys. Rev. Lett.* 110.25 (2013), p. 251102. DOI: 10.1103/PhysRevLett.110.251102. arXiv: 1303.1995 [hep-th].

[83] Roberto Emparan, Ryotaku Suzuki, and Kentaro Tanabe. "Quasinormal modes of (Anti-)de Sitter black holes in the 1/D expansion." In: *JHEP* 04 (2015), p. 085. DOI: 10.1007/JHEP04(2015)085. arXiv: 1502.02820 [hep-th].

[84] Dam T. Son and Andrei O. Starinets. "Minkowski space correlators in AdS / CFT correspondence: Recipe and applications." In: *JHEP* 09 (2002), p. 042. DOI: 10.1088/1126-6708/2002/09/042. arXiv: hep-th/0205051 [hep-th].

[85] Vitor Cardoso and Jose P. S. Lemos. "Scalar, electromagnetic and Weyl perturbations of BTZ black holes: Quasinormal modes." In: *Phys. Rev.* D63 (2001), p. 124015. DOI: 10.1103/PhysRevD.63.124015. arXiv: gr-qc/0101052 [gr-qc].

[86] Danny Birmingham. "Choptuik scaling and quasinormal modes in the anti-de Sitter space/conformal-field theory correspondence." In: *Phys. Rev. D* 64 (6 2001), p. 064024. DOI: 10.1103/PhysRevD.64.064024. URL: https://link.aps.org/doi/10.1103/PhysRevD.64.064024.

[87] Sebastian de Haro, Sergey N. Solodukhin, and Kostas Skenderis. "Holographic reconstruction of space-time and renormalization in the AdS / CFT correspondence." In: *Commun. Math. Phys.* 217 (2001), pp. 595–622. DOI: 10.1007/s002200100381. arXiv: hep-th/0002230 [hep-th].

[88] Veronika E. Hubeny. "Holographic insights and puzzles." In: *Fortsch. Phys.* 59 (2011), pp. 586–601. DOI: 10.1002/prop.201100041. arXiv: 1103.1999 [hep-th].

[89] Sebastian Fischetti and Donald Marolf. "Flowing Funnels: Heat sources for field theories and the AdS_3 dual of CFT_2 Hawking radiation." In: *Class. Quant. Grav.* 29 (2012), p. 105004. DOI: 10.1088/0264-9381/29/10/105004. arXiv: 1202.5069 [hep-th].

[90] Roberto Emparan and Marina Martinez. "Black String Flow." In: *JHEP* 09 (2013), p. 068. DOI: 10.1007/JHEP09(2013)068. arXiv: 1307.2276 [hep-th].

[91] Donald Marolf, Mukund Rangamani, and Toby Wiseman. "Holographic thermal field theory on curved spacetimes." In: *Class. Quant. Grav.* 31 (2014), p. 063001. DOI: 10.1088/0264-9381/31/6/063001. arXiv: 1312.0612 [hep-th].

[92] Oscar J. C. Dias, Jorge E. Santos, and Benson Way. "Numerical Methods for Finding Stationary Gravitational Solutions." In: *Class. Quant. Grav.* 33.13 (2016), p. 133001. DOI: 10.1088/0264-9381/33/13/133001. arXiv: 1510.02804 [hep-th].

[93] Paul M. Chesler and Laurence G. Yaffe. "Horizon Formation and Far-From-Equilibrium Isotropization in Supersymmetric Yang-Mills Plasma." In: *Phys. Rev. Lett.* 102 (2009), p. 211601. DOI: 10.1103/PhysRevLett.102.211601. arXiv: 0812.2053 [hep-th].

[94] Dennis M. DeTurck. "Deforming metrics in the direction of their Ricci tensors." In: *J. Differential Geom.* 18.1 (1983), pp. 157–162. DOI: 10.4310/jdg/1214509286. URL: https://doi.org/10.4310/jdg/1214509286.

[95] Toby Wiseman. "Numerical construction of static and stationary black holes." In: *Black Holes in Higher Dimensions*. Cambridge University Press, 2011, pp. 233–270. arXiv: 1107.5513 [gr-qc].

[96] Timothy A. Davis. "Algorithm 832: UMFPACK V4.3—an Unsymmetric-pattern Multifrontal Method." In: *ACM Trans. Math. Softw.* 30.2 (June 2004), pp. 196–199. ISSN: 0098-3500. DOI: 10.1145/992200.992206. URL: http://doi.acm.org/10.1145/992200.992206.

[97] Pierre C Hohenberg and Bertrand I Halperin. "Theory of dynamic critical phenomena." In: *Reviews of Modern Physics* 49.3 (1977), p. 435.

[98] Philip JW Moll, Pallavi Kushwaha, Nabhanila Nandi, Burkhard Schmidt, and Andrew P Mackenzie. "Evidence for hydrodynamic electron flow in PdCoO2." In: *Science* 351.6277 (2016), pp. 1061–1064.

[99] Jesse Crossno, Jing K Shi, Ke Wang, Xiaomeng Liu, Achim Harzheim, Andrew Lucas, Subir Sachdev, Philip Kim, Takashi Taniguchi, Kenji Watanabe, et al. "Observation of the Dirac fluid and the breakdown of the Wiedemann-Franz law in graphene." In: *Science* 351.6277 (2016), pp. 1058–1061.

[100] K. S. Novoselov, A. K. Geim, S. V. Morozov, D. Jiang, M. I. Katsnelson, I. V. Grigorieva, S. V. Dubonos, and A. A. Firsov. "Two-dimensional gas of massless Dirac fermions in graphene." In: *Nature* 438 (2005), p. 197. DOI: 10.1038/nature04233. arXiv: cond-mat/0509330 [cond-mat.mes-hall].

[101] Markus Müller, Jörg Schmalian, and Lars Fritz. "Graphene: A Nearly Perfect Fluid." In: *Phys. Rev. Lett.* 103 (2 2009), p. 025301. DOI: 10.1103/PhysRevLett.103.025301. arXiv: 0903.4178 [cond-mat.mes-hall].

[102] Iacopo Torre, Andrea Tomadin, Andre K. Geim, and Marco Polini. "Nonlocal transport and the hydrodynamic shear viscosity in graphene." In: *Phys. Rev. B* 92 (16 2015), p. 165433. DOI: 10.1103/PhysRevB.92.165433. URL: https://link.aps.org/doi/10.1103/PhysRevB.92.165433.

[103] Vincent E. Dorgan, Myung-Ho Bae, and Eric Pop. "Mobility and saturation velocity in graphene on SiO2." In: *Applied Physics Letters* 97.8 (2010), p. 082112. DOI: 10.1063/1.3483130. eprint: https://doi.org/10.1063/1.3483130. URL: https://doi.org/10.1063/1.3483130.

[104] Andrew G Green and SL Sondhi. "Nonlinear quantum critical transport and the Schwinger mechanism for a superfluid-Mott-insulator transition of bosons." In: *Physical review letters* 95.26 (2005), p. 267001.

[105] A. G. Green, J. E. Moore, S. L. Sondhi, and A. Vishwanath. "Current noise in the vicinity of the 2D superconductor-insulator quantum critical point." In: *Physical review letters* 97.22 (2006), p. 227003.

[106] Sebastian Fischetti and Benson Way. "Towards Fluid Instabilities of Stationary Non-Killing Horizons." In: *Class. Quant. Grav.* 33.24 (2016), p. 245009. DOI: 10.1088/0264-9381/33/24/245009. arXiv: 1606.00838 [hep-th].

[107] Boris N. Narozhny, Igor V. Gornyi, Alexander D. Mirlin, and Jörg Schmalian. "Hydrodynamic Approach to Electronic Transport in Graphene." In: *Annalen der Physik* 529.11 (2017), p. 1700043. DOI: 10.1002/andp.201700043. eprint: https://onlinelibrary.wiley.com/doi/pdf/10.1002/andp.201700043. URL: https://onlinelibrary.wiley.com/doi/abs/10.1002/andp.201700043.

[108] Andrew Lucas and Kin Chung Fong. "Hydrodynamics of Electrons in Graphene." In: *J. Phys. Condens. Matter* 30.5 (2018), p. 053001. DOI: 10.1088/1361-648X/aaa274. arXiv: 1710.08425 [cond-mat.str-el].

[109] John Toner, Yuhai Tu, and Sriram Ramaswamy. "Hydrodynamics and phases of flocks." In: *Annals of Physics* 318.1 (2005). Special Issue, pp. 170 –244. ISSN: 0003-4916. DOI: https://doi.org/10.1016/j.aop.2005.04.011. URL: http://www.sciencedirect.com/science/article/pii/S0003491605000540.

[110] Yashodhan Hatwalne, Sriram Ramaswamy, Madan Rao, and R. Aditi Simha. "Rheology of Active-Particle Suspensions." In: *Phys. Rev. Lett.* 92 (11 2004), p. 118101. DOI: 10.1103/PhysRevLett.92.118101. URL: https://link.aps.org/doi/10.1103/PhysRevLett.92.118101.

[111] Andrew C Callan-Jones and Frank Jülicher. "Hydrodynamics of active permeating gels." In: *New Journal of Physics* 13.9 (2011), p. 093027.

[112] Sebastian Fürthauer, Marc Neef, Stefan W Grill, Karsten Kruse, and Frank Jülicher. "The Taylor–Couette motor: spontaneous flows of active polar fluids between two coaxial cylinders." In: *New Journal of Physics* 14.2 (2012), p. 023001.

[113] Alberto Nicolis, Riccardo Penco, Federico Piazza, and Riccardo Rattazzi. "Zoology of Condensed Matter: Framids, Ordinary Stuff, Extra-Ordinary Stuff." In: *JHEP* 06 (2015), p. 155. DOI: 10.1007/JHEP06(2015)155. arXiv: 1501.03845 [hep-th].

[114] Ted Jacobson and David Mattingly. "Gravity with a Dynamical Preferred Frame." In: *Phys. Rev.* D64 (2001), p. 024028. DOI: 10.1103/PhysRevD.64.024028. arXiv: gr-qc/0007031 [gr-qc].

[115] Jan de Boer, Jelle Hartong, Niels A. Obers, Watse Sybesma, and Stefan Vandoren. "Perfect Fluids." In: *SciPost Phys.* 5.1 (2018), p. 003. DOI: 10.21468/SciPostPhys.5.1.003. arXiv: 1710.04708 [hep-th].

[116] Jan de Boer, Jelle Hartong, Niels A. Obers, Watse Sybesma, and Stefan Vandoren. "Hydrodynamic Modes of Homogeneous and Isotropic Fluids." In: *SciPost Phys.* 5.2 (2018), p. 014. DOI: 10.21468/SciPostPhys.5.2.014. arXiv: 1710.06885 [hep-th].

[117] Napat Poovuttikul and Watse Sybesma. "First order non-Lorentzian fluids, entropy production and linear instabilities." In: (2019). arXiv: 1911.00010 [hep-th].

[118] Jyotirmoy Bhattacharya, Sayantani Bhattacharyya, and Mukund Rangamani. "Non-dissipative hydrodynamics: Effective actions versus entropy current." In: *JHEP* 02 (2013), p. 153. DOI: 10.1007/JHEP02(2013)153. arXiv: 1211.1020 [hep-th].

[119] Nabamita Banerjee, Jyotirmoy Bhattacharya, Sayantani Bhattacharyya, Sachin Jain, Shiraz Minwalla, and Tarun Sharma. "Constraints on Fluid Dynamics from Equilibrium Partition Functions." In: *JHEP* 09 (2012), p. 046. DOI: 10.1007/JHEP09(2012)046. arXiv: 1203.3544 [hep-th].

[120] Kristan Jensen, Matthias Kaminski, Pavel Kovtun, Rene Meyer, Adam Ritz, and Amos Yarom. "Towards hydrodynamics without an entropy current." In: *Phys. Rev. Lett.* 109 (2012), p. 101601. DOI: 10.1103/PhysRevLett.109.101601. arXiv: 1203.3556 [hep-th].

[121] V. Bargmann. "On Unitary ray representations of continuous groups." In: *Annals Math.* 59 (1954), pp. 1–46. DOI: 10.2307/1969831.

[122] Roel Andringa, Eric Bergshoeff, Sudhakar Panda, and Mees de Roo. "Newtonian Gravity and the Bargmann Algebra." In: *Class. Quant. Grav.* 28 (2011), p. 105011. DOI: 10.1088/0264-9381/28/10/105011. arXiv: 1011.1145 [hep-th].

[123] Kristan Jensen and Andreas Karch. "Revisiting Non-Relativistic Limits." In: *JHEP* 04 (2015), p. 155. DOI: 10.1007/JHEP04(2015)155. arXiv: 1412.2738 [hep-th].

[124] Michael Geracie, Kartik Prabhu, and Matthew M. Roberts. "Fields and Fluids on Curved Non-Relativistic Spacetimes." In: *JHEP* 08 (2015), p. 042. DOI: 10.1007/JHEP08(2015)042. arXiv: 1503.02680 [hep-th].

[125] D. T. Son. "Vanishing Bulk Viscosities and Conformal Invariance of Unitary Fermi Gas." In: *Phys. Rev. Lett.* 98 (2007), p. 020604. DOI: 10.1103/PhysRevLett.98.020604. arXiv: cond-mat/0511721 [cond-mat].

[126] Carlos Hoyos, Bom Soo Kim, and Yaron Oz. "Lifshitz Hydrodynamics." In: *JHEP* 11 (2013), p. 145. DOI: 10.1007/JHEP11(2013)145. arXiv: 1304.7481 [hep-th].

[127] Carlos Hoyos, Bom Soo Kim, and Yaron Oz. "Lifshitz Field Theories at Non-Zero Temperature, Hydrodynamics and Gravity." In: *JHEP* 03 (2014), p. 029. DOI: 10.1007/JHEP03(2014)029. arXiv: 1309.6794 [hep-th].

[128] Carlos Hoyos, Bom Soo Kim, and Yaron Oz. "Bulk Viscosity in Holographic Lifshitz Hydrodynamics." In: *JHEP* 03 (2014), p. 050. DOI: 10.1007/JHEP03(2014)050. arXiv: 1312.6380 [hep-th].

[129] Christopher Eling and Yaron Oz. "Horava-Lifshitz Black Hole Hydrodynamics." In: *JHEP* 11 (2014), p. 067. DOI: 10.1007/JHEP11(2014)067. arXiv: 1408.0268 [hep-th].

[130] Carlos Hoyos, Adiel Meyer, and Yaron Oz. "Parity Breaking Transport in Lifshitz Hydrodynamics." In: *JHEP* 09 (2015), p. 031. DOI: 10.1007/JHEP09(2015)031. arXiv: 1505.03141 [hep-th].

[131] Marika Taylor. "Lifshitz holography." In: *Class. Quant. Grav.* 33.3 (2016), p. 033001. DOI: 10.1088/0264-9381/33/3/033001. arXiv: 1512.03554 [hep-th].

[132] Jelle Hartong, Niels A. Obers, and Marco Sanchioni. "Lifshitz Hydrodynamics from Lifshitz Black Branes with Linear Momentum." In: *JHEP* 10 (2016), p. 120. DOI: 10.1007/JHEP10(2016)120. arXiv: 1606.09543 [hep-th].

[133] Richard A. Davison, Sašo Grozdanov, Stefan Janiszewski, and Matthias Kaminski. "Momentum and charge transport in non-relativistic holographic fluids from Hořava gravity." In: *JHEP* 11 (2016), p. 170. DOI: 10.1007/JHEP11(2016)170. arXiv: 1606.06747 [hep-th].

[134] Markus Garbiso and Matthias Kaminski. "Dispersion relations in non-relativistic two-dimensional materials from quasinormal modes in Hořava Gravity." In: *JHEP* 10 (2019), p. 087. DOI: 10.1007/JHEP10(2019)087. arXiv: 1905.11993 [hep-th].

[135] Daniel Fernandez, Aruna Rajagopal, and Larus Thorlacius. "Non-equilibrium steady states in quantum critical systems with Lifshitz scaling." In: (2019). arXiv: 1909.06377 [hep-th].

[136] Jan de Boer, Jelle Hartong, Emil Have, Niels A. Obers, and Watse Sybesma. "Non-Boost Invariant Fluid Dynamics." In: *SciPost Phys.* 9.2 (2020), p. 018. DOI: 10.21468/SciPostPhys.9.2.018. arXiv: 2004.10759 [hep-th].

[137] Jay Armas and Akash Jain. "Effective field theory for hydrodynamics without boosts." In: (Oct. 2020). arXiv: 2010.15782 [hep-th].

[138] Johanna Erdmenger, Ioannis Matthaiakakis, René Meyer, and David Rodríguez Fernández. "Strongly coupled electron fluids in the Poiseuille regime." In: *Phys. Rev. B* 98.19 (2018), p. 195143. DOI: 10.1103/PhysRevB.98.195143. arXiv: 1806.10635 [cond-mat.mes-hall].

[139] Steven A. Orszag. "Accurate solution of the Orr-Sommerfeld stability equation." In: *Journal of Fluid Mechanics* 50.4 (1971), 689?703. DOI: 10.1017/S0022112071002842.

[140] Brian Higgins. *Solution of the Orr-Sommerfeld Equation for Plane Poiseuille Flow: A Spectral Collocation Method*. June 2019.

[141] Lloyd N. Trefethen. *Spectral Methods in MatLab*. USA: Society for Industrial and Applied Mathematics, 2000. ISBN: 0898714656.

[142] Sean A. Hartnoll and Christopher P. Herzog. "Ohm's Law at strong coupling: S duality and the cyclotron resonance." In: *Phys. Rev.* D76 (2007), p. 106012. DOI: 10.1103/PhysRevD.76.106012. arXiv: 0706.3228 [hep-th].

Thank you for reading.

COLOPHON

This document was typeset using the typographical look-and-feel `classicthesis` developed by André Miede. The style was inspired by Robert Bringhurst's seminal book on typography "*The Elements of Typographic Style*". `classicthesis` is available for both LaTeX and LyX:

https://bitbucket.org/amiede/classicthesis/

Happy users of `classicthesis` usually send a real postcard to the author, a collection of postcards received so far is featured here:

http://postcards.miede.de/